

Copyright Warning & Restrictions

The copyright law of the United States (Title 17, United States Code) governs the making of photocopies or other reproductions of copyrighted material.

Under certain conditions specified in the law, libraries and archives are authorized to furnish a photocopy or other reproduction. One of these specified conditions is that the photocopy or reproduction is not to be “used for any purpose other than private study, scholarship, or research.” If a user makes a request for, or later uses, a photocopy or reproduction for purposes in excess of “fair use” that user may be liable for copyright infringement,

This institution reserves the right to refuse to accept a copying order if, in its judgment, fulfillment of the order would involve violation of copyright law.

Please Note: The author retains the copyright while the New Jersey Institute of Technology reserves the right to distribute this thesis or dissertation

Printing note: If you do not wish to print this page, then select “Pages from: first page # to: last page #” on the print dialog screen



The Van Houten library has removed some of the personal information and all signatures from the approval page and biographical sketches of theses and dissertations in order to protect the identity of NJIT graduates and faculty.

1) EXPERIMENTAL EVALUATION
OF
PROCESS ZONE DEFORMATION
IN CONCRETE

BY

1) CHERNG-MAOU MENG
=

Thesis submitted to the faculty of the graduate school
of the New Jersey Institute of Technology in partial
fulfillment of the requirements for the degree of
Master of Science in Civil Engineering

1990

APPROVAL OF THESIS

Title of Thesis : Experimental Evaluation of
Process Zone Deformation
In Concrete

Name of Candidate : Cherng-Maou Meng
Master of Science in Civil
Engineering , 1990

Thesis and Abstract approved by :

Date

Farhad Ansari, Ph.D.

Associate Professor

Department of Civil and Environmental Engineering

Date

Signature of other Member
of the Thesis Committee

VITA

Name : Cherng-Maou Meng

Degree & Date : Master of Science in Civil Engineering 1990

Secondary education : Tsi-Shiu High School

Collegiate Institute	Date	Degree	Date Graduated
----------------------	------	--------	----------------

Tamkang University	1982-1986	B.S. Civil Eng.	June , 1986
--------------------	-----------	-----------------	-------------

New Jersey Institute of Technology	1988-1990	M.S. Civil Eng.	May , 1990
---------------------------------------	-----------	-----------------	------------

Major : Structure Engineering

Position Held :

1989-1990 : Teaching Assistant at NJIT , NJ

1990-Present : Junior Structure Engineer , Formosa Plastics
CO. USA , NJ U.S.A.

ABSTRACT

Title of thesis : Experimental Evaluation of Process
Zone Deformation in Concrete

Name: Cherng-Maou Meng
Master of Science in Civil Engineering

Thesis directed by : Dr. Farhad Ansari

Concrete structures are often subjected to a variety of loading conditions. Under ultimate load design , concrete structures can resist these loads without evident deformation. However , under service , tension cracks will develop and depending on their location , they may impair load carrying capacity.

It is generally believed that microcrack development is preceded by formation of a relatively long microcracked region. A large number of studies have indicated that due to formation of this process zone (microcracked zone) , Linear

Elastic Fracture Mechanics (LEFM) principles are not applicable to concrete. However , a number of nonlinear models can be developed if the length of this zone can be determined. Determination of process zone length is a difficult experimental problem , mainly due to difficulties involved in accurate detection of microcracks during loading in a typical experiment. Furthermore , as some recent studies indicate , surface microcracks progress further than their internal counterparts. Determination of internal deformations and microcracks are even more challenging than the mere surface flaw detection mentioned earlier. Survey of technical literature indicate , inexistence of an accurate internal deformation measuring technique for concrete.

In the present study , a new technique is developed for measurement of internal deformation in cementitious composites. main emphasis is given to the development of the technique , and measurement of deformations in the process zone. Results from experiments on compact tension , and three point bend specimen are presented.

Blank Page

ACKNOWLEDGEMENTS

The author wishes to acknowledge the help of the following persons who contributed to this research in a variety of ways :

To Dr. Farhad Ansari , my graduate advisor , for his valuable guidance throughout the entire project.

To Mr. Quij Chen , for his help in doing fiber optics.

TABLE OF CONTENTS

Chapter	Page
I. Introduction and Research objectives	1
II. Experimental Program	4
II.1 Experimental Investigation	4
II.2 Methodology	4
II.3 Fiber Optics Crack Opening Displacement (COD) Gage	6
II.4 Instrumentation and Calibration	9
II.4.1 Sensor Intrumentation and Calibration	9
II.4.2 Closed Loop Testing and Data Acquisition	13
II.5 Details of Test Specimen	31
II.6 Experimental procedure	32
III. Analysis and Result	38

IV. Conclusion137

 IV.1 Conclusion137

 IV.2 Future Research138

Appendix A139

LIST OF TABLE

Table	Page
Table 1 - Specimen types and designation	39

LIST OF FIGURES

Figure	Page
Fig.1 - Basic for light transmission in optical fibers ...	5
Fig.2 - Light loss in the optical fiber due to deformation	7
Fig.3 - Plan view of fiber optic COD gage	9
Fig.4 - Block diagram of fiber optic sensor operations ..	10
Fig.5 - Plan view of the calibration instrument	12
Fig.6 - Calibration data for channel#1	14
Fig.7 - Calibration data for channel#1	15
Fig.8 - Calibration data for channel#1	16
Fig.9 - Lower range cali. curve for channel#1	17
Fig.10 - Calibration data for channel#2	18
Fig.11 - Calibration data for channel#2	19
Fig.12 - Calibration data for channel#2	20
Fig.13 - Lower range cali. curve for channel#2	21
Fig.14 - Calibration data for channel#3	22
Fig.15 - Calibration data for channel#3	23
Fig.16 - Calibration data for channel#3	24
Fig.17 - Lower range cali. curve for channel#3	25
Fig.18 - Calibration data for channel#4	26
Fig.19 - Calibration data for channel#4	27
Fig.20 - Calibration data for channel#4	28

Fig.21 - Lower range cali. curve for channel#4	29
Fig.22 - Block diagram of experimental setup	30
Fig.23.1 - Compact tension specimen and location of sensors.....	33
Fig.23.2 - Three point bend specimen and location of specimen	34
Fig.23.3 - Compact tension specimen in the loading fram	35
Fig.23.4 - Three point bend specimen in the loading frame and the optical setup	36
Fig.24 - Internal deformation data for J31	40
Fig.25 - Internal deformation data for J31	41
Fig.26 - Internal deformation data for J31	42
Fig.27 - Internal deformation data for J31	43
Fig.28 - Internal deformation data for F2	44
Fig.29 - Internal deformation data for F2	45
Fig.30 - Internal deformation data for F2	46
Fig.31 - Internal deformation data for F2	47
Fig.32 - Internal deformation data for F3#2	48
Fig.33 - Internal deformation data for F3#2	49
Fig.34 - Internal deformation data for F3#2	50
Fig.35 - Internal deformation data for F3#2	51
Fig.36 - Internal deformation data for F8	52
Fig.37 - Internal deformation data for F8	53
Fig.38 - Internal deformation data for F8	54
Fig.39 - Internal deformation data for F8	55
Fig.40 - Internal deformation data for F10	56
Fig.41 - Internal deformation data for F10	57
Fig.42 - Internal deformation data for F10	58

Fig.43 - Internal deformation data for F10	59
Fig.44 - Internal deformation data for F11	60
Fig.45 - Internal deformation data for F11	61
Fig.46 - Internal deformation data for F11	62
Fig.47 - Internal deformation data for F11	63
Fig.48 - Internal deformation data for F12	64
Fig.49 - Internal deformation data for F12	65
Fig.50 - Internal deformation data for F12	66
Fig.51 - Internal deformation data for F12	67
Fig.52 - Internal deformation data for F19A	68
Fig.53 - Internal deformation data for F19A	69
Fig.54 - Internal deformation data for F19A	70
Fig.55 - Internal deformation data for F19A	71
Fig.56 - Internal deformation data for F19B	72
Fig.57 - Internal deformation data for F19B	73
Fig.58 - Internal deformation data for F19B	74
Fig.59 - Internal deformation data for F19B	75
Fig.60 - Internal deformation data for F19C	76
Fig.61 - Internal deformation data for F19C	77
Fig.62 - Internal deformation data for F19C	78
Fig.63 - Internal deformation data for F19C	79
Fig.64 - Internal deformation data for F19D	80
Fig.65 - Internal deformation data for F19D	81
Fig.66 - Internal deformation data for F19D	82
Fig.67 - Internal deformation data for F19D	83
Fig.68 - Internal deformation data for F28A	84
Fig.69 - Internal deformation data for F28A	85

Fig.70 - Internal deformation data for F28A	86
Fig.71 - Internal deformation data for F28A	87
Fig.72 - Internal deformation data for F28B	88
Fig.73 - Internal deformation data for F28B	89
Fig.74 - Internal deformation data for F28B	90
Fig.75 - Internal deformation data for F28B	91
Fig.76 - Internal deformation data for F28C	92
Fig.77 - Internal deformation data for F28C	93
Fig.78 - Internal deformation data for F28C	94
Fig.79 - Internal deformation data for F28C	95
Fig.80 - Internal deformation data for M1A	96
Fig.81 - Internal deformation data for M1A	97
Fig.82 - Internal deformation data for M1A	98
Fig.83 - Internal deformation data for M1A	99
Fig.84 - Internal deformation data for M1B	100
Fig.85 - Internal deformation data for M1B	101
Fig.86 - Internal deformation data for M1B	102
Fig.87 - Internal deformation data for M1B	103
Fig.88 - Internal deformation for J31	104
Fig.89 - Internal deformation for F2	105
Fig.90 - Internal deformation for F3#2.....	106
Fig.91 - Internal deformation for F8	107
Fig.92 - Internal deformation for F11	108
Fig.93 - Internal deformation for F12	109
Fig.94 - Internal deformation for F19B	110
Fig.95 - Internal deformation for F19D	111
Fig.96 - Internal deformation for F28A	112

Fig.97 - Internal deformation for F28C	113
Fig.98 - Internal deformation for M1A	114
Fig.99 - Internal deformation for M1B	115
Fig.100 - Defor. pattern at diff. load F2	117
Fig.101 - Defor. pattern at diff. load F8	118
Fig.102 - Defor. pattern at diff. load F11	119
Fig.103 - Defor. pattern at diff. load F12	120
Fig.104 - Defor. pattern at diff. load F19B.....	121
Fig.105 - Defor. pattern at diff. load F19D.....	122
Fig.106 - Defor. pattern at diff. load F28A	123
Fig.107 - Defor. pattern at diff. load F28C	124
Fig.108 - Defor. pattern at diff. load M1A	125
Fig.109 - Defor. pattern at diff. load M1B	126
Fig.110 - Defor. pattern without COD F2	127
Fig.111 - Defor. pattern without COD F8	128
Fig.112 - Defor. pattern without COD F11	129
Fig.113 - Defor. pattern without COD F12	130
Fig.114 - Defor. pattern without COD F19B	131
Fig.115 - Defor. pattern without COD F19D	132
Fig.116 - Defor. pattern without COD F28A	133
Fig.117 - Defor. pattern without COD F28C	134
Fig.118 - Defor. pattern without COD M1A	135
Fig.119 - Defor. pattern without COD M1B	136

CHAPTER I Introduction and Research Objectives

Formation and growth of microcracks play an important role in the performance of plain , reinforced , and prestressed concrete. For instance , cracking of concrete in tension is a significant factor contributing to the non-linear behavior of reinforced concrete. Therefore , logical design concepts ought to be based on realistic theoretical models that take crack formation and propagation into account. Recent advances in fracture mechanics and application of numerical methods have given possibilities for the establishment of realistic models for concrete fracture¹⁻². It is recognized that fracture toughness of concrete can not be evaluated using linear elastic fracture mechanics unless proper modifications are applied. Studies on the fracture behavior of concrete reveal some fracture characteristics that differ from those normally observed in metallic materials³⁻⁶. Among these characteristics is the existence of a microcracking zone or process zone at the tip of an advancing crack. Since the process zone is believed to be relatively large in concrete , calculation of fracture parameters should include the effects of this zone. Lack of data on the experimentally observed zone of microcracking , the COD-crack growth relationship , and the inelastic behavior has forced the investigators to make assumptions pertaining to process zone. The determination of the fracture process zone in concrete is a difficult

experimental problem , because the resulting deformation is strongly localized. The extent of the crack tip at the crack front and the location for the tip of the advancing microcrack that forms that zone is almost impossible to detect.

Dugale-Barrenblatt model⁷⁻⁸ for modeling metal fracture in the presence of large scale yielding has been extensively applied to concrete treating the fracture process zone as the strip yield zone⁹⁻¹⁰. Assumptions regarding the crack length and crack opening resistance of the fracture process zone were all different in above-mentioned models. Bazant¹¹ developed a nonlinear fracture concept , modeling the fracture process zone extension through nonlinear programming. In another report¹⁰ , double clip-on gage technique was used to infer the location of the process zone in crack-line wedge-loaded double cantilever beams. In a simplified model proposed by Jenq and Shah a closing pressure of zero was assumed as a starting value in the interactive solution that adjusted the effective crack length to yield the value of CMOD from the experiments.

Inconsistency of results reported by many investigators and comparison of their approach in order to model fracture behavior of concrete suggest the nonlinear effects associated with crack propagation in concrete as the major source of inconsistency. Values reported in the technical literature for fracture toughness vary widely even for essentially similar materials depending on the size of the

test specimen^{3,11-13}. The primary reason for the discrepancy in the reported values is the effect of microcracking zone or fracture process zone ahead of the crack tip.

Microcracking zone is also responsible for the slow crack growth in concrete. One impractical way to evaluate a size independent fracture toughness for concrete is to test very large specimen so that the uncracked portion of the segment in front of the crack is much larger than the fracture process zone. The alternative approach would be to test practical size specimen and develop an experimental technique such that information regarding the localized displacement field in front of the moving crack and the extent of microcracks can be determined. Once this information is acquired, then the effect of fracture process zone can be introduced in the numerical modeling with the least number of simplified assumption.

Based on above considerations, the main objective of the research reported here is to develop an experimental technique for direct full field measurement of internal deformations and microcrack widths in the process zone of concrete specimen.

CHAPTER II EXPERIMENTAL PROGRAM

II.1 Experimental Investigation

Microcracking is the essential aspect of the fracture process zone in concrete , therefore , there is a need for a testing technique that would be accurate enough to detect and measure the displacement associated with microcracks. Moreover , it is very important to make internal measurement of the deformation associated with microcracking in order to distinguish in between the structural and nonstructural development of microcracks , such as the surface microcracks developed due to shrinkage at the hydration stage.

II.2 Methodology

Transmission of light through optical fibers can be explained by the Snell's law and the concept of total internal reflection. According to Fig.1 , when light travels from the fiber core that has a high refractive index into the cladding with a lower index , the lightwave totally reflects back into the core. This is true , provided that the diameter of the core is chosen so as to force the lightwave to propagate according to a certain critical angle of incidence. However , if the fiber is stretched or bent at any point along it's length , the change in the angle of incidence will cause some of the light to escape out through

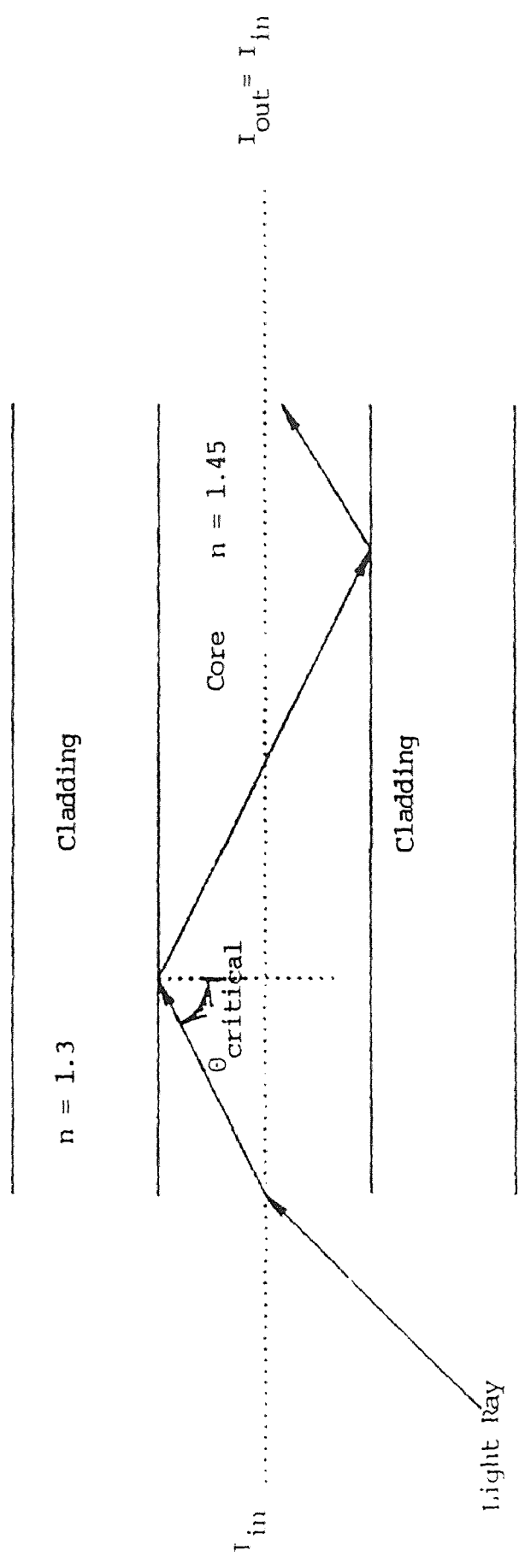


Fig.1 Basis for light transmission in optical fibers.

the cladding (Fig.2). The intensity of light at the output end of the fiber will decrease due to this loss , and it can be directly related to the amount of deformation if properly calibrated. Employing light intensity loss sensors in structural applications is simple since these sensors make use of modulation schemes which perturb the fiber itself , so that the fiber is both the transmission medium and the transducer. In other words , a thin optical fiber is all that is needed for embedment within a concrete member.

II.3 Fiber Optic Crack Opening Displacement (COD)Gage

Practical application of fiber optics to displacement measurements , particularly to COD measurements in concrete require special arrangement for placement of the optical fiber within the concrete , as well as attainment of sufficient sensitivity in measurements. The arrangement shown in Fig.3 provides optimum configuration of the fiber optics for COD measurements. It also satisfies the sensitivity requirements as bending of an optical fiber will result in increased light intensity loss through mode coupling. In other words , the microbending of an optical fiber , steepens the angle of light incidence at the core-cladding interface which in turn brings about increased light intensity loss.

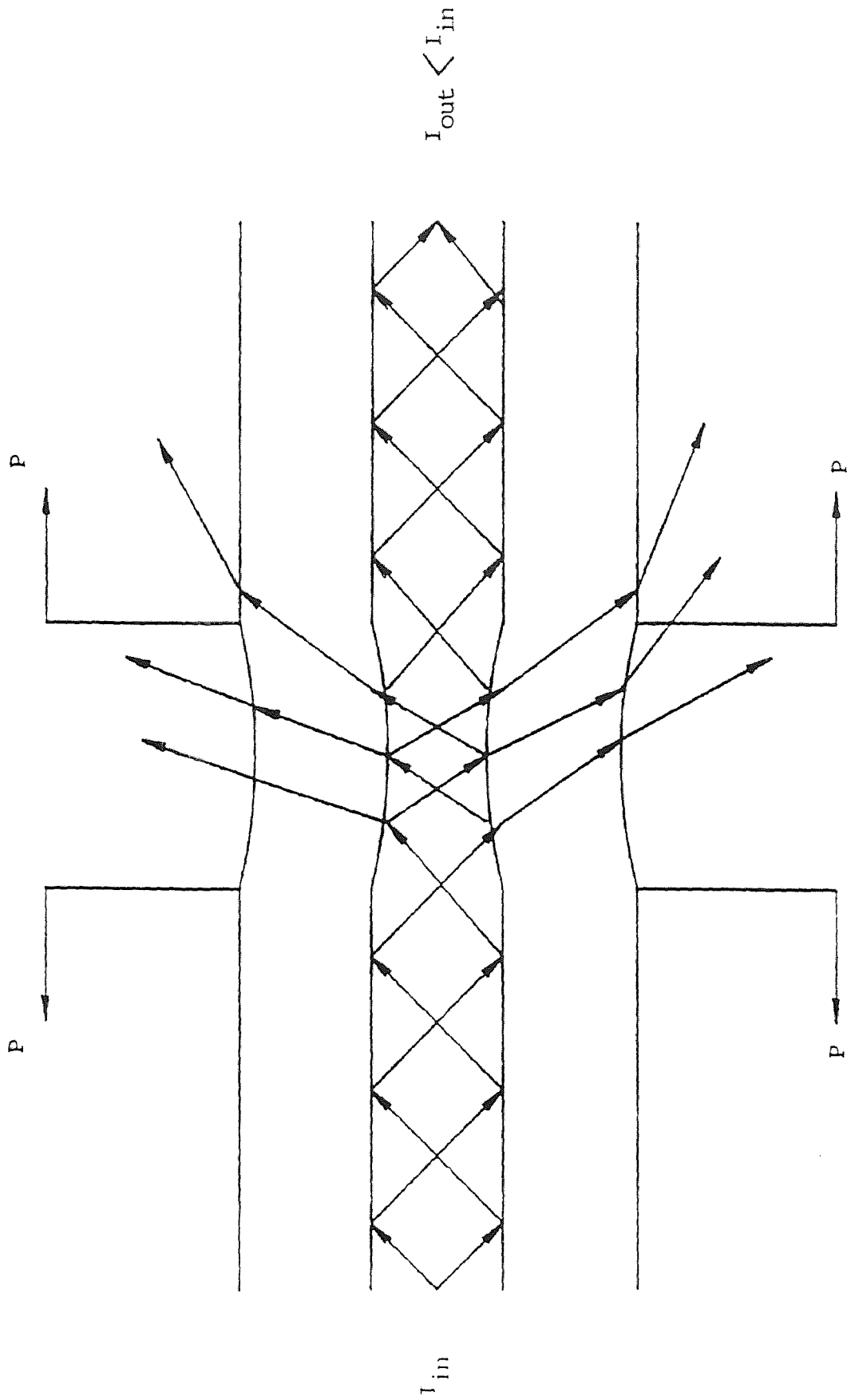


Fig. 2 Light loss in the optical fiber due to deformation.

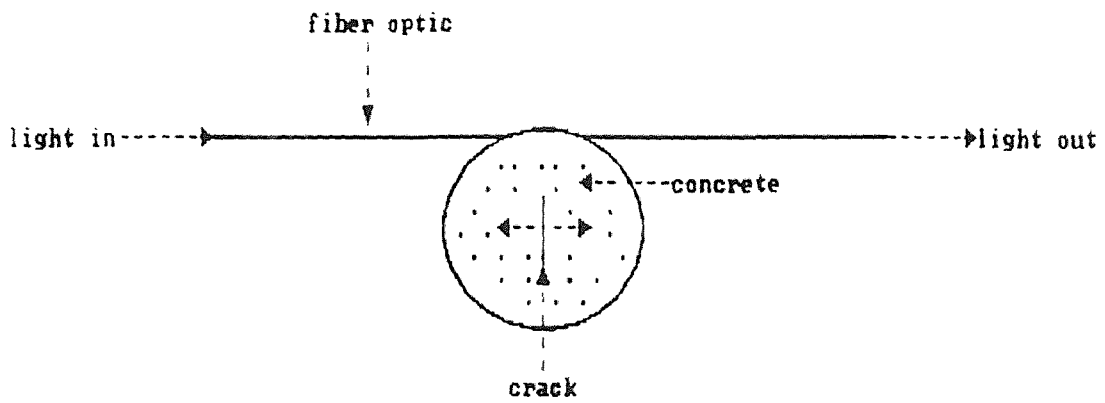


Fig.3 Plan View of Fiber Optic COD Gage

II.4 Instrumentation and Calibration

Progress of the microcracking zone was monitored by using four fiber optic COD sensors within the uncracked ligament for which details will be given in a later section. Experiments were performed in a closed loop mechanical testing machine so as to provide the capability of monitoring the descending branch of load-displacement relationship. Details in regard to various instrumentation techniques in performing the experiments , and acquiring pertinent data are given in the following subsections.

II.4.1 Sensor Intrumentation and Calibration

Instrumentation , specific to the operation of the fiber optic sensor are outlined in Fig.4. A 25 mW Helium-Neon laser source provide the input light source. At the coupler stage , light is divided into four equal divisions for use with four sensors. As explained earlier , in a particular sensor , the light output will decrease in proportion to the amount of displacement. This output is detected by a photodiode that in turn is amplified at the amplifier stage. At this point , data is converted to digital signals through a multichannel data acquisition board , and is transferred to a microcomputer.

Conversion of light intensity data (in Volts) to appropriate displacement values ,i.e. in milli-inch units ,

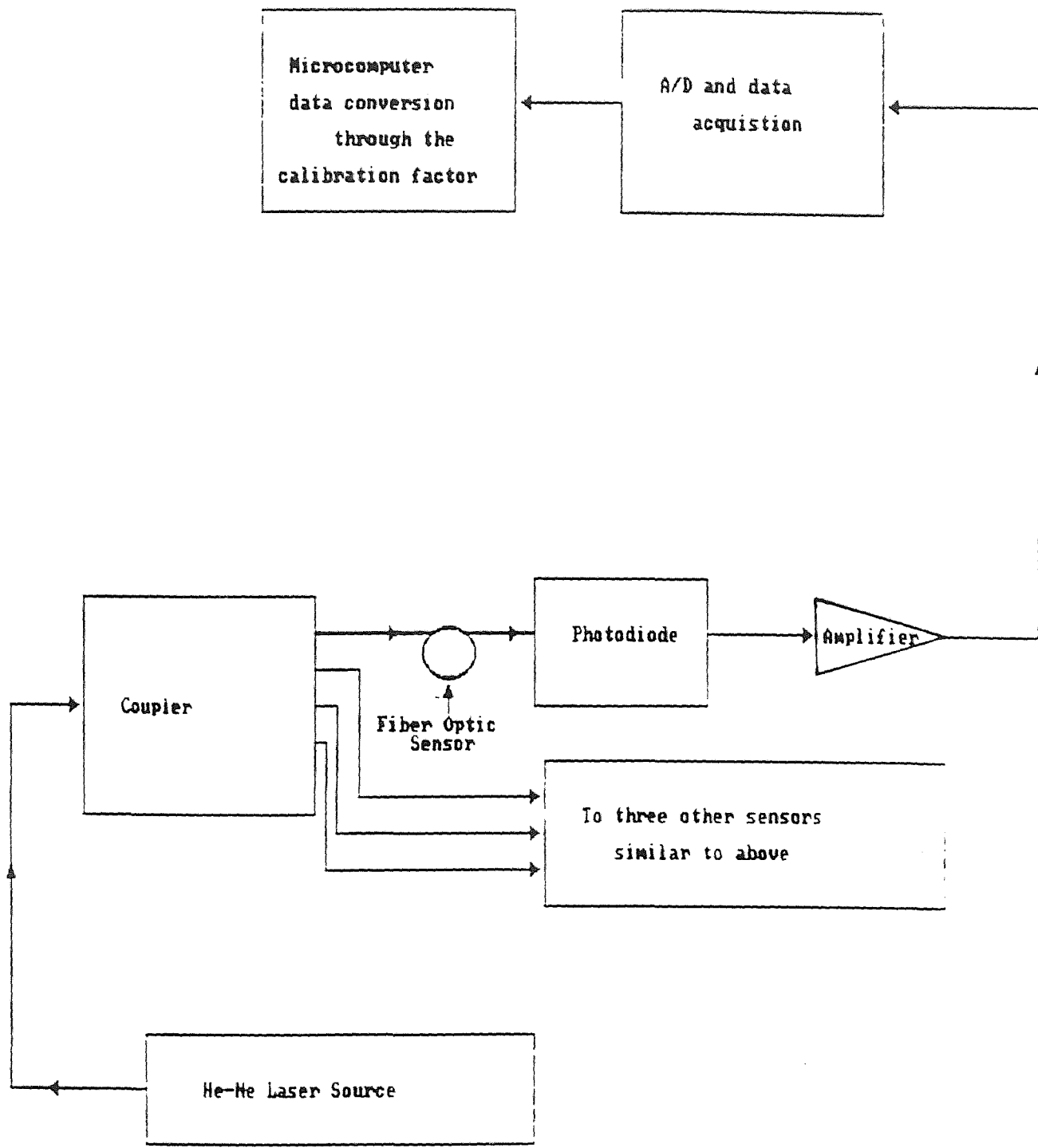


Fig.4 Block diagram of Fiber Optic Sensor operations

is accomplished through calibration. A calibration instrument is specifically designed for the fiber optic sensor (Fig.5). Calibration of the sensor is performed according to the following steps :

- 1) Fiber optic is wrapped around a disjoining cylinder whose diameter is 1.25 inchs (Fig.5). A groove is provided on the cylinder so as to facilitate fastening of the fiber optic into a perfect circle of 1.25 diameter. This is an important stage in the procedure , since variations in diameter result in inaccurate calibrations.
- 2) Stretch the fiber in a straight position by the motorized positioner. Hold it in position by an adhesive tape.
- 3) Use an epoxy to glue the fiber to the disjoining cylinder.
- 4) Once the epoxy is hardened (after 60 minutes) , apply another half inch of cement paste on top of the epoxy to insure perfect bonding.
- 5) Once cement is hardened (after 24 hours) , the fiber ends are connected to the laser source and the photodiode.
- 6) Amplifier's output is adjusted to six volts , and the output sensitivity is checked.
- 7) LVDT's core is adjusted to a halfway position.
- 8) Data acquisition rate is set at twenty Hertz for a period of ten seconds , and the computer is initialized.
- 9) At this point , the motorized positioner is turned on to separate the disjoining cylinder , and as a result , create loss in the intensity of input light due to

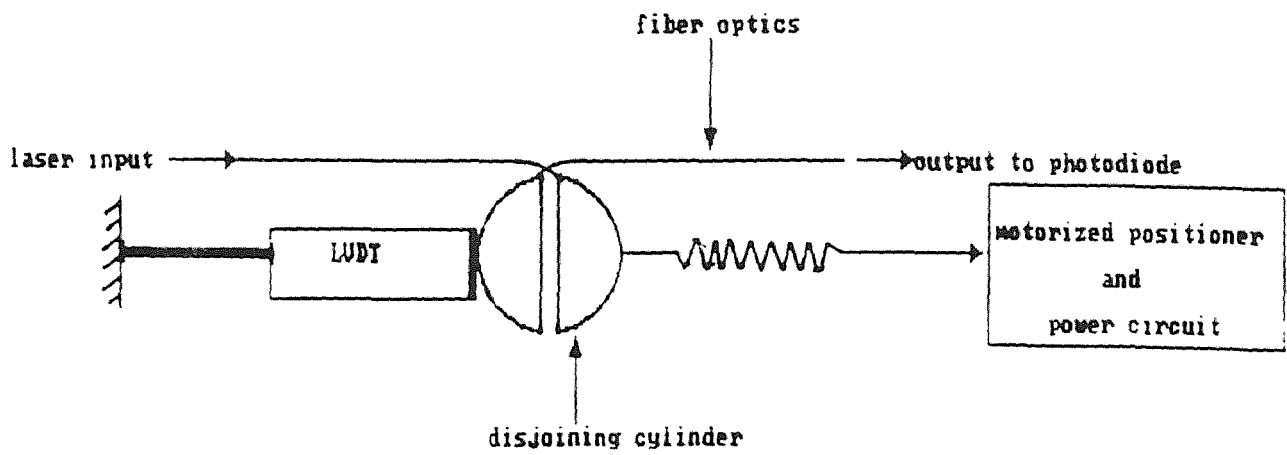


Fig.5 Plan View of The Calibration Instrument

separation of the cylinder halves.

10) By design , the LVDT core and the two halves of the cylinder displace identically , and therefore the light intensity loss measurements can be directly related to the opening of the cylinder halves.

Calibration results obtained in this way are automatically stored in the microcomputer via the data acquisition system. each of the four sensors were calibrated individually , and results are shown in Fig.6 thru Fig.21. A calibration constant relating the loss in the intensity of light to the displacement for each of the sensors can be obtained from the slope of Figs.8 , 12 , 16 , and 20. The calibration constants calculated in this way are : 34.4575volts/in. , 50.6821volts/in. , 75.43volts/in. , and 67.245volts/in. for channel 1 thru 4 respectively.

II.4.2 Closed Loop testing and Data acquisition

It is essential to study the prepeak response as well as post peak softening behavior of concrete. Therefore , specimen were tested in a screw-driven microcomputer-based closed loop testing system. An Apple II microcomputer was employed in generating testing program signals (Fig.22). The system is capable of controlling the movement of optical components as well as providing closed-loop feedback control for loading of specimen so as to maintain a constant rate of increase in the deformation of specimens. details regarding

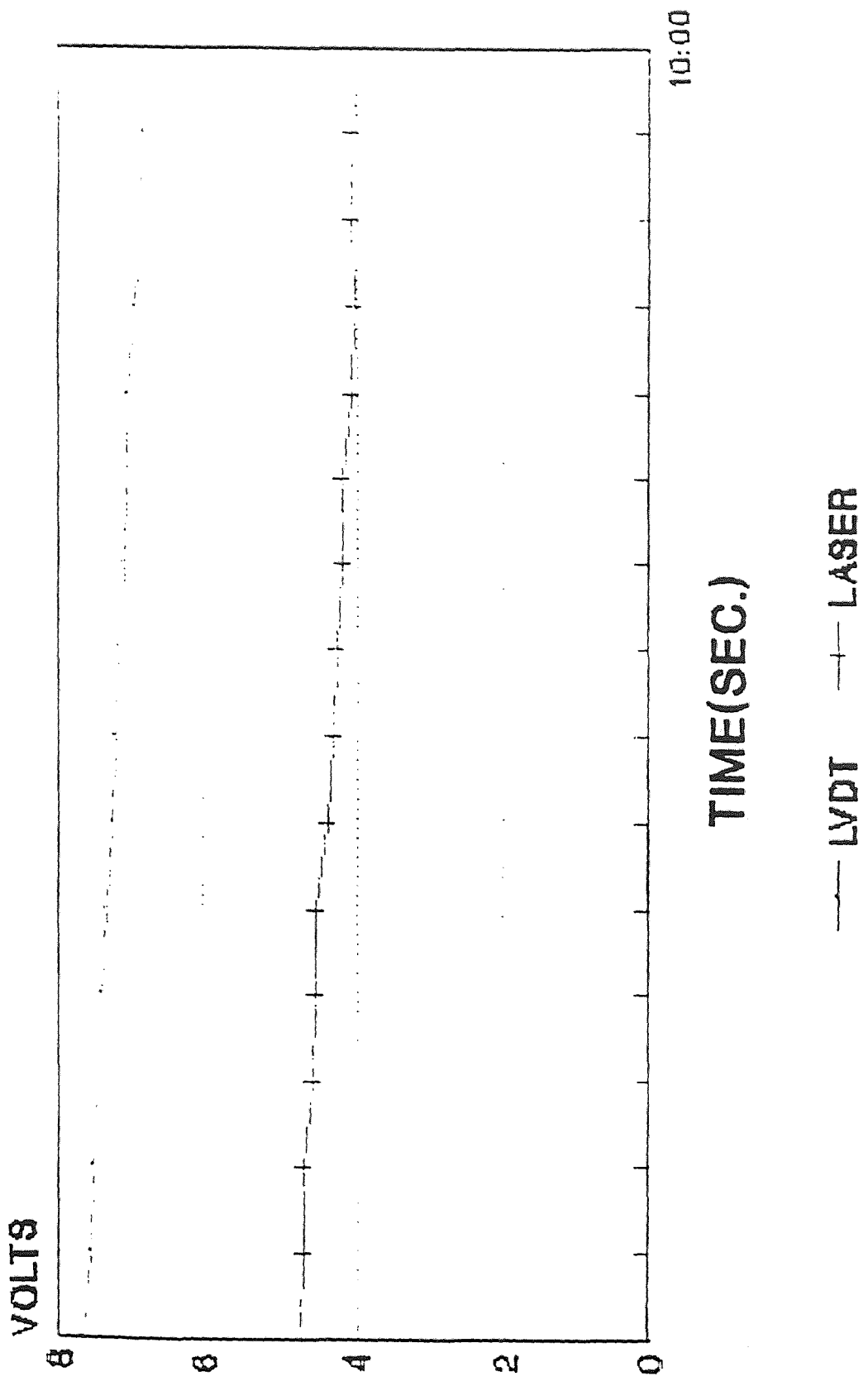


Fig.6 Calibration data for channel#1

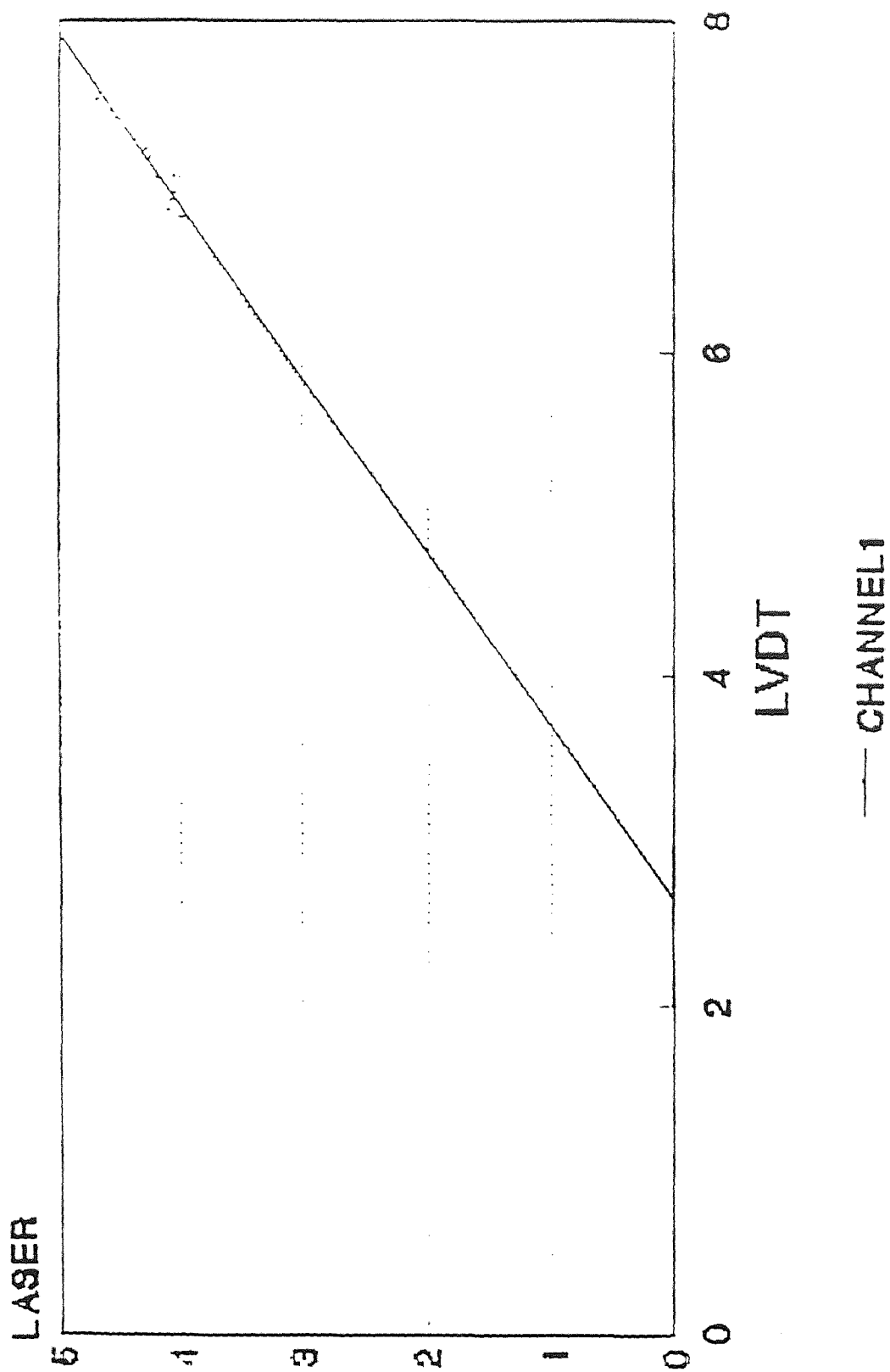


Fig.7 Light Inten. loss vs. LYDT for CH1

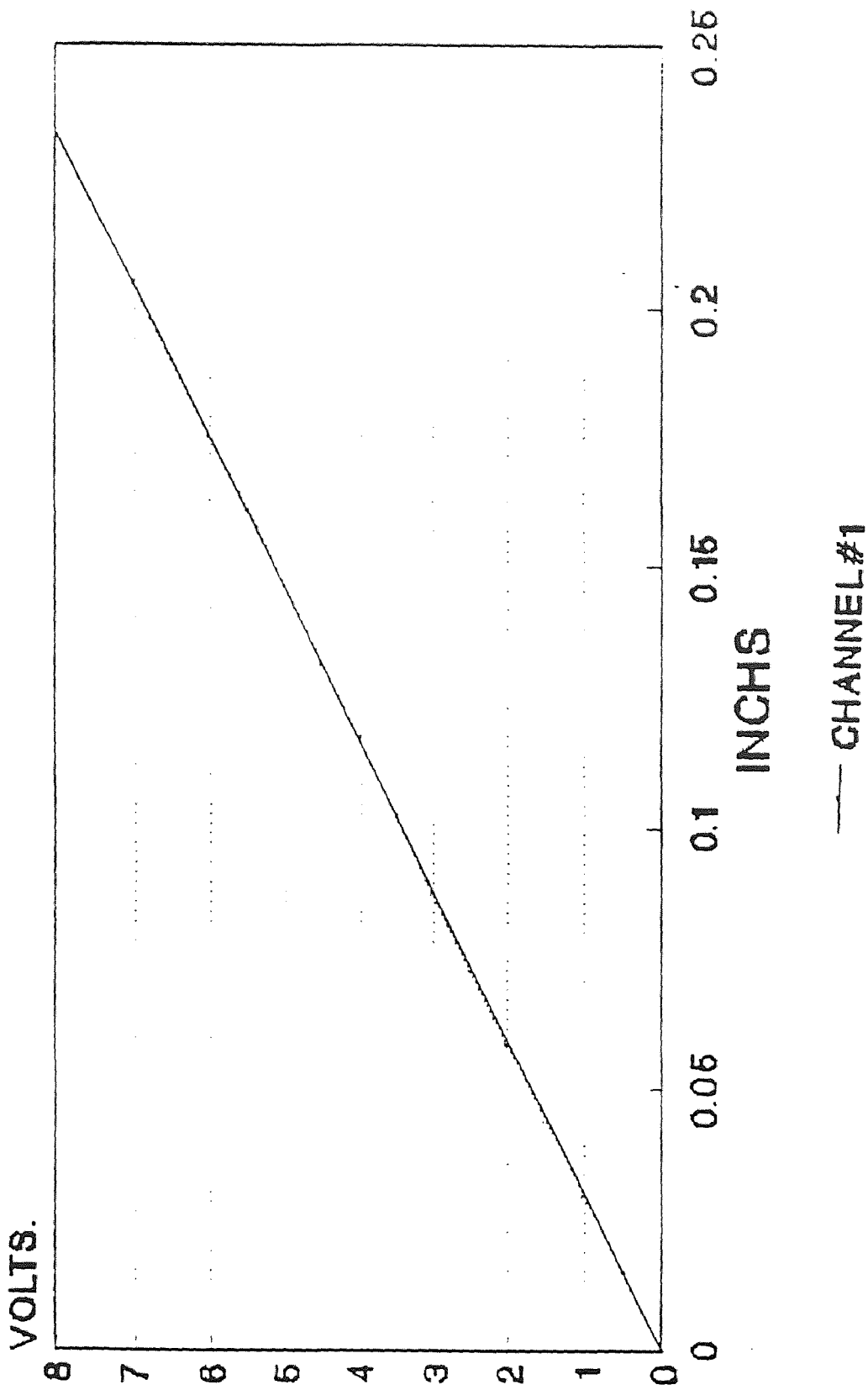


Fig.8 Light Inten. loss vs. dia. for CH1

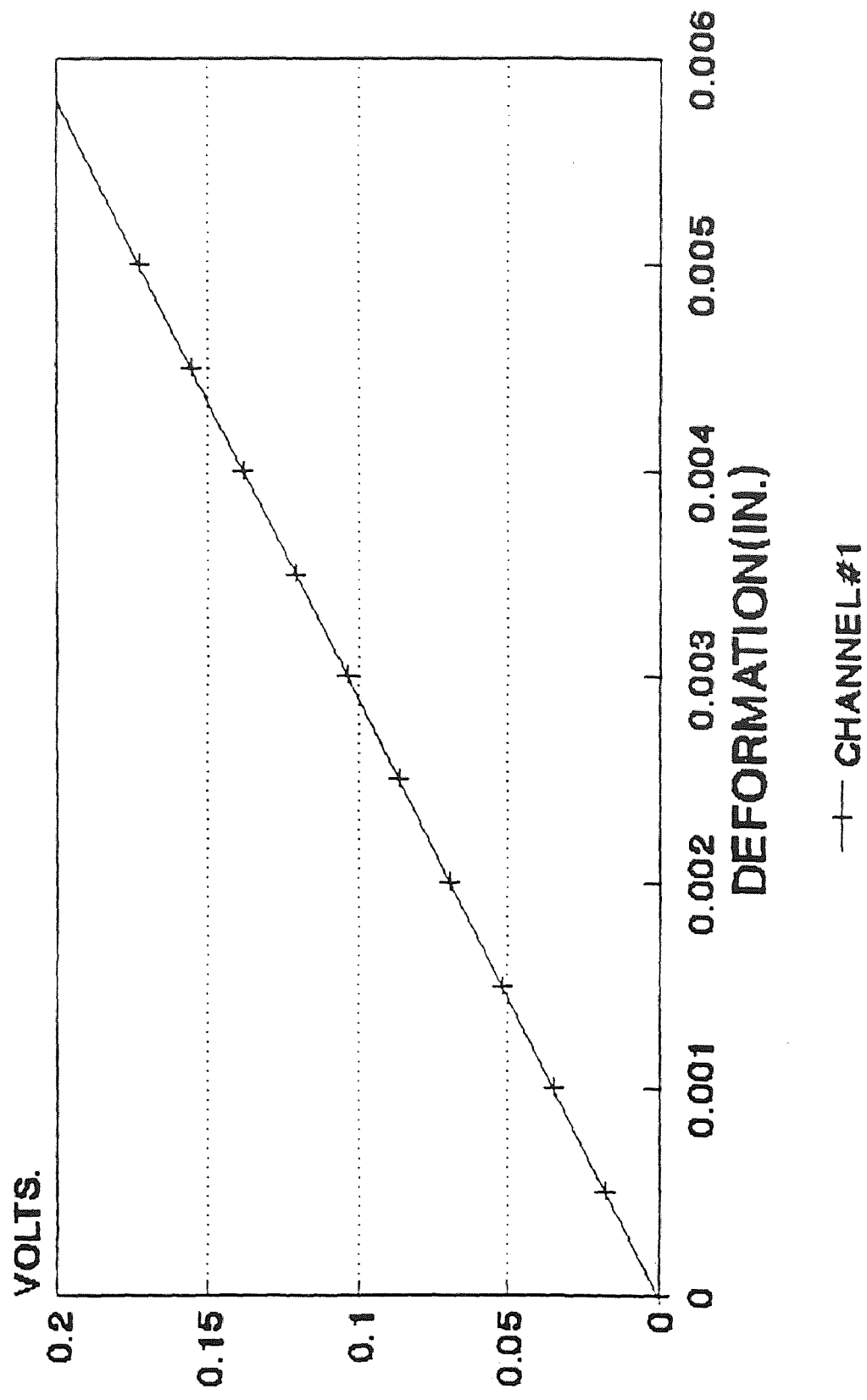


Fig.9 Lower range call. curve for CH.1

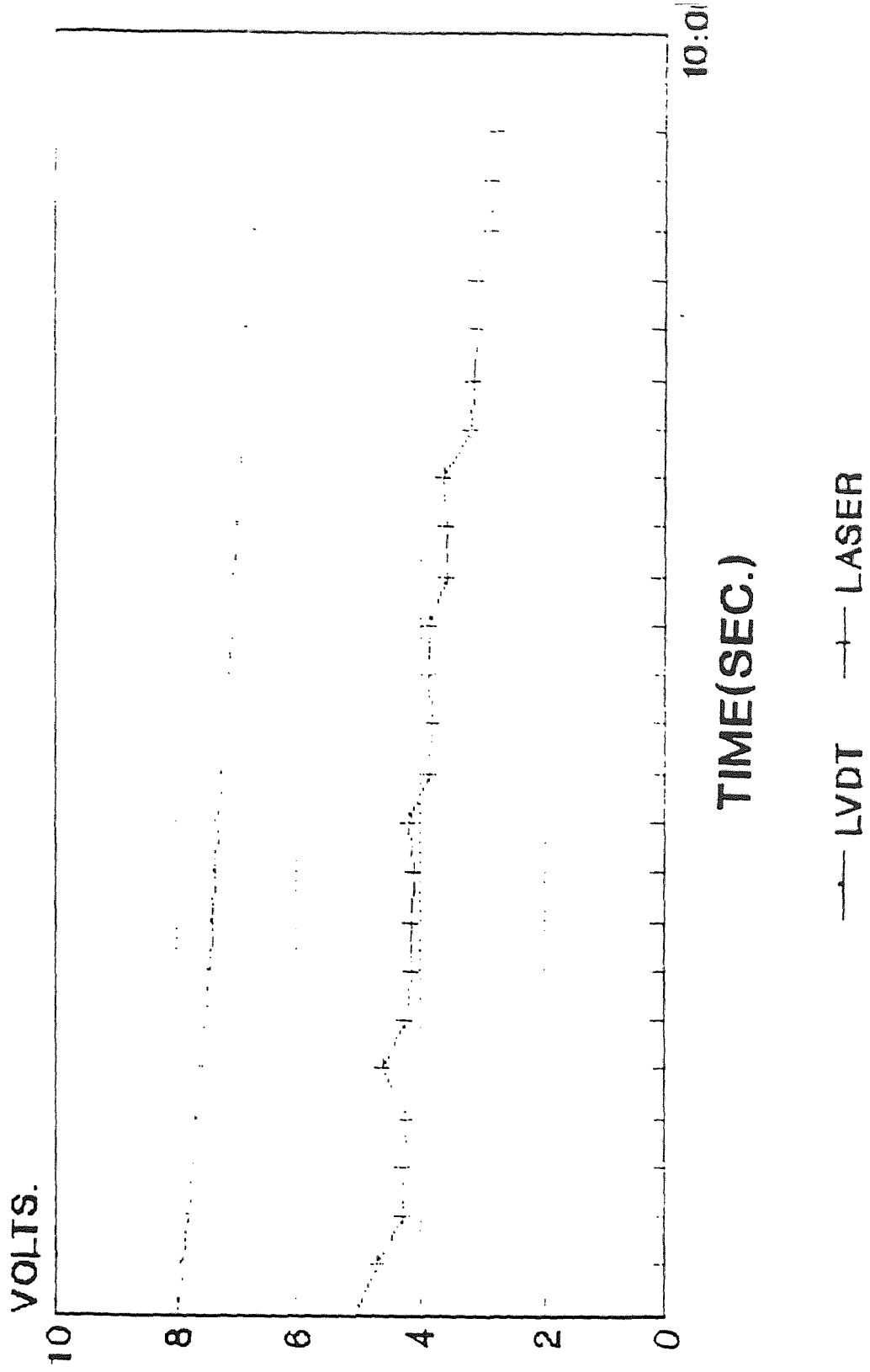


Fig.10 Calibration data for channel#2

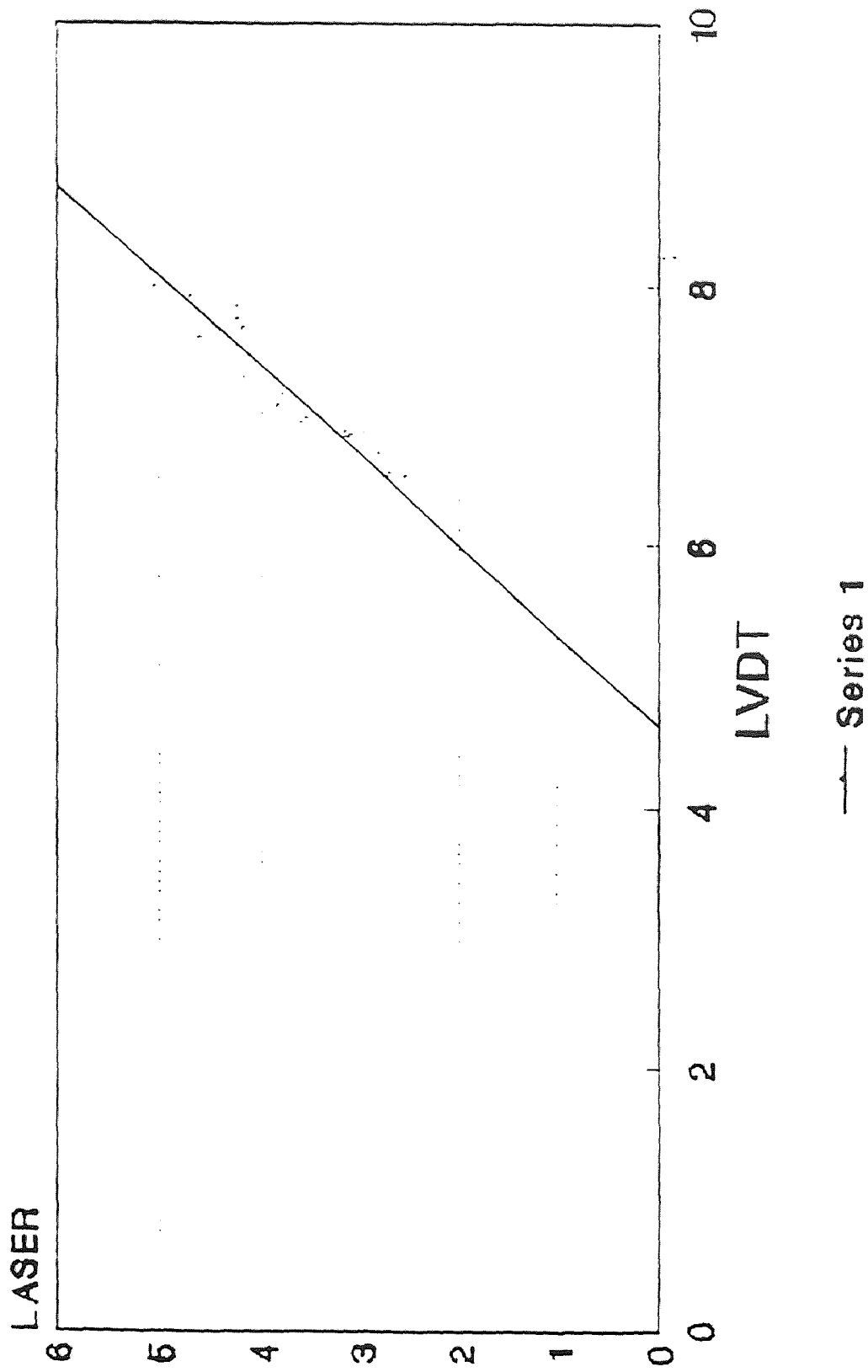


Fig.11 Light Inten. loss vs. LVDT forCH2

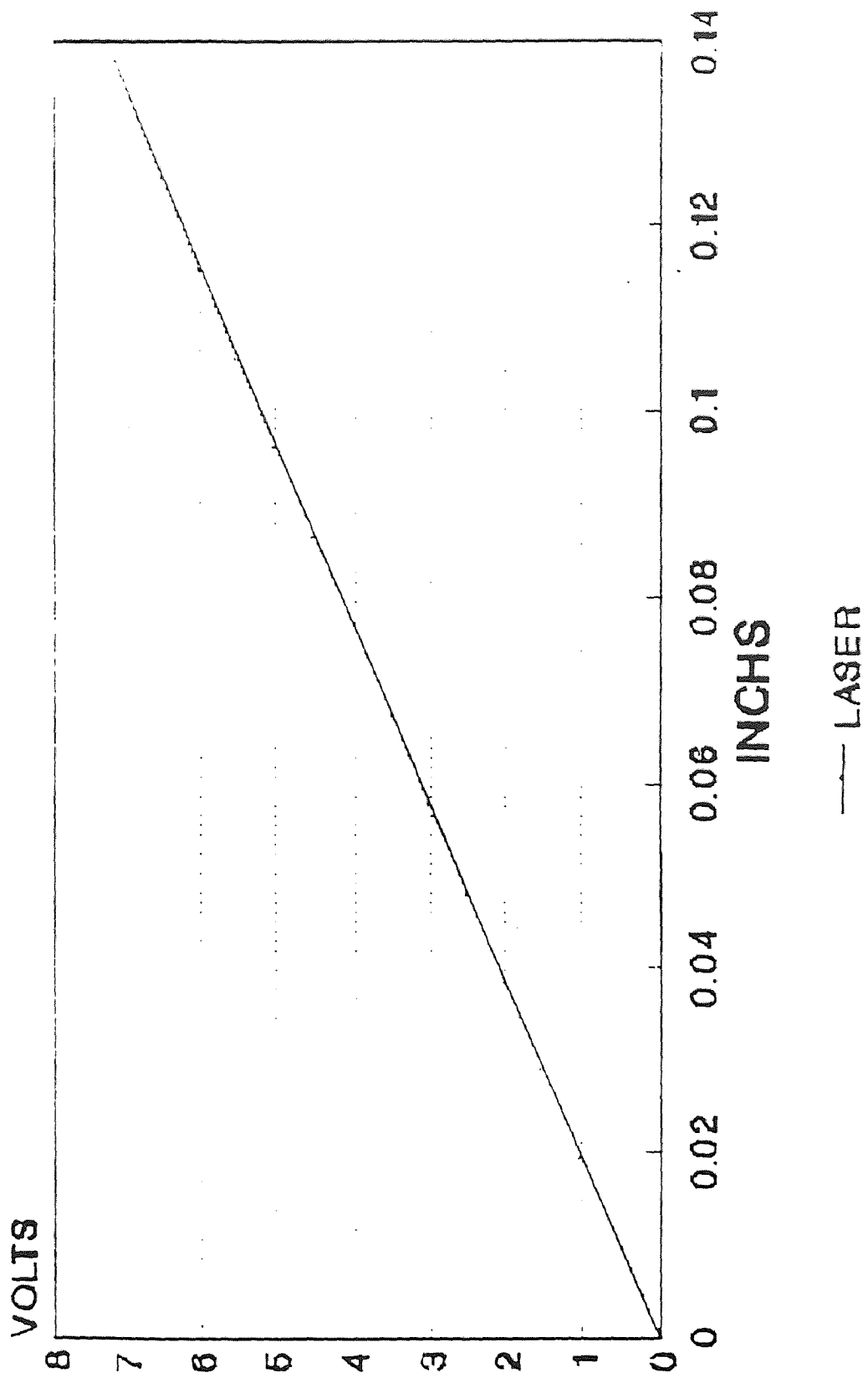


Fig.12 Light Inten. loss vs. dis. forCH2

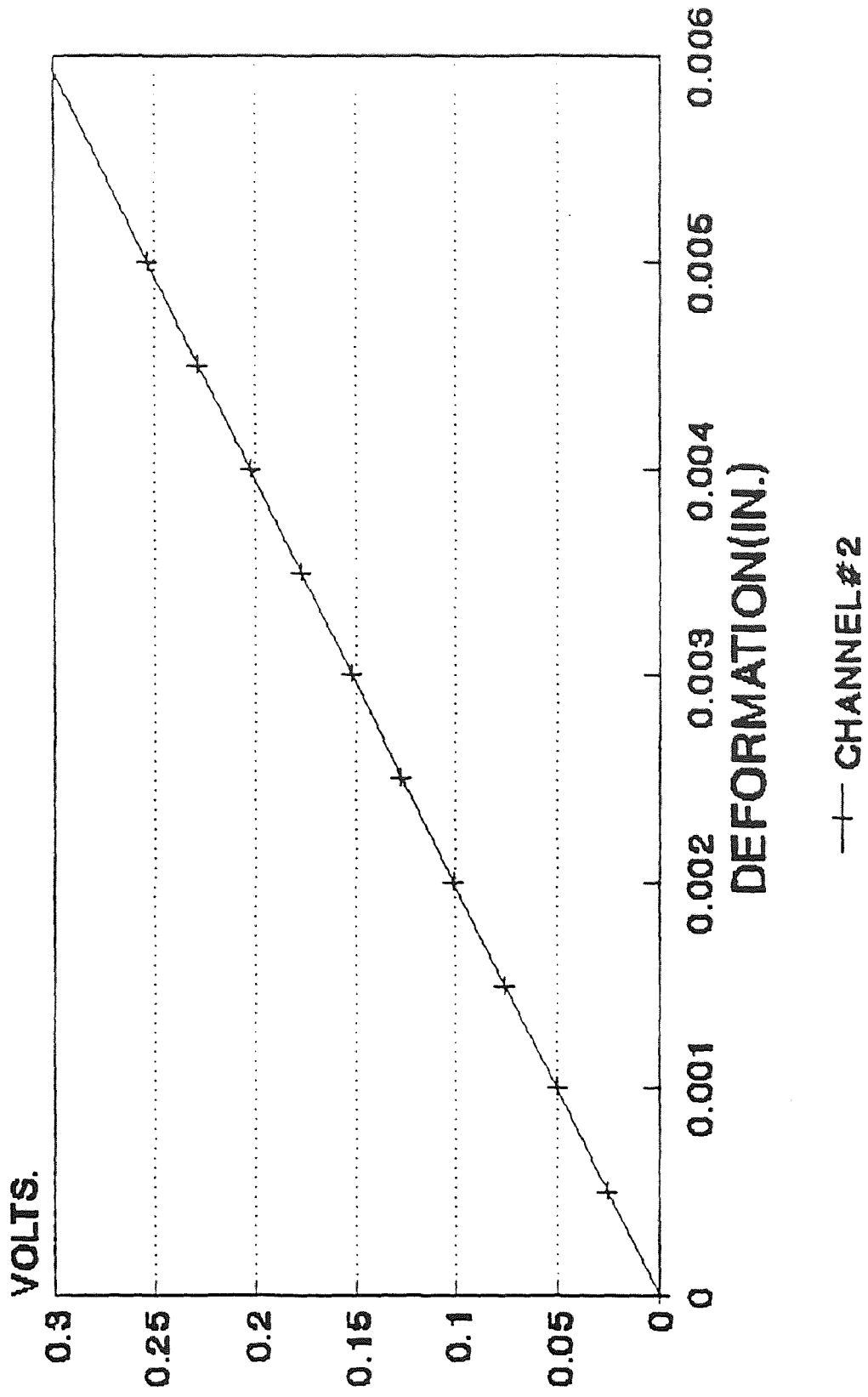


Fig.13 Lower range cal. curve for CH.2

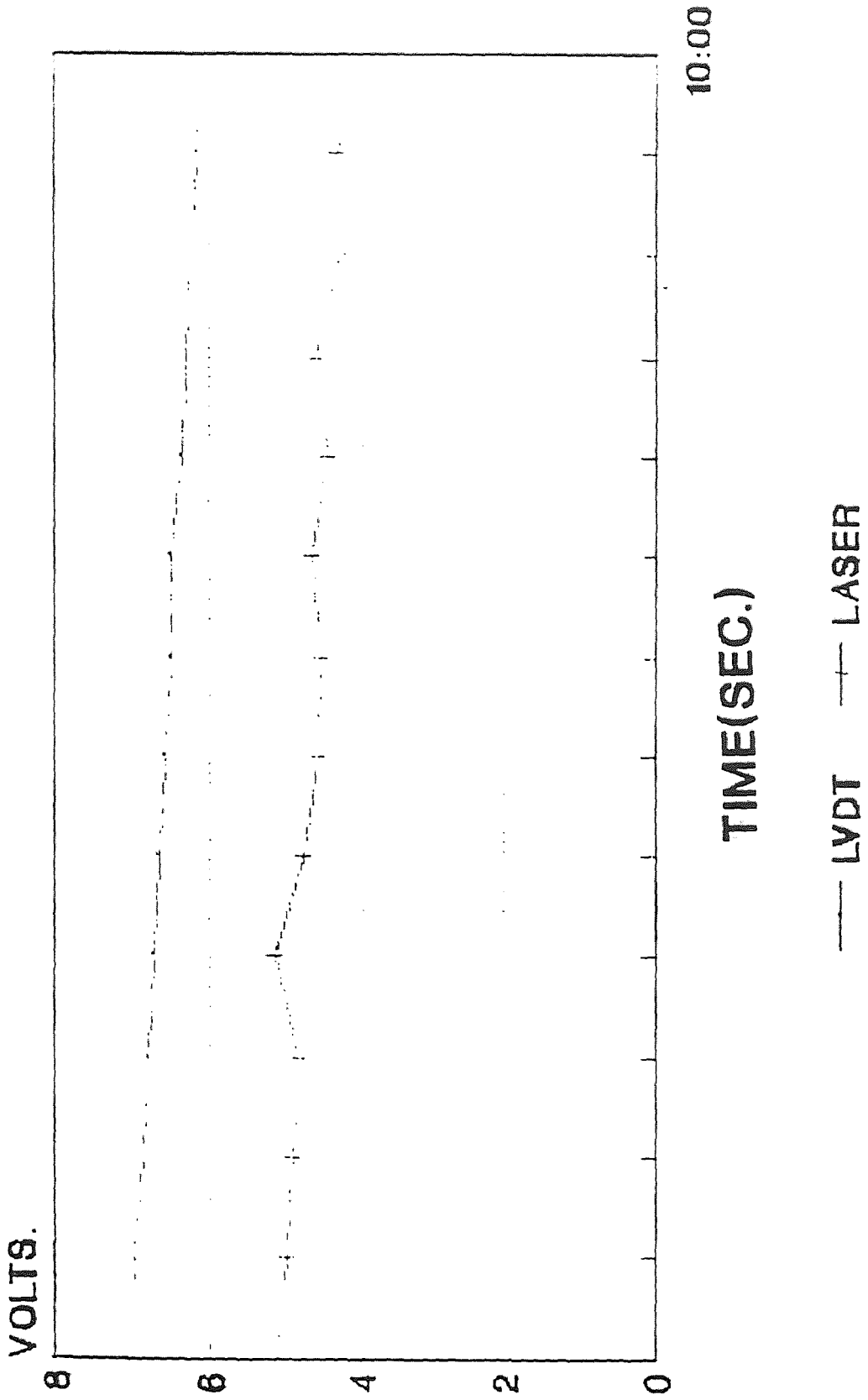


Fig.14 Calibration data for channel#3

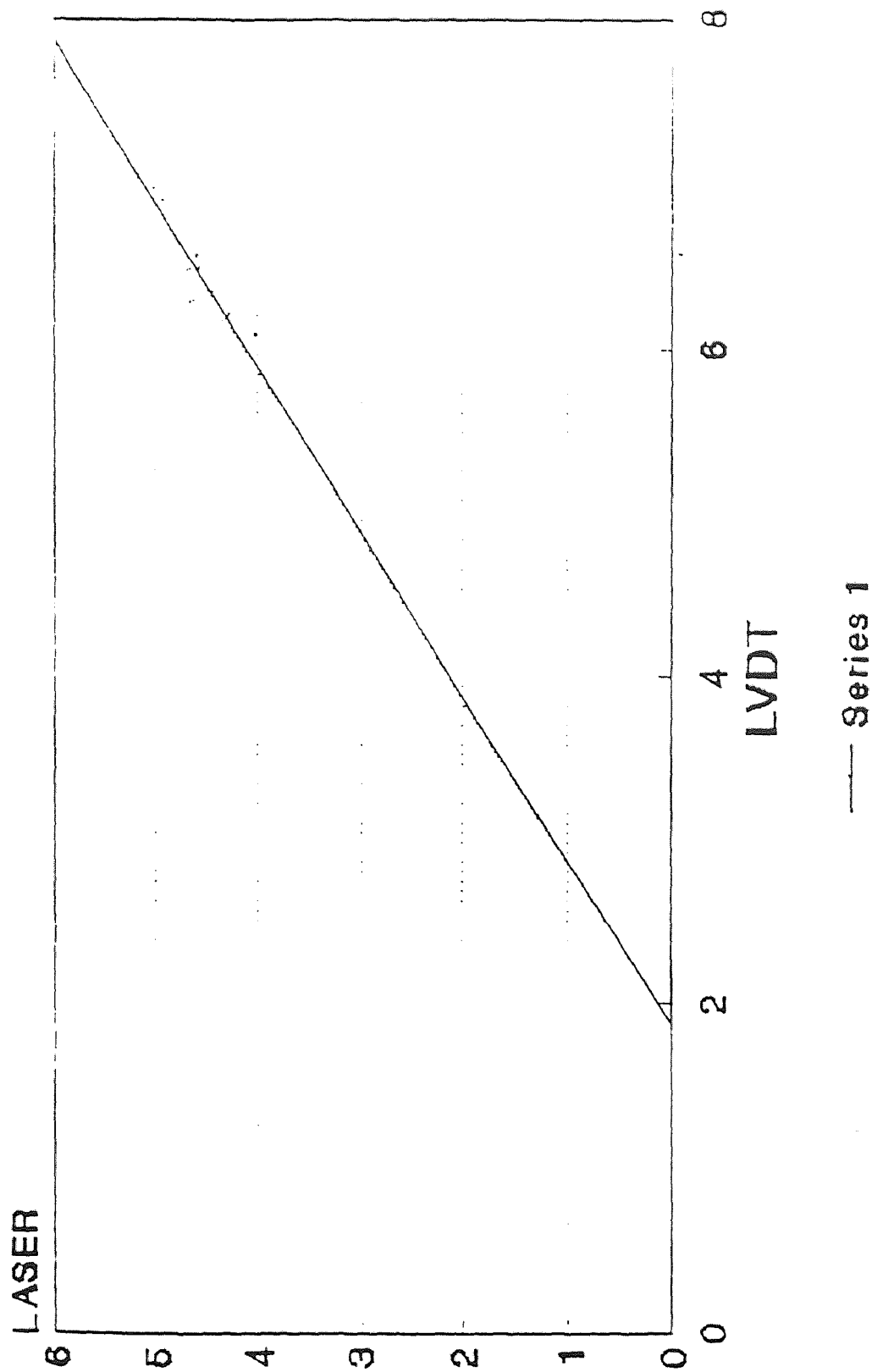


Fig.16 Light Inten. loss vs. LVDT forCH3

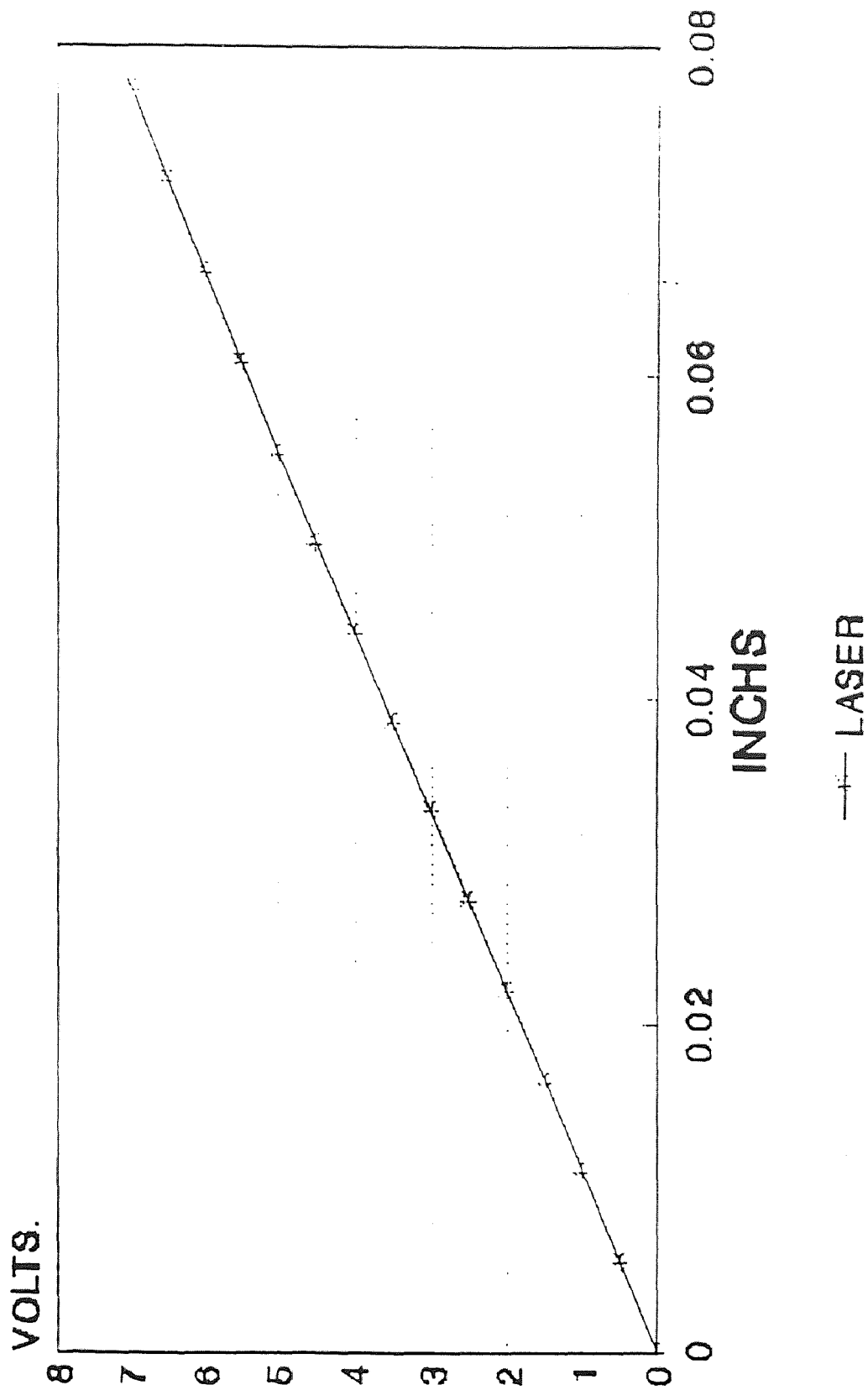


Fig.16 Light Inten. loss vs. dis. forCH3

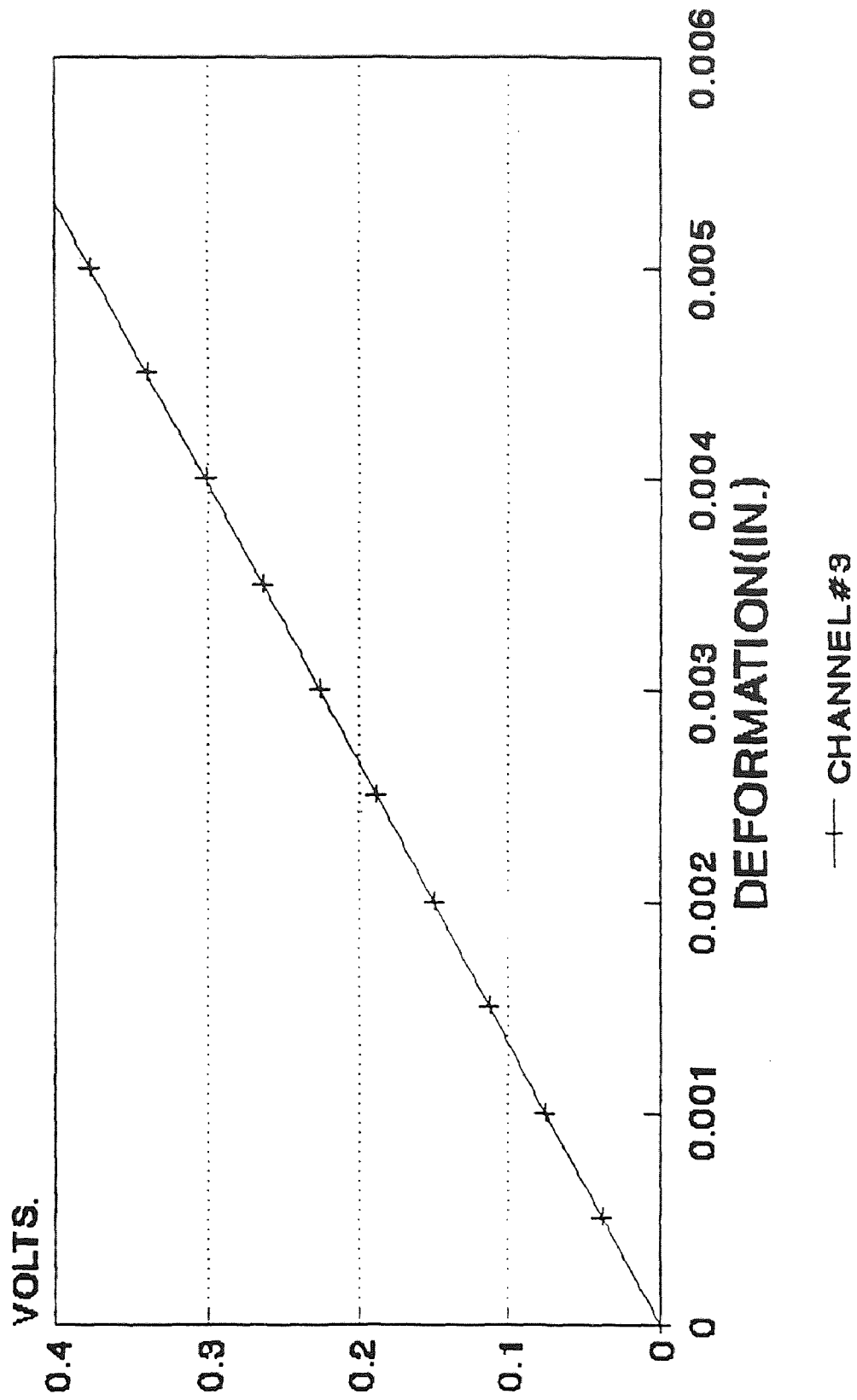


Fig.17 Lower range call. curve for CH.3

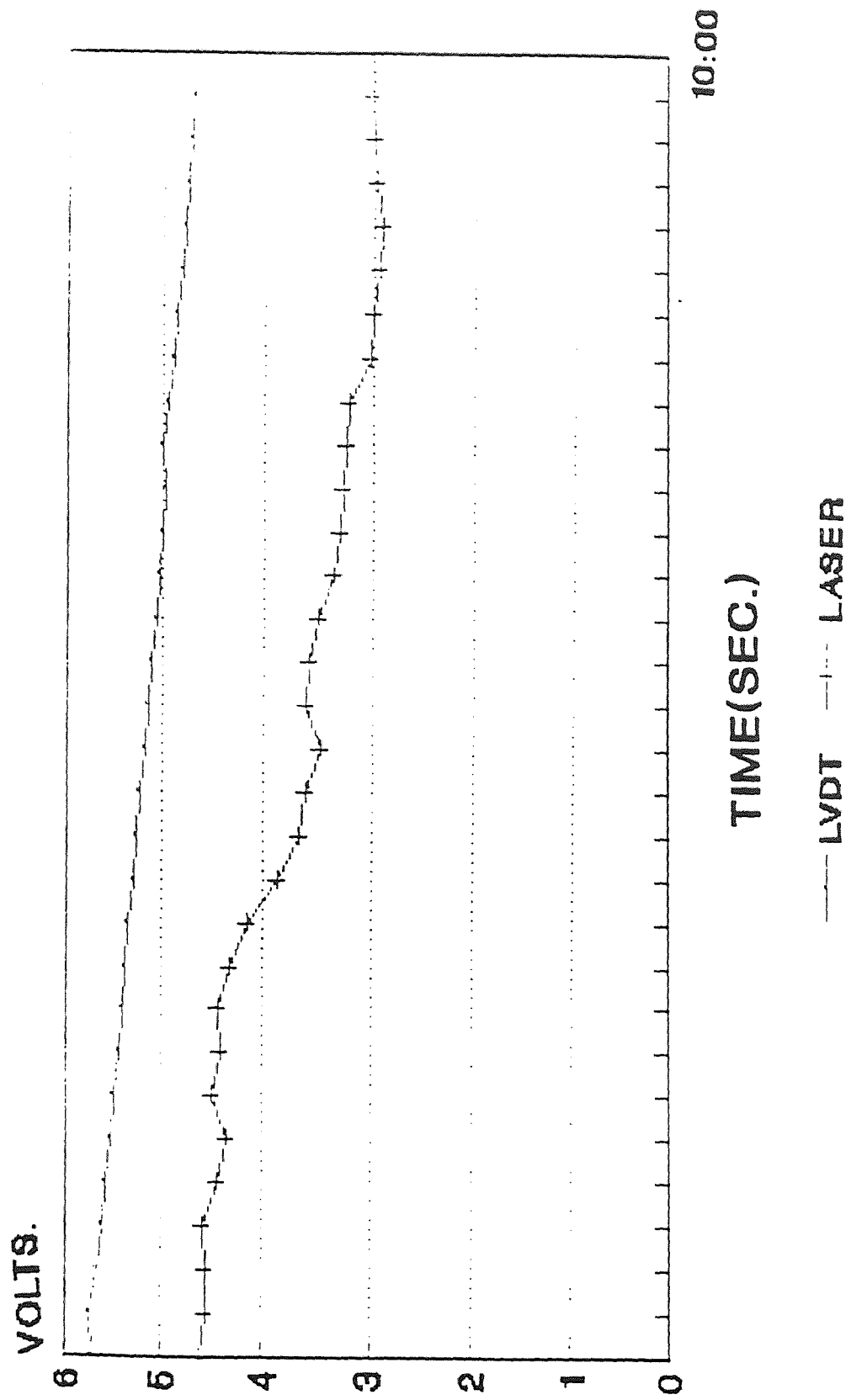


Fig.18 Calibration data for channel#4

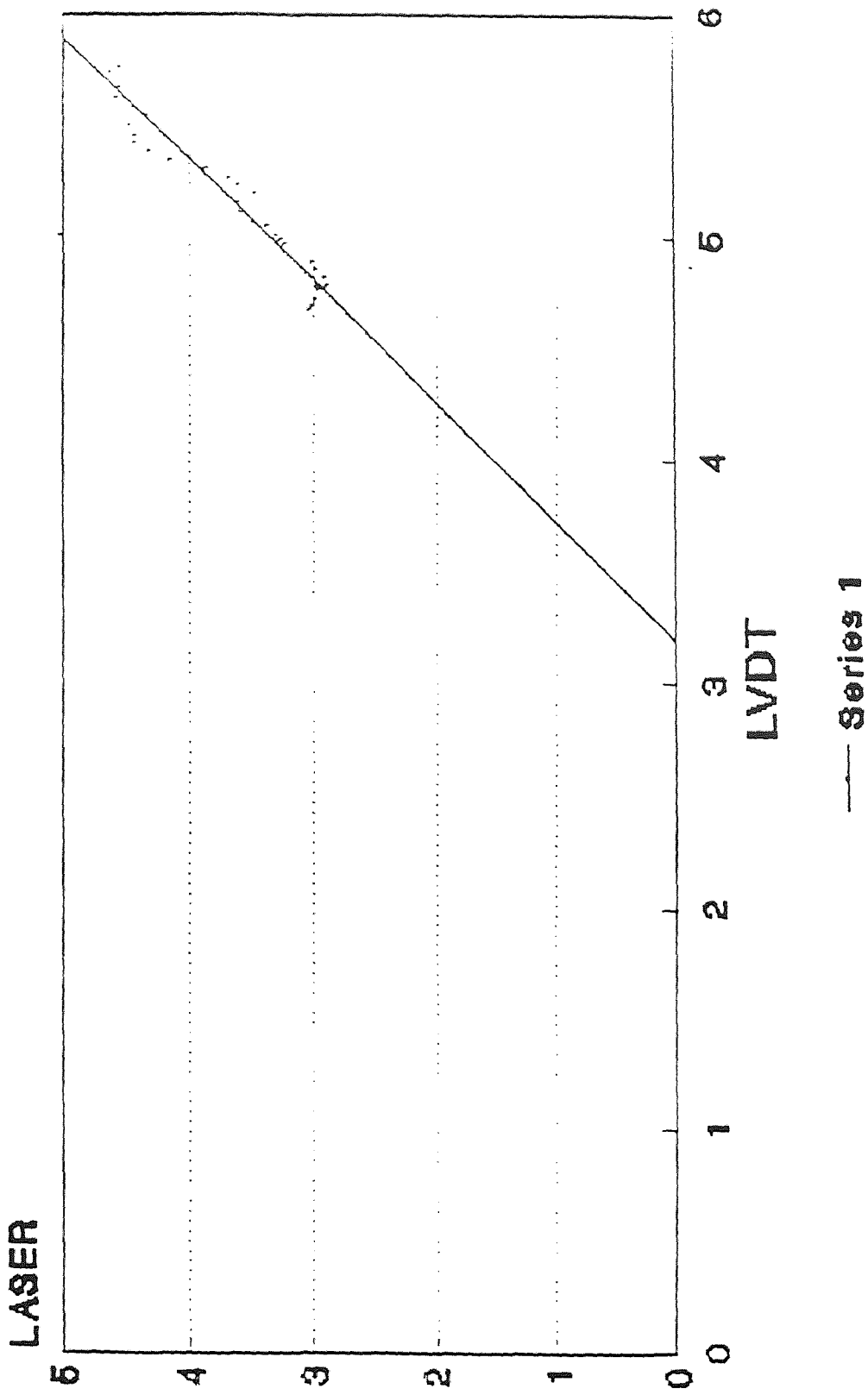


Fig.19 Light Inten. loss vs. LVDT forCH4

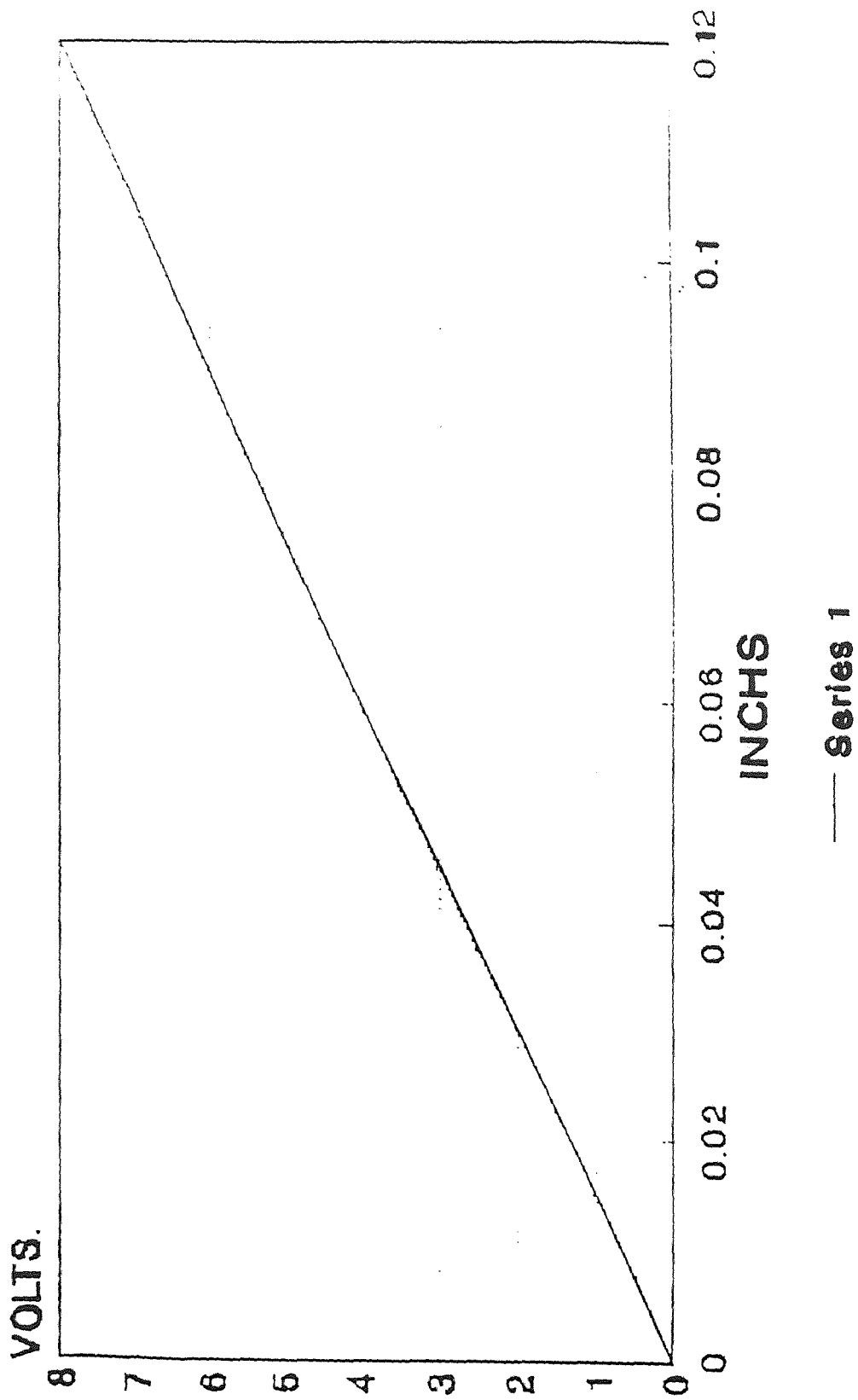


Fig.20 Light Inten. loss vs. dia. for CH4

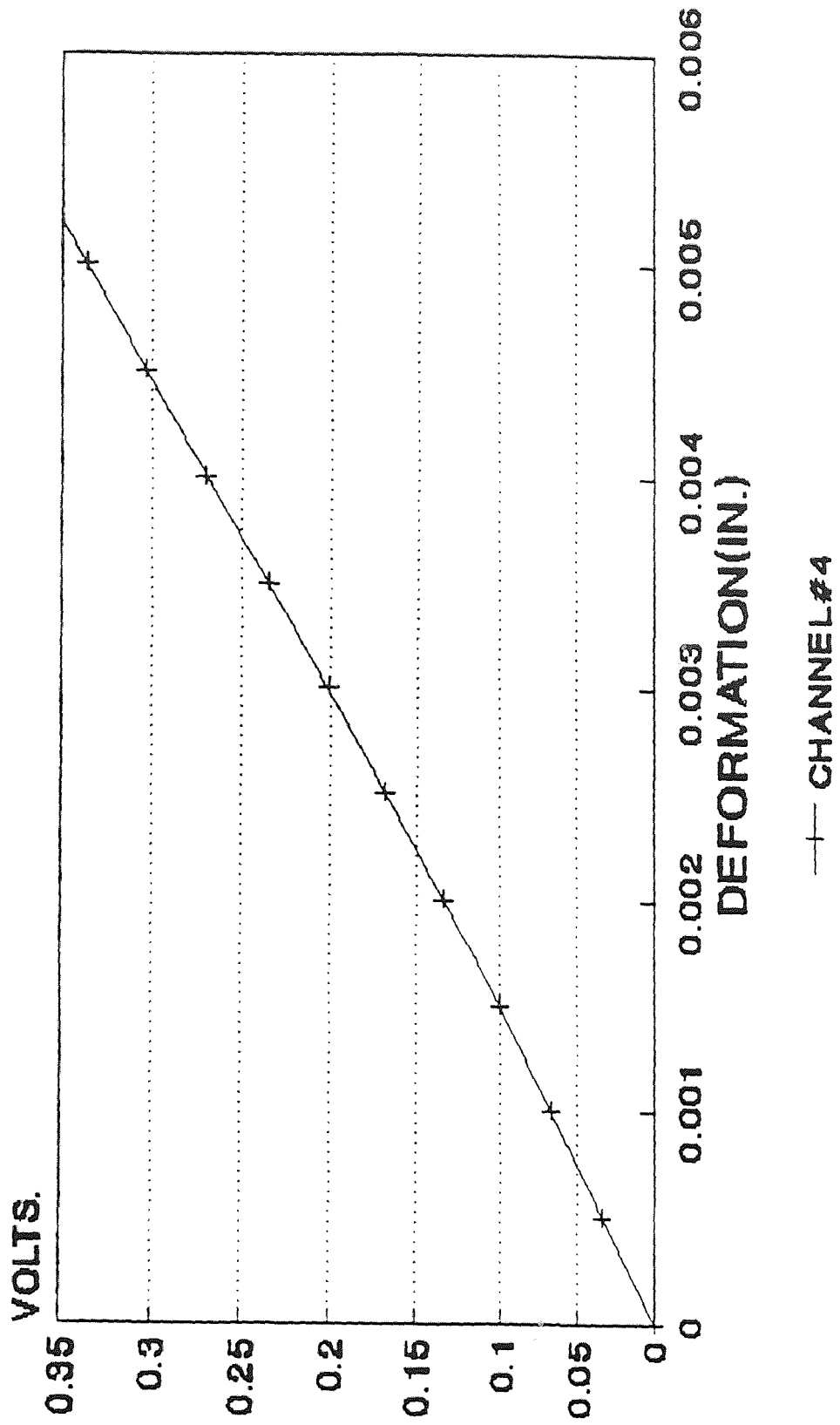
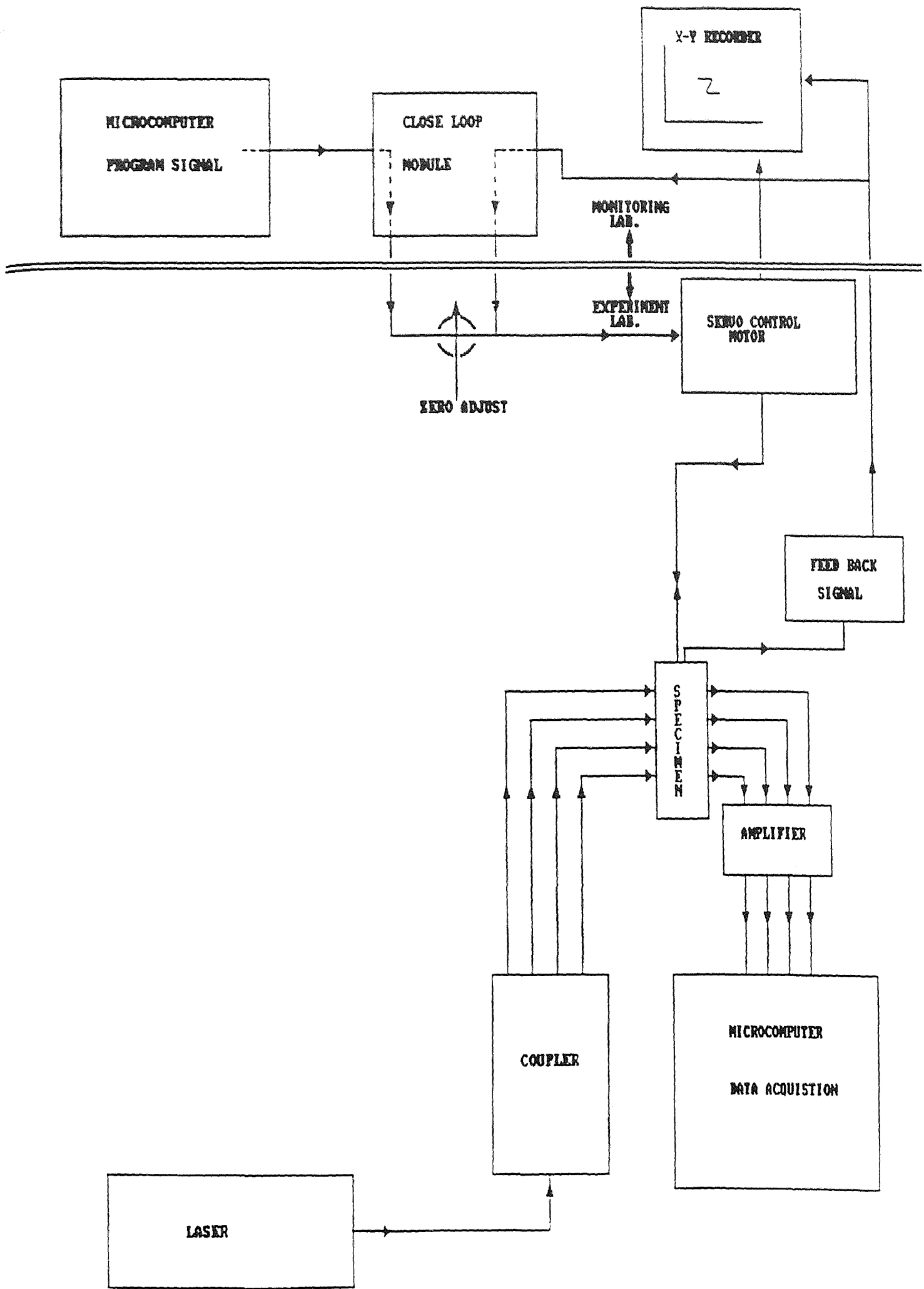


Fig.21 Lower range cell. curve for CH.4



the design and fabrication of the system are given elsewhere¹⁴. Feedback signal for loading was provided by an LVDT at the precast notch mouth. In other words , for both the three point bend and the compact tension specimen , COD was used as a feedback signal. A second LVDT was employed for measuring the Load Point Deformation. Calibration data for these LVDT's are given as :

LVDT for COD measurements : 1 inch = 33.87 volts.

LVDT for LPD measurements : 1 inch = 35.7 volts.

As mentioned earlier , four optical sensors were embedded in each specimen through equal division of laser light source by a coupler as shown in Fig.22. A data acquisition program , DASH-16 was modified by BASIC programming and employed for data handling from seven channels. Data acquisition channels included , load , two LVDT's , and four fiber optic sensors. Program modification was performed through a BASIC program , MENG.BAS , that will be given in detail in the Appendix. Sampling rate was set at 20 HZ , for 25 minutes. a total of 30,000 data points were acquired per specimen.

II.5 Details of test specimen

A mix proportion of 1:2:2:0.55 , by weight of cement : sand : gravel : water was employed. Type III portland cement conforming to ASTM c 150 , ASTM NO.2 grade river sand passing through sieve NO.8 , maximum coarse aggregate size

passing 0.375 inch (9.5mm) and retained on NO.4 sieve was used. Specimen were cast in plexiglass molds. Freshly cast specimens were left at room temperature for 24 hours. They were then demolded and air-dried before testing. Average age of specimen at testing time ranged between 21 to 30 days. Specimen geometry and location of sensors are shown in Fig.23.1 and 23.2. Fig.23.3 and Fig.23.4 depict the compact tension and the three point bend specimen with associated optical setup in the loading frame respectively.

II.6 Experimental procedure

Beams were tested under three point load and Compact Tension specimen were tested under direct tension in a testing frame on a vibration isolated table. Experiments were monitored from an adjacent room employing a microcomputer as discussed earlier. Following are steps taken during testing :

- 1, Load "MCCLSS" program into microcomputer(Apple II) , which is a program for closed-loop system.
- 2, Place the specimen into the load machine very carefully , and connect the laser to the corresponding channels , and then connect the other ends of the fiber sensor to the amplifier.
- 3, Turn on the microcomputer (IBM) for data acquisition. Load "LABTECH" , data acquisition software for checking

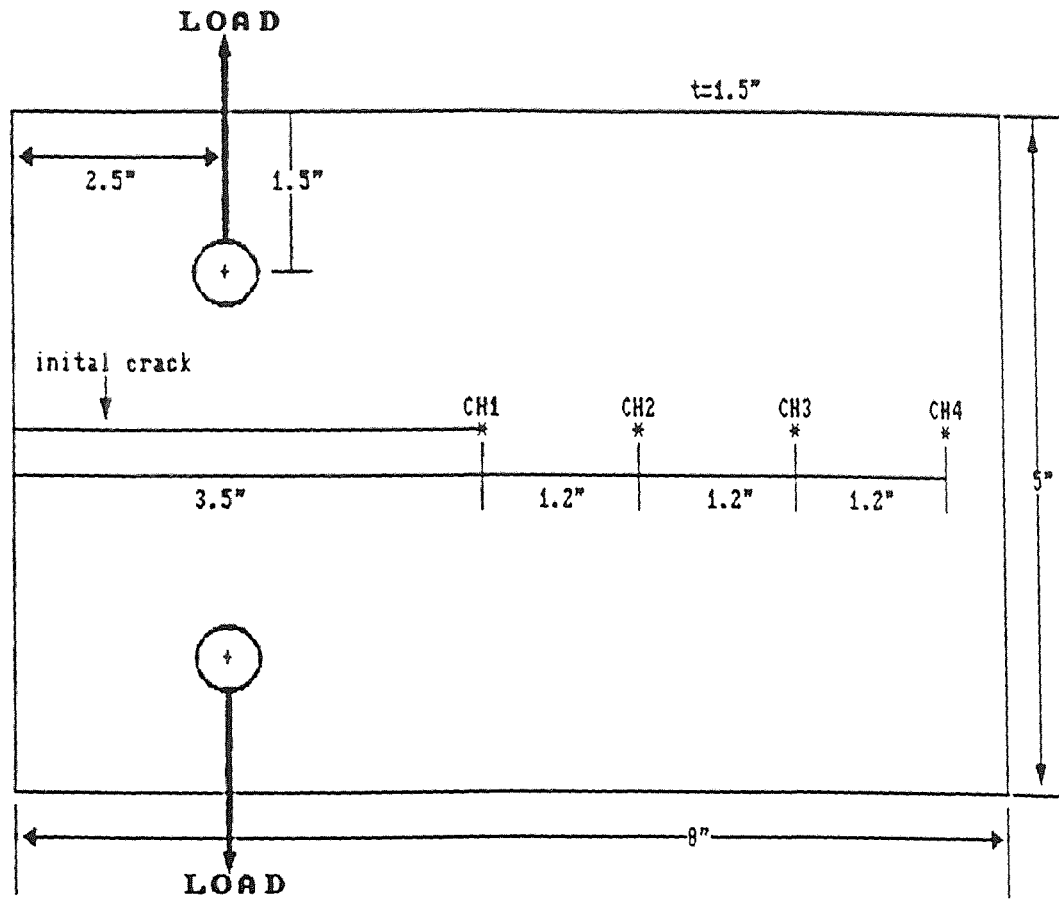


Fig.23.1 Compact tension specimen and location of sensors

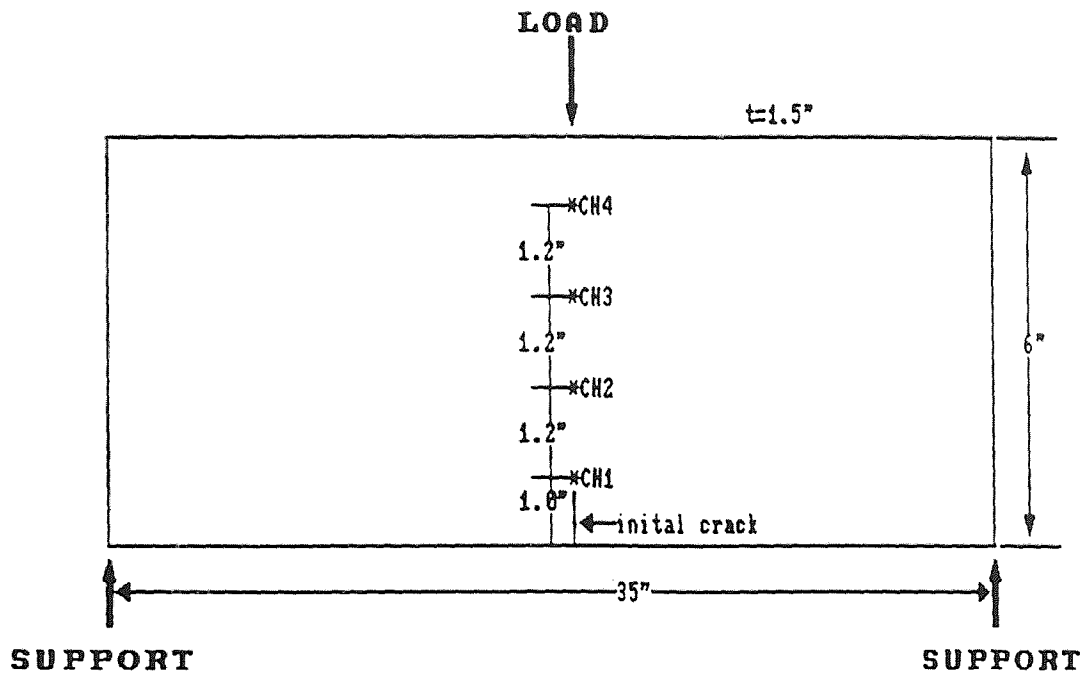


Fig.23.2 Three point bend specimen and location of sensors

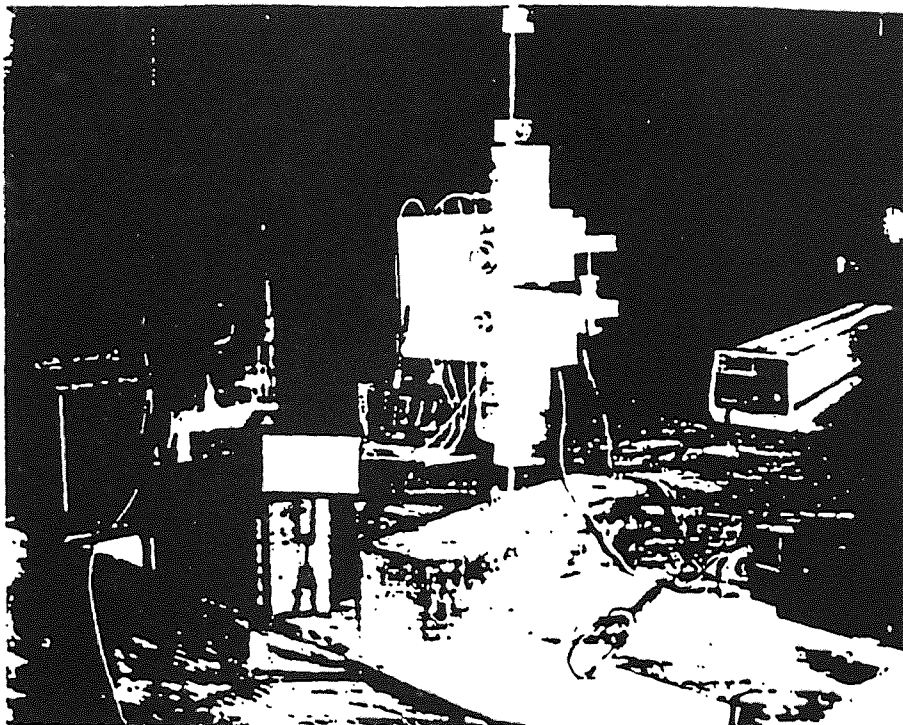
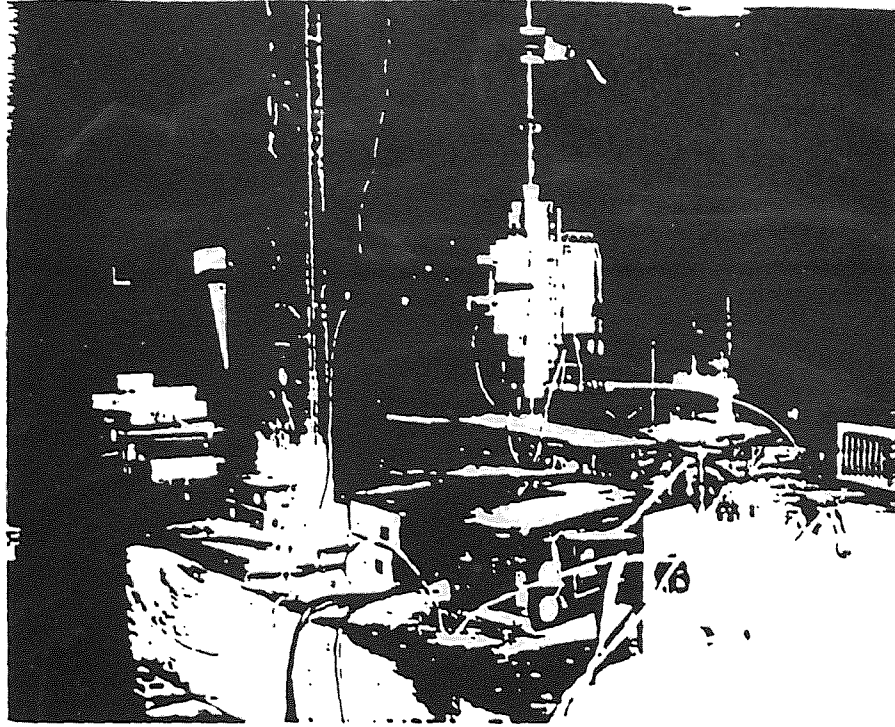


Fig.23.3 Compact tension specimen in the
loading fram

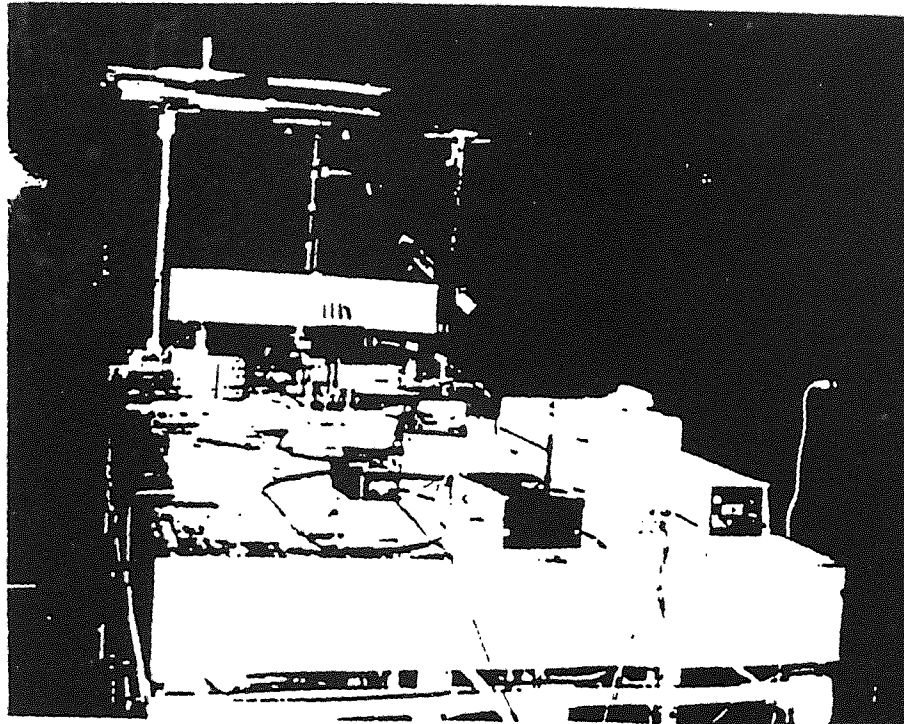
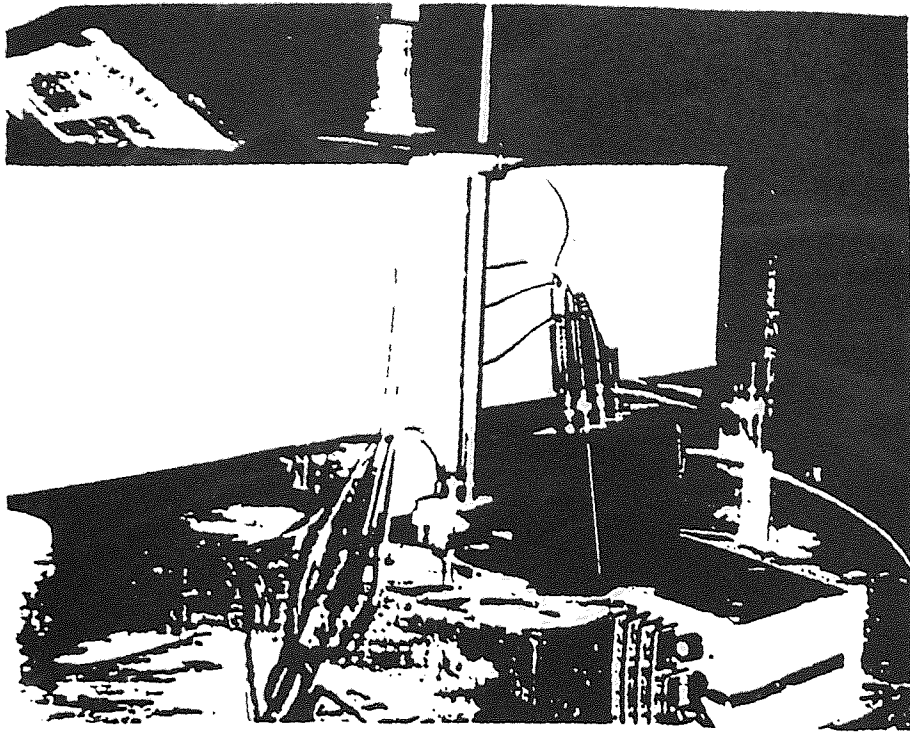


Fig.23.4 Three point bend specimen in the loading frame and the optical setup

proper operation of all the channels.

- 4, Load "DASH-16" and "MENG.BAS" into micro-computer for data acquisition .
- 5, Following steps are required for zero adjustment of the closed-loop testing system :
 - (a), Loosen the drive belt in order not to damage the specimen.
 - (b), Adjust the LVDT at the crack mouth for zero adjustment.
 - (c), Adjust the load controlling switch so as to get the exact zero point on the specimen.
- 6, Use "MCCLSS" to set all the required parameters into the program in order to operate the testing system.(While doing compact tension specimen use an exposure time of 0.09 min. , for BEAM tests use 0.2 min..)
- 7, Run "MENG.BAS" in the IBM microcomputer for data acquisition.
- 8, After the test turn off all system.

CHAPTER III Analysis and Results

This chapter presents experimental results , their analysis and a discussion of observed trend. As shown in Table 1, sixteen concrete specimens were tested. Seven specimens were tested under tension and the rest were tested under three point load.

Experimental data acquired by the computer , representing load , load point displacement , COD , and the four sensor outputs are given in direct data acquisition voltage units in Figs.24 thru 87.

These figures represent raw experimental data. Program CHAN.FOR , DEF.FOR , and TOT.FOR that are explained in detailed in the Appendix and the HARVARD GRAPHICS software were employed to convert the raw data into corresponding load , COD , LVDT , and deformation values.

Load versus corresponding COD , LPD , and internal deformations are shown in Figs.88 thru 99.

Experimental results indicated that specimen F2 , F8 , F11 , F12 , F19D , F28A , M1A , and M1B showed consistent results , whereas , the rest of the specimen did not provide good results. These bad results were due to either deficiencies in the specimen such as damages due to precast notch , or fracture of the compact tension arms prior to the completion of tests. Experimental data indicates that in

Table I Specimen types and designations

CONCRETE SPECIMEN		
NUMBER	NAME	TYPE
1	J31	CT
2	F2	CT
3	F3#2	CT
4	F8	CT
5	F10	CT
6	F11	CT
7	F12	CT
8	F19A	BEAM
9	F19B	BEAM
10	F19C	BEAM
11	F19D	BEAM
12	F28A	BEAM
13	F28B	BEAM
14	F28C	BEAM
15	M1A	BEAM
16	M1B	BEAM

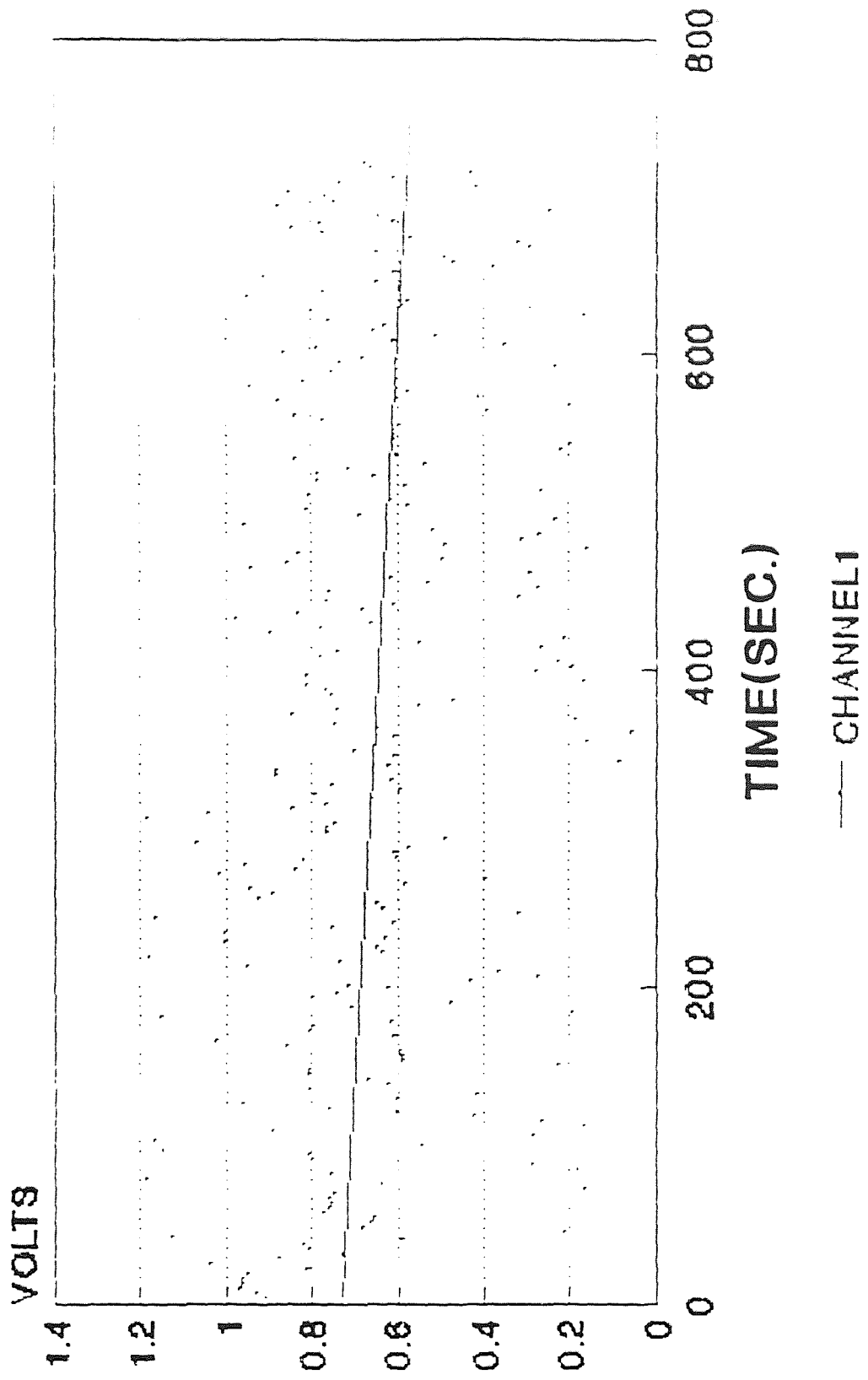


Fig.24 Internal deformation for J31

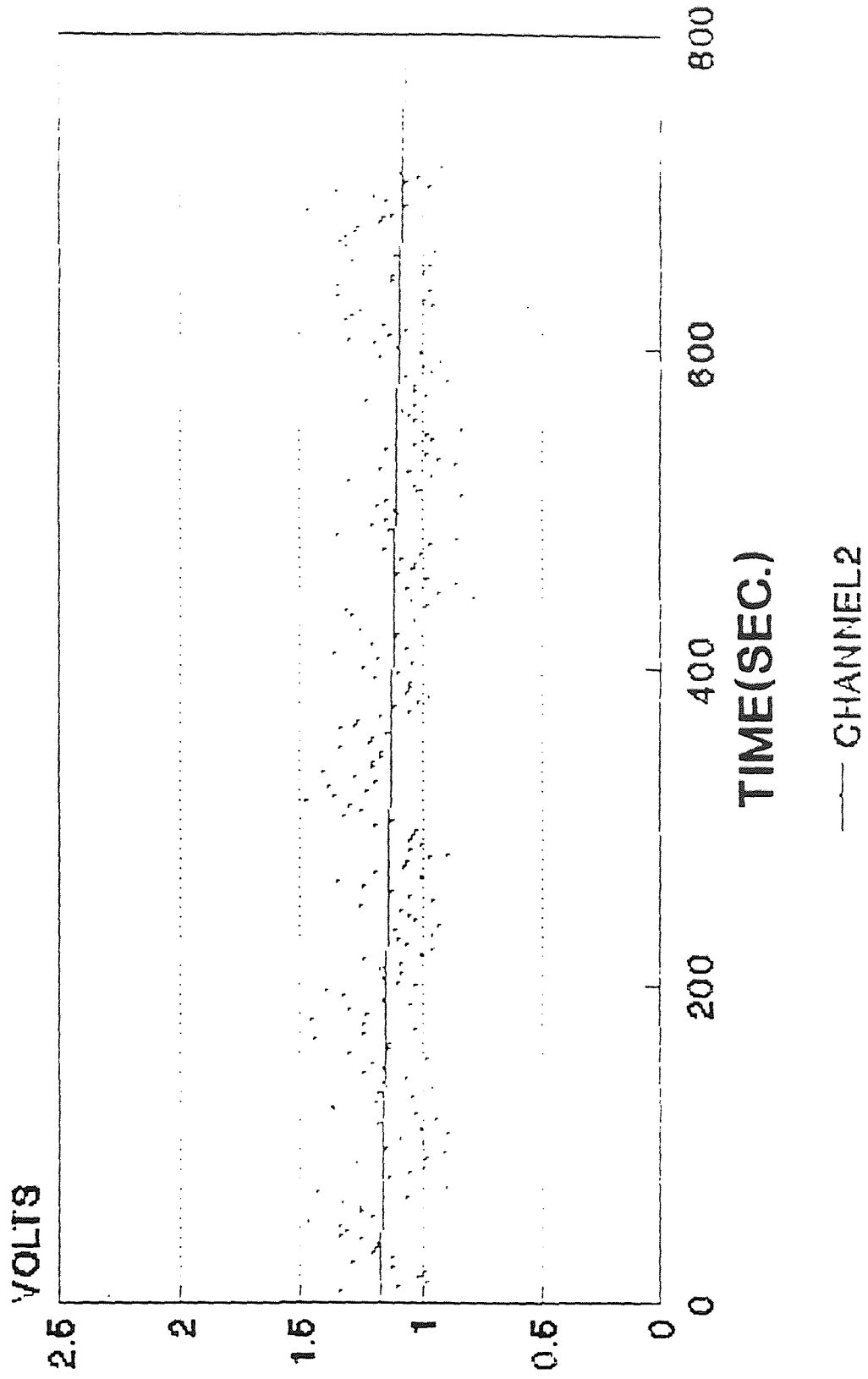


Fig.25 Internal deformation data for J31

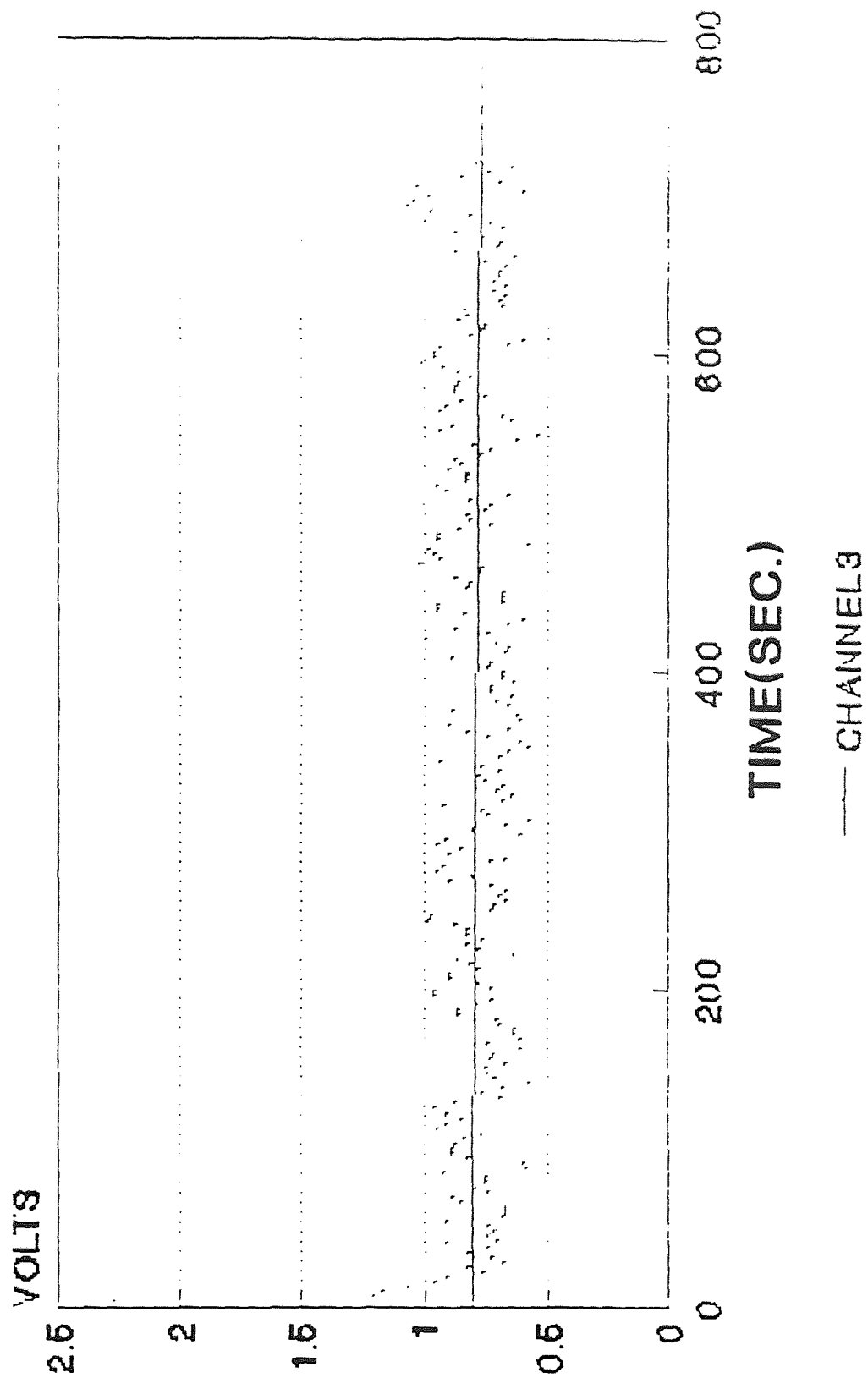


Fig.26 Internal deformation data for J31

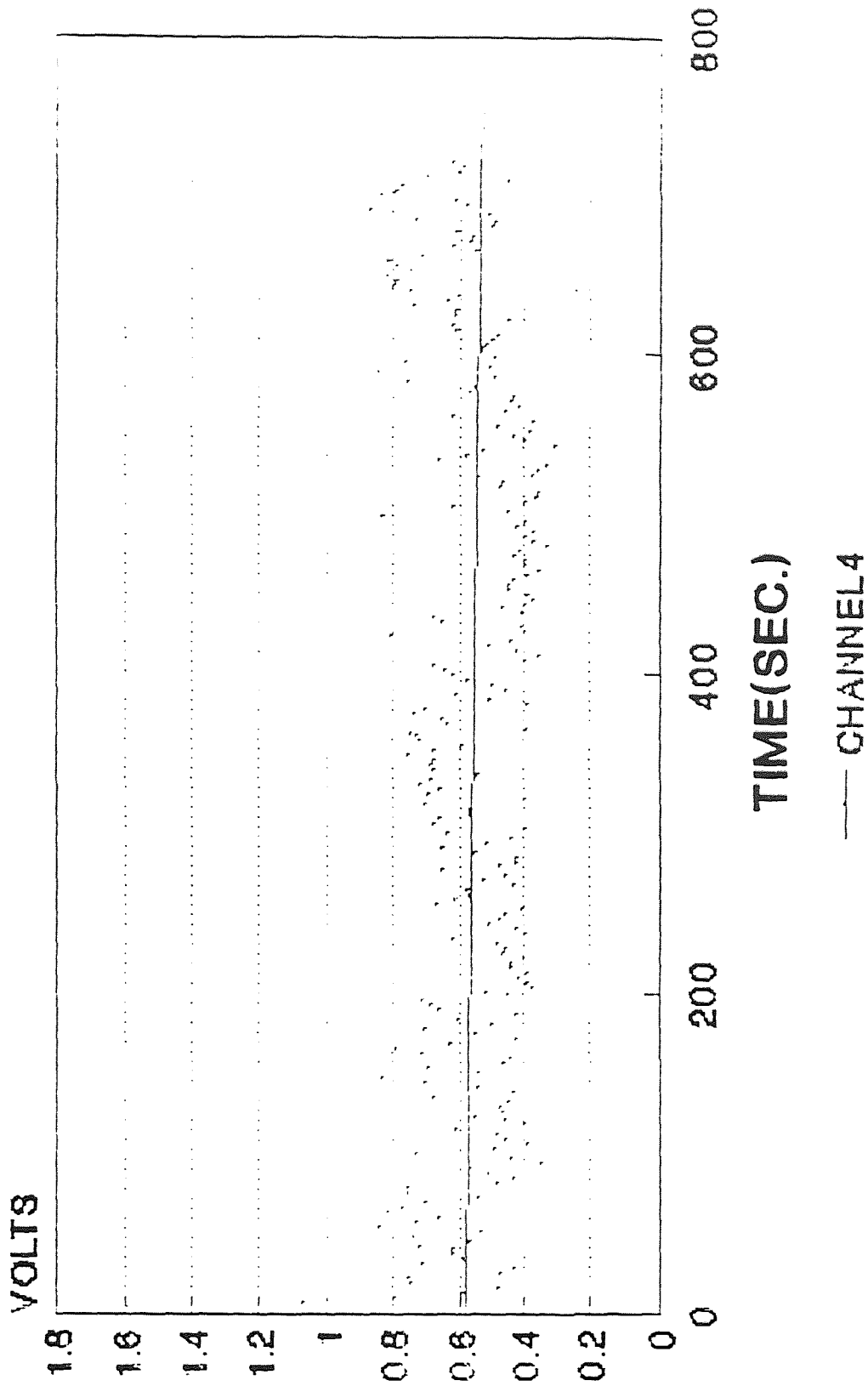


Fig.27 Internal deformation data f J31

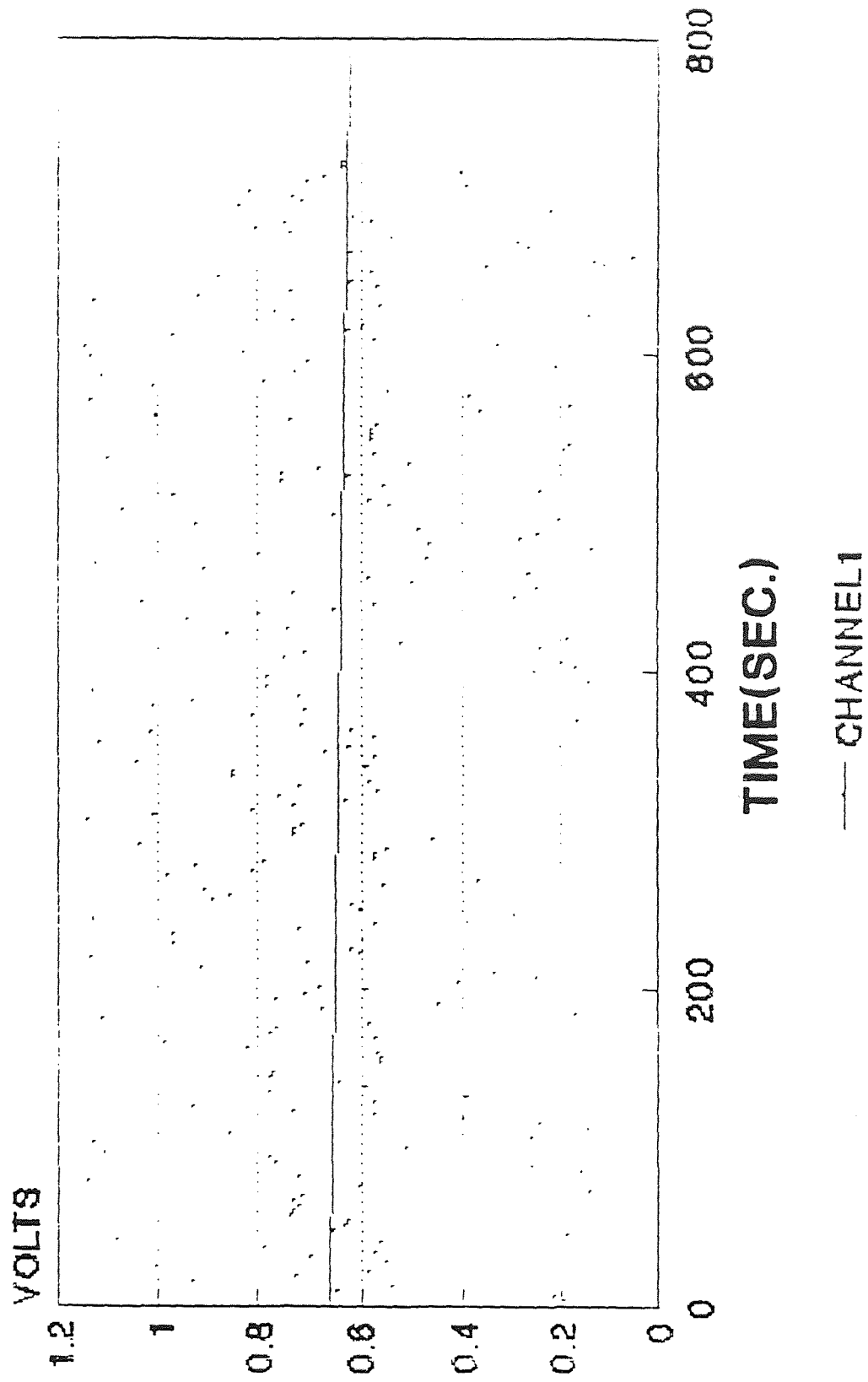


Fig.28 Internal deformation data for F2

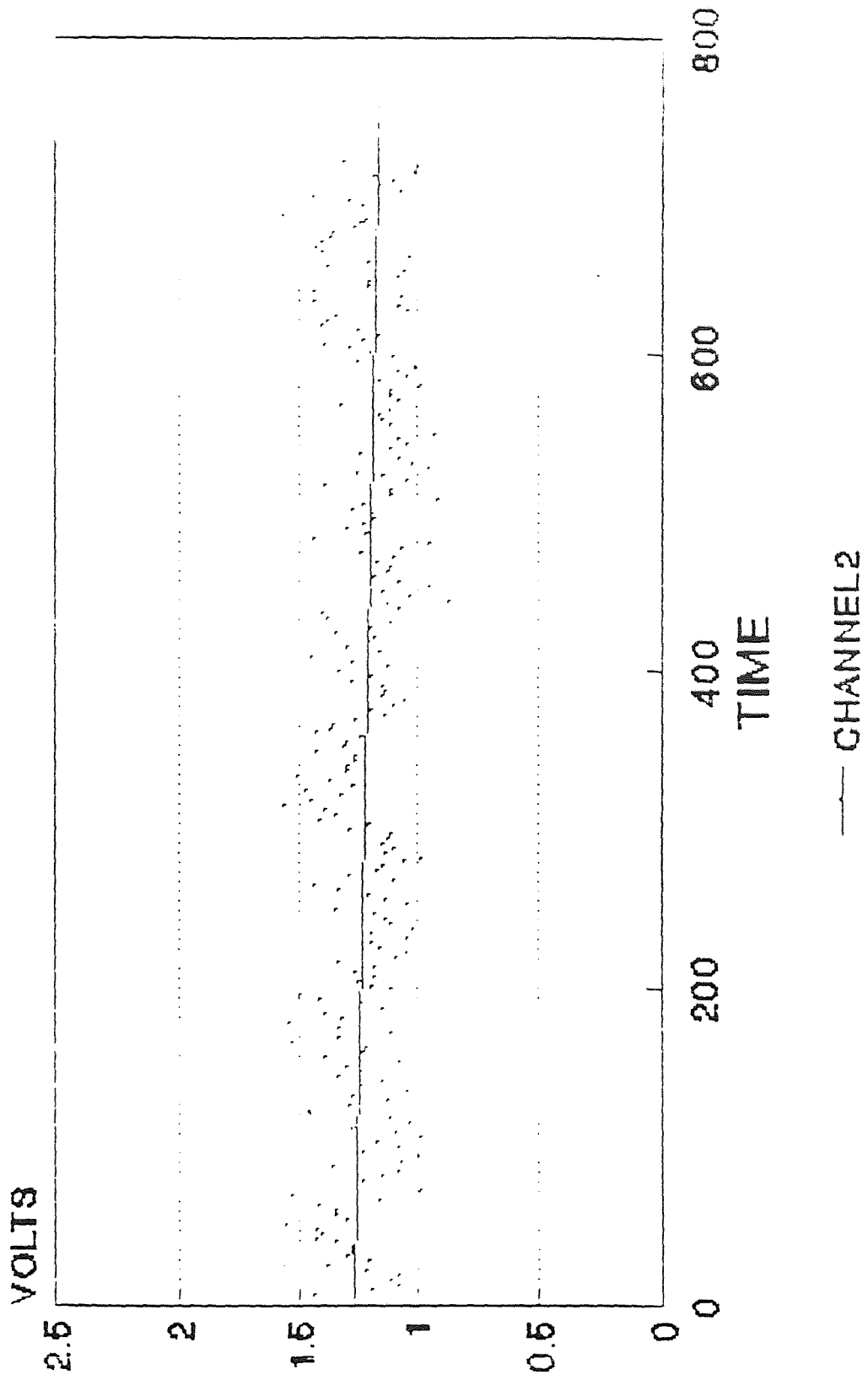


Fig.29 Internal deformation data for F2

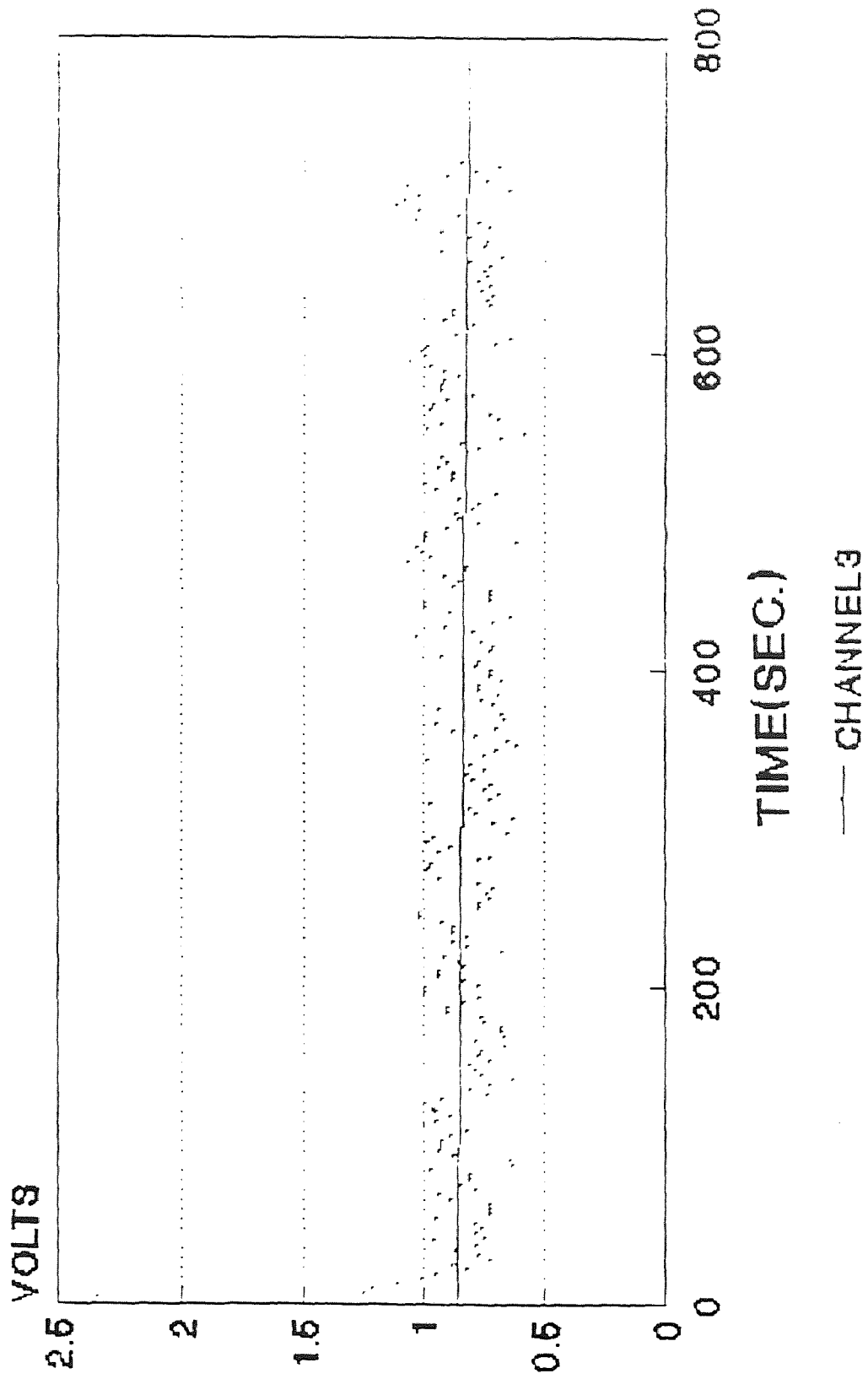


Fig.30 Internal deformation data for F2

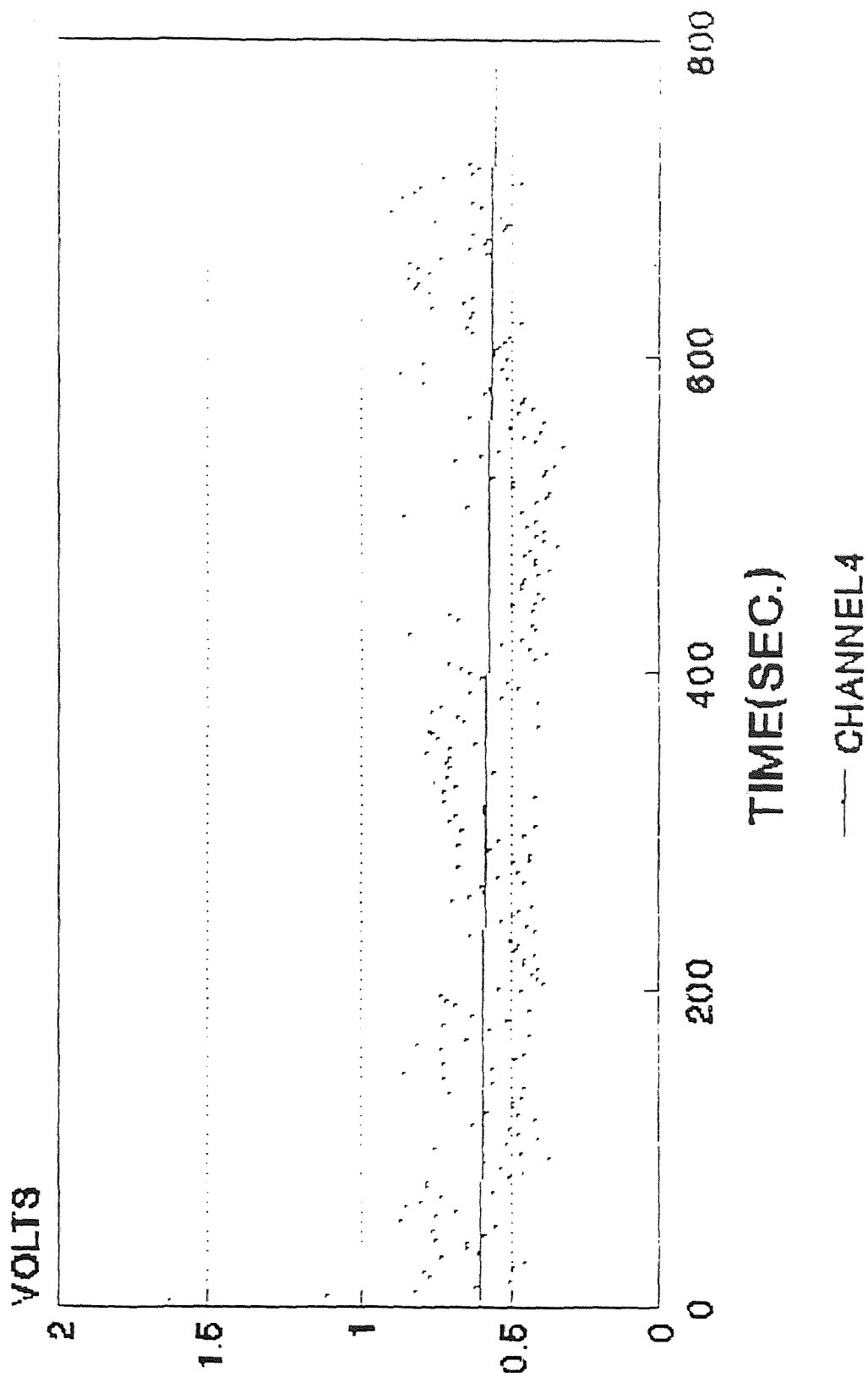


Fig.31 Internal deformation data for F2

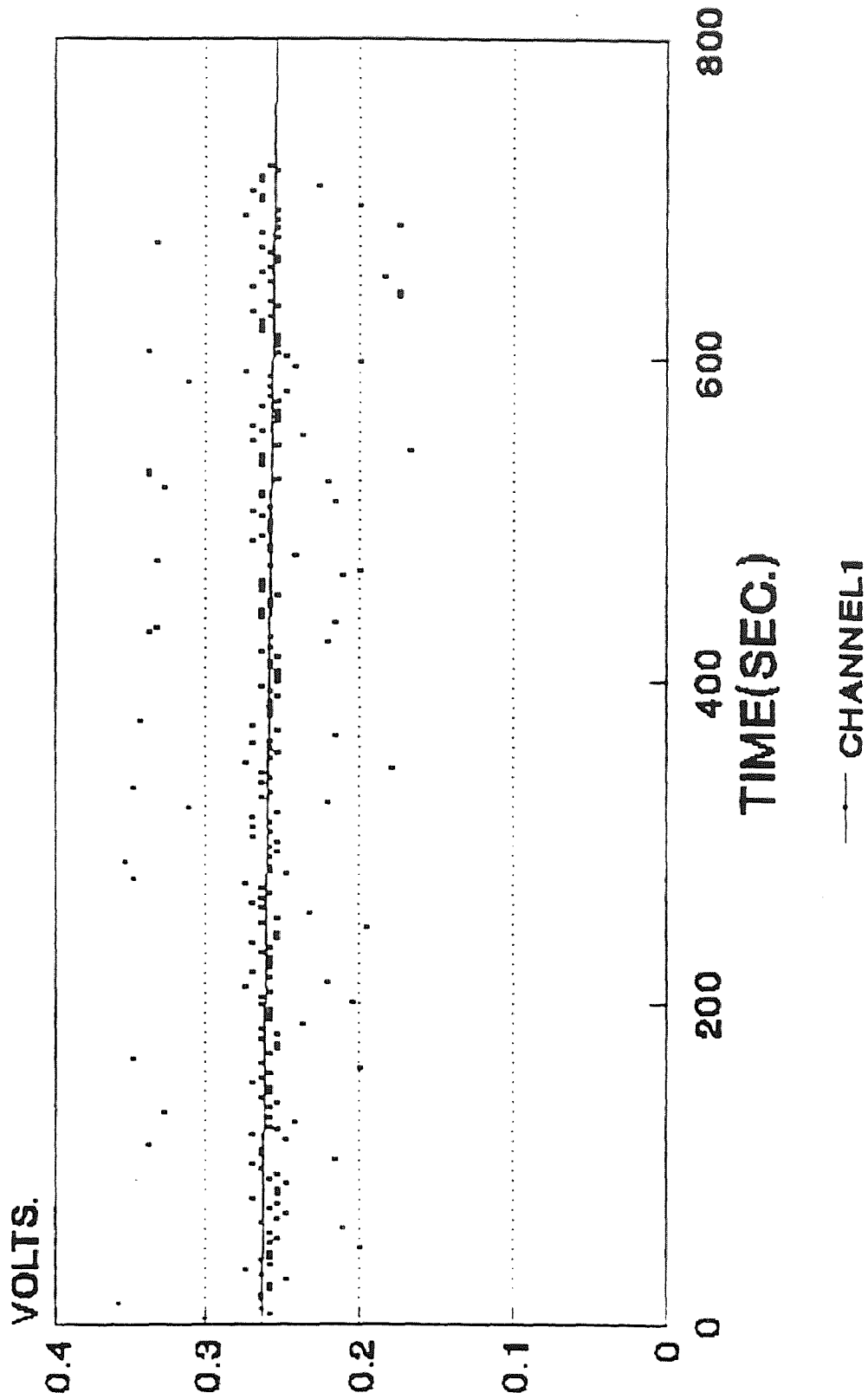


Fig.32 Internal deformation data for F3 #2

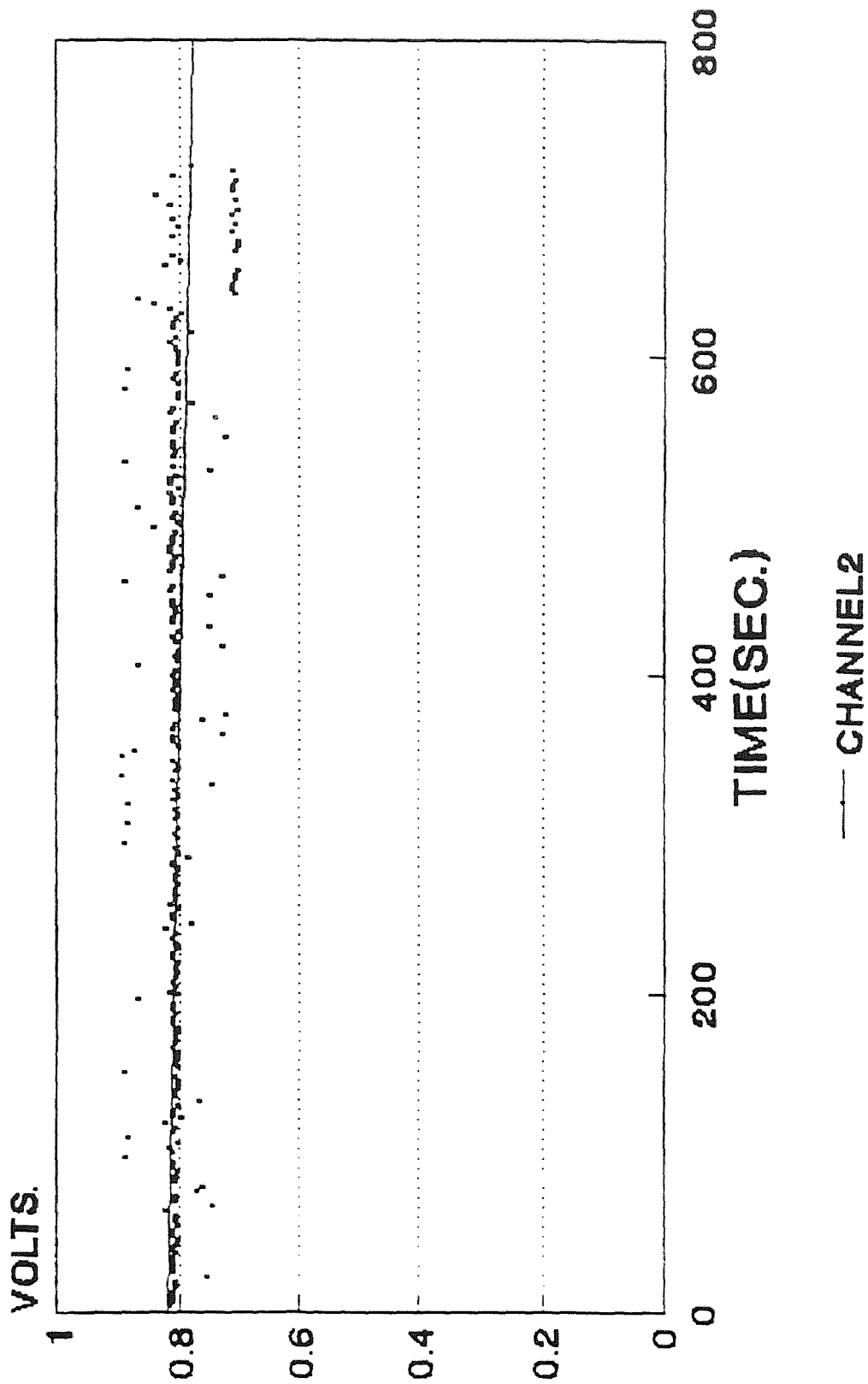


Fig.33 Internal deformation data for F3#2

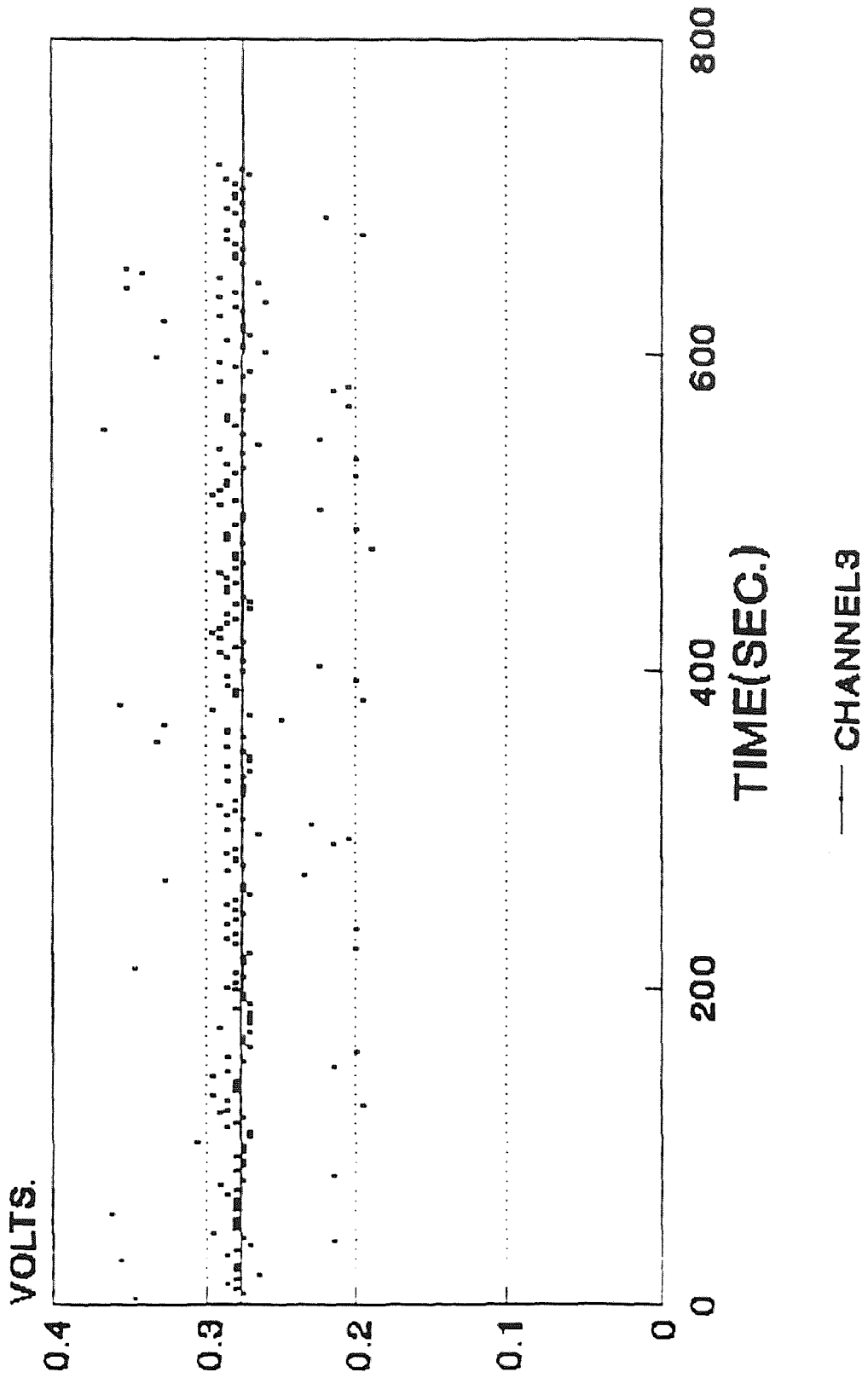


Fig.34 Internal deformation data for F3#2

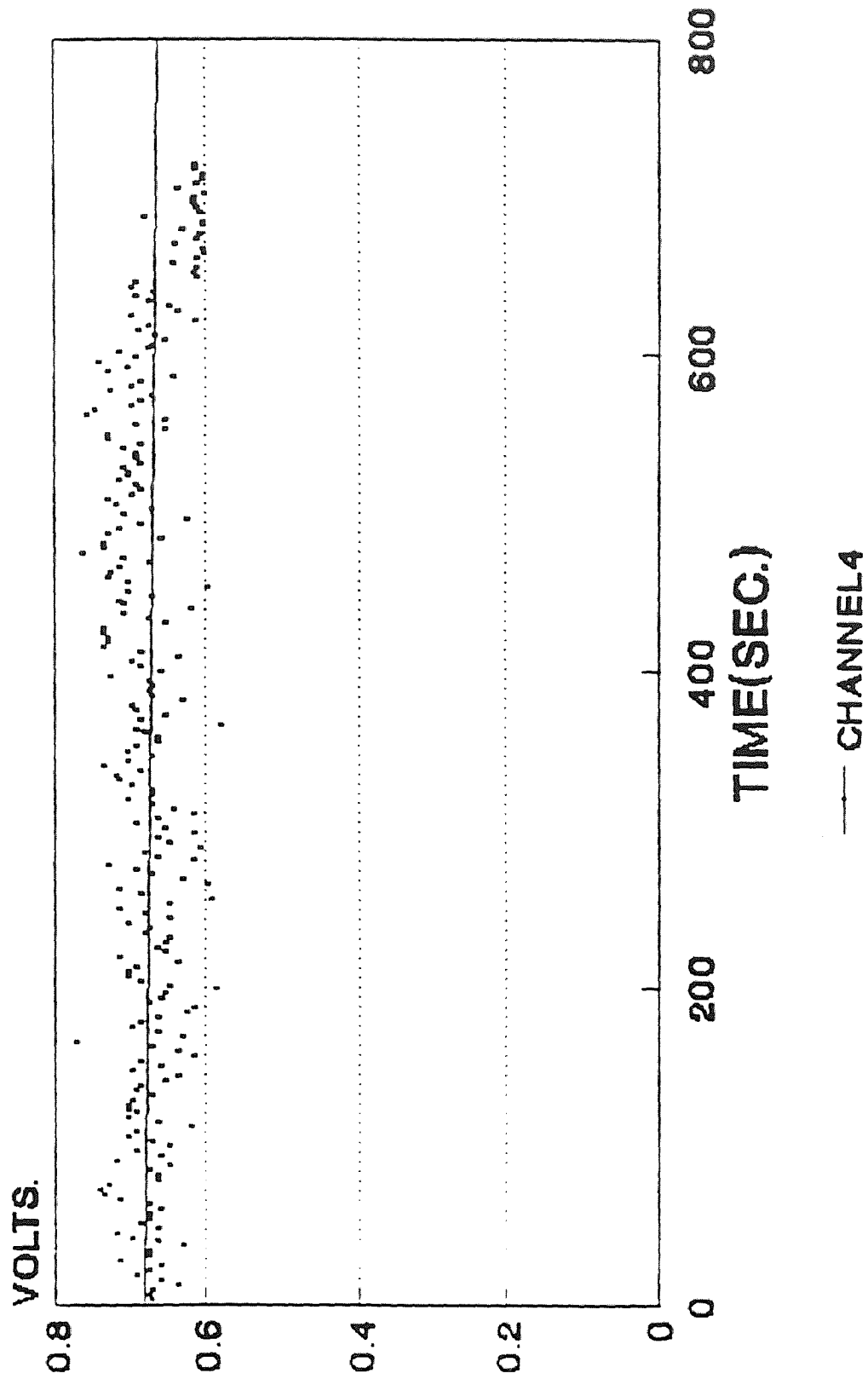


Fig. 35 Internal deformation data for F3#2

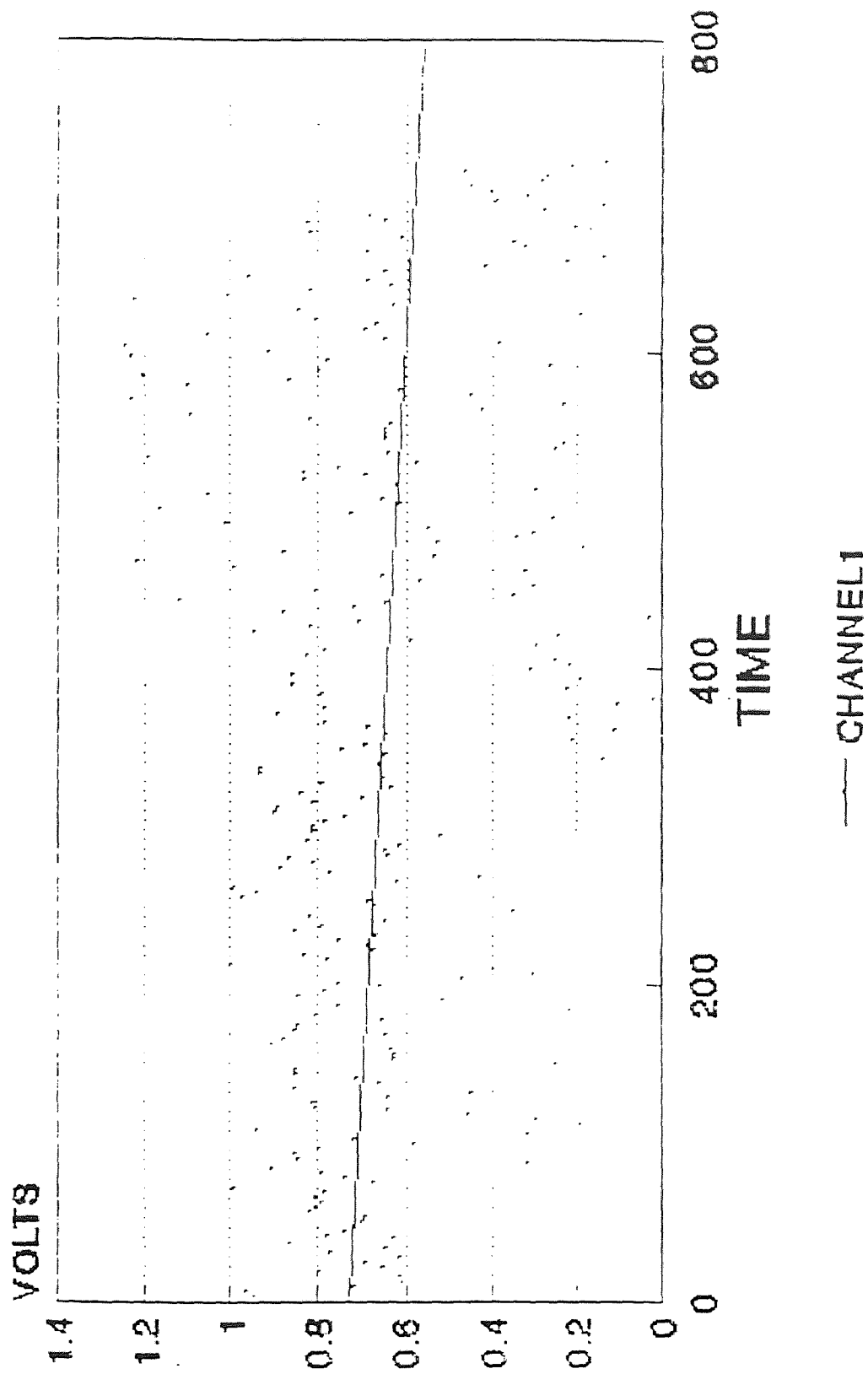


Fig.36 Internal deformation data for F8

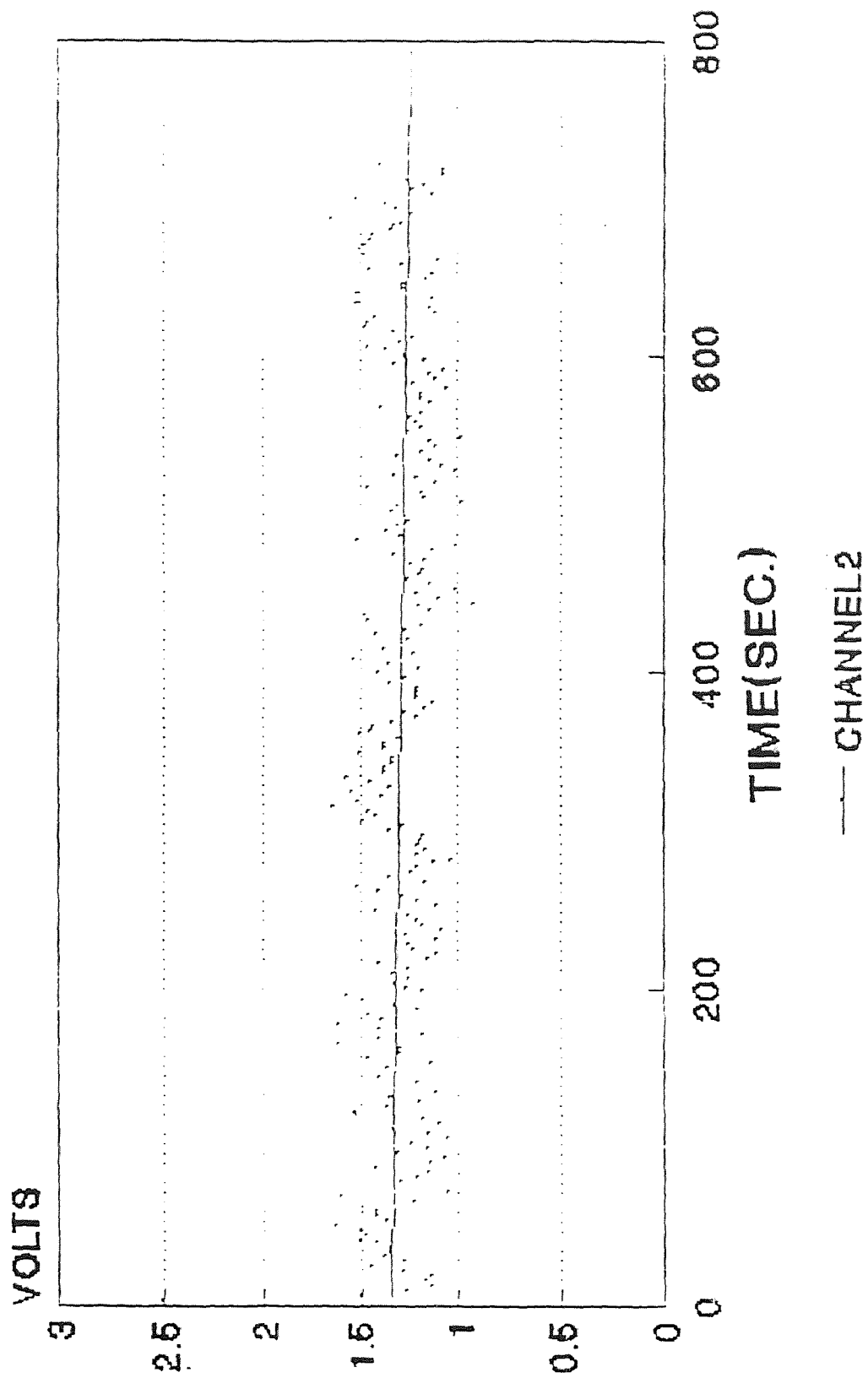


Fig.37 Internal deformation data for F8

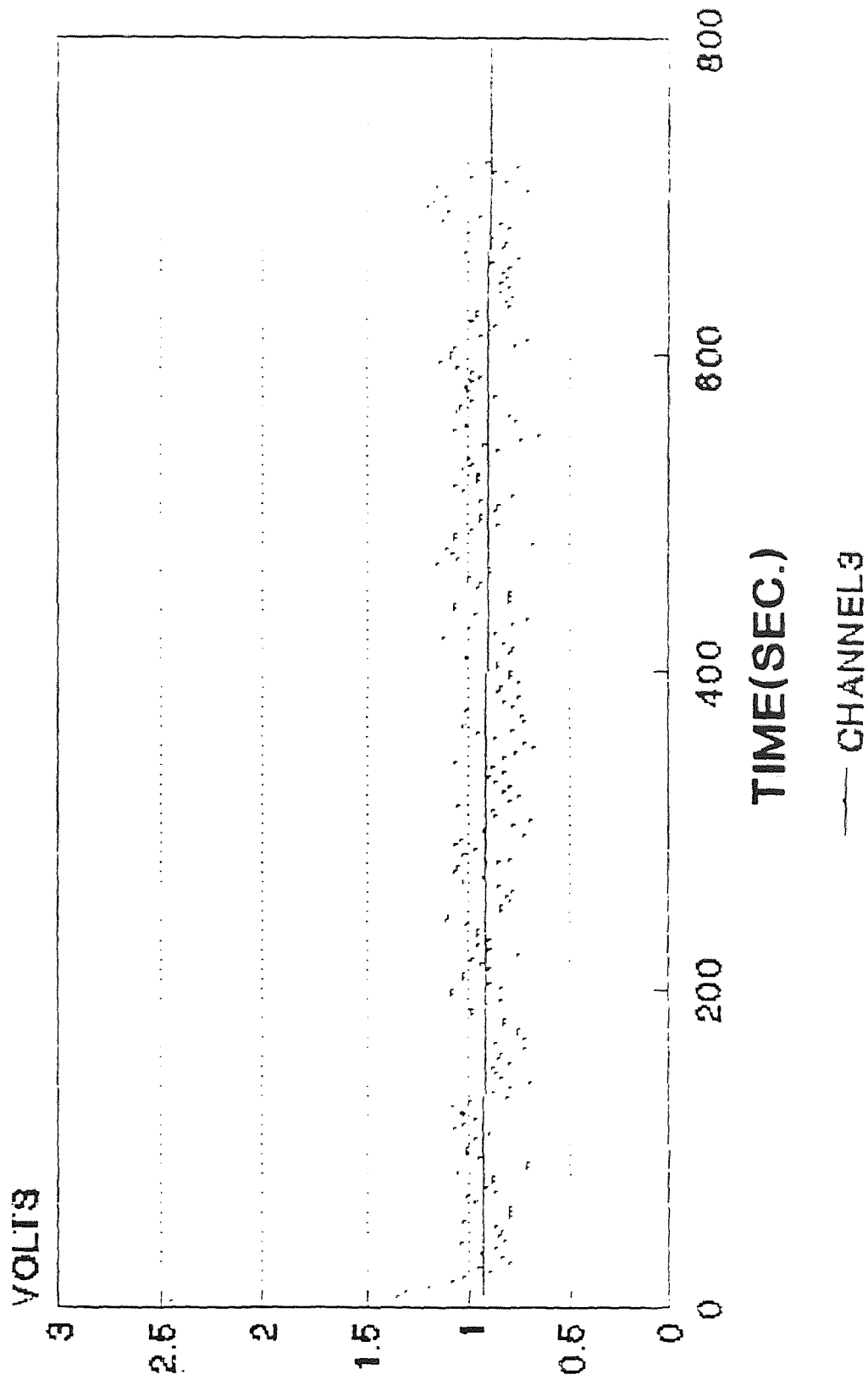


Fig.38 Internal deformation data for F8

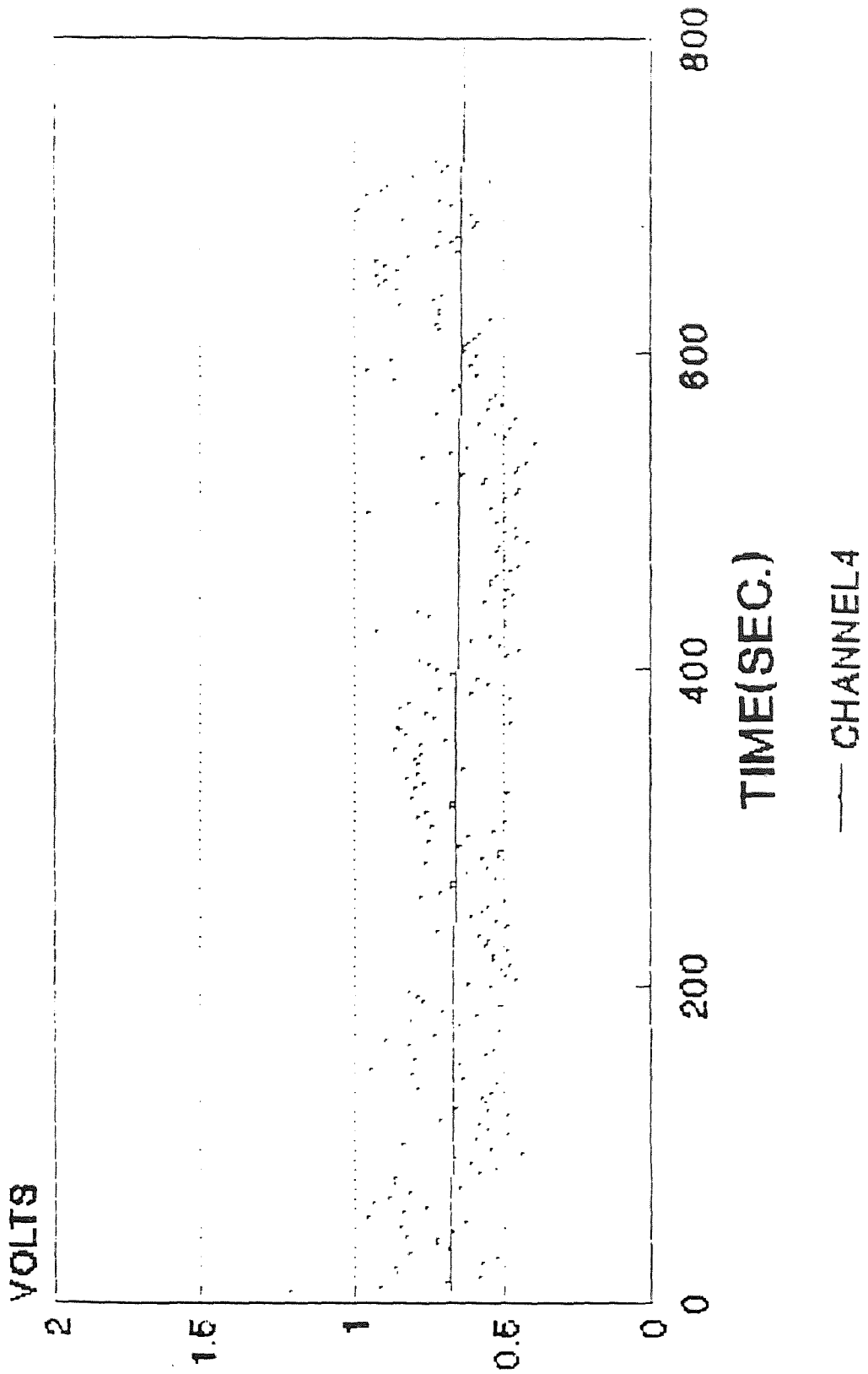


Fig.39 Internal deformation data for F8

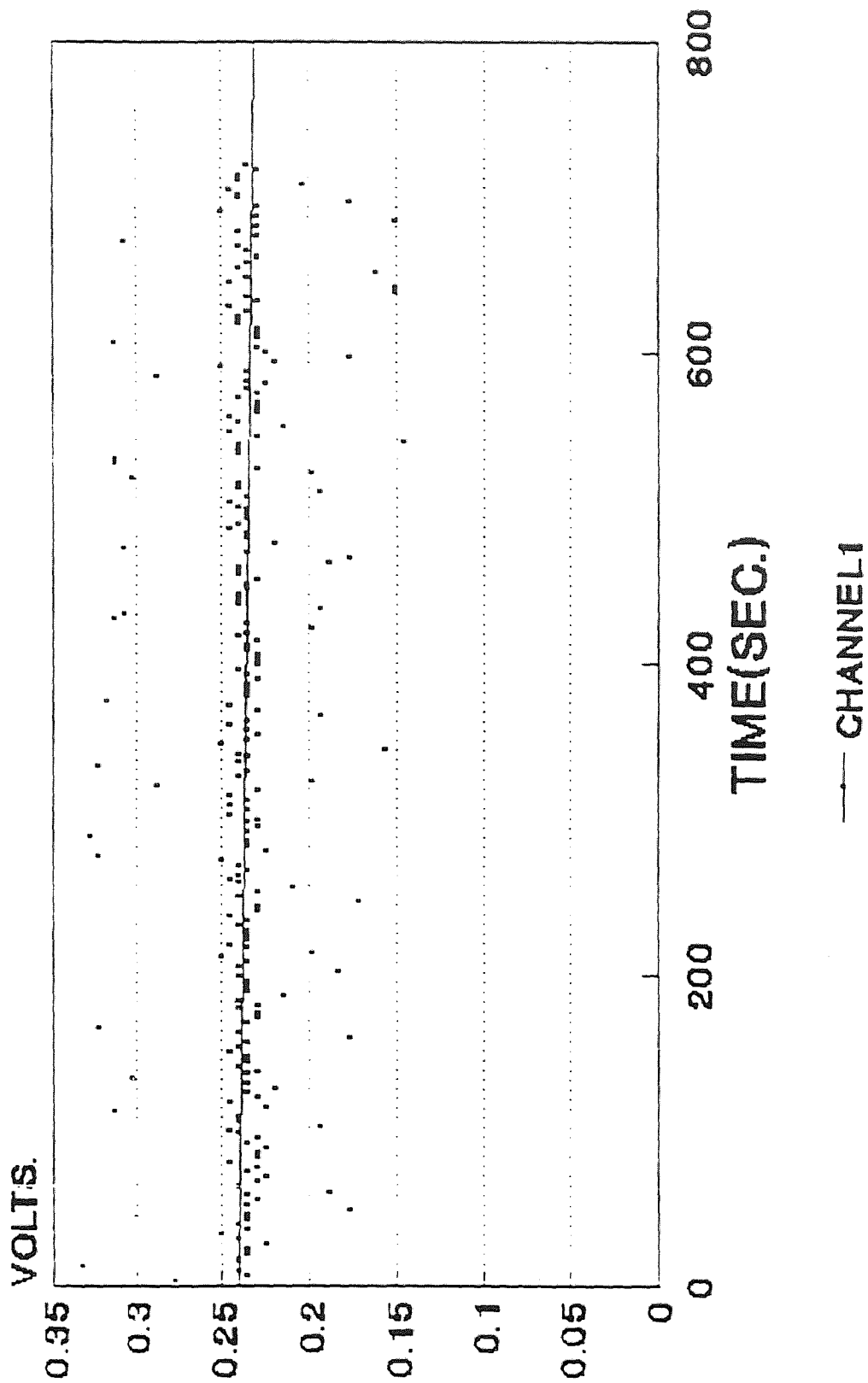
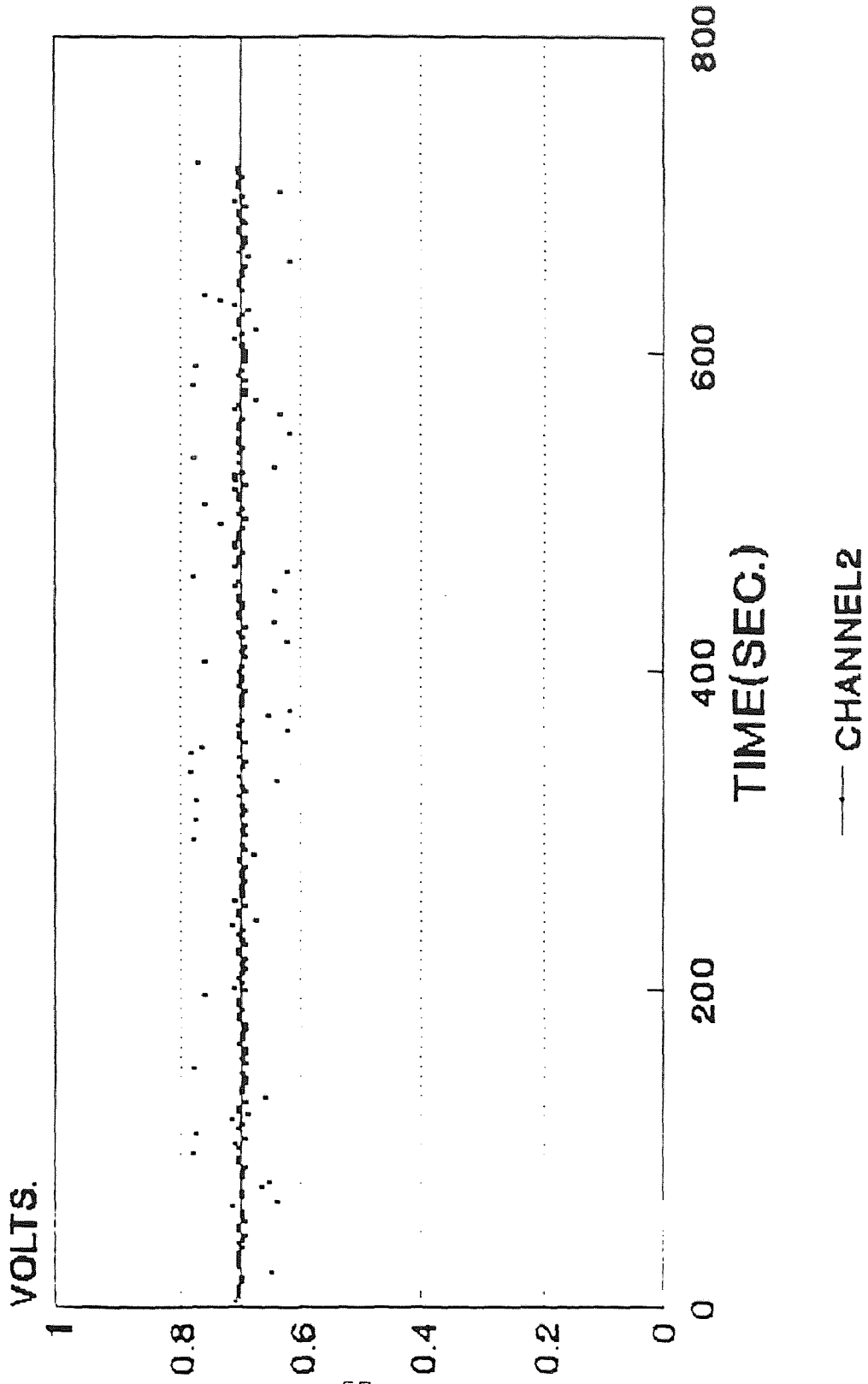


Fig.40 Internal deformation data for F10



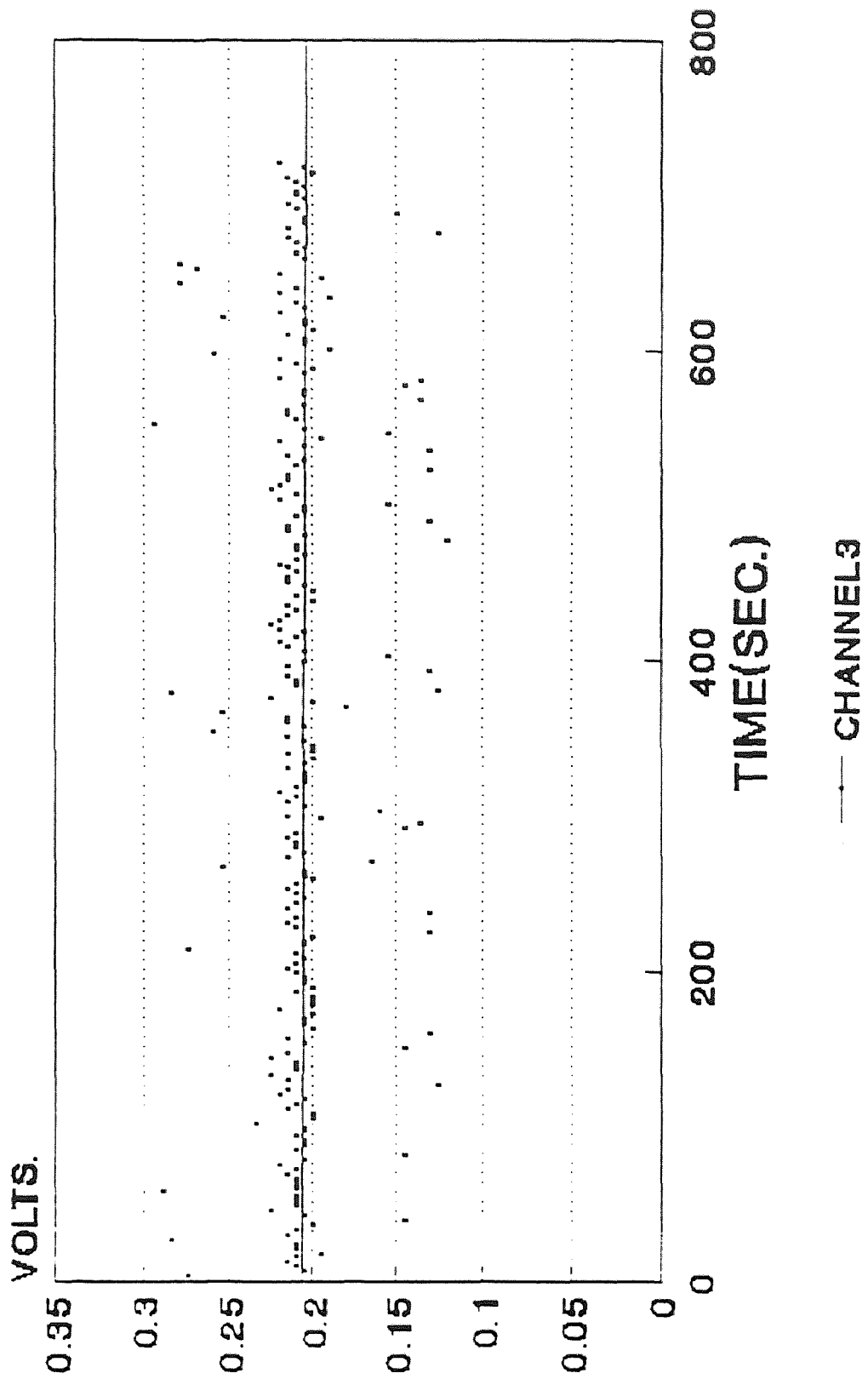


Fig.42 Internal deformation data for F10

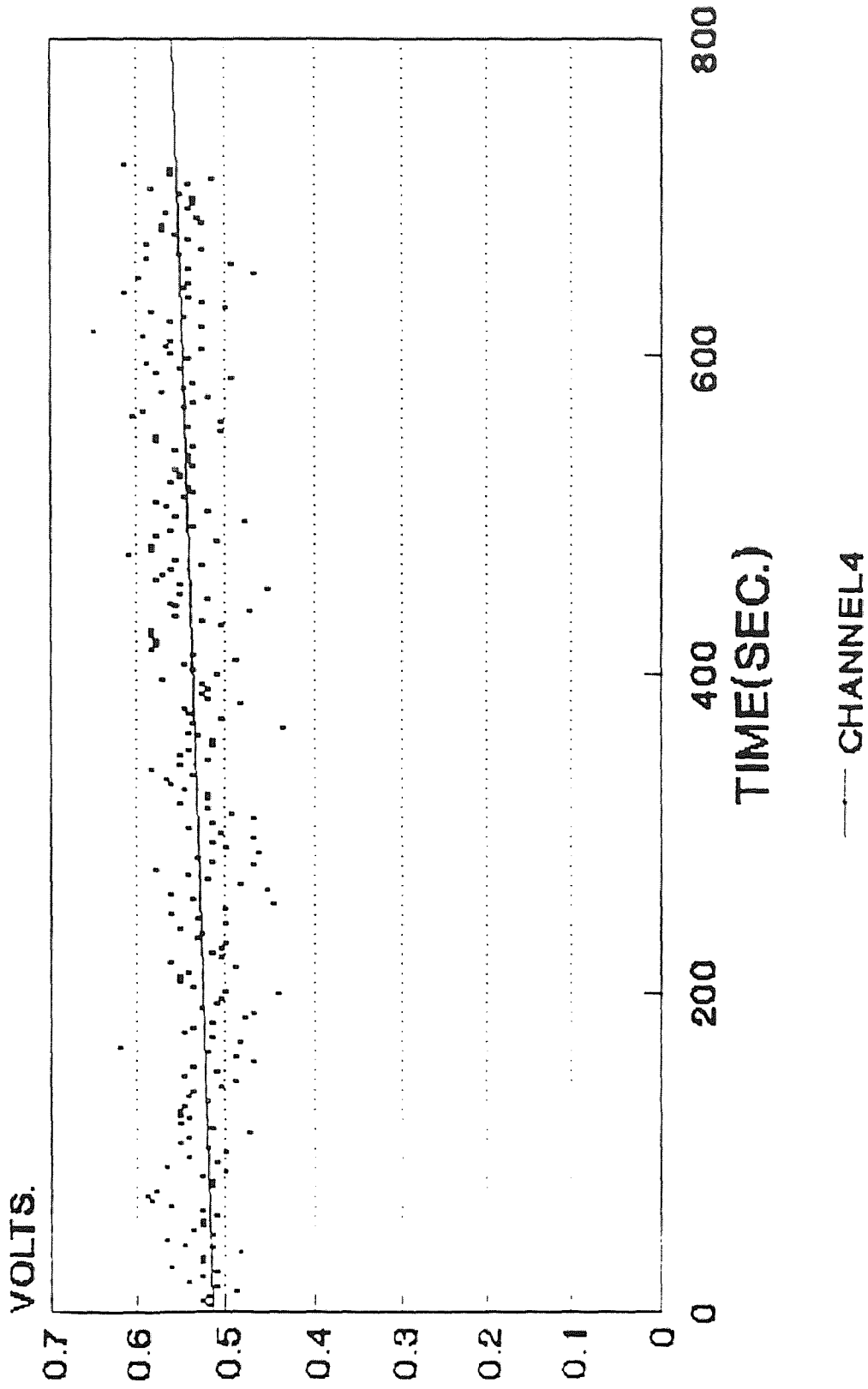


Fig.43 Internal deformation data for F10

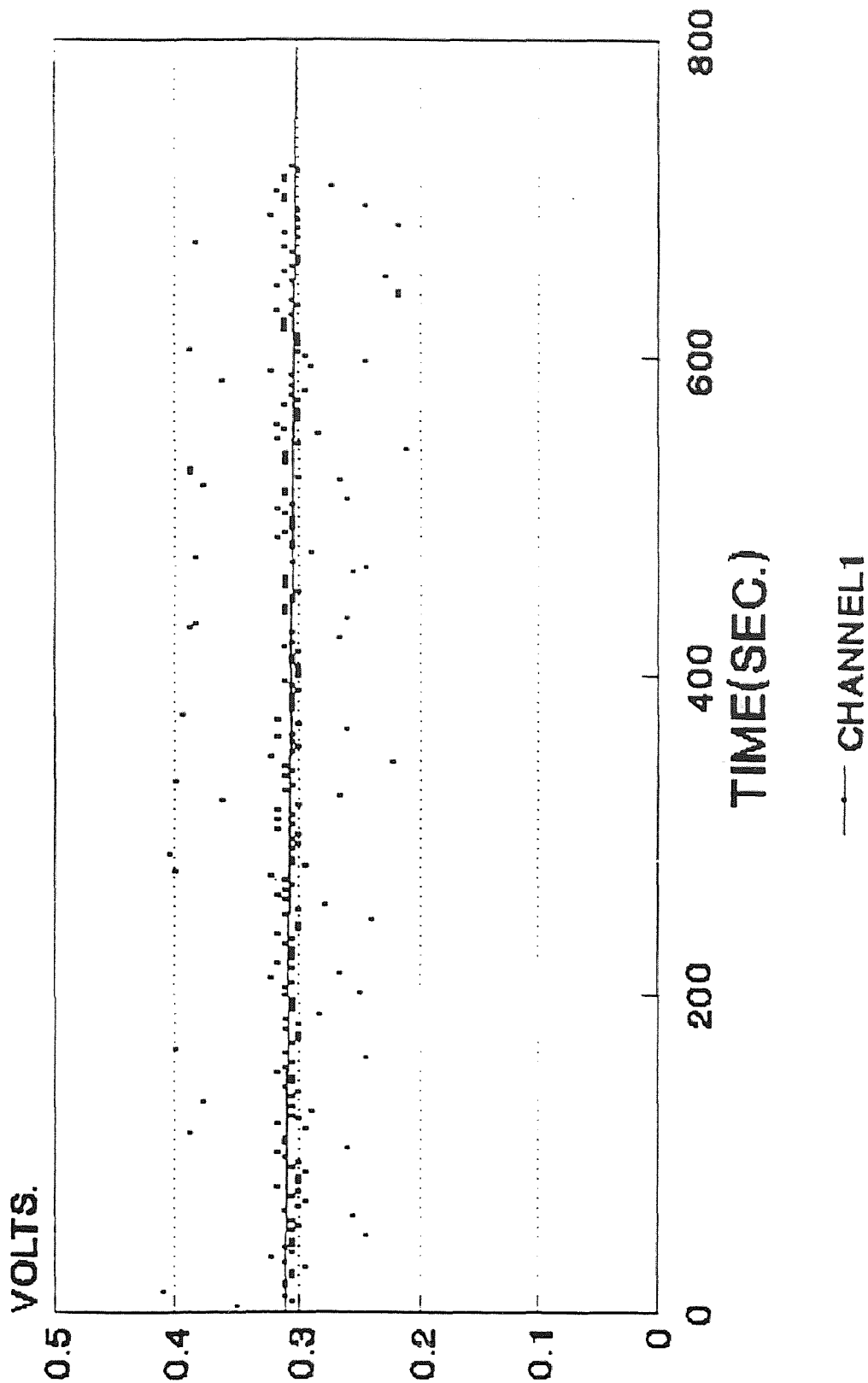


Fig.44 Internal deformation data for F11

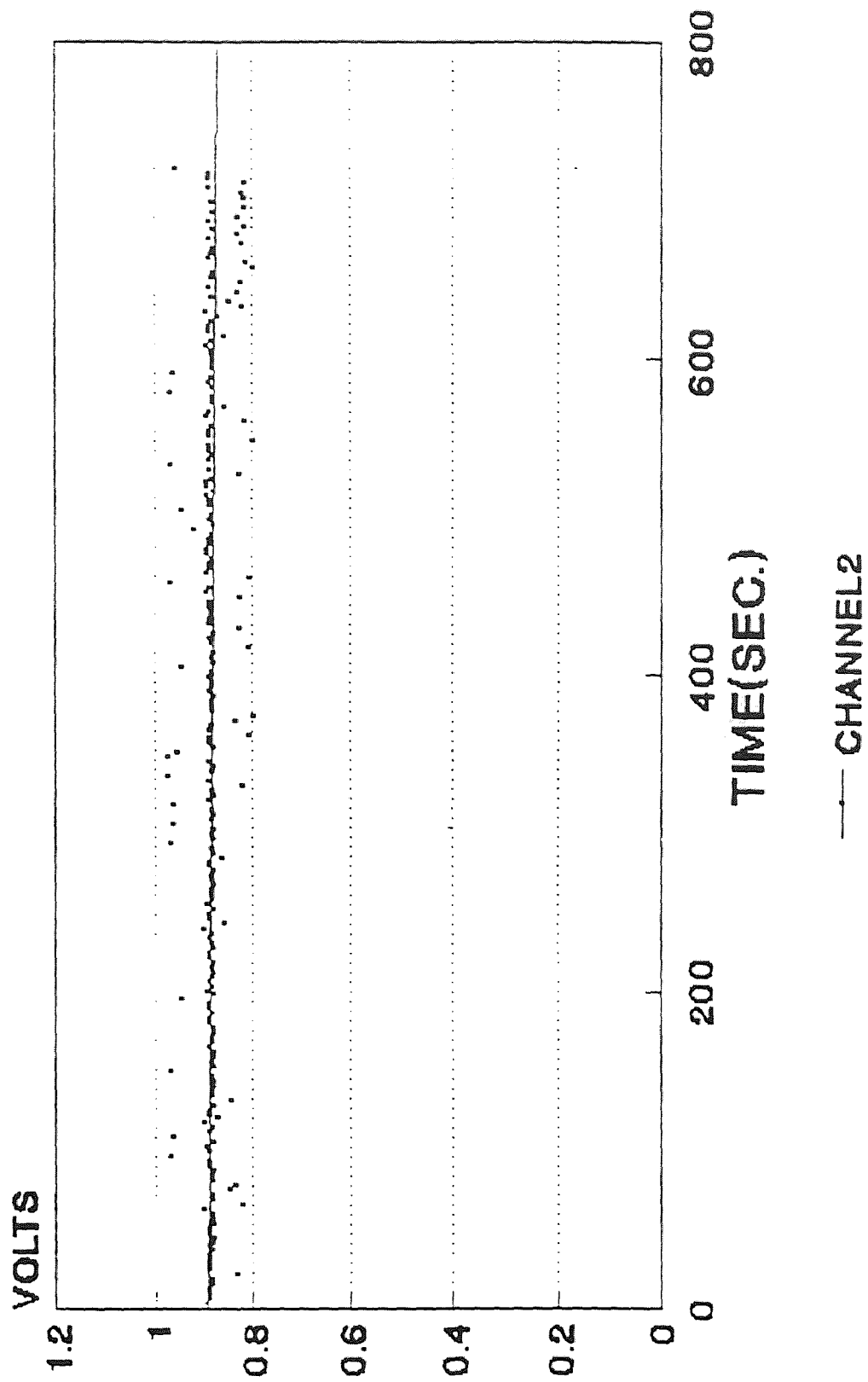


Fig.45 Internal deformation data for F1.

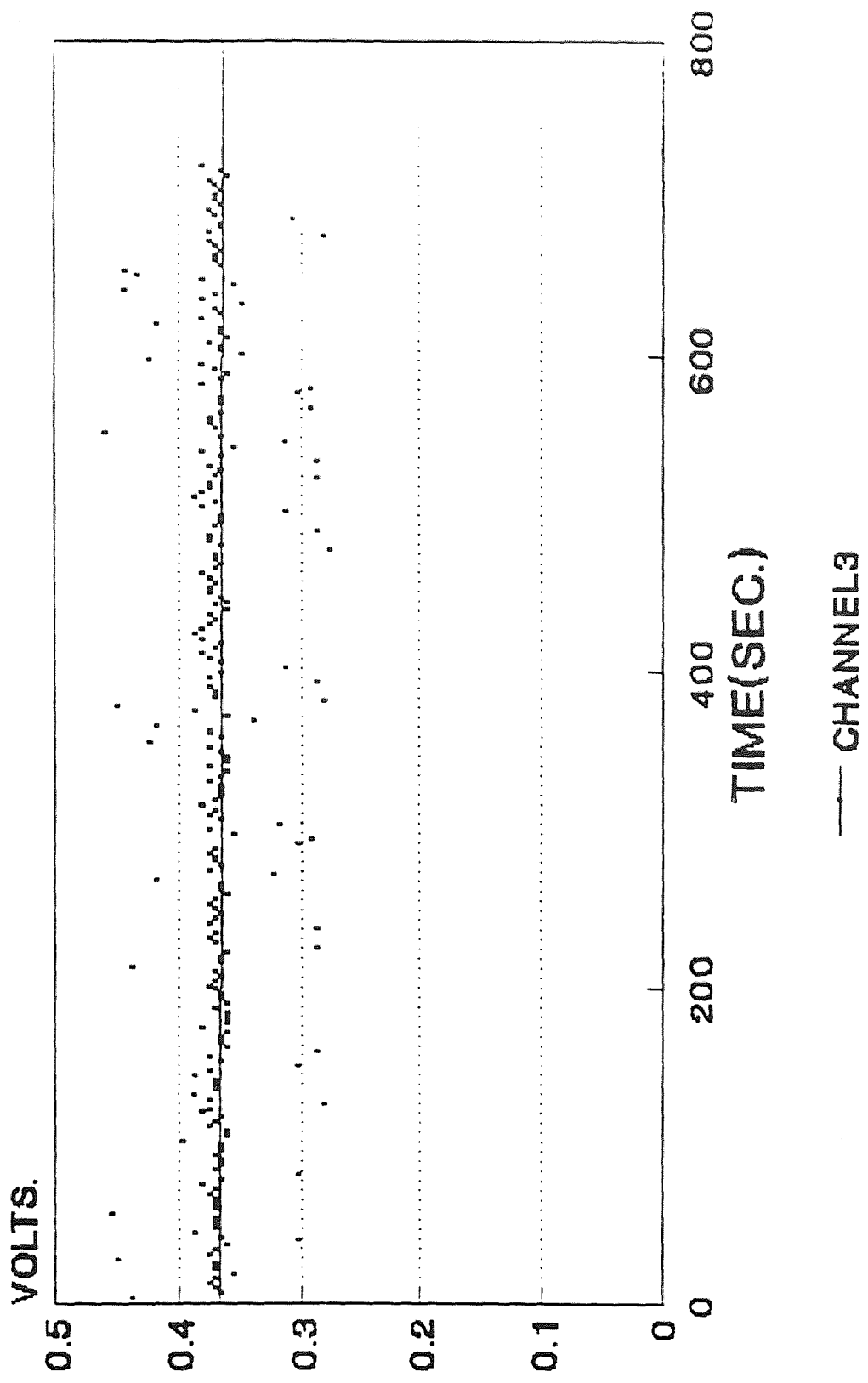


Fig.46 Internal deformation data for F11

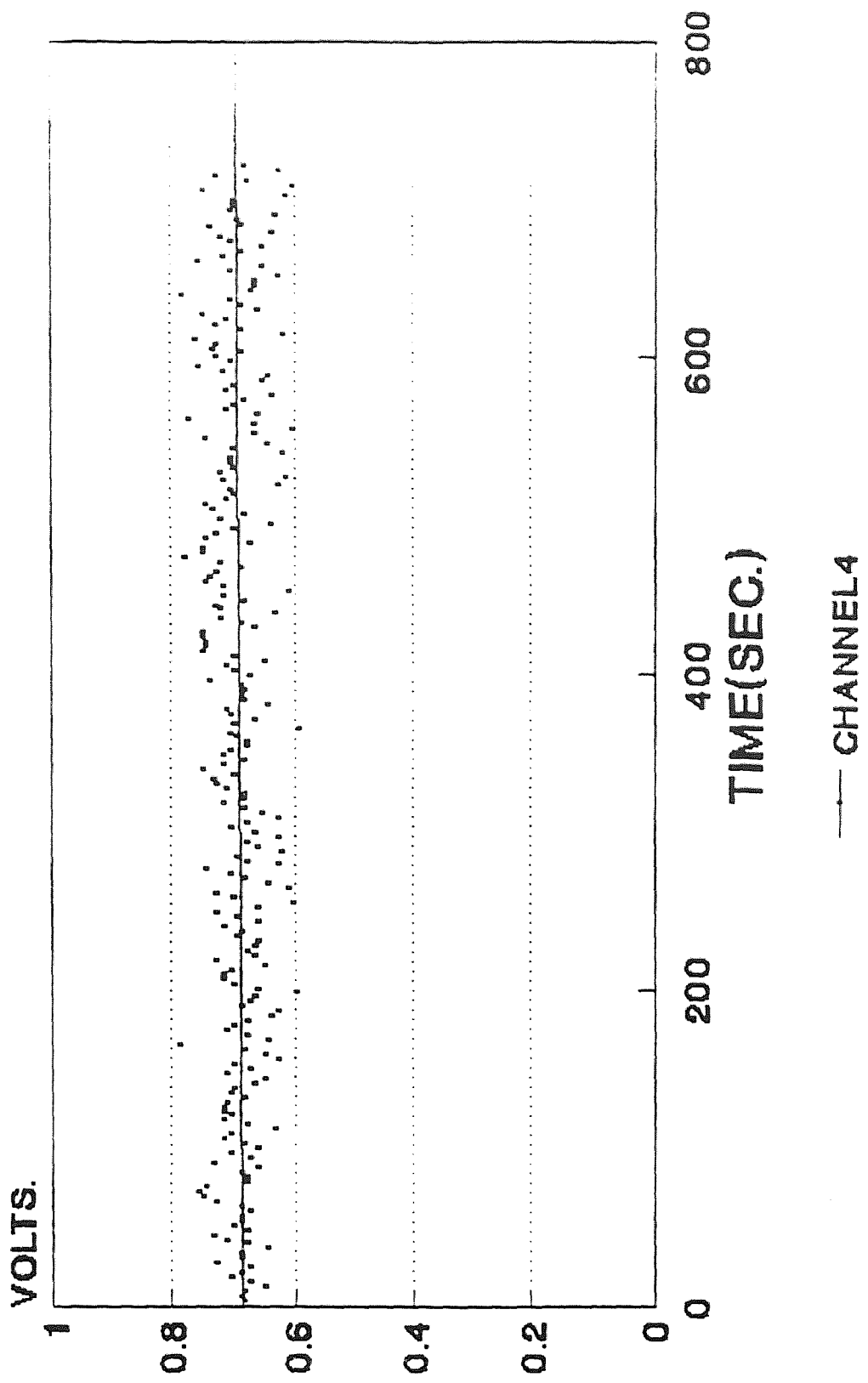


Fig.47 Internal deformation data for Ft1

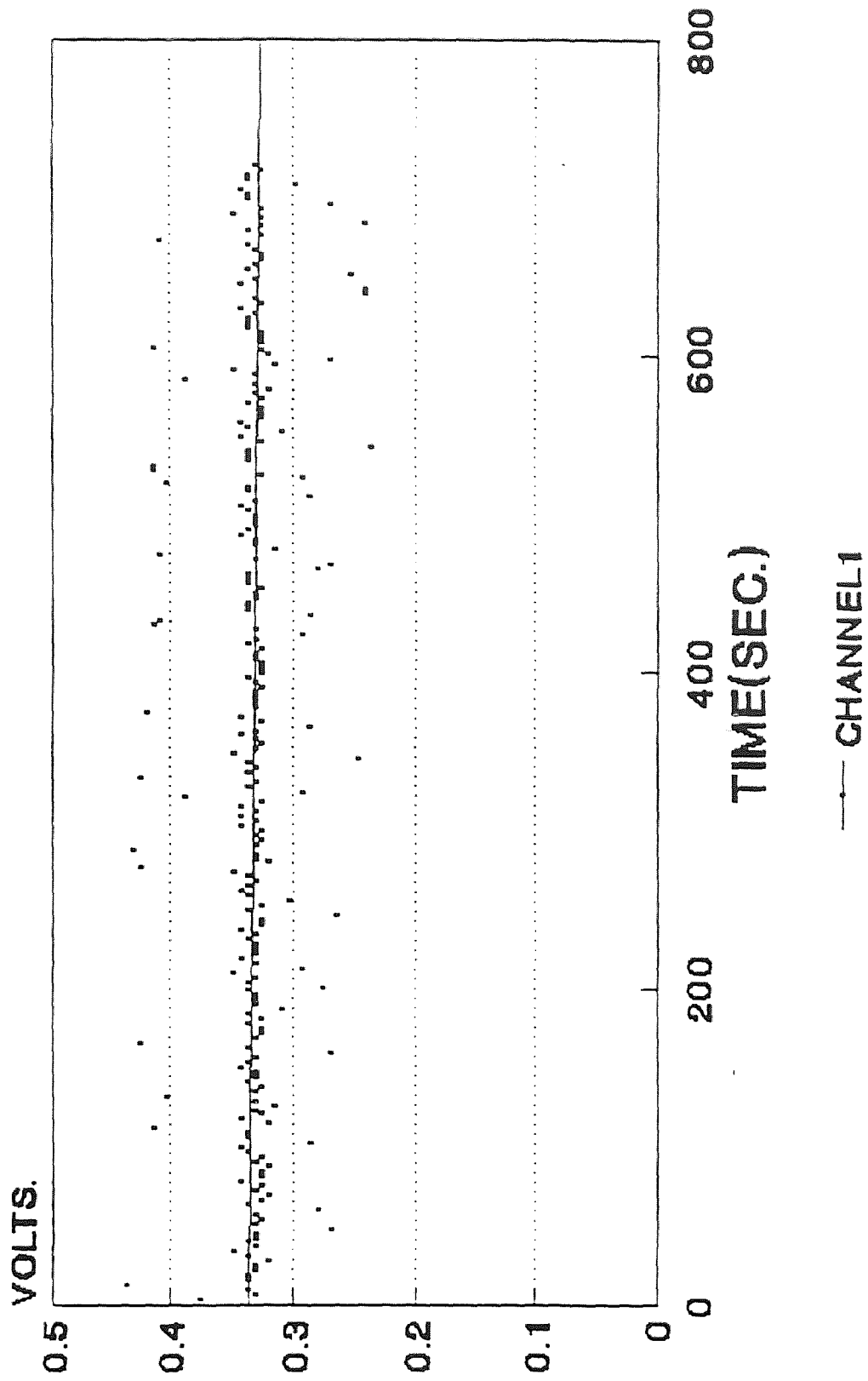


Fig.48 Internal deformation data for F12

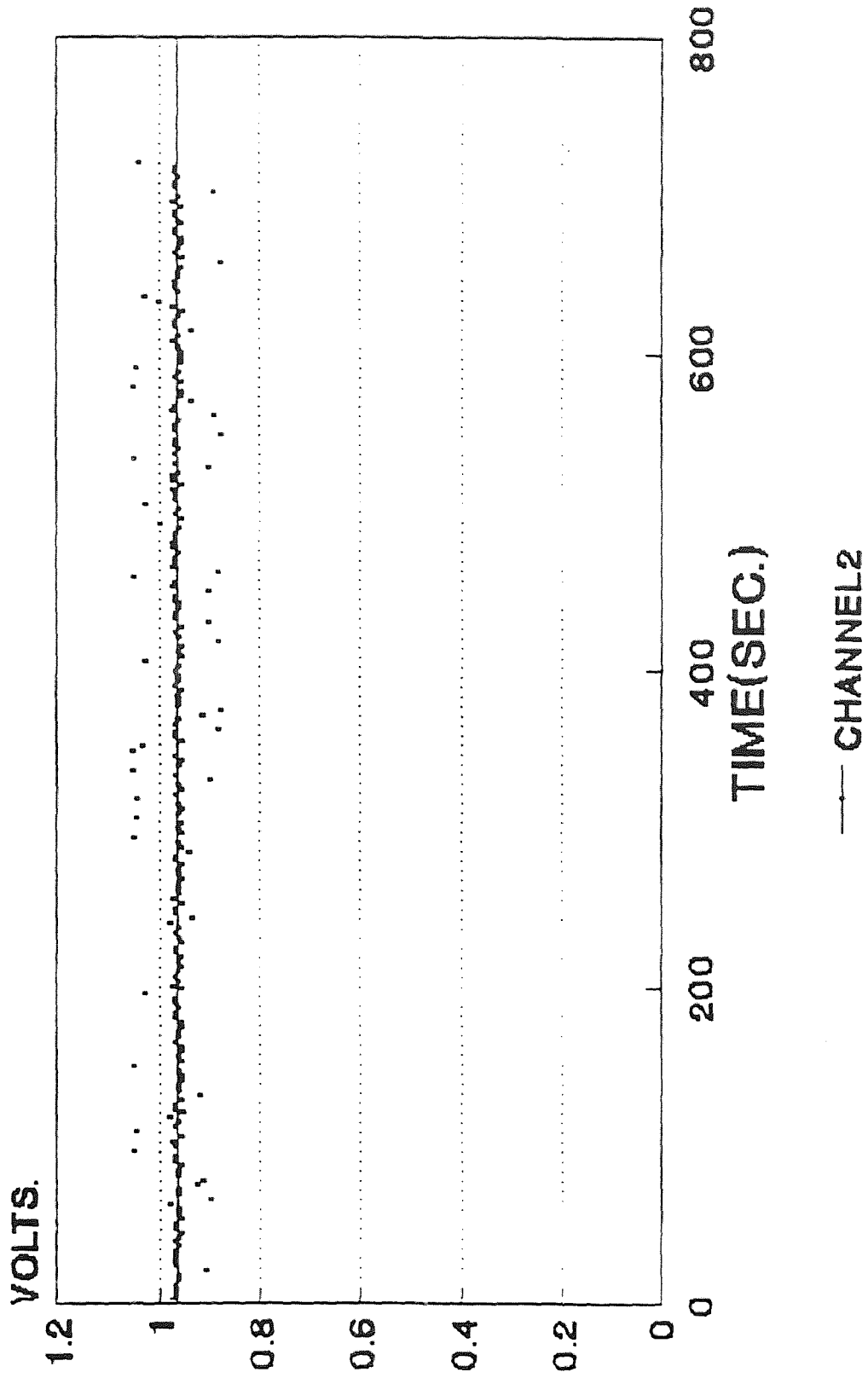


Fig.49 Internal deformation data for F12

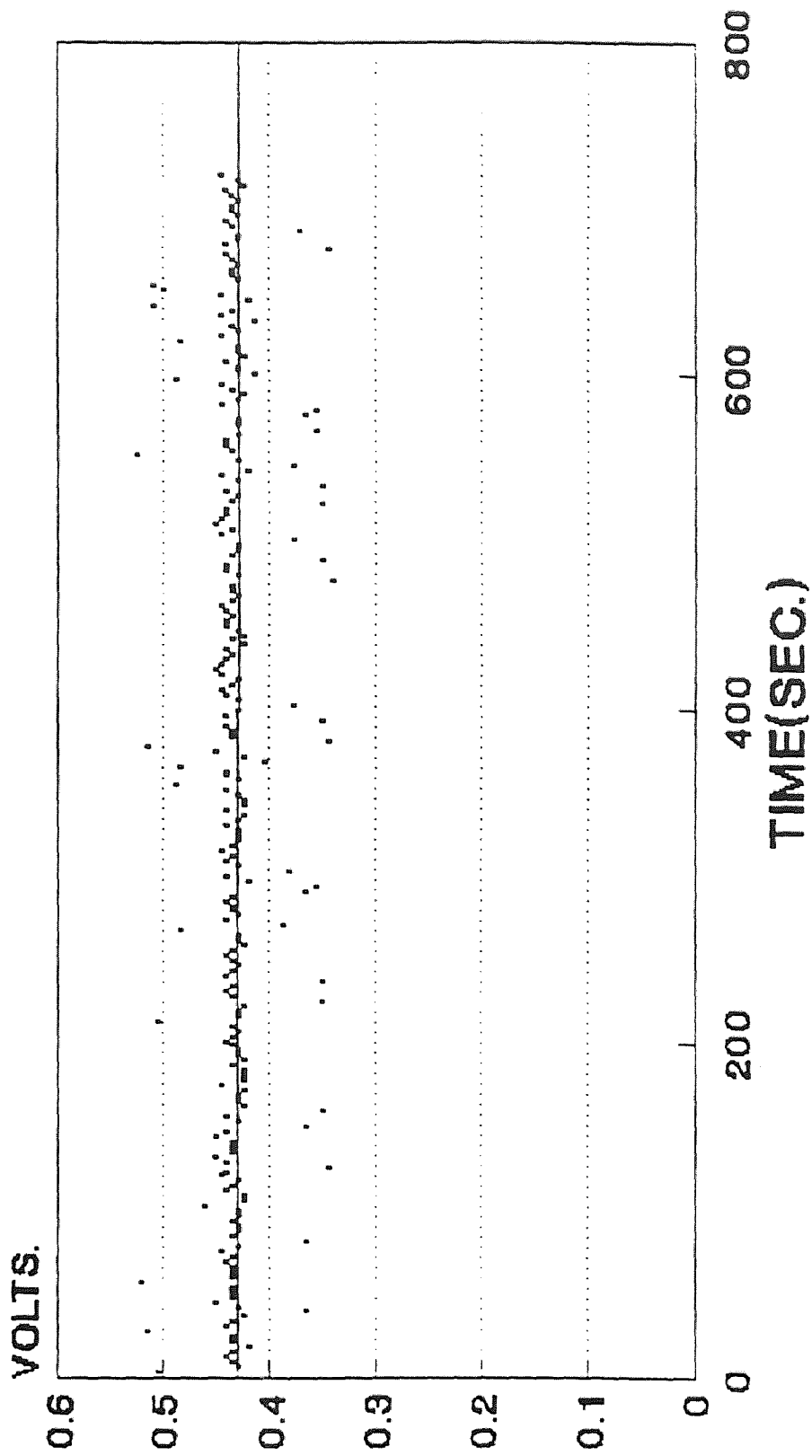


Fig.50 Internal deformation data for F12

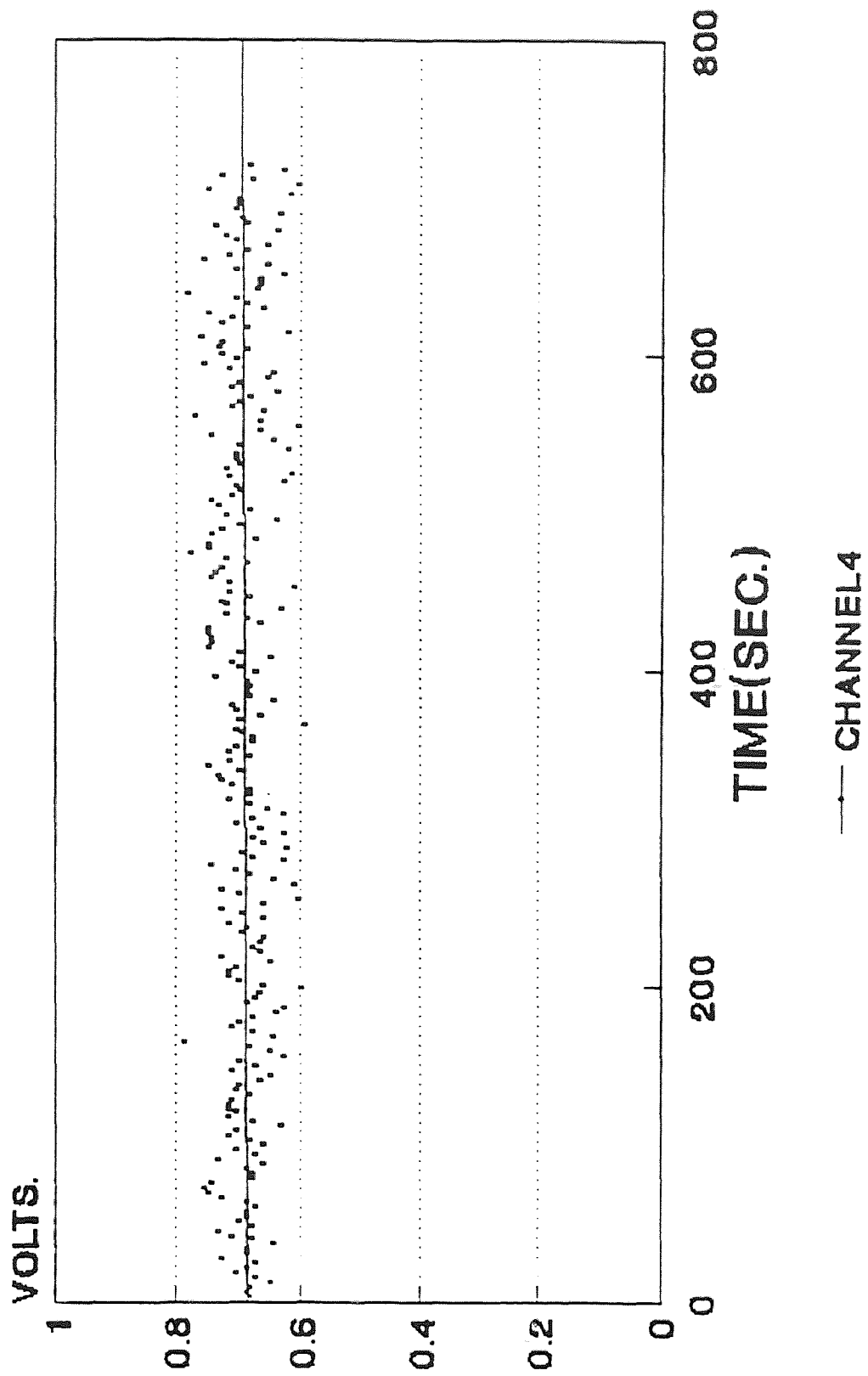


Fig.51 Internal deformation data for F12

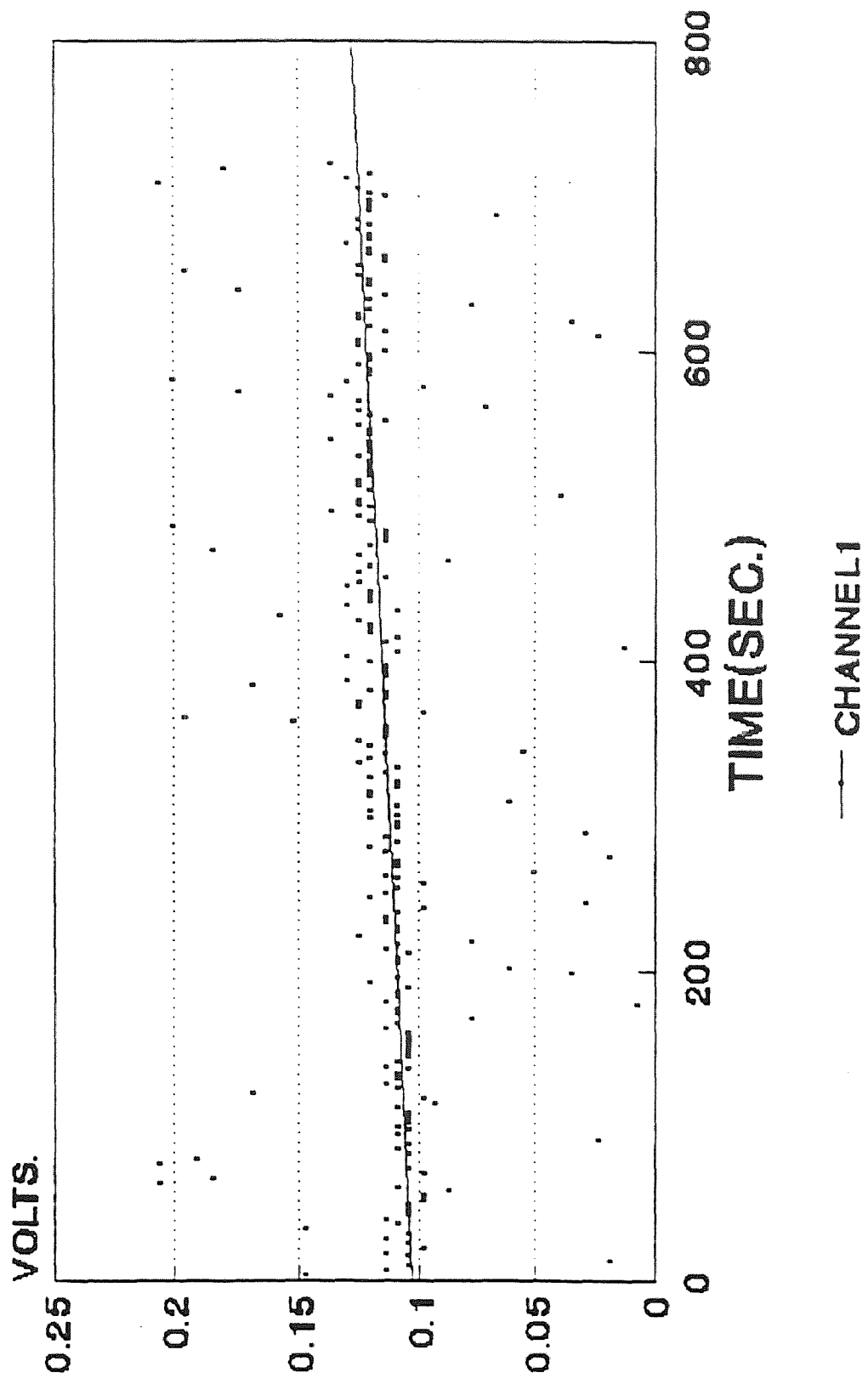


Fig.52 Internal deformation data for F19A

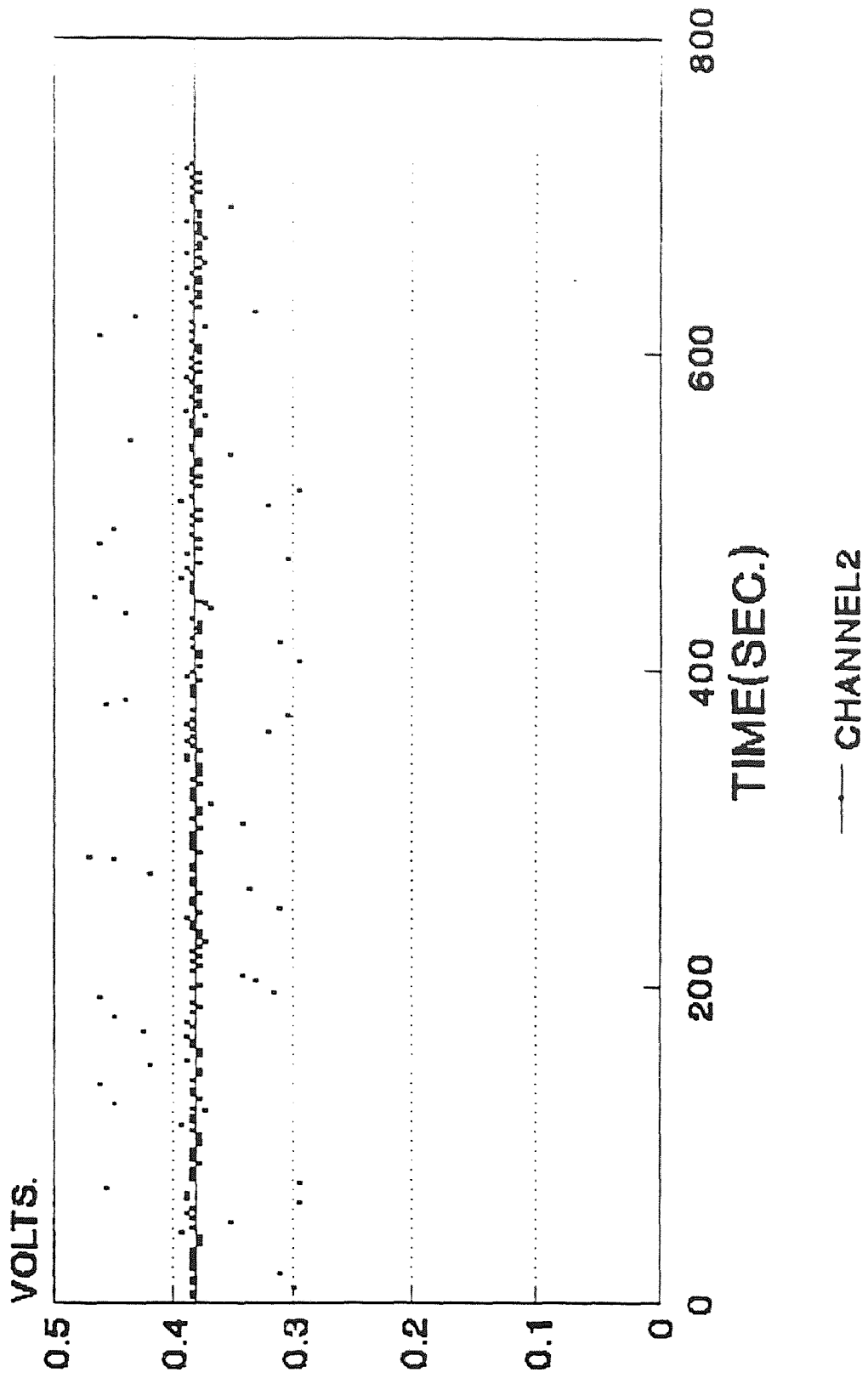


Fig.53 Internal deformation data for F19A

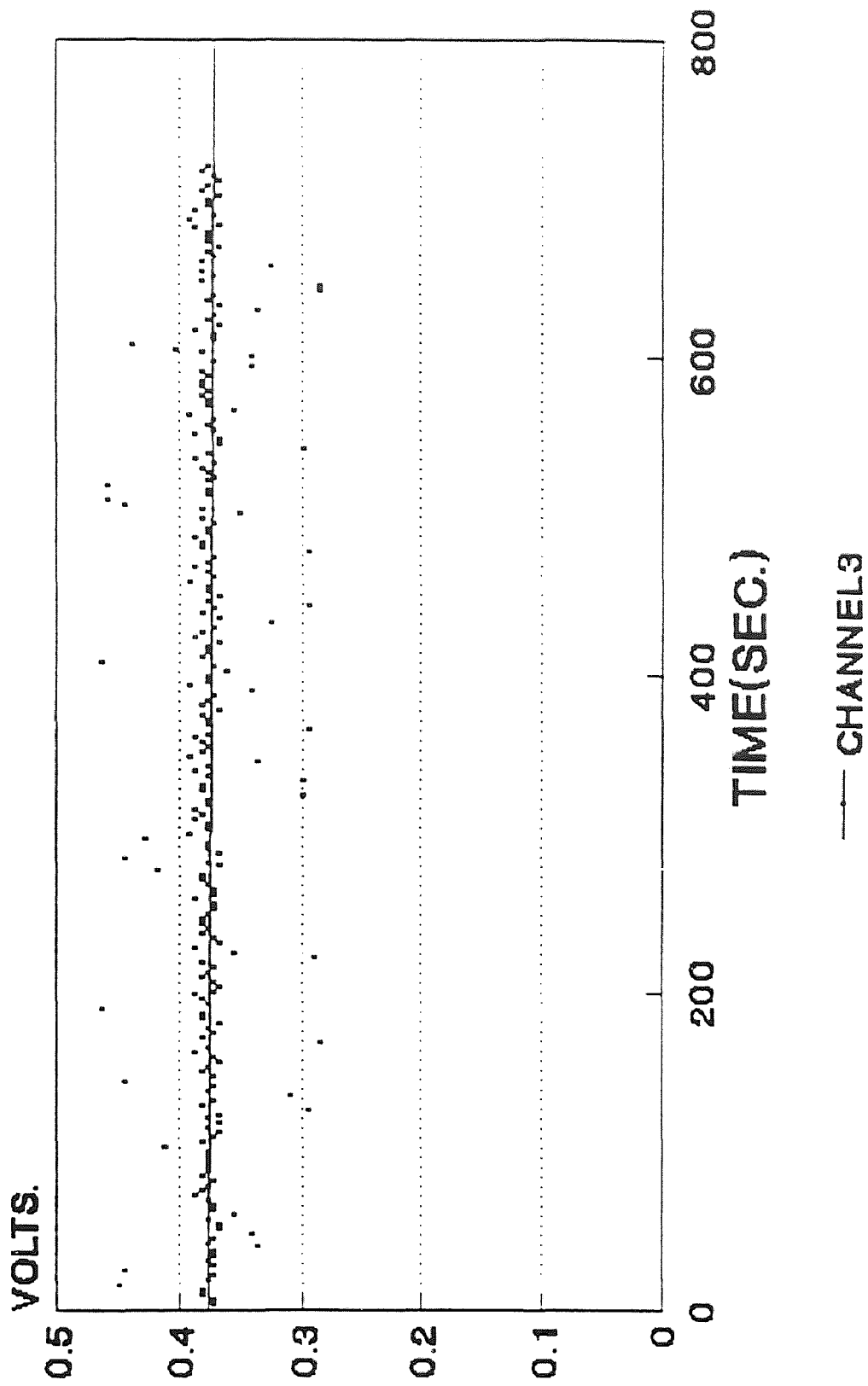


Fig.54 Internal deformation data forF

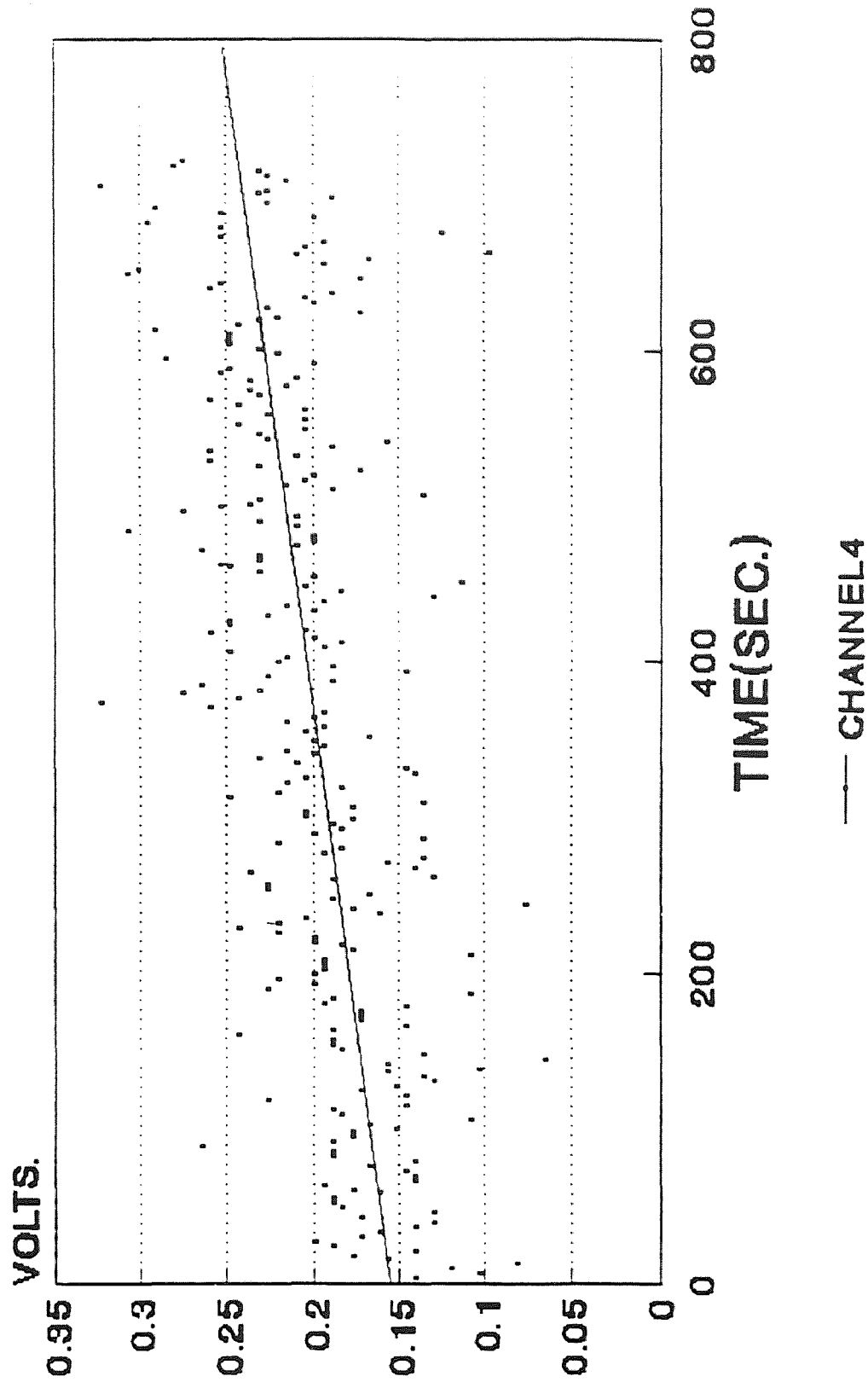


Fig.55 Internal deformation data for F19A

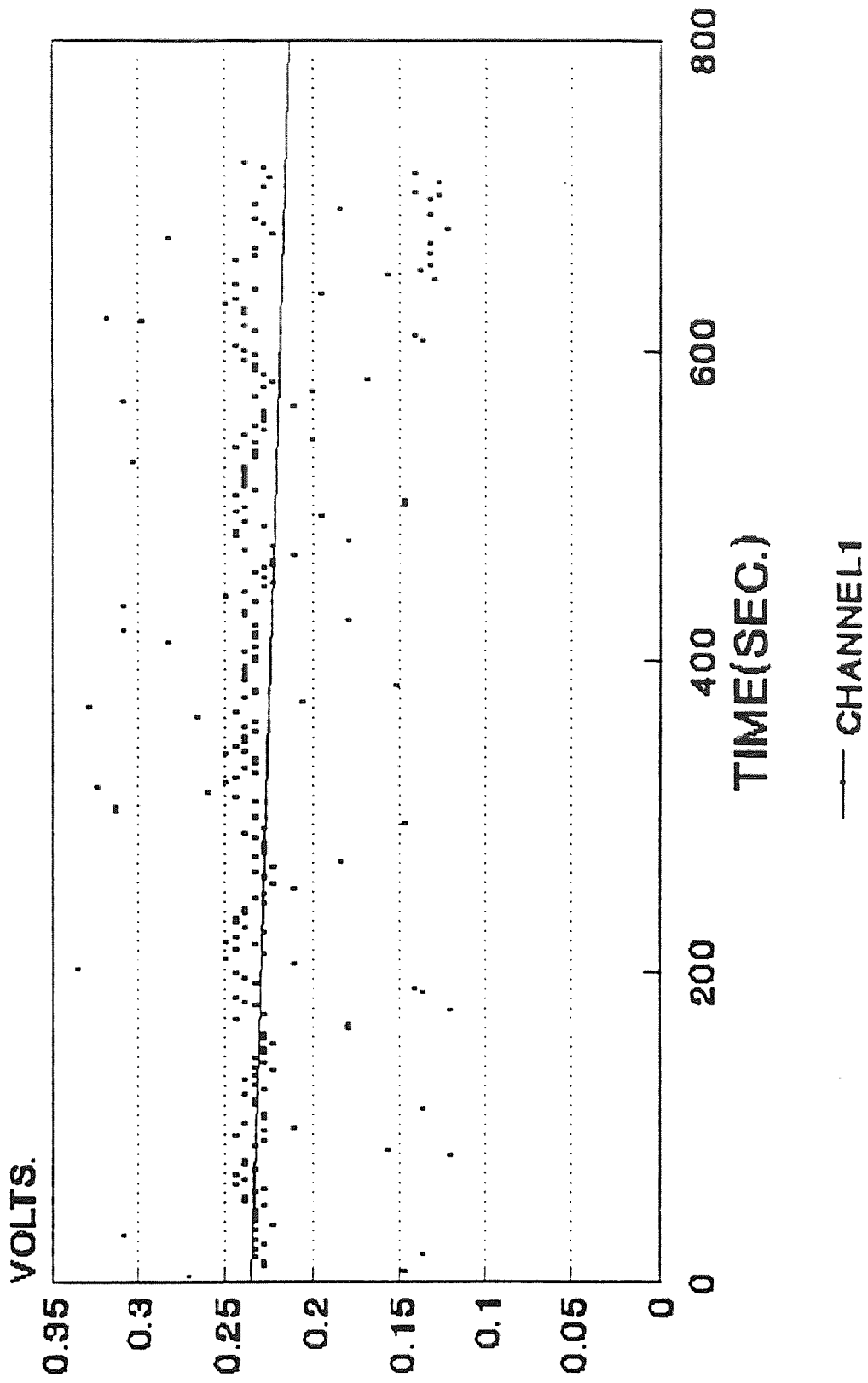


Fig.56 Internal deformation data for19B

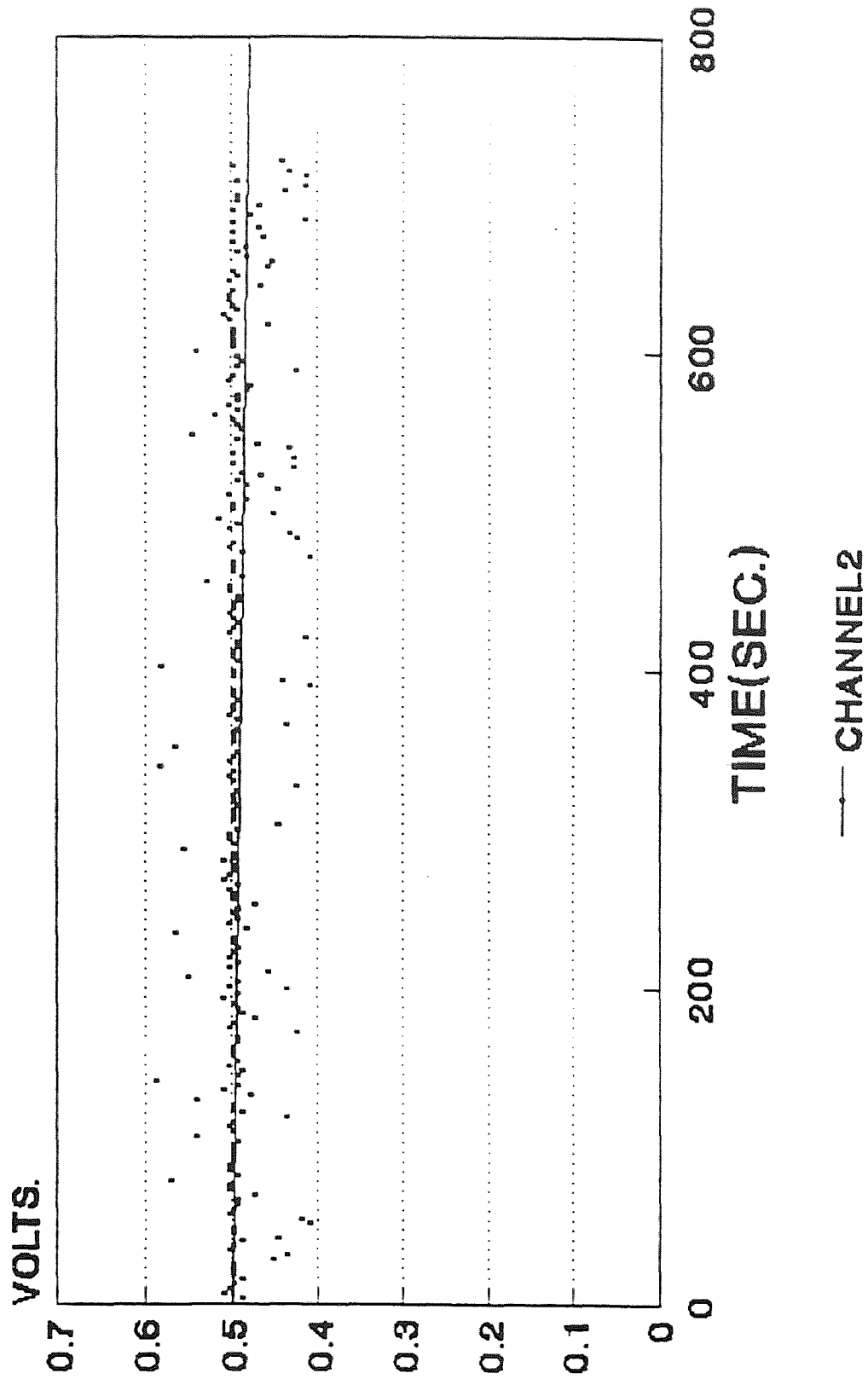


Fig.57 Internal deformation data for F19B

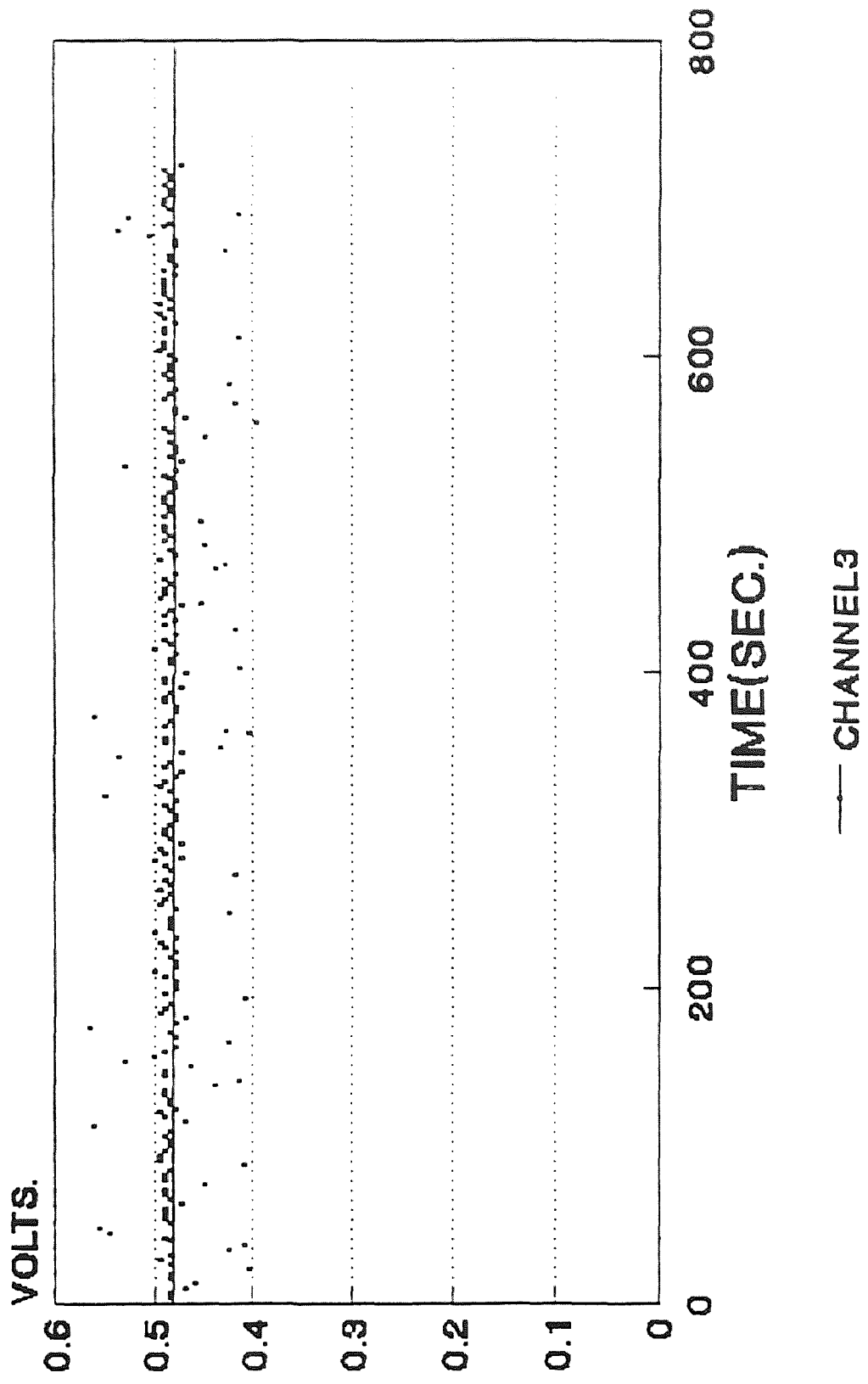


Fig. 58 Internal deformation data for F10B

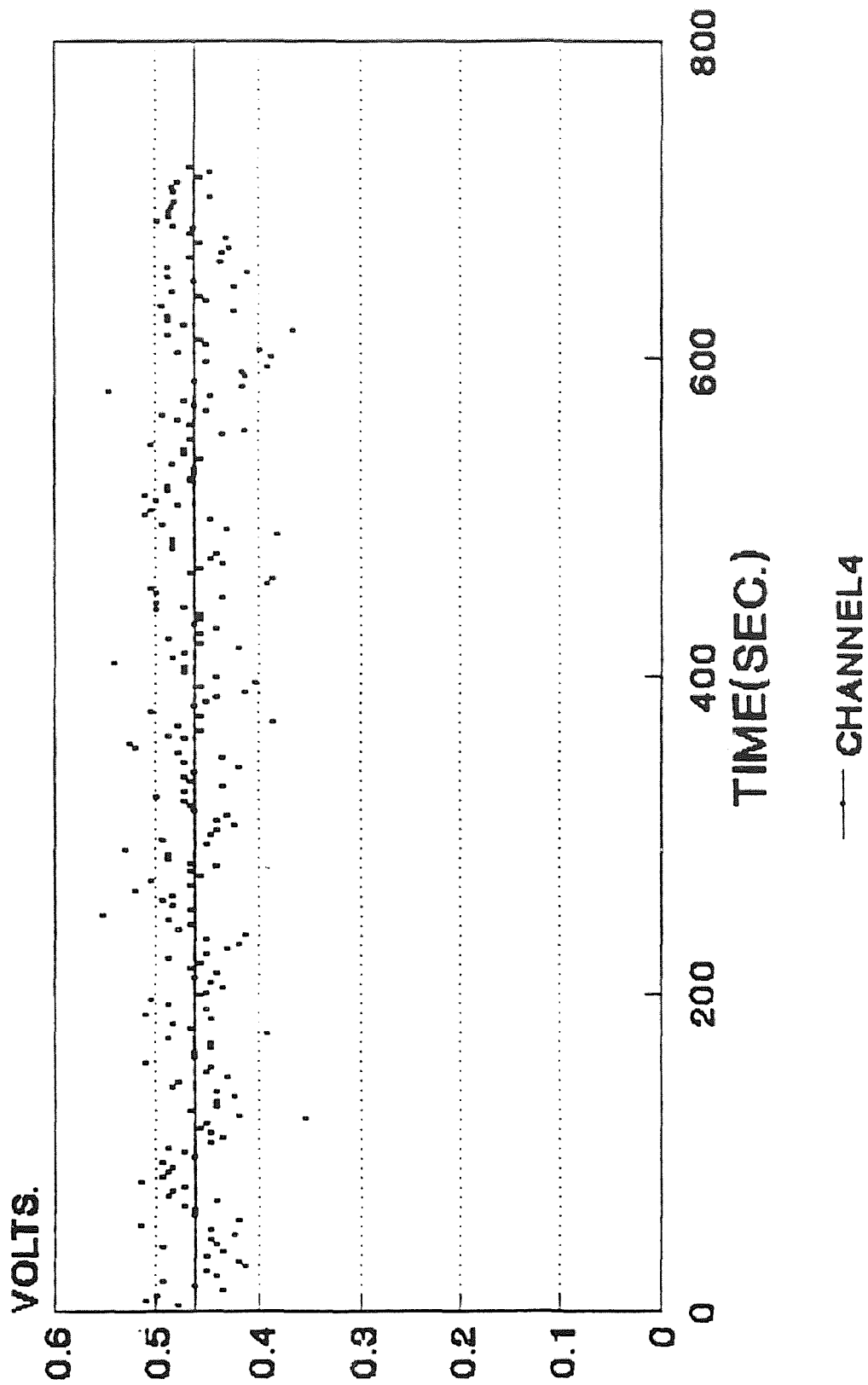


Fig.59 Internal deformation data for F107

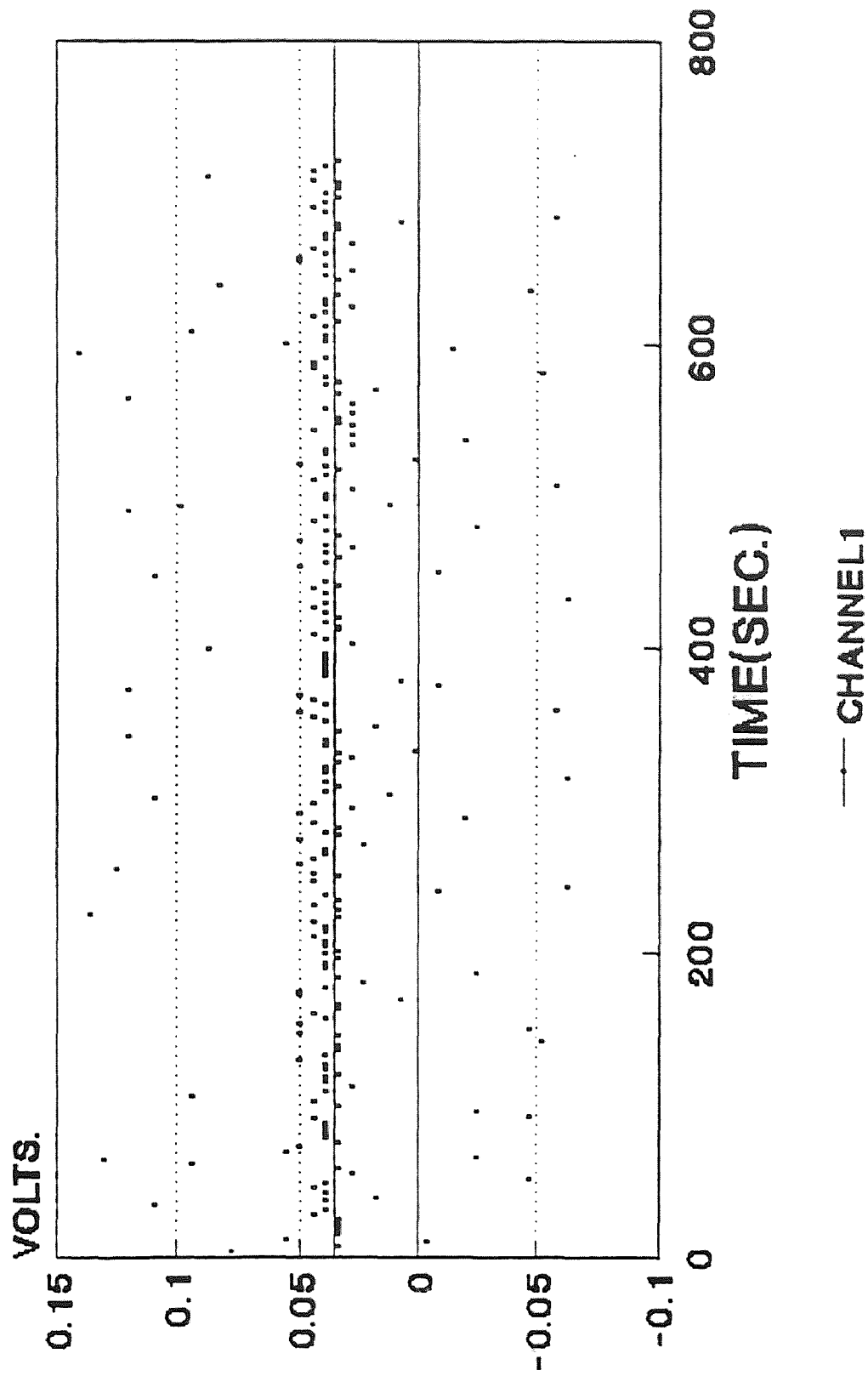


Fig.60 Internal deformation data for F19C

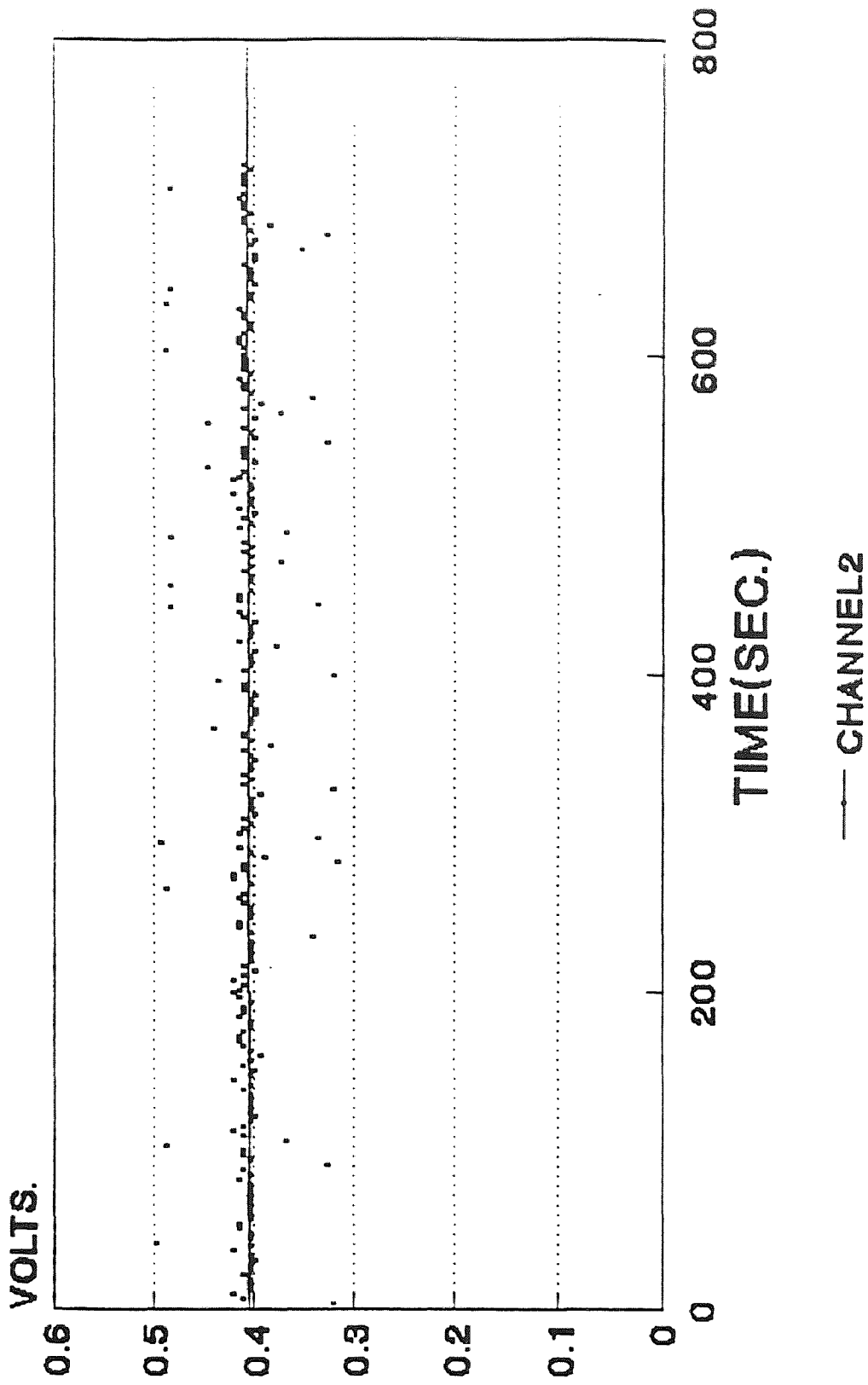


Fig.61 Internal deformation data for F18C

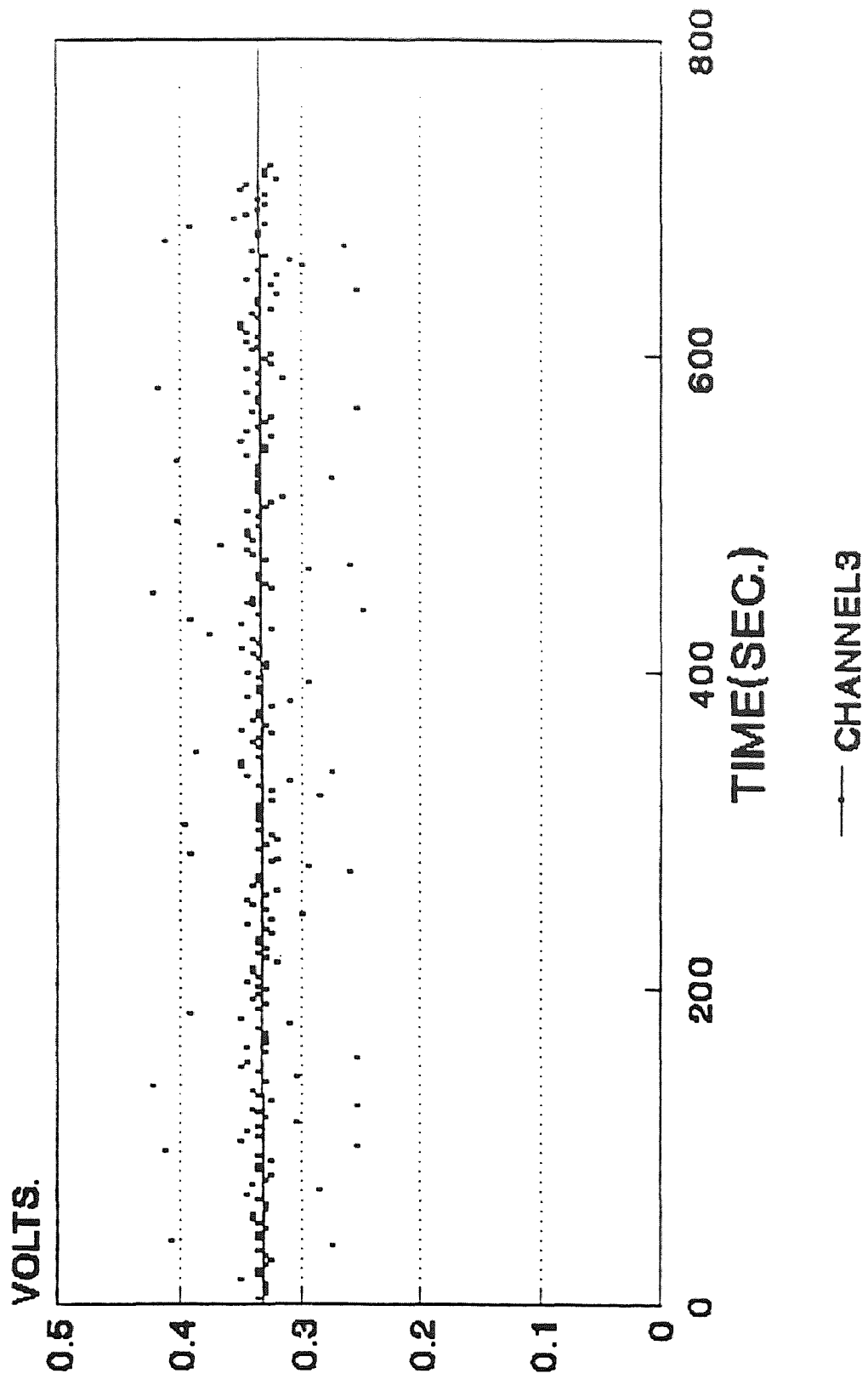


Fig. 62 Internal deformation data F19C

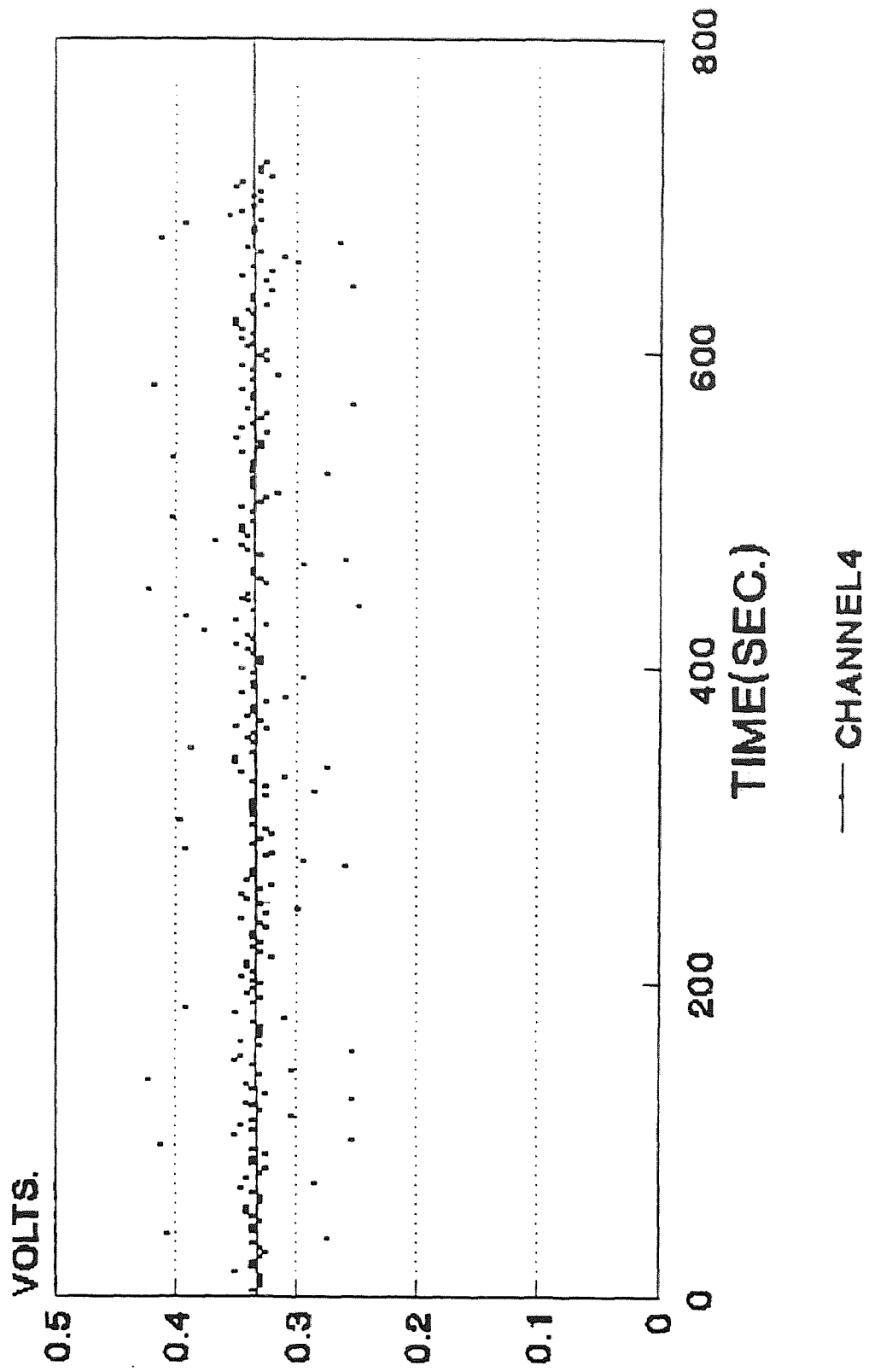


Fig.63 Internal deformation data for T2C

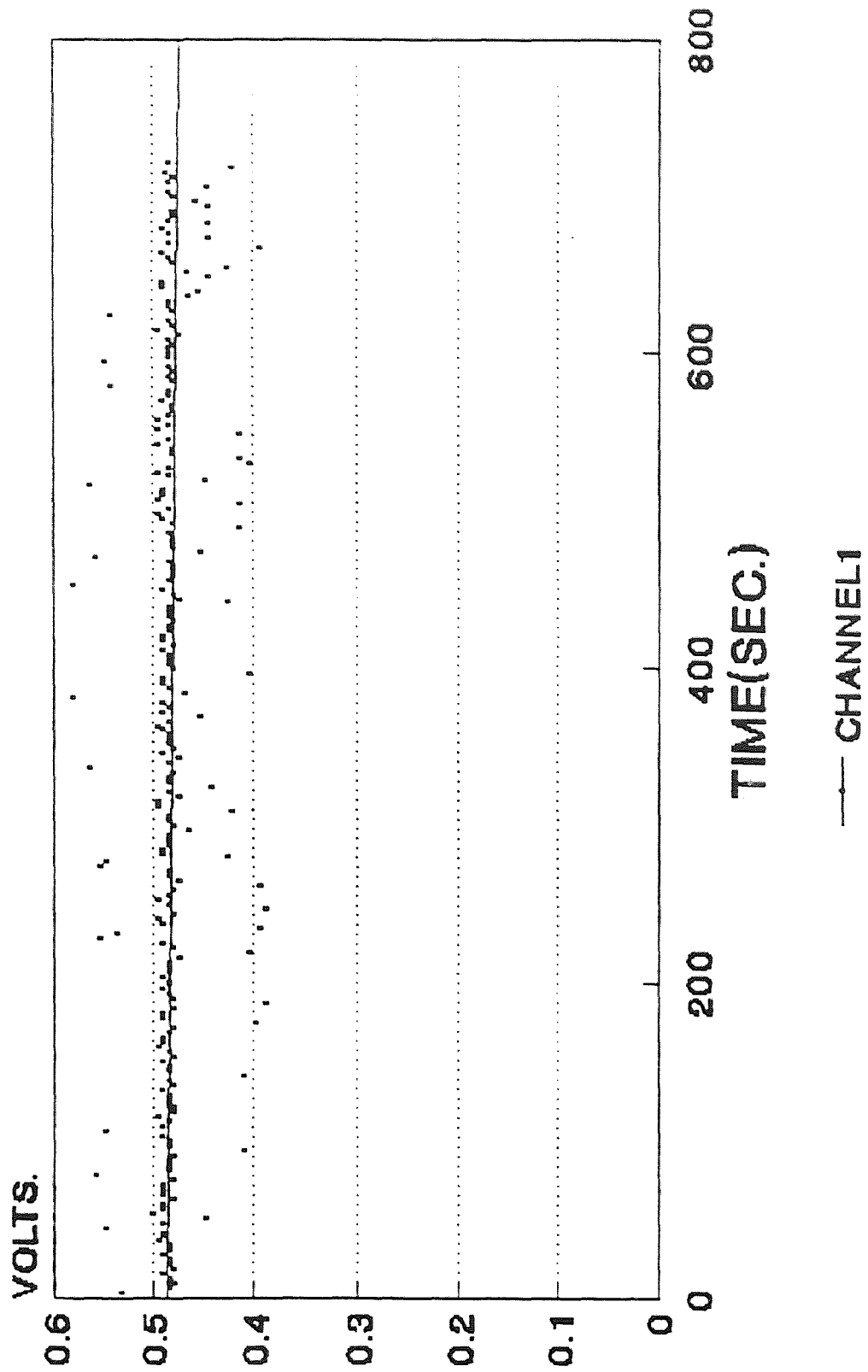


Fig.64 Internal deformation data for F10D

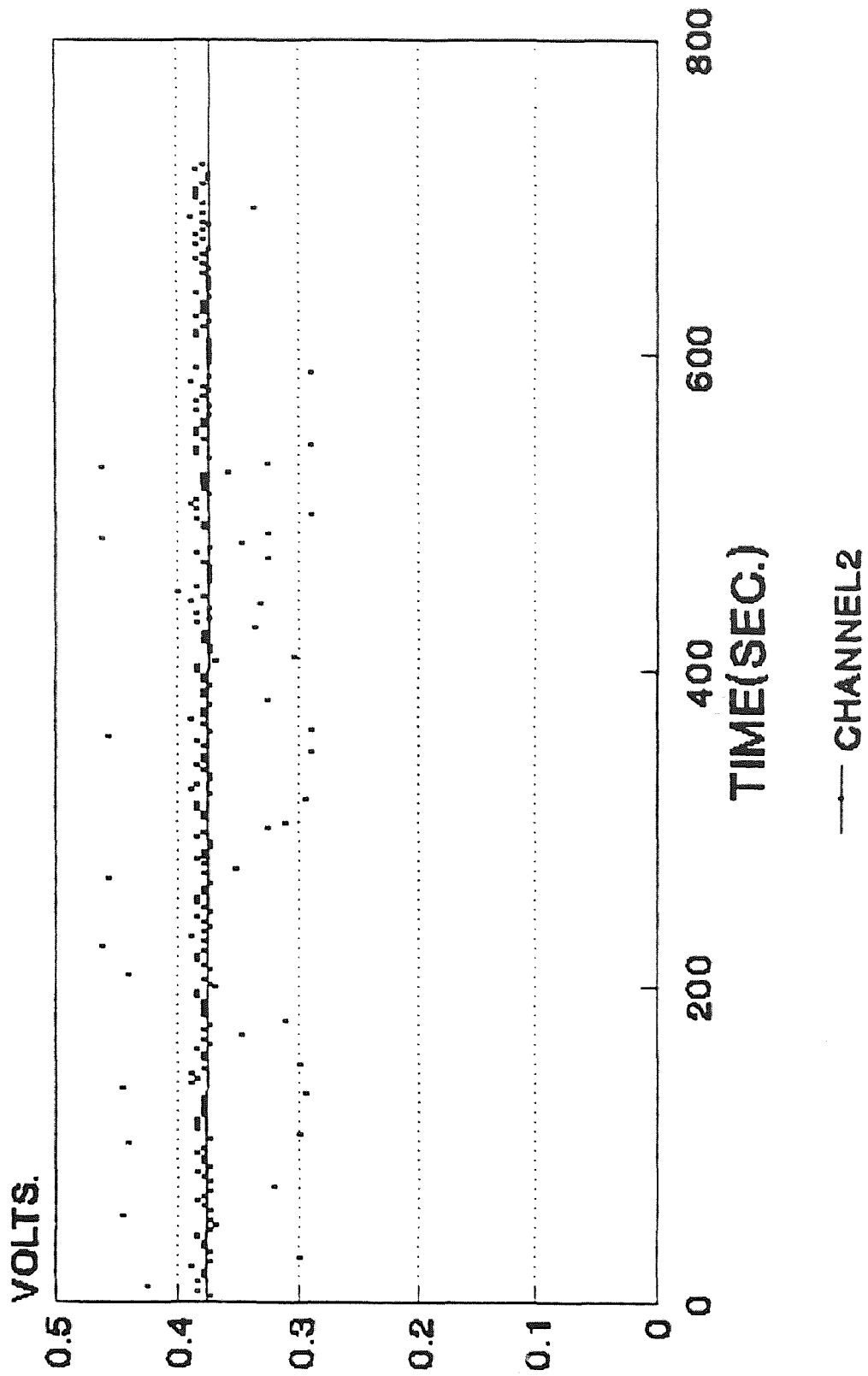


Fig.65 Internal deformation data for F19

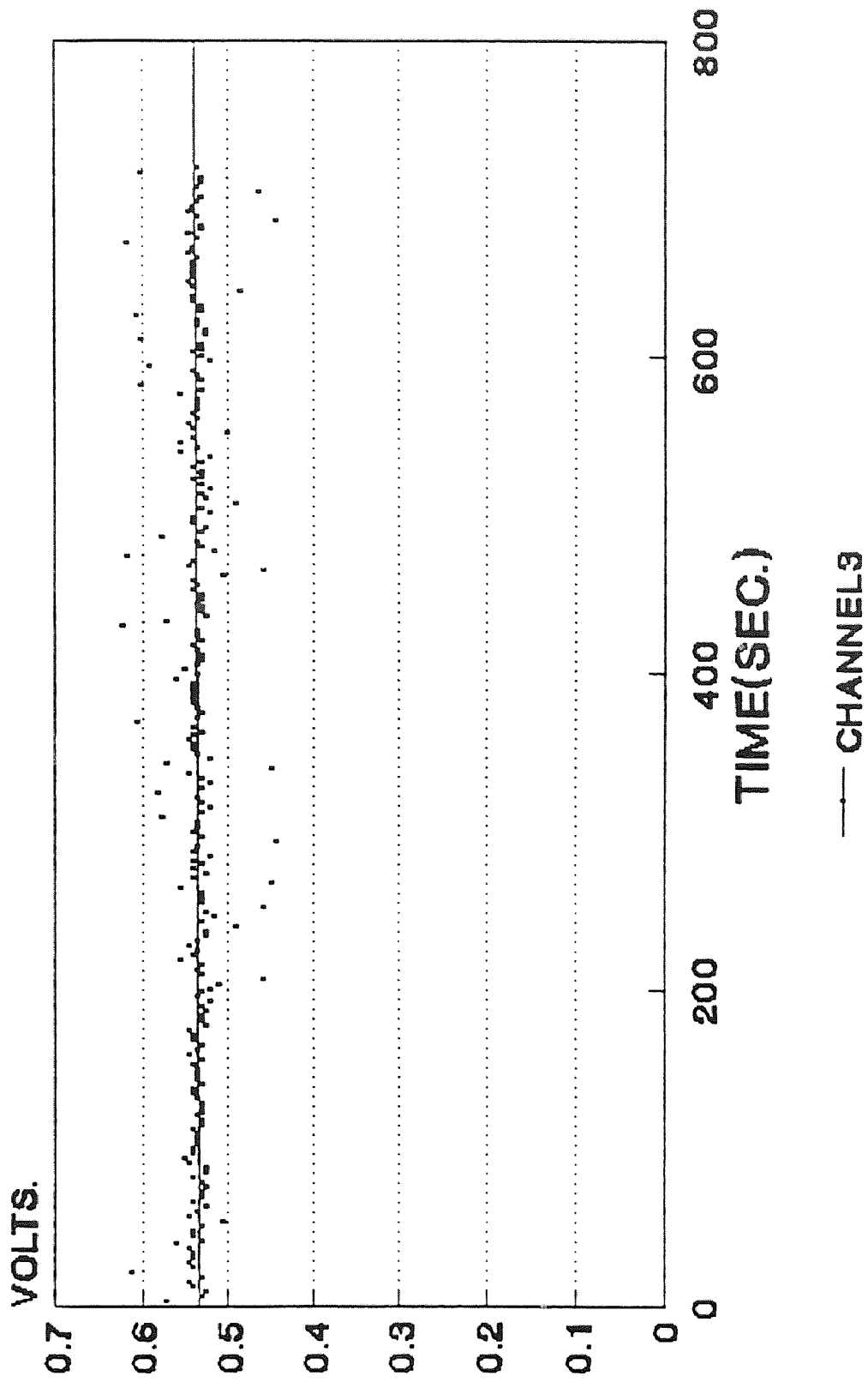


Fig.66 Internal deformation data for F19D

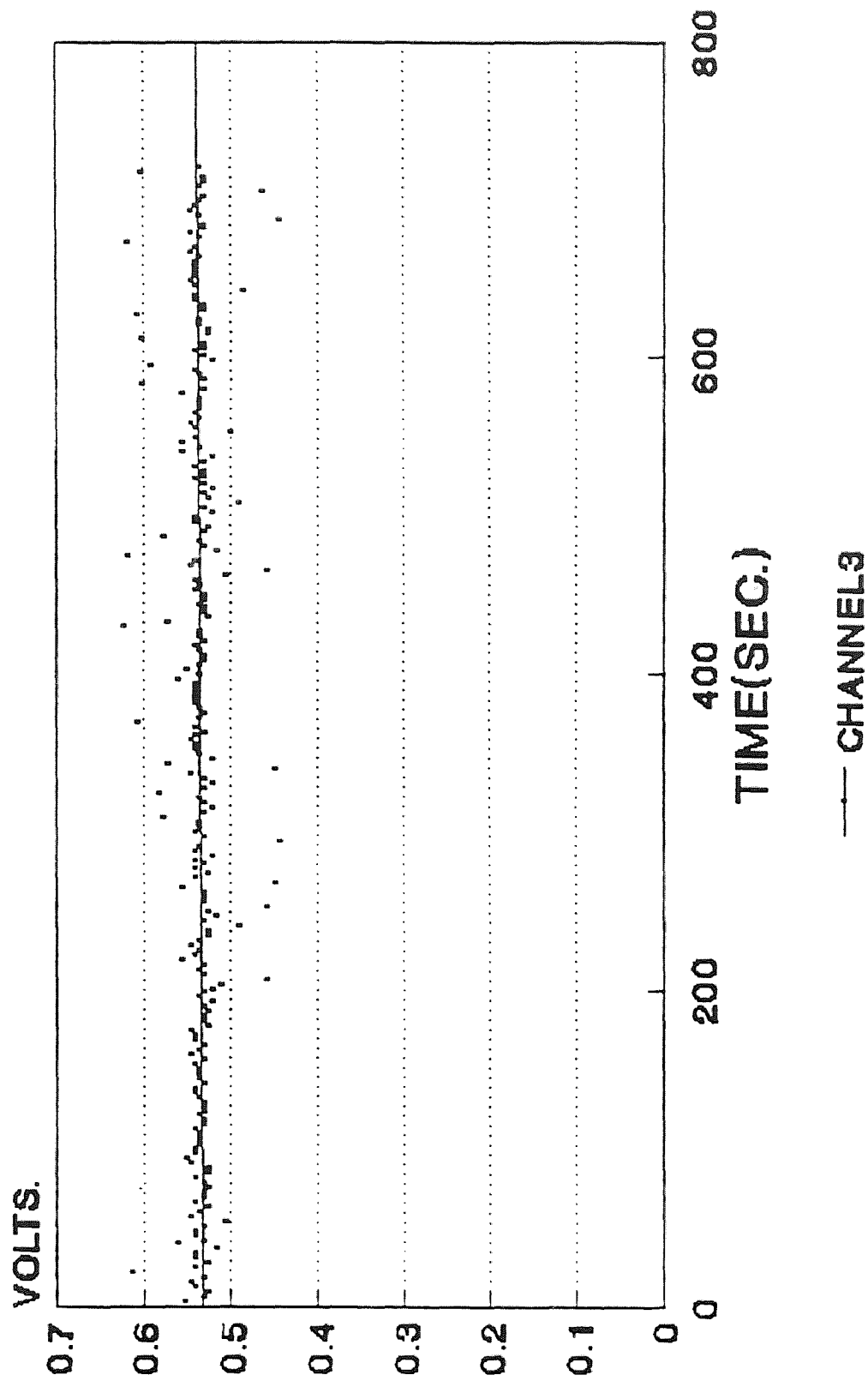


Fig.67 Internal deformation data for F19D

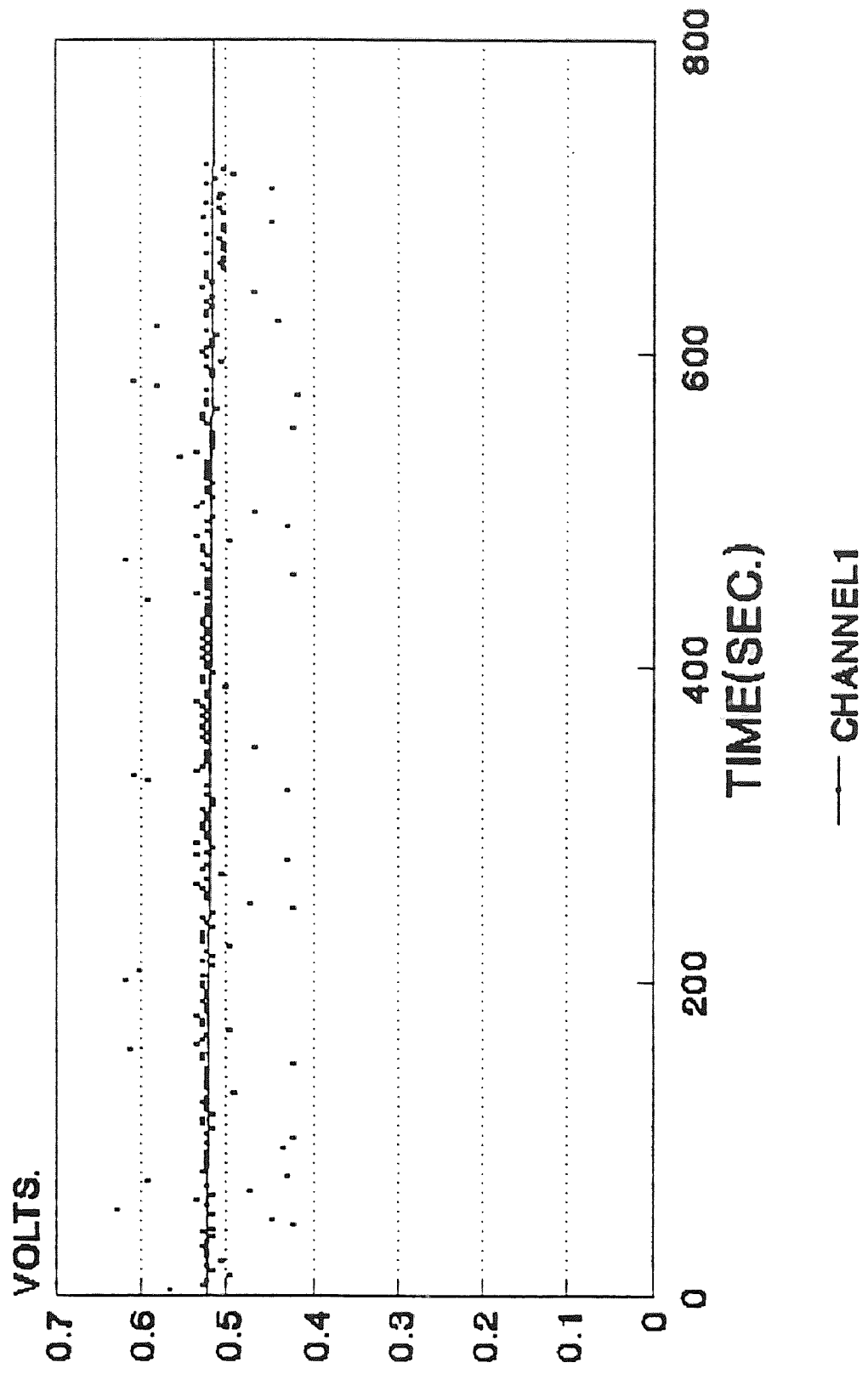


Fig.68 Internal deformation data for F28A

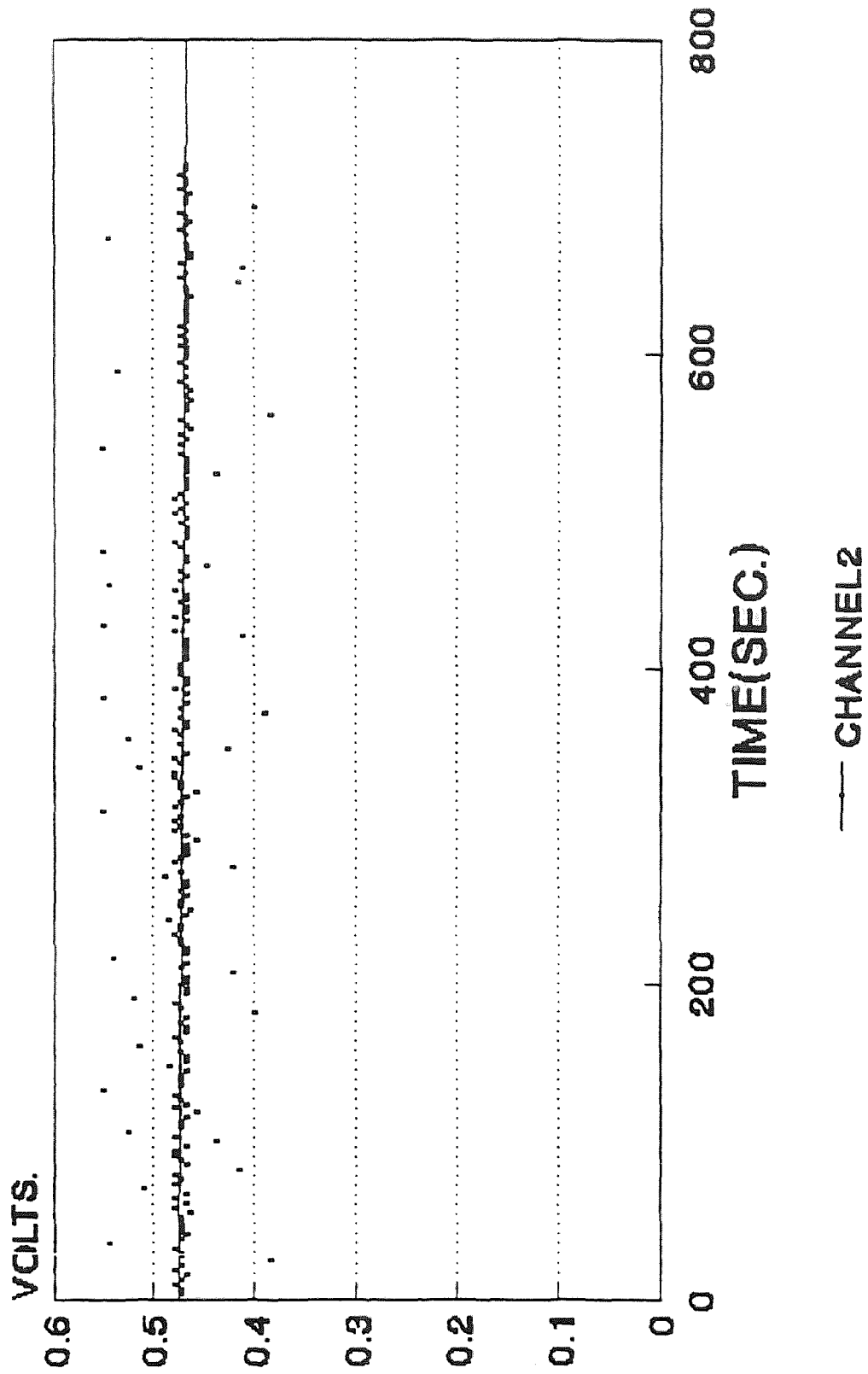


Fig. 69 Internal deformation data for F2.

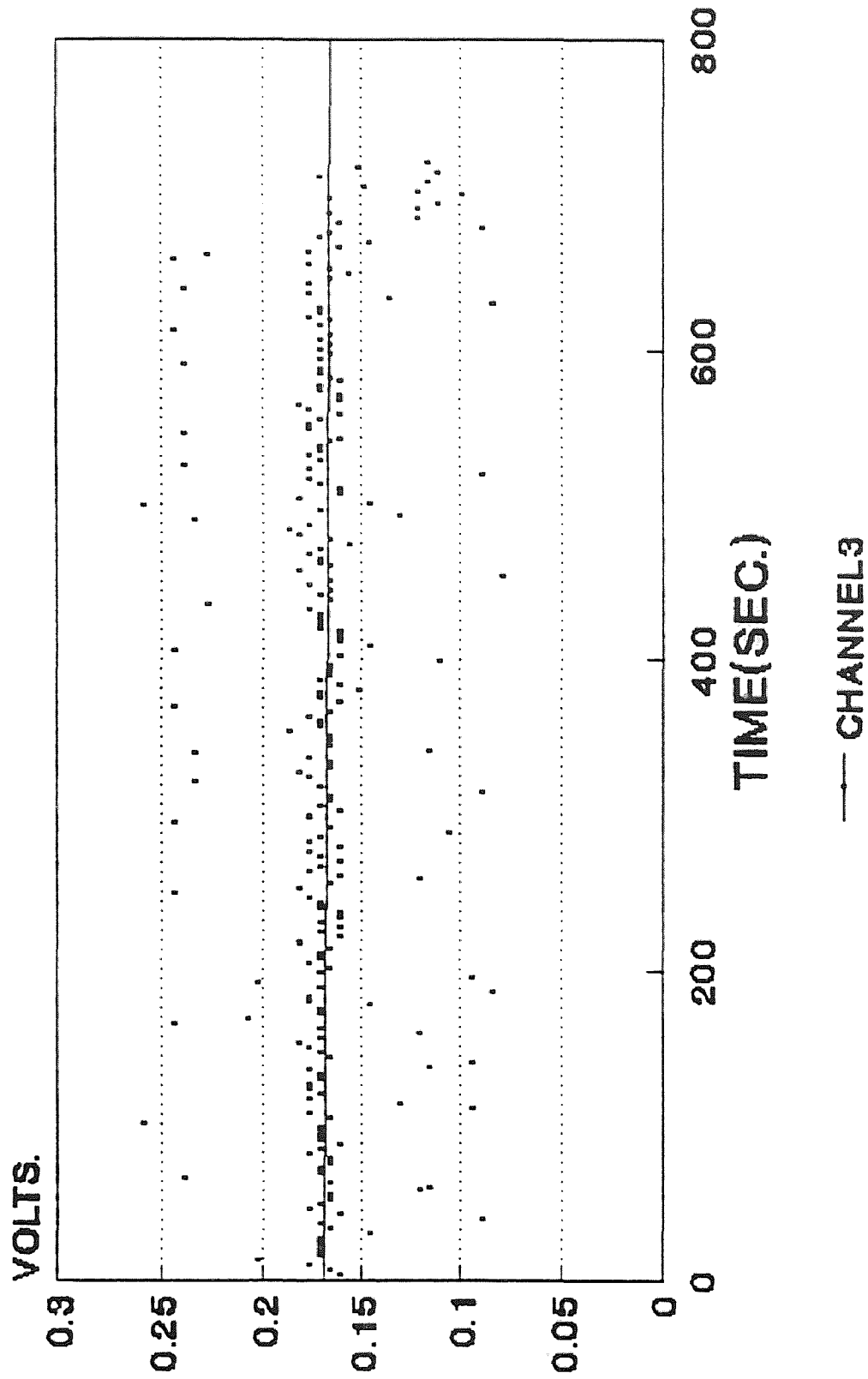


Fig.70 Internal deformation data for F28

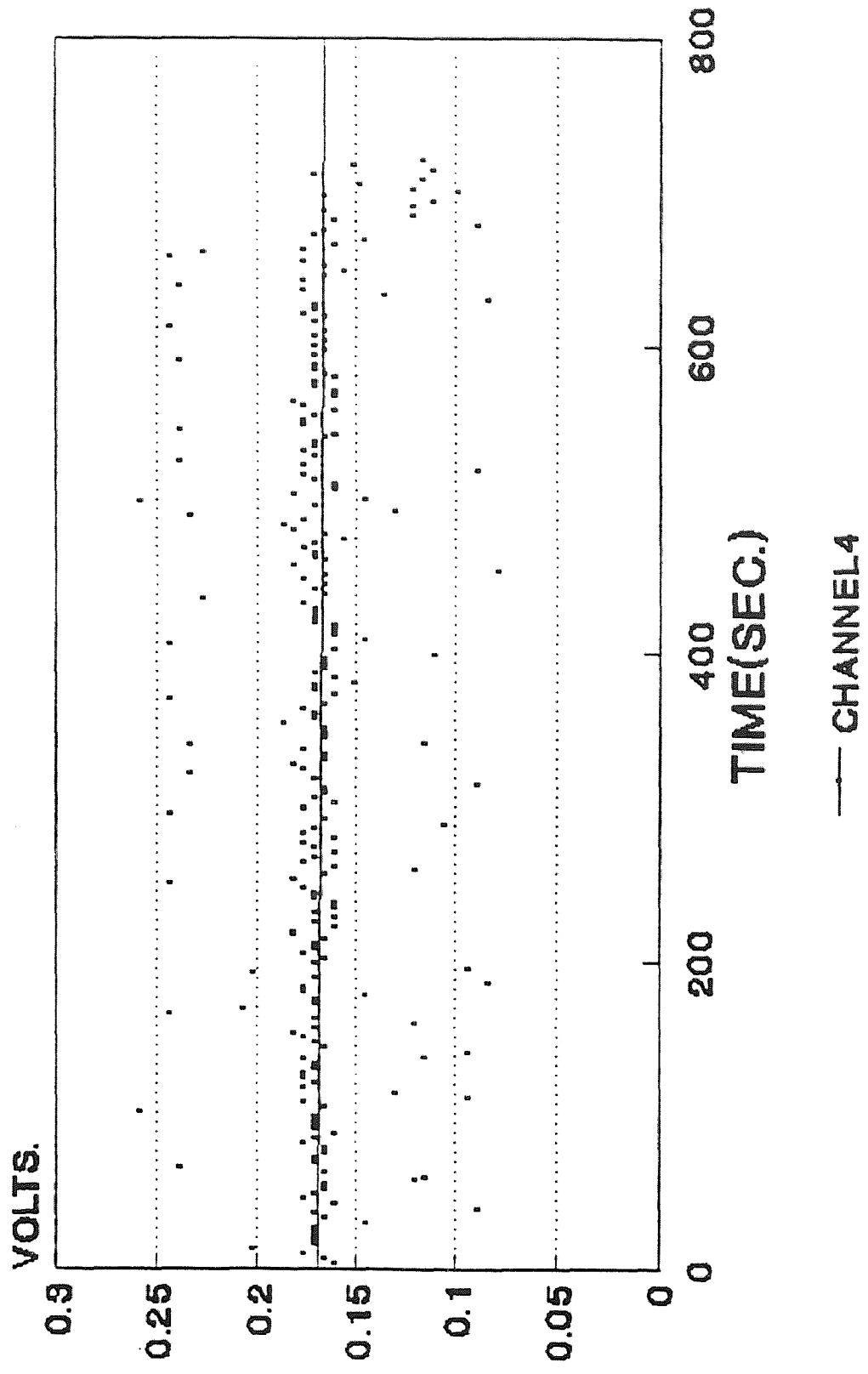


Fig.71 Internal deformation data for i 3A

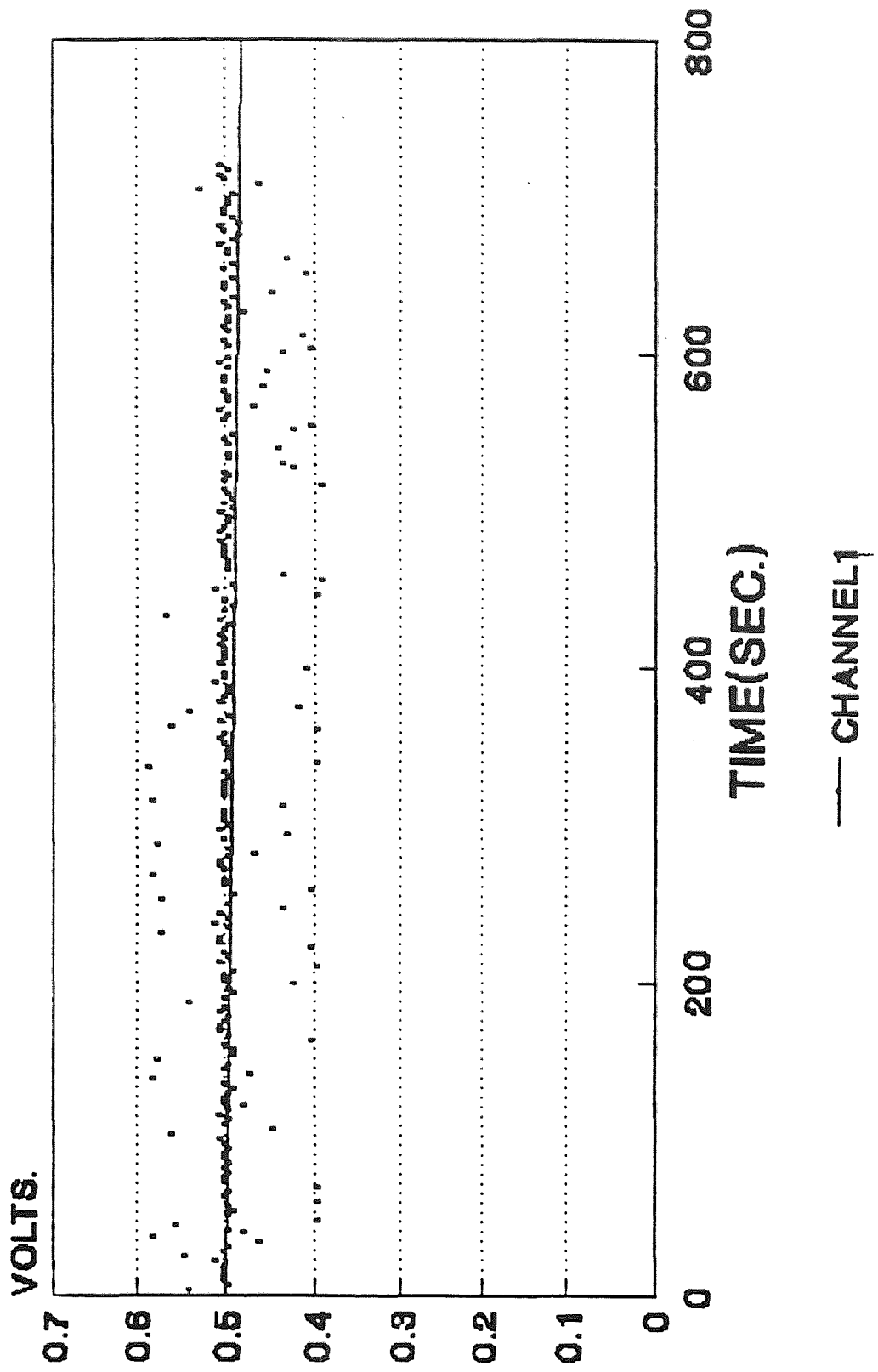


Fig.72 Internal deformation data forF.

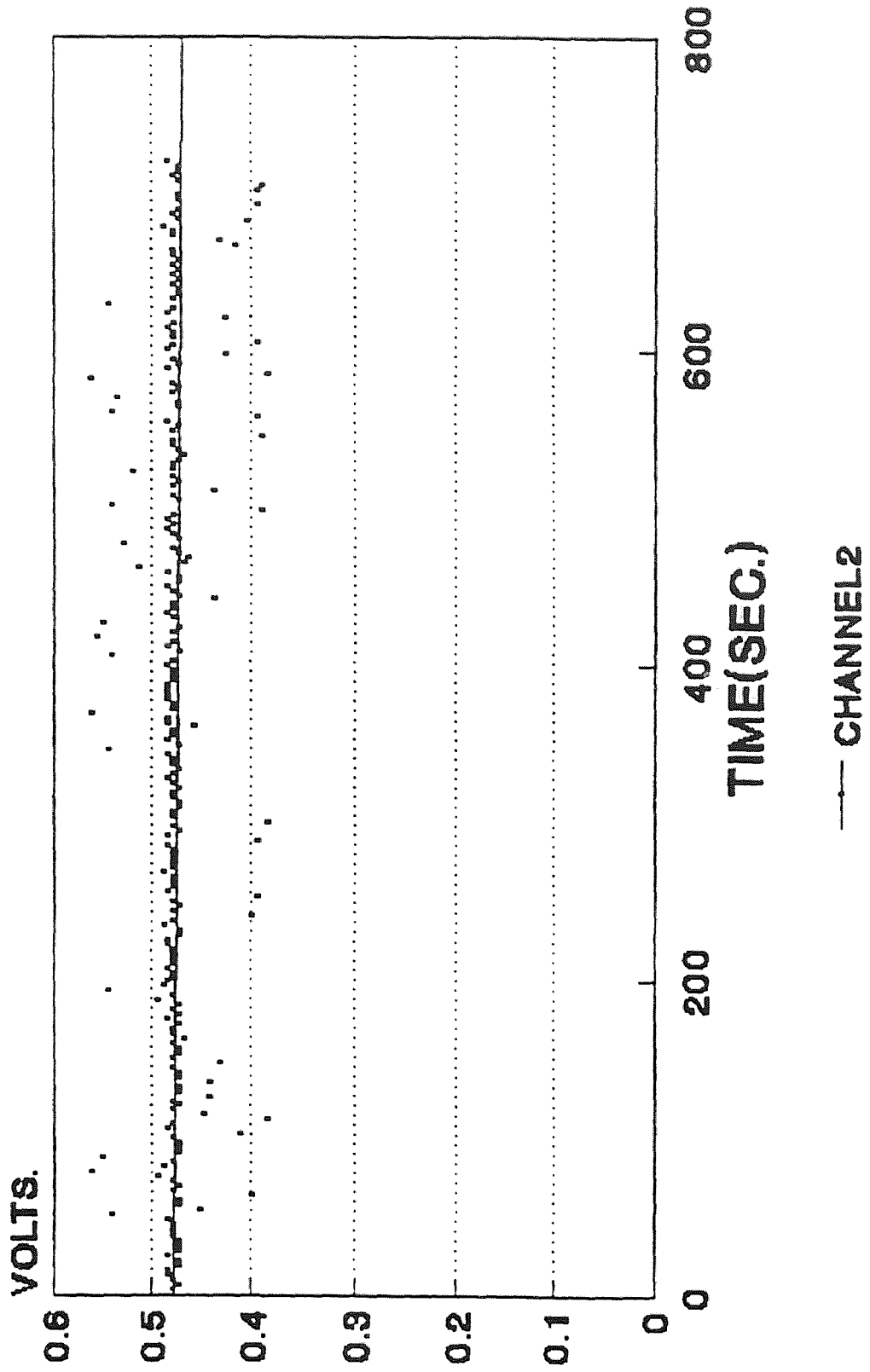


Fig.73 Internal deformation data for F28B

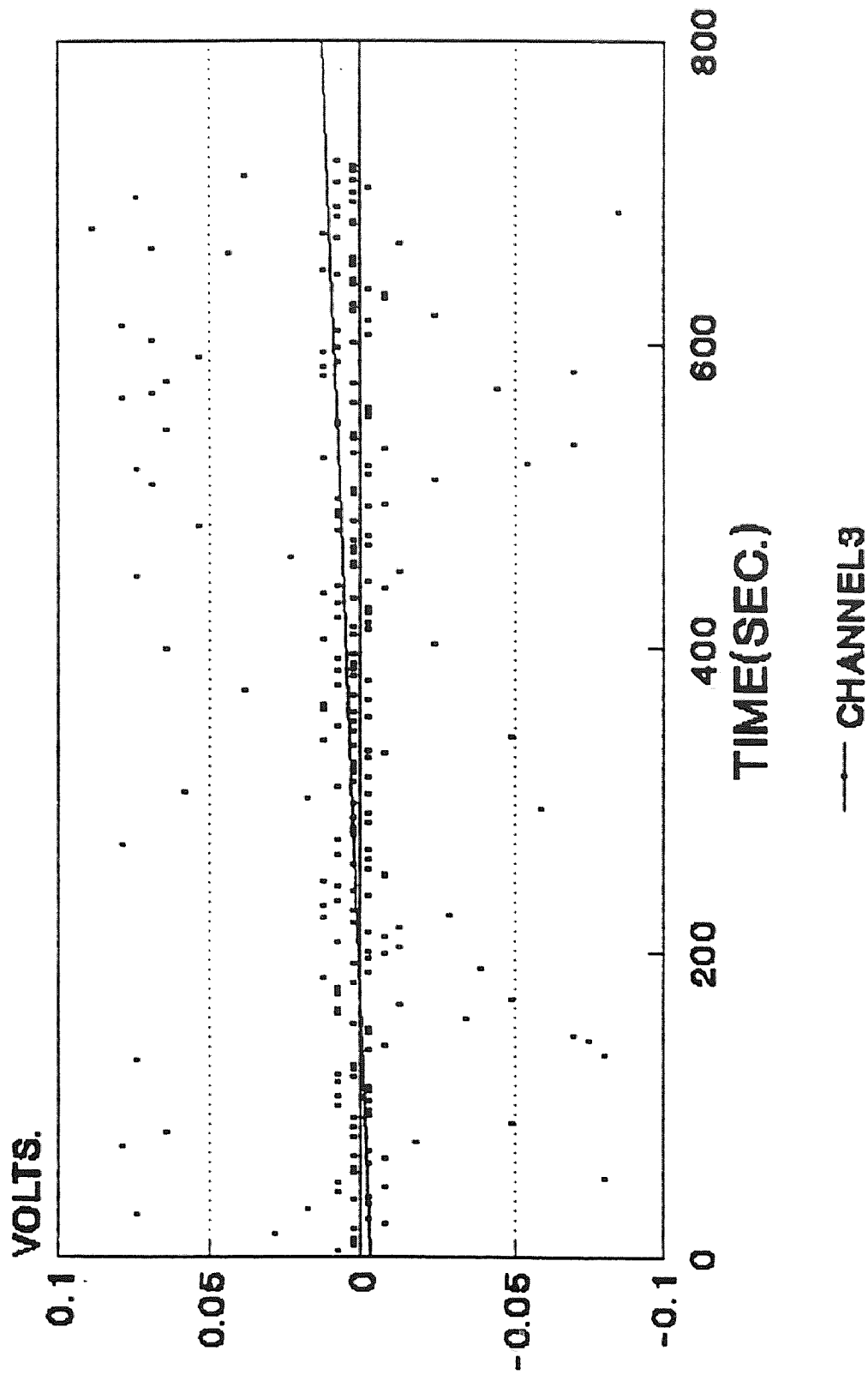


Fig.7.4 Internal deformation data for F28B

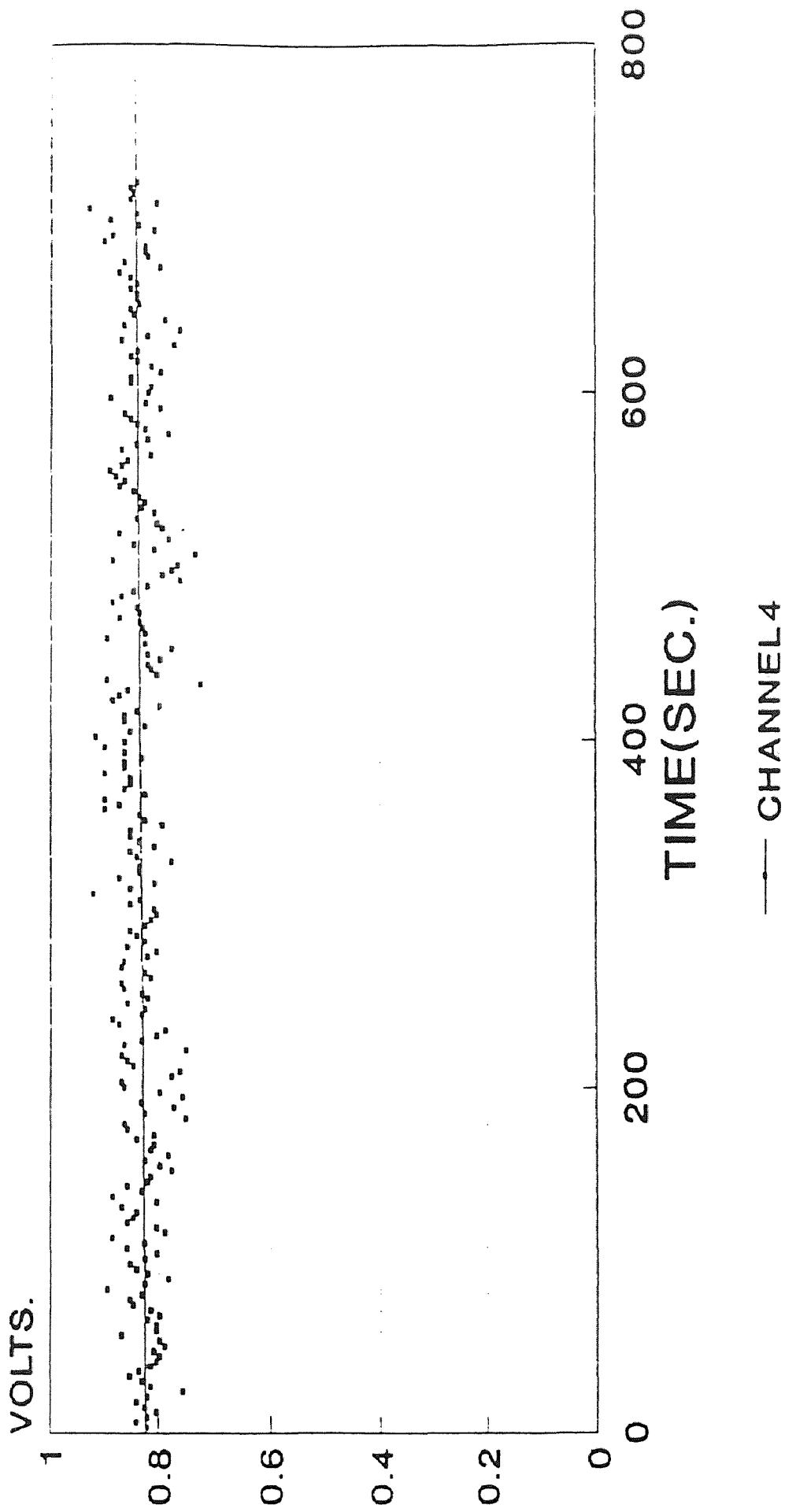


Fig.75 Internal deformation data for F28B

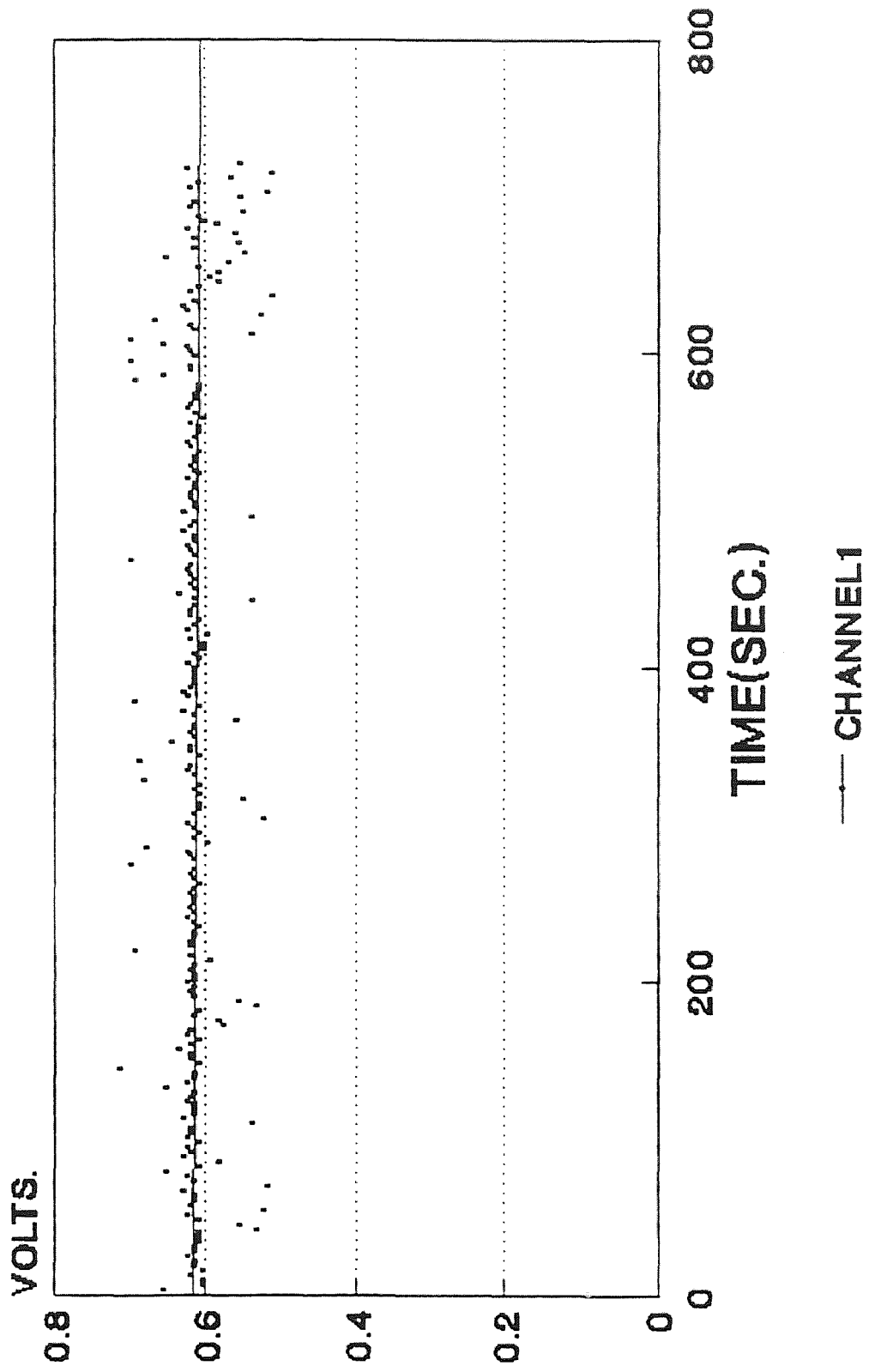


Fig.76 Internal deformation data ForF28C

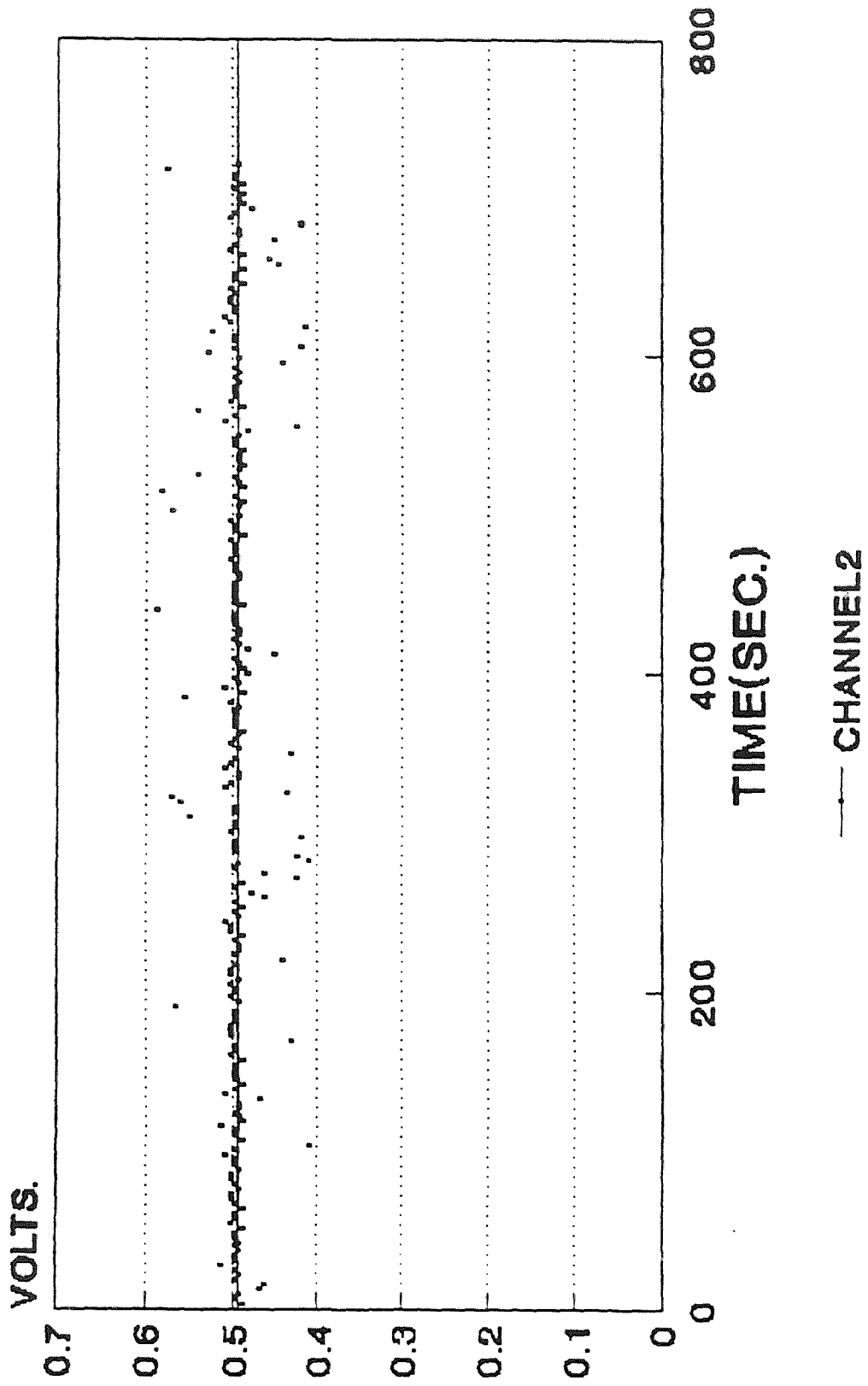


Fig.77 Internal deformation data for F28C

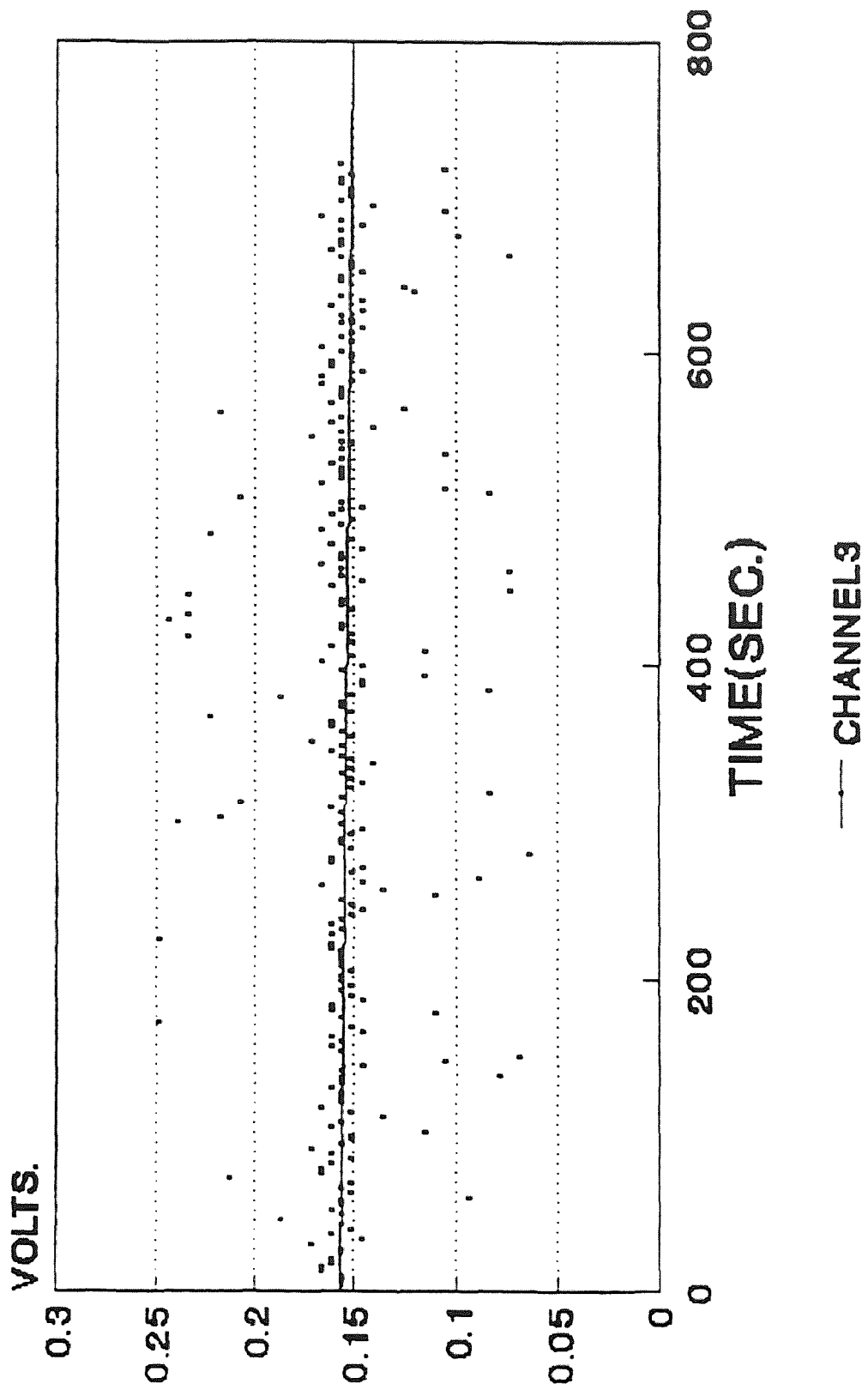


Fig.78 Internal deformation data for F28C

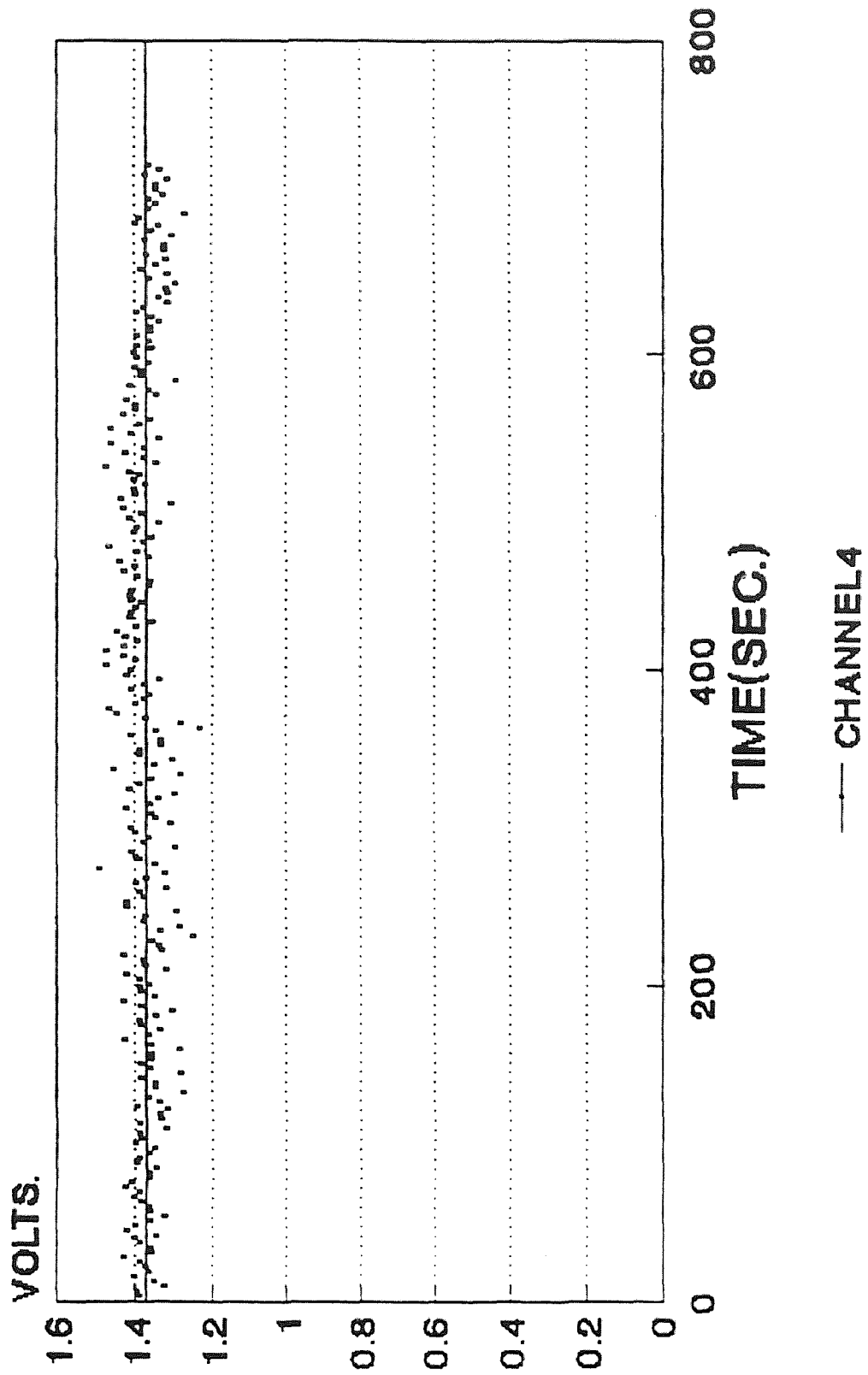


Fig.79 Internal deformation data for F28C

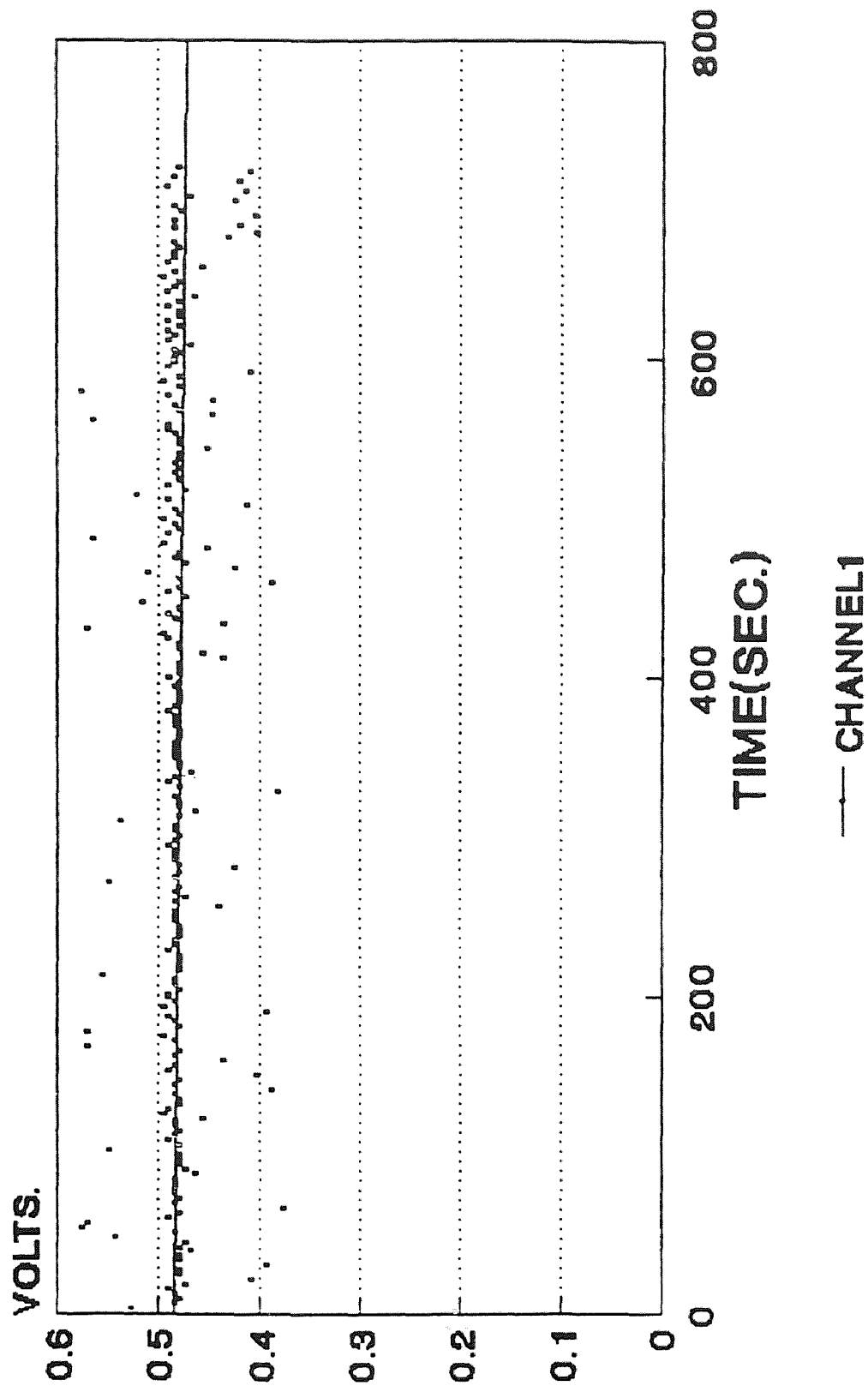


Fig.80 Internal deformation data for M1A

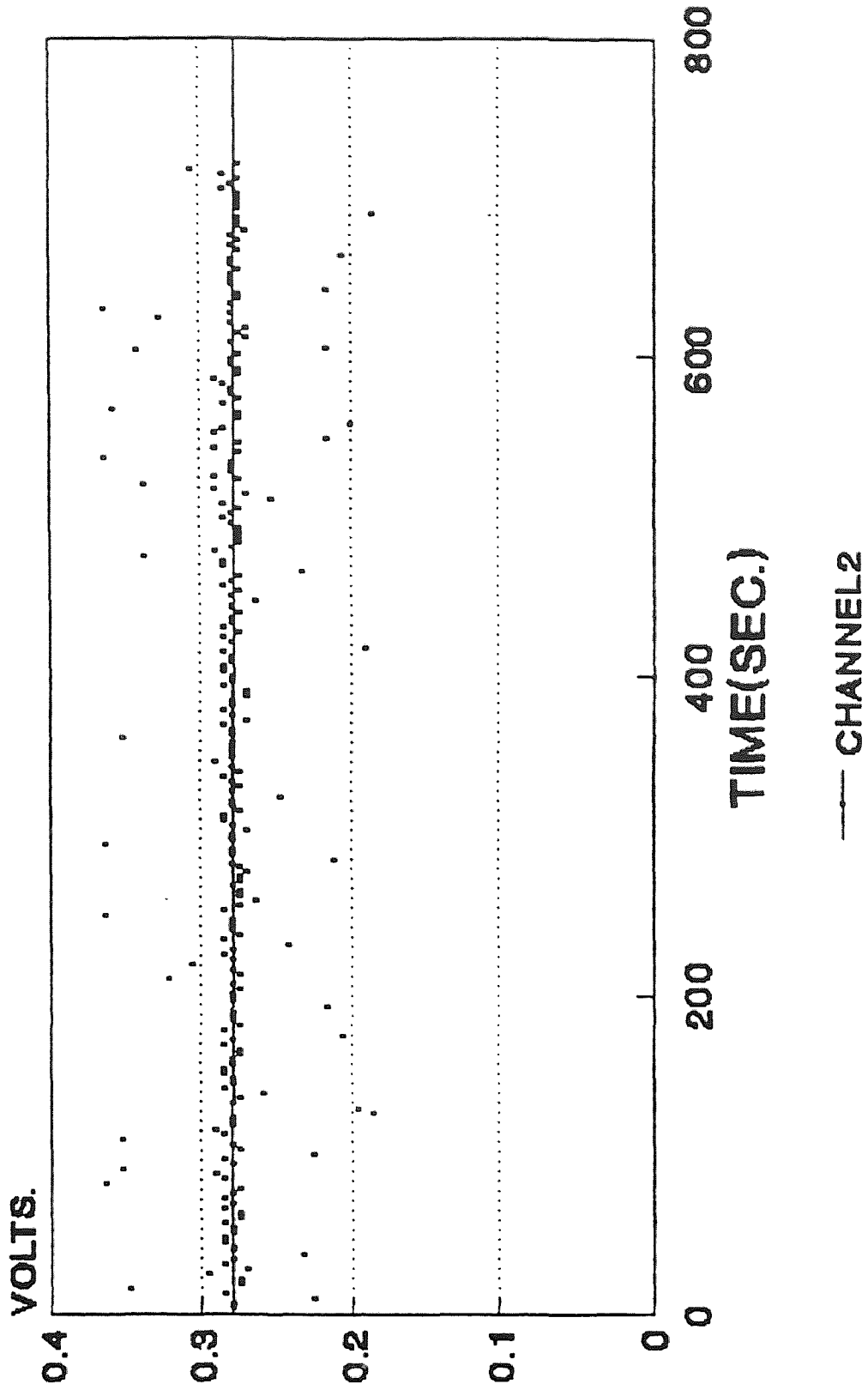


Fig.81 Internal deformation data fo.

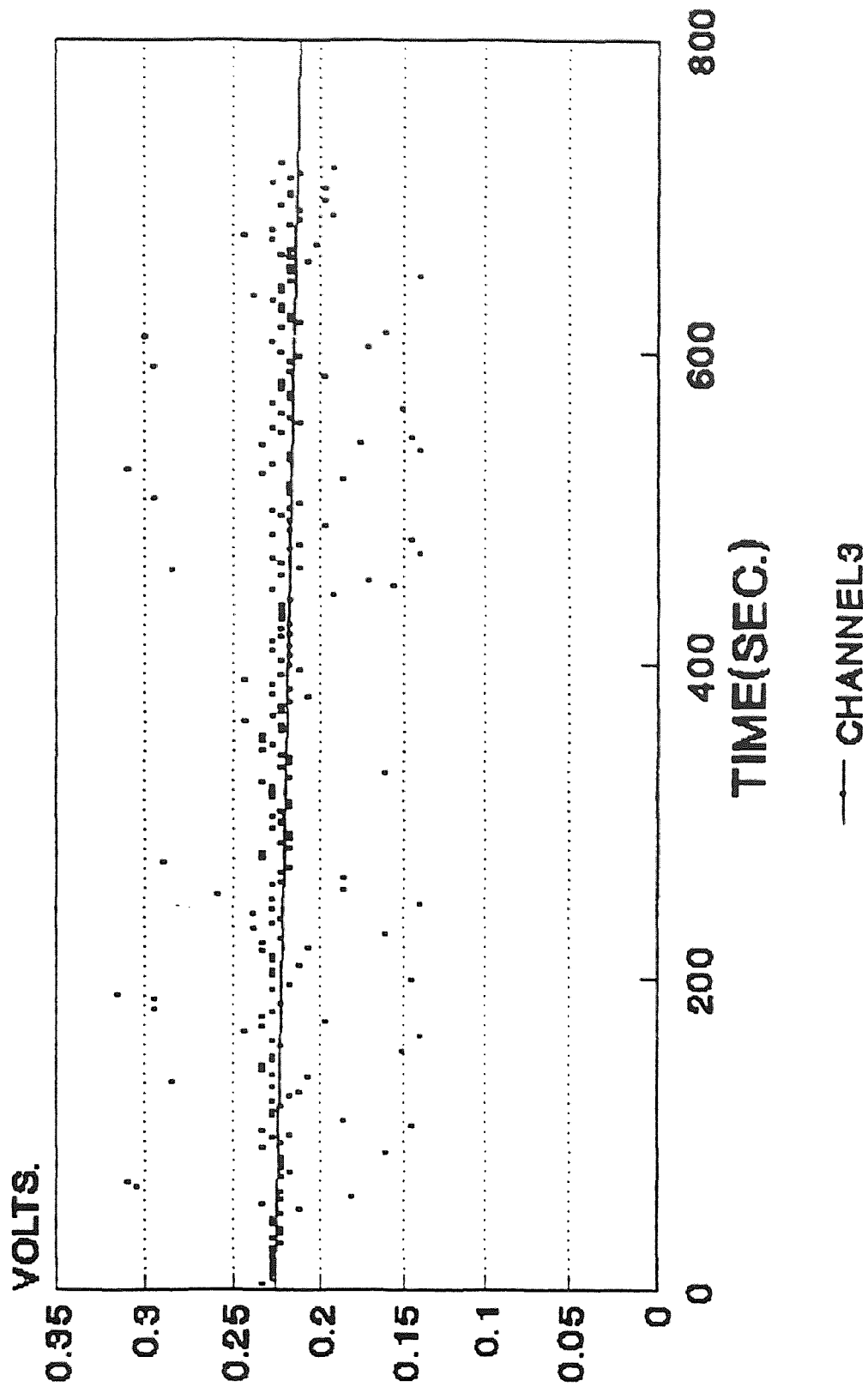


Fig.82 Internal deformation data fo

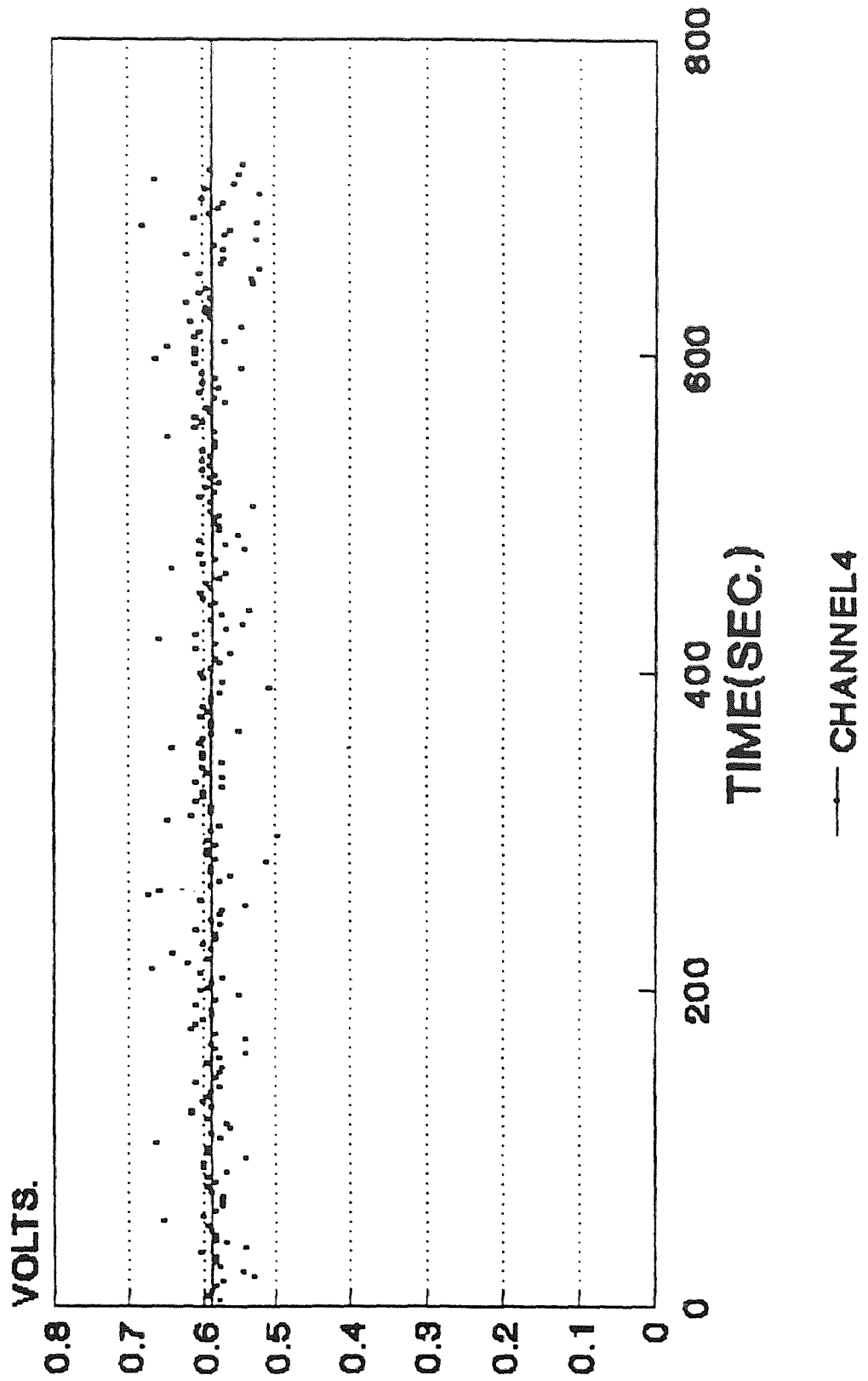


Fig.83 Internal deformation data for M1A

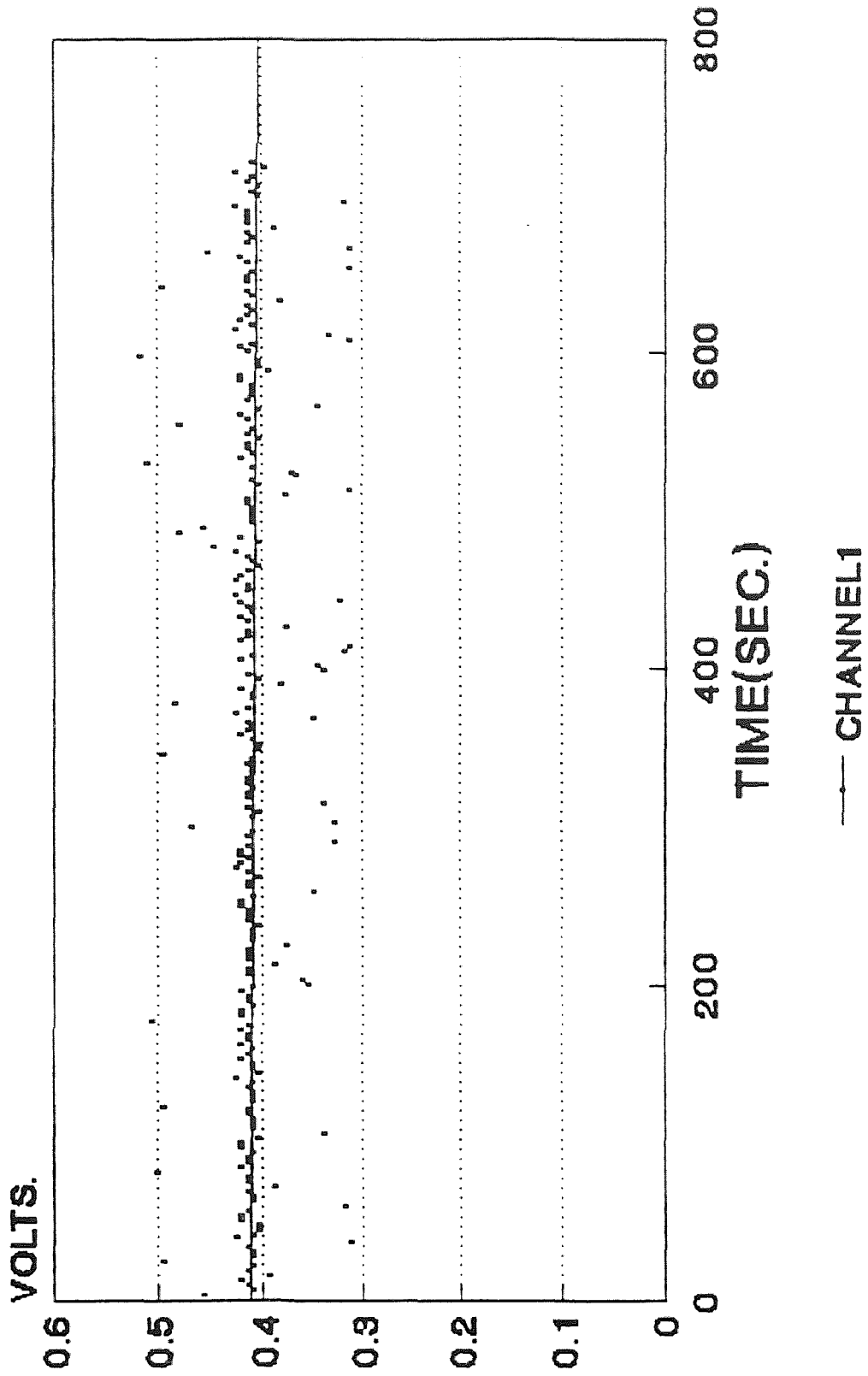


Fig.84 Internal deformation data for MIB

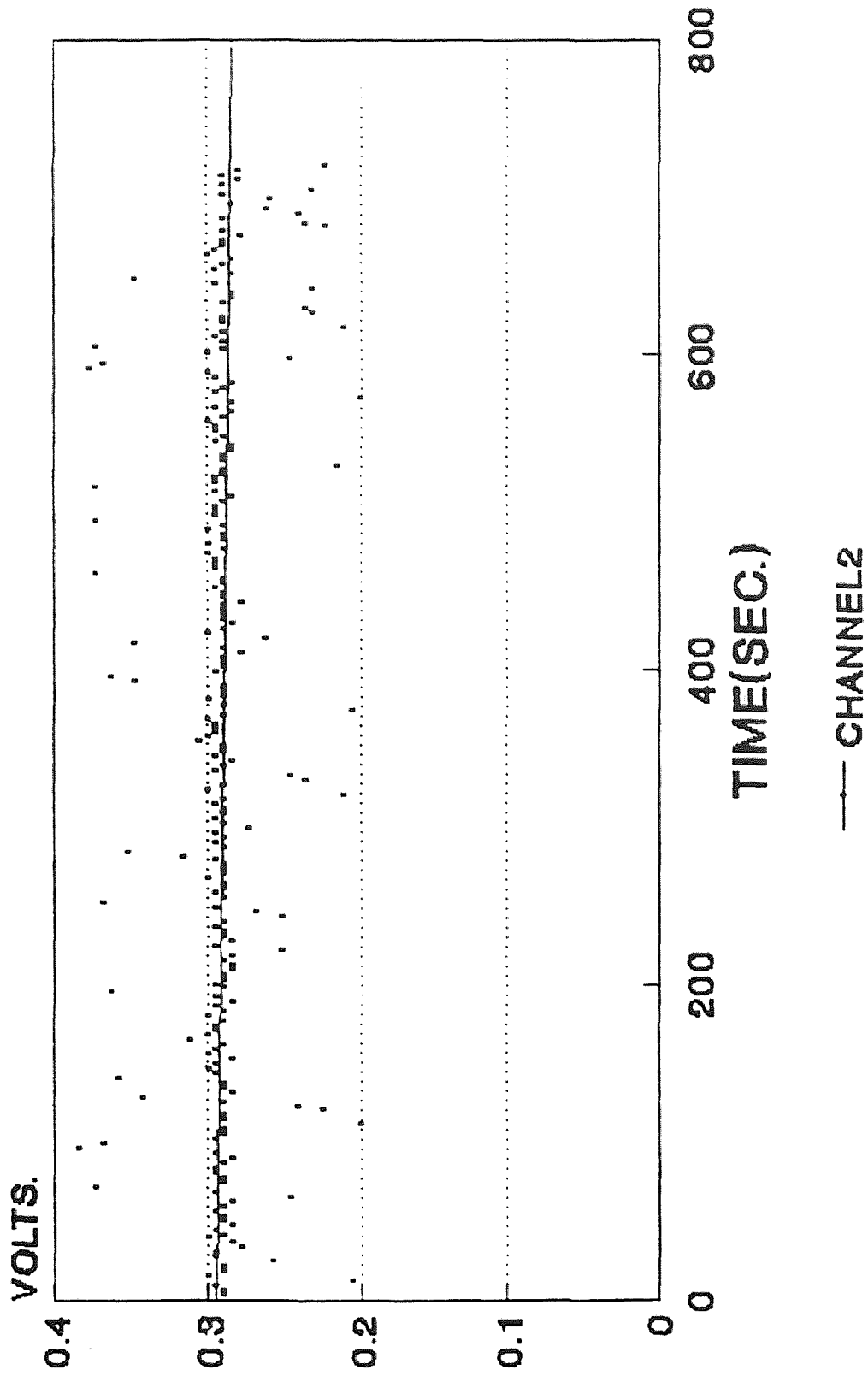


Fig.85 Internal deformation data M1B

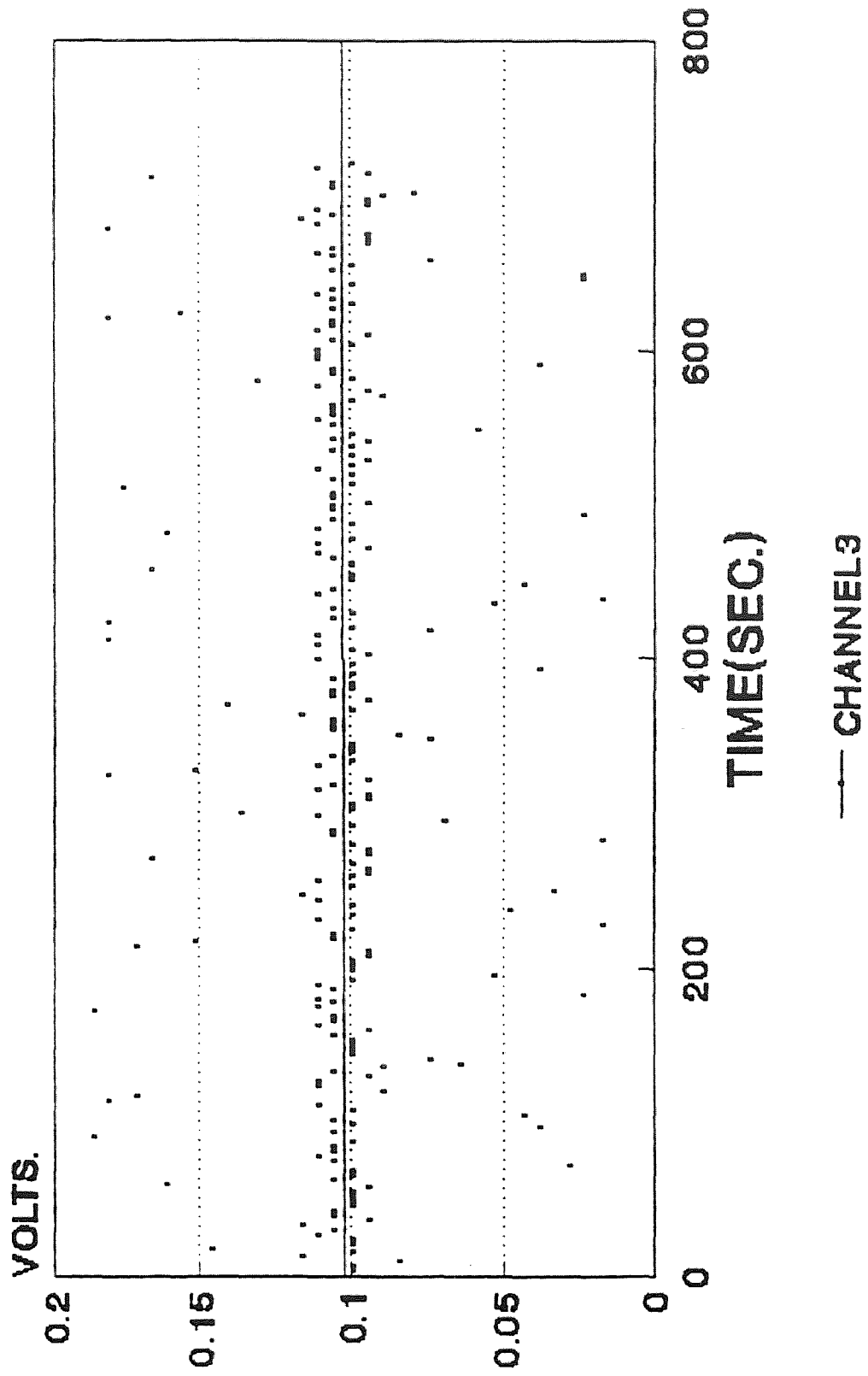


Fig.86 Internal deformation data .IB

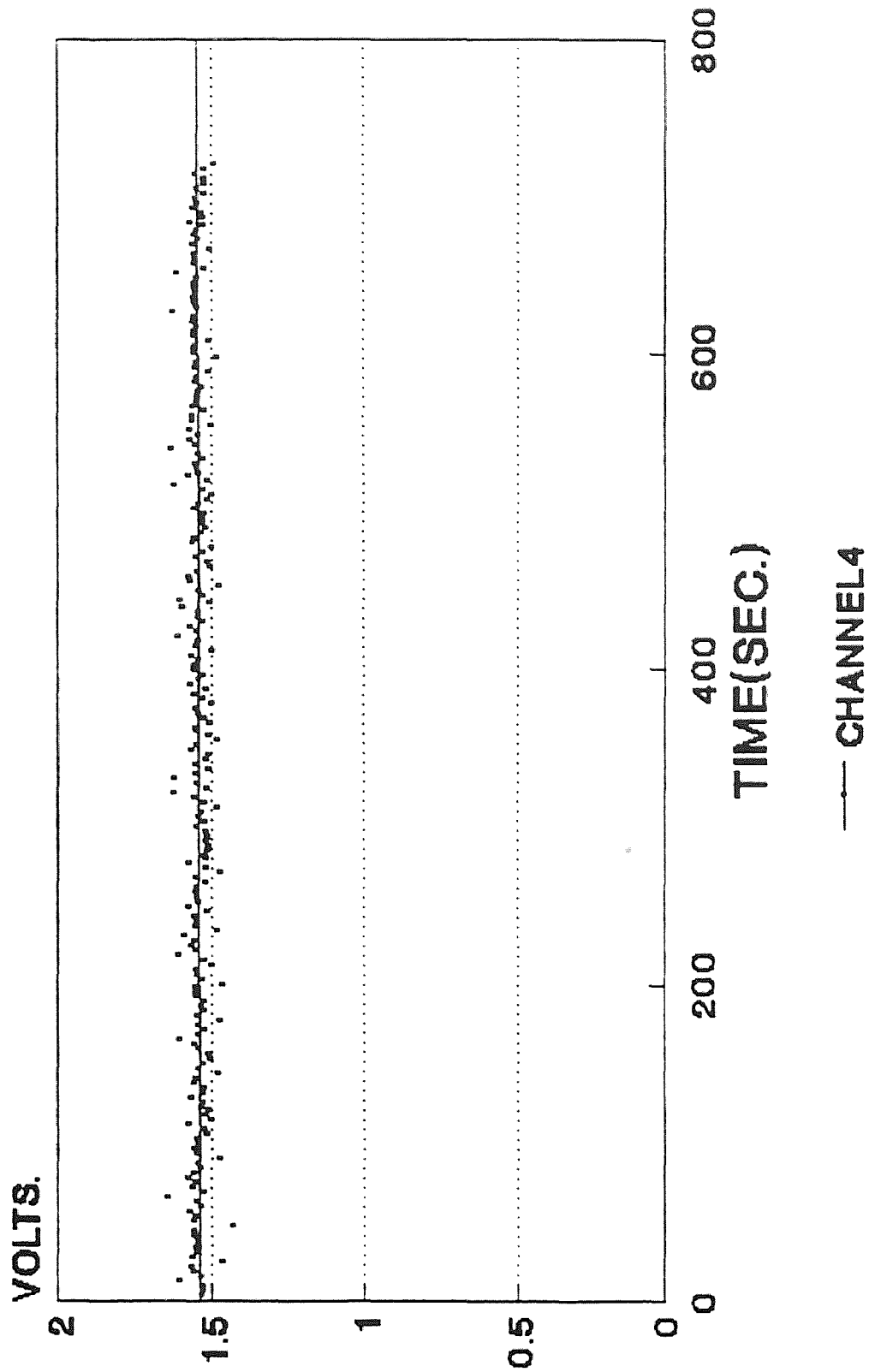


Fig.87 Internal deformation data for M1B

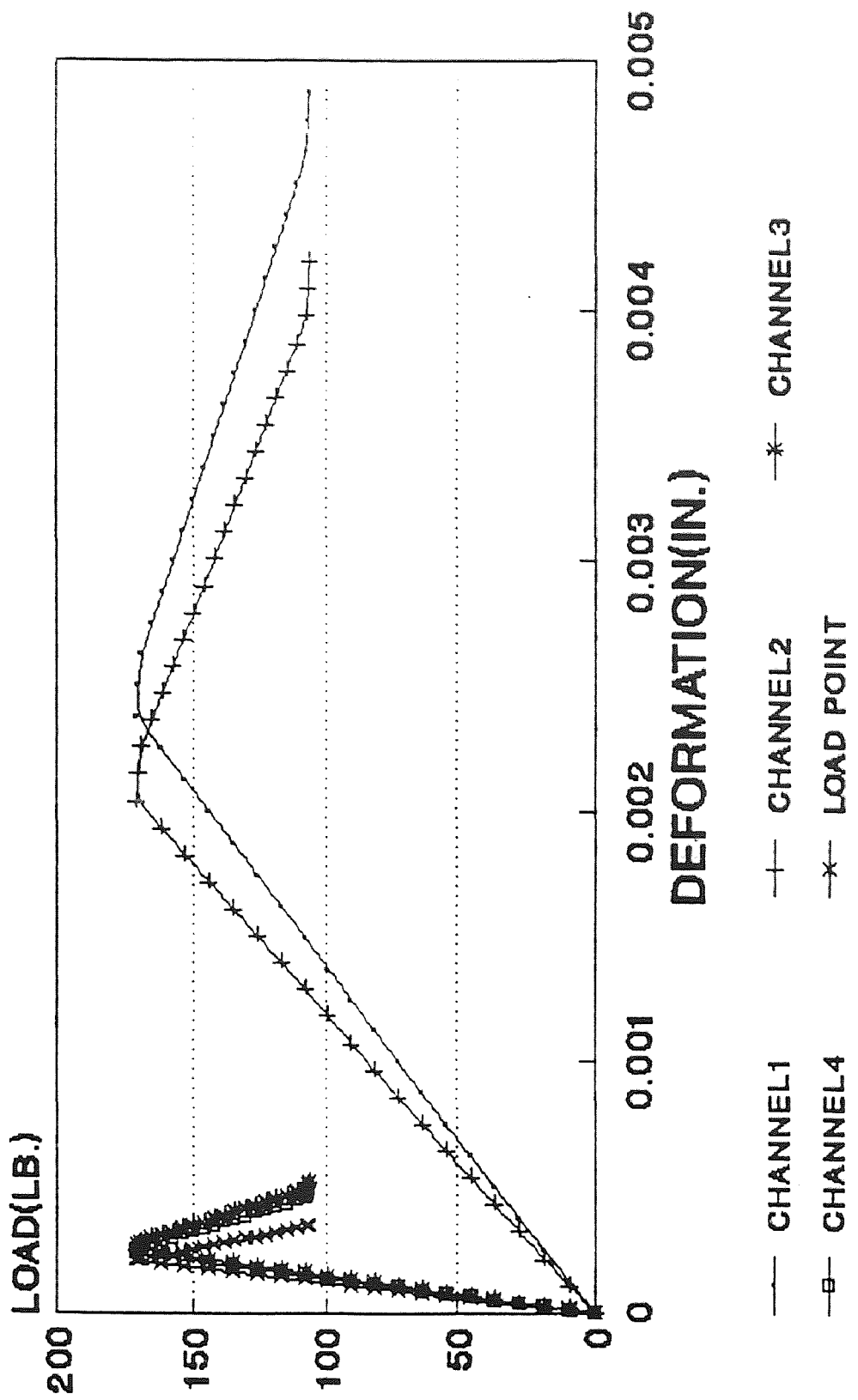


Fig. 88 Internal deformation for .J31

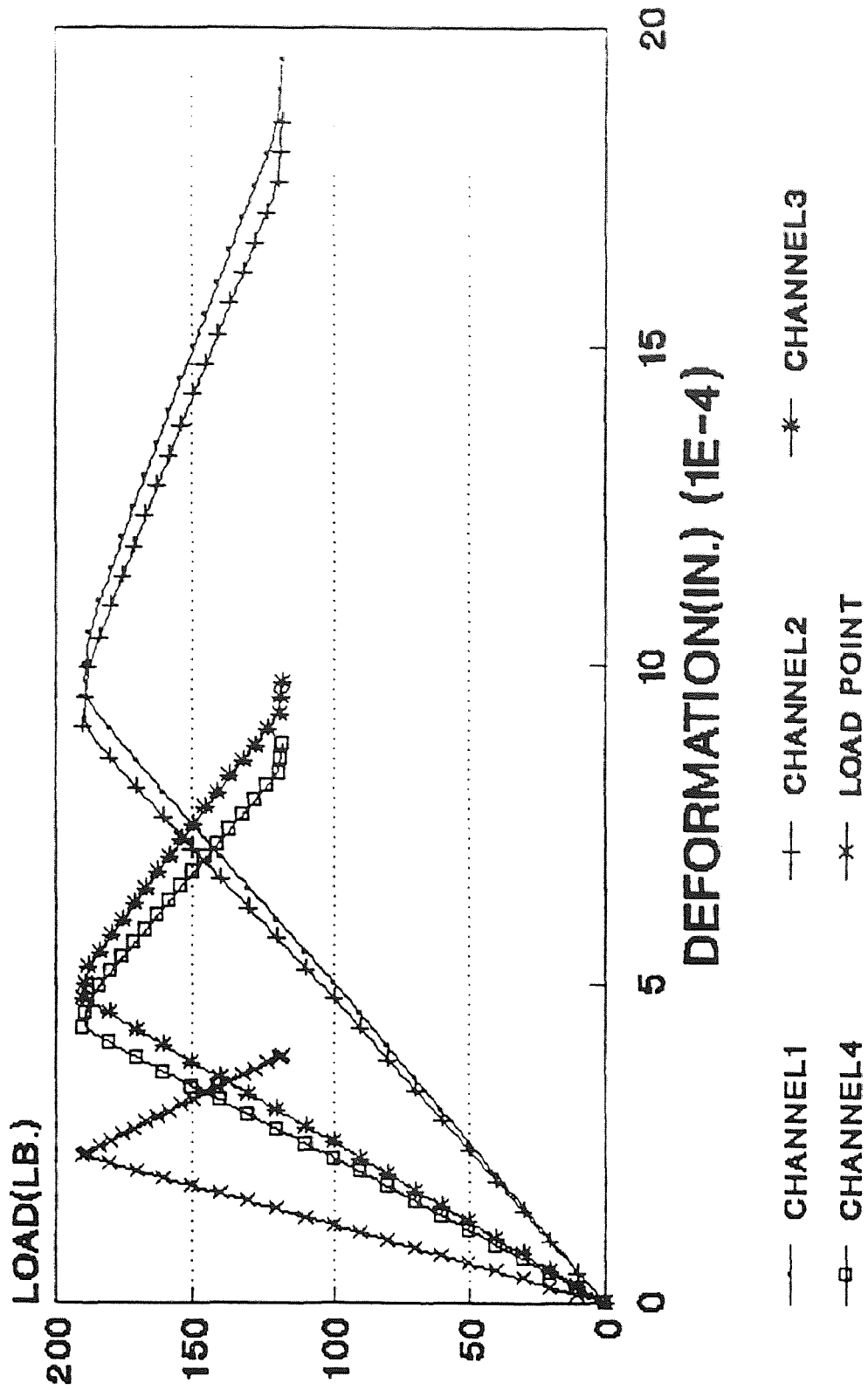


Fig.89 Internal deformation for F2

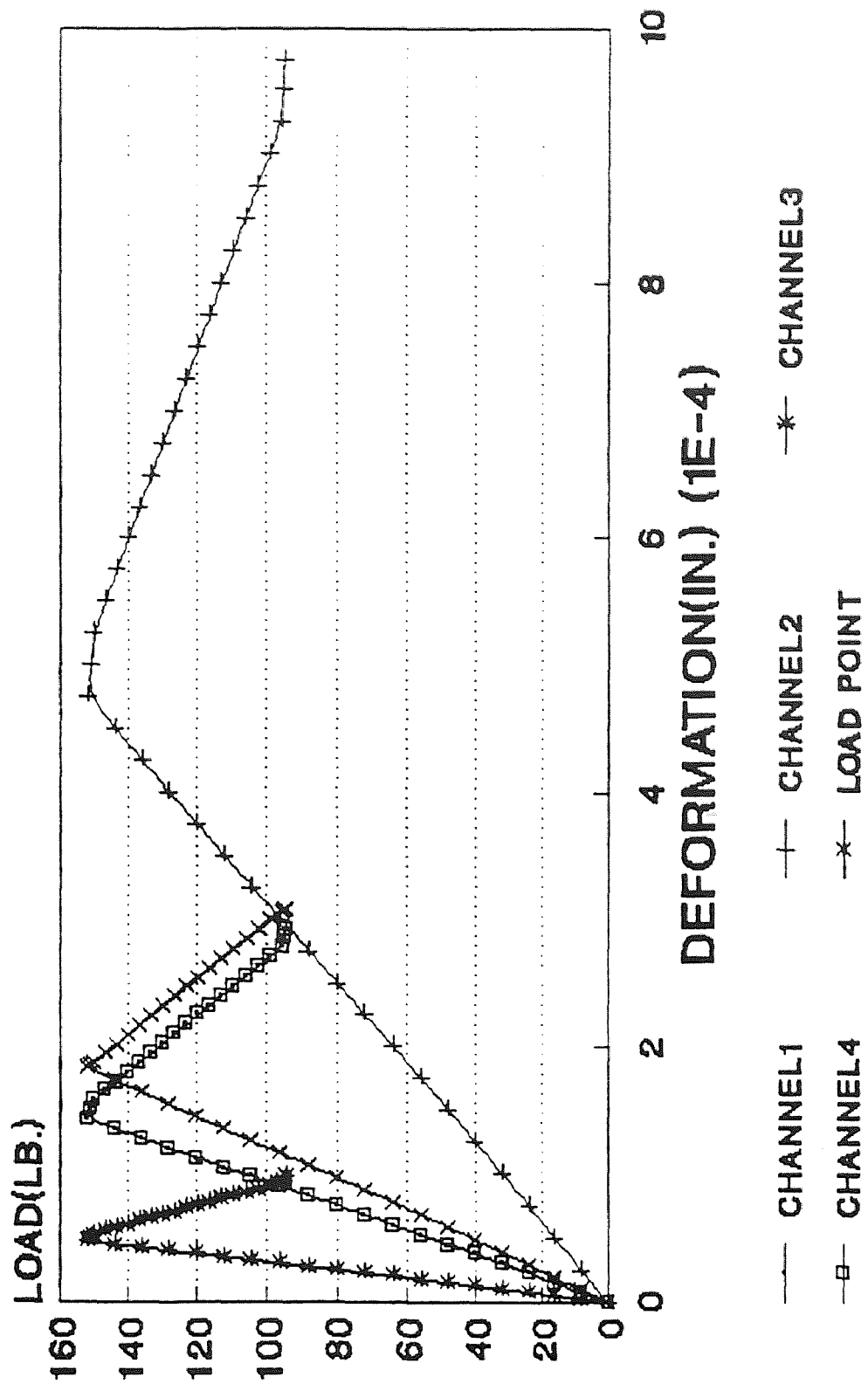


Fig.90 Internal deformation for Fig.72

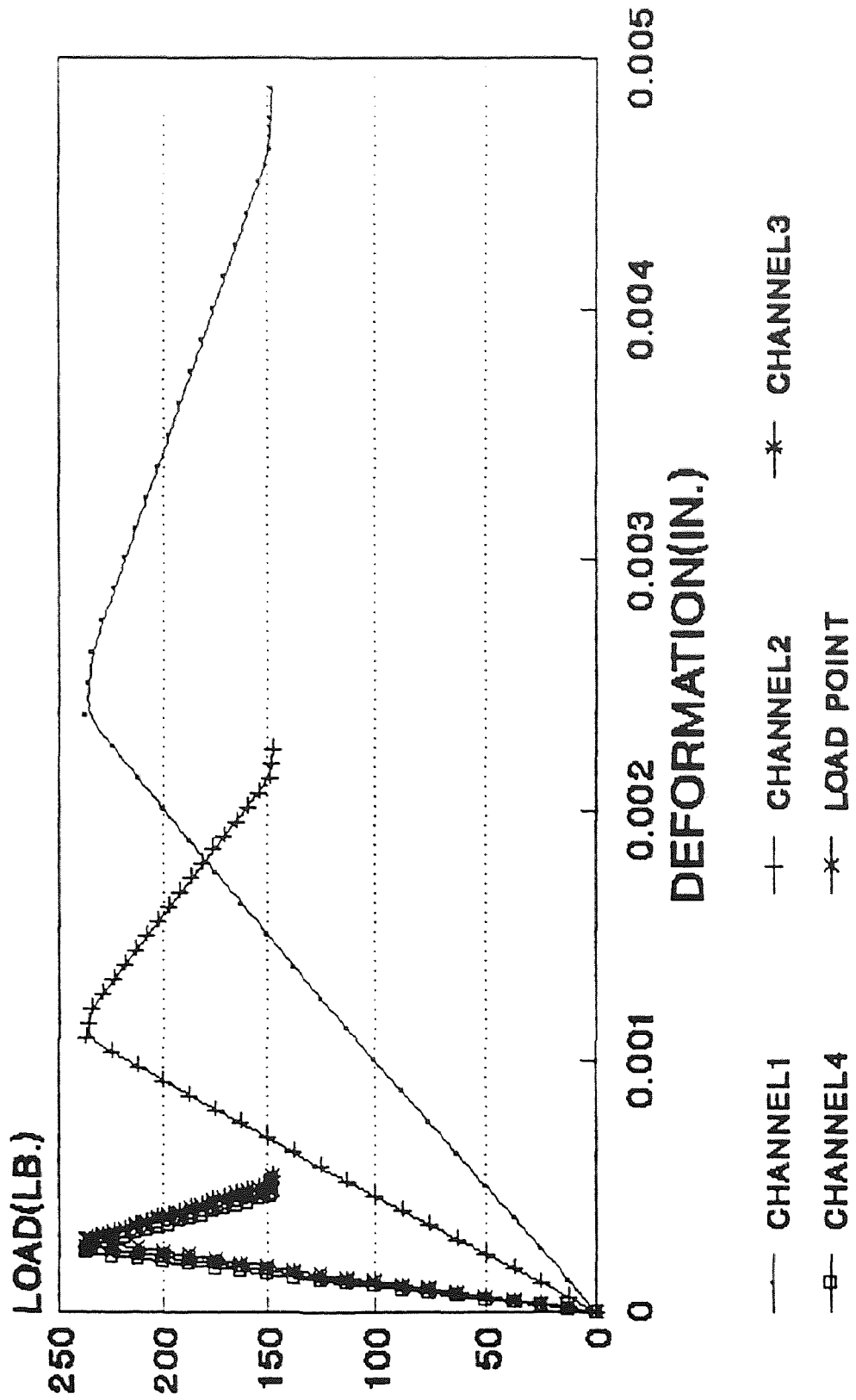


Fig.91 Internal deformation for F

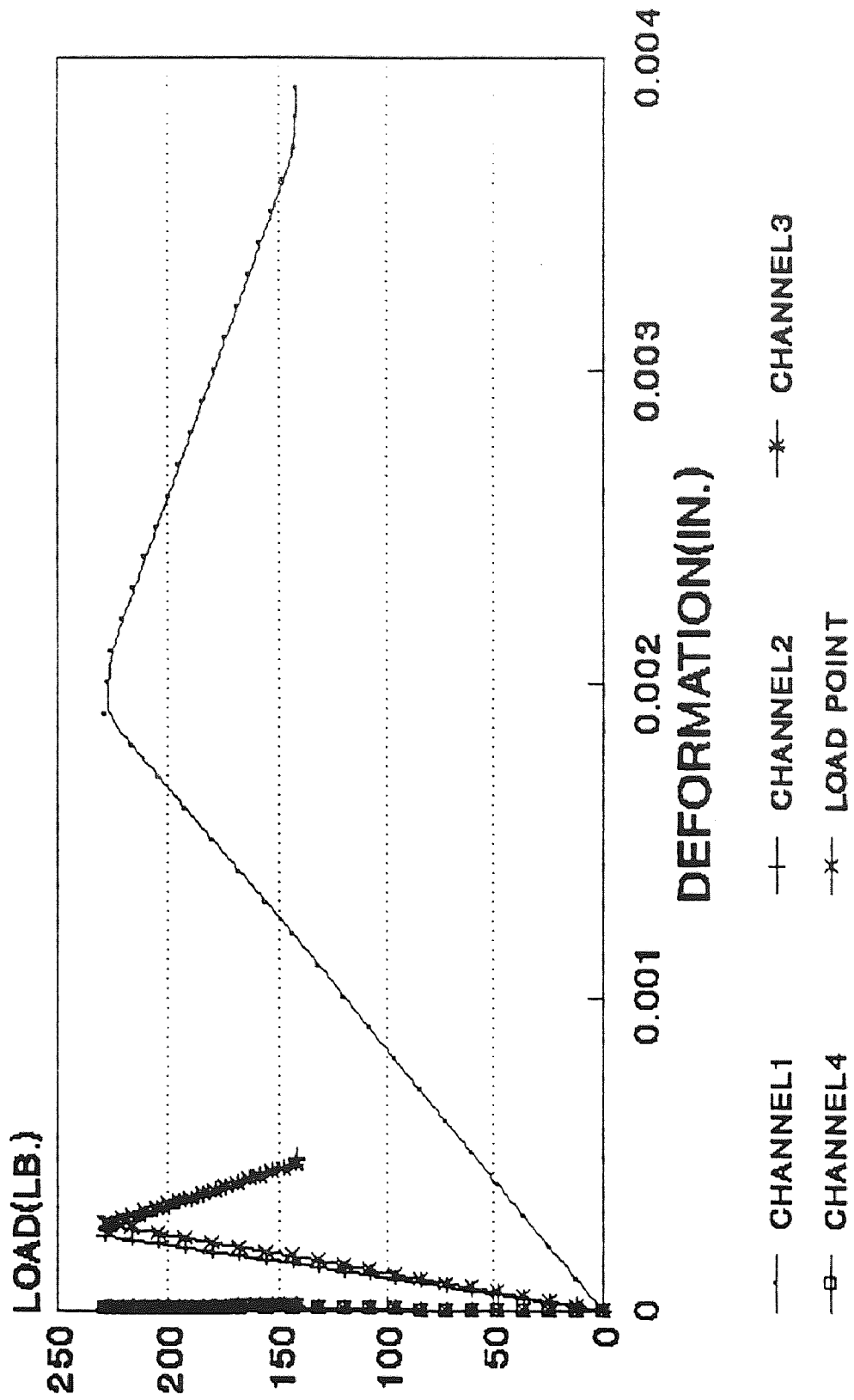


Fig.92 Internal deformation for F11

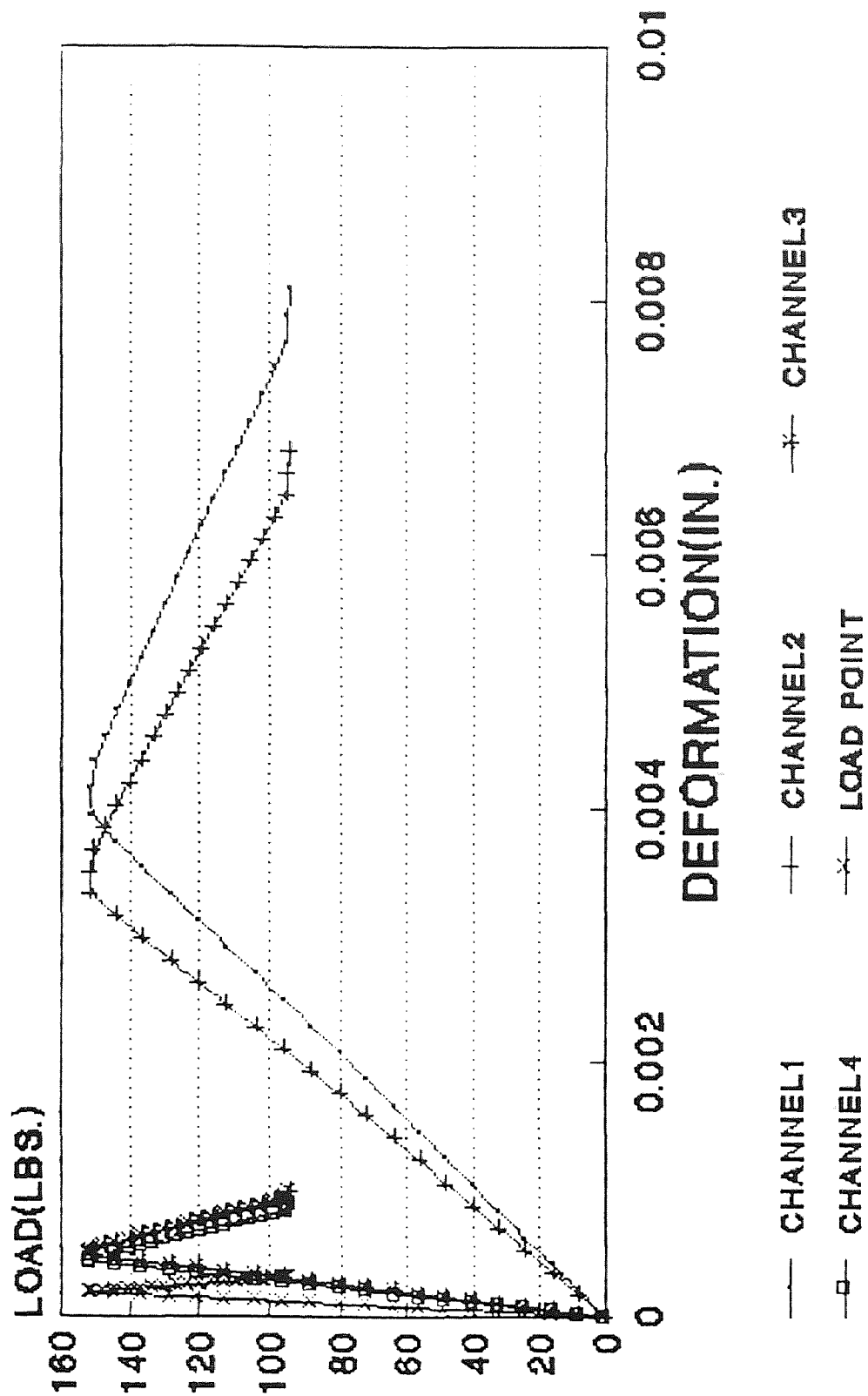


Fig.93 Internal deformation for F12

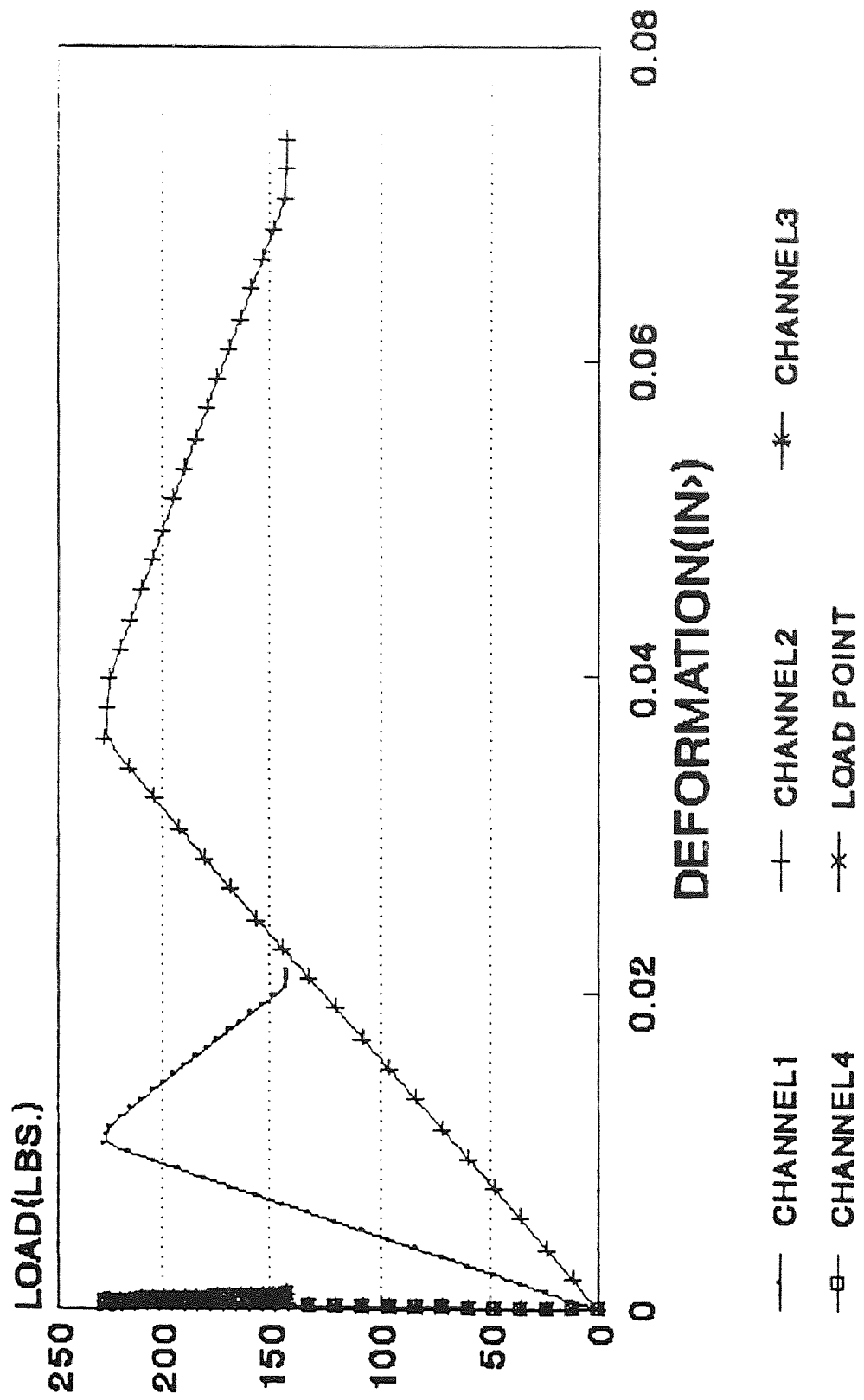


Fig.94 Internal deformation .9B

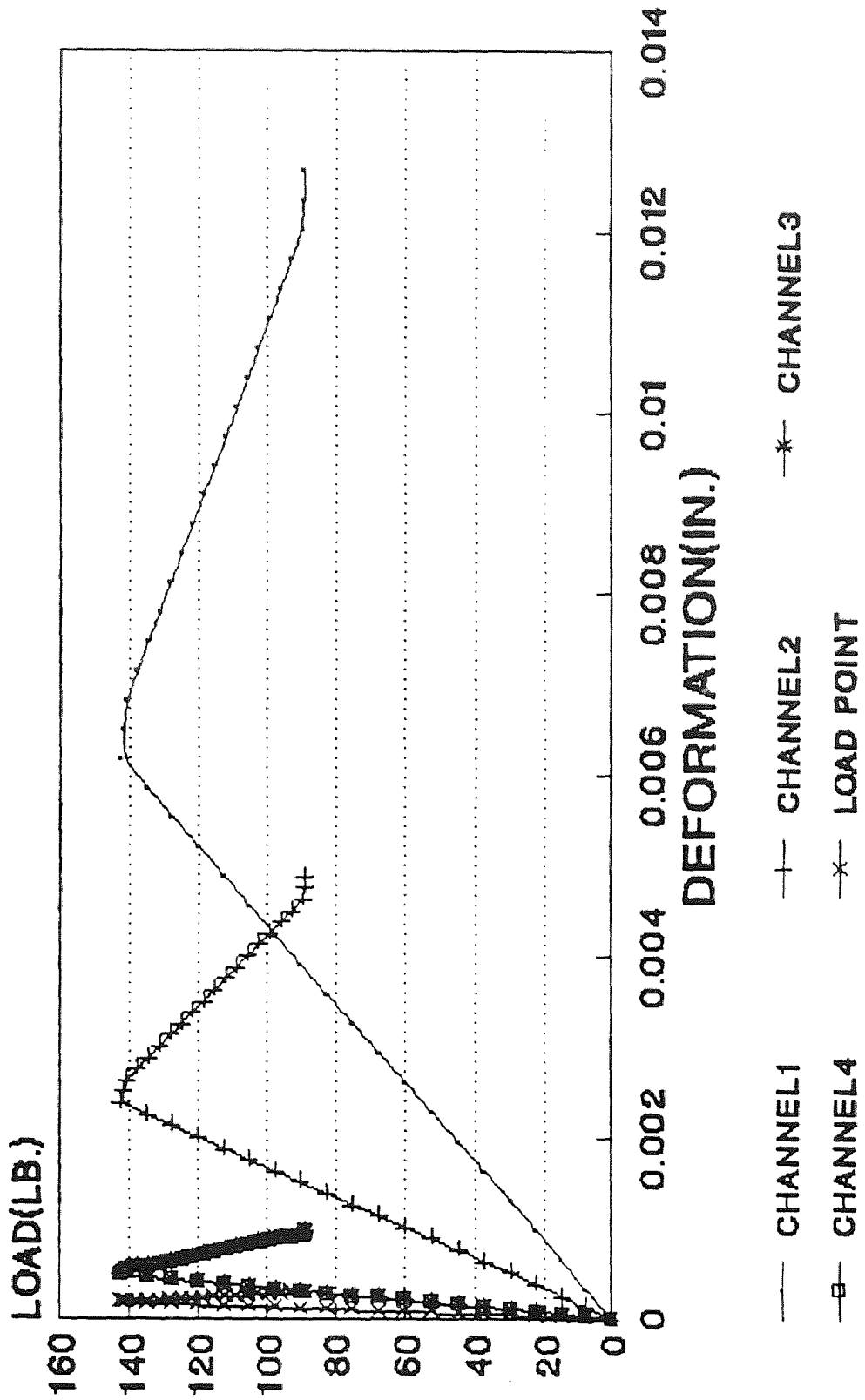


Fig.95 Internal deformation for F19D

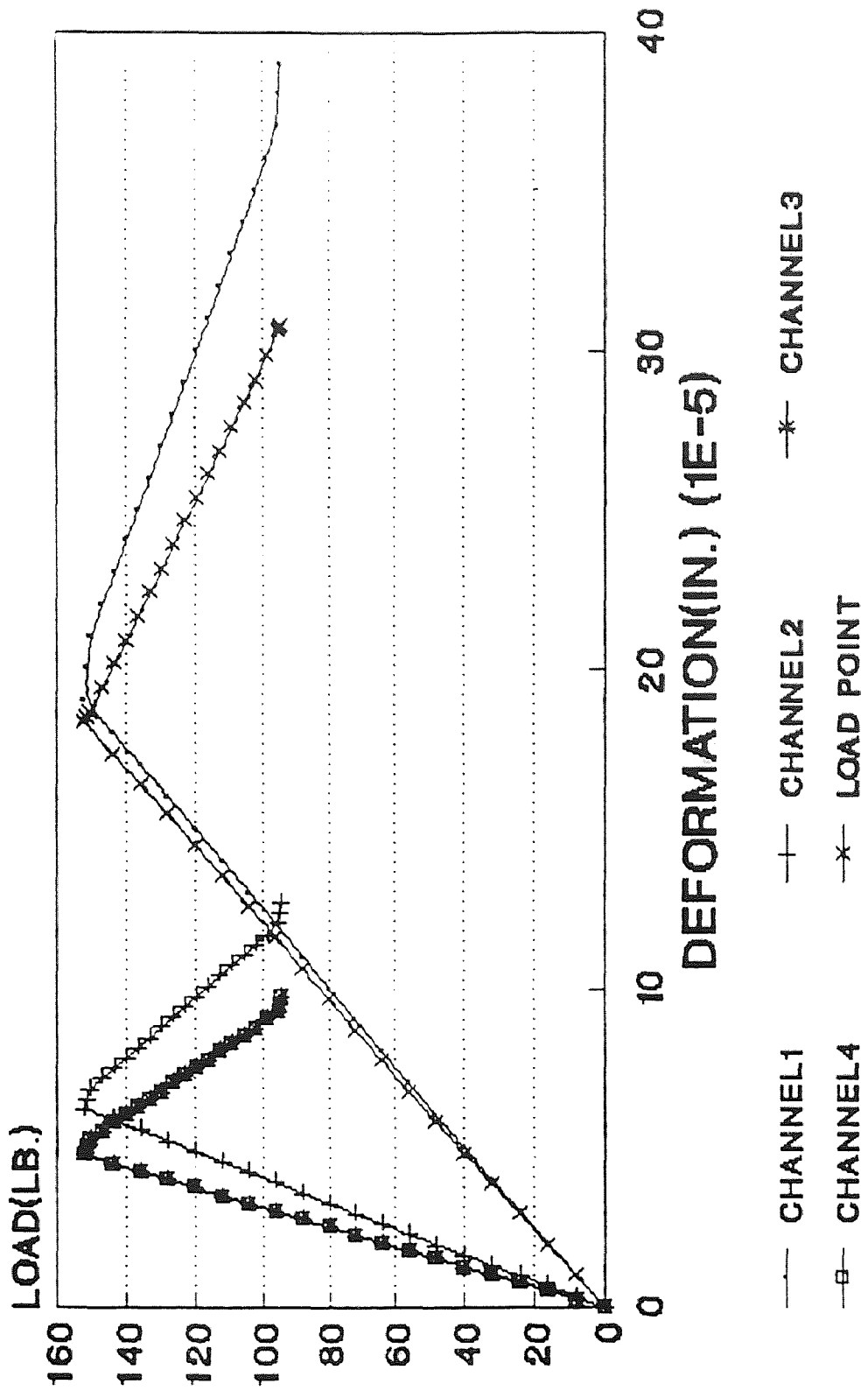


Fig.96 Internal deformation for F28a

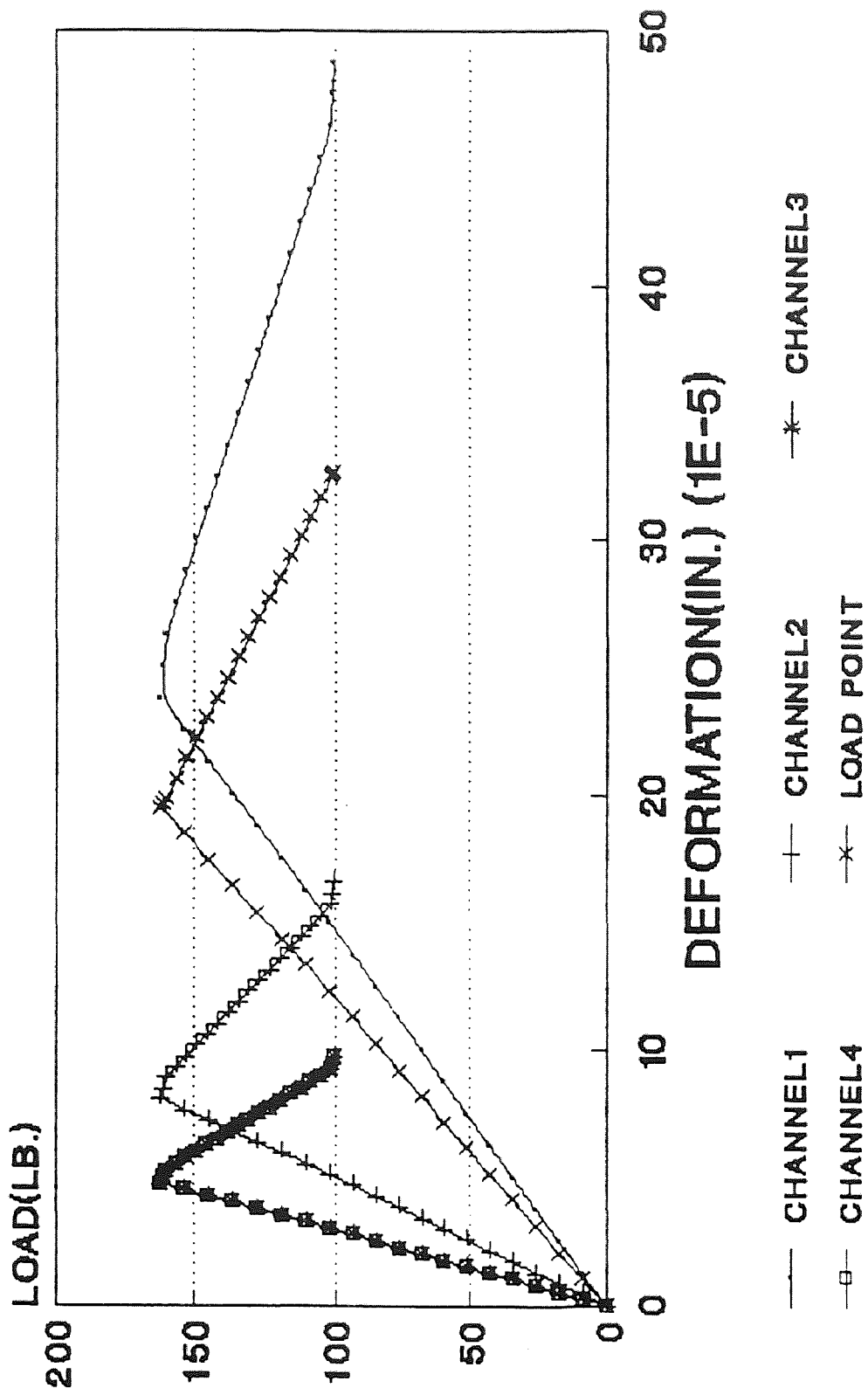


Fig.97 Internal deformation for F28C

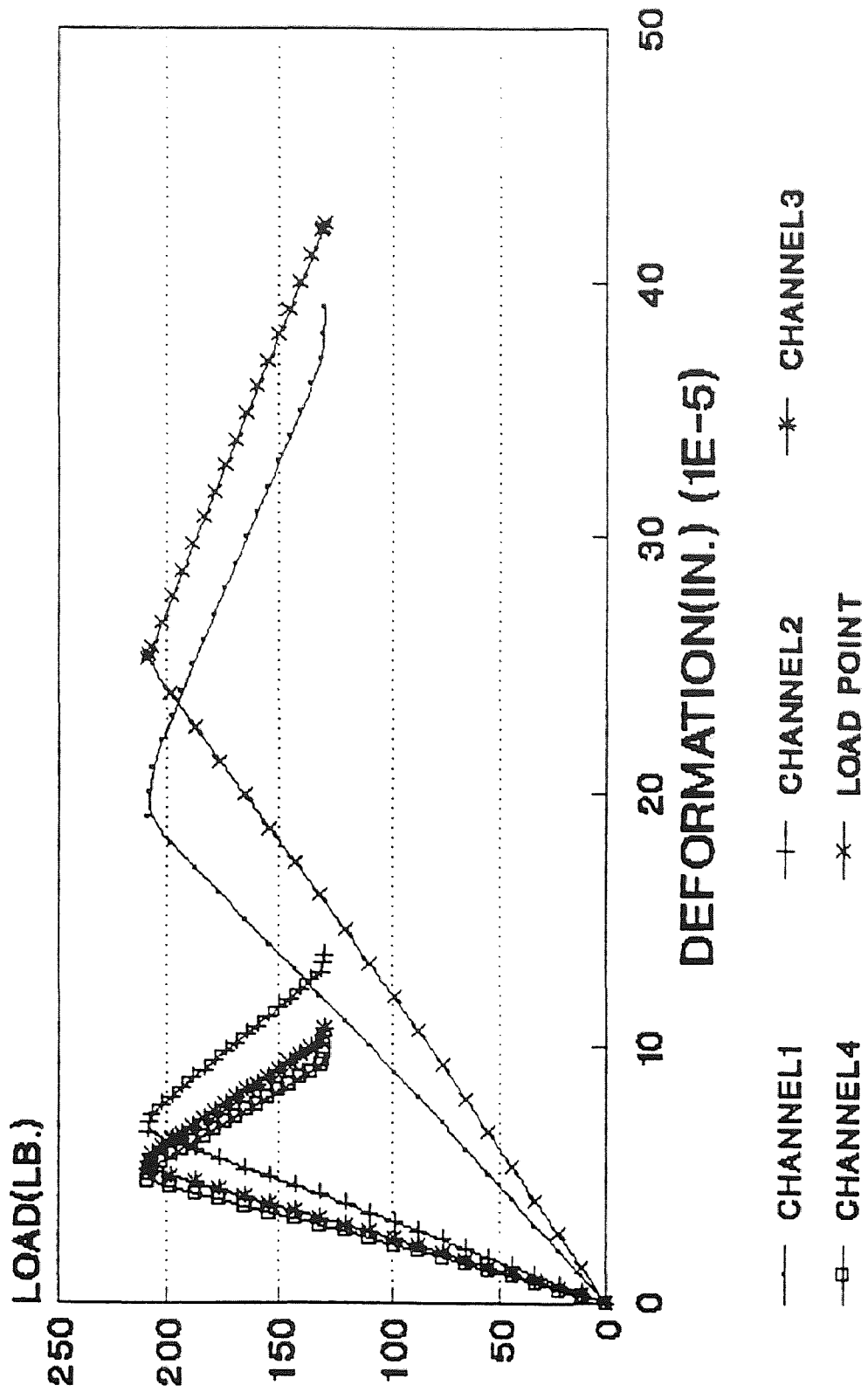


Fig.98 Internal deformation for M1A

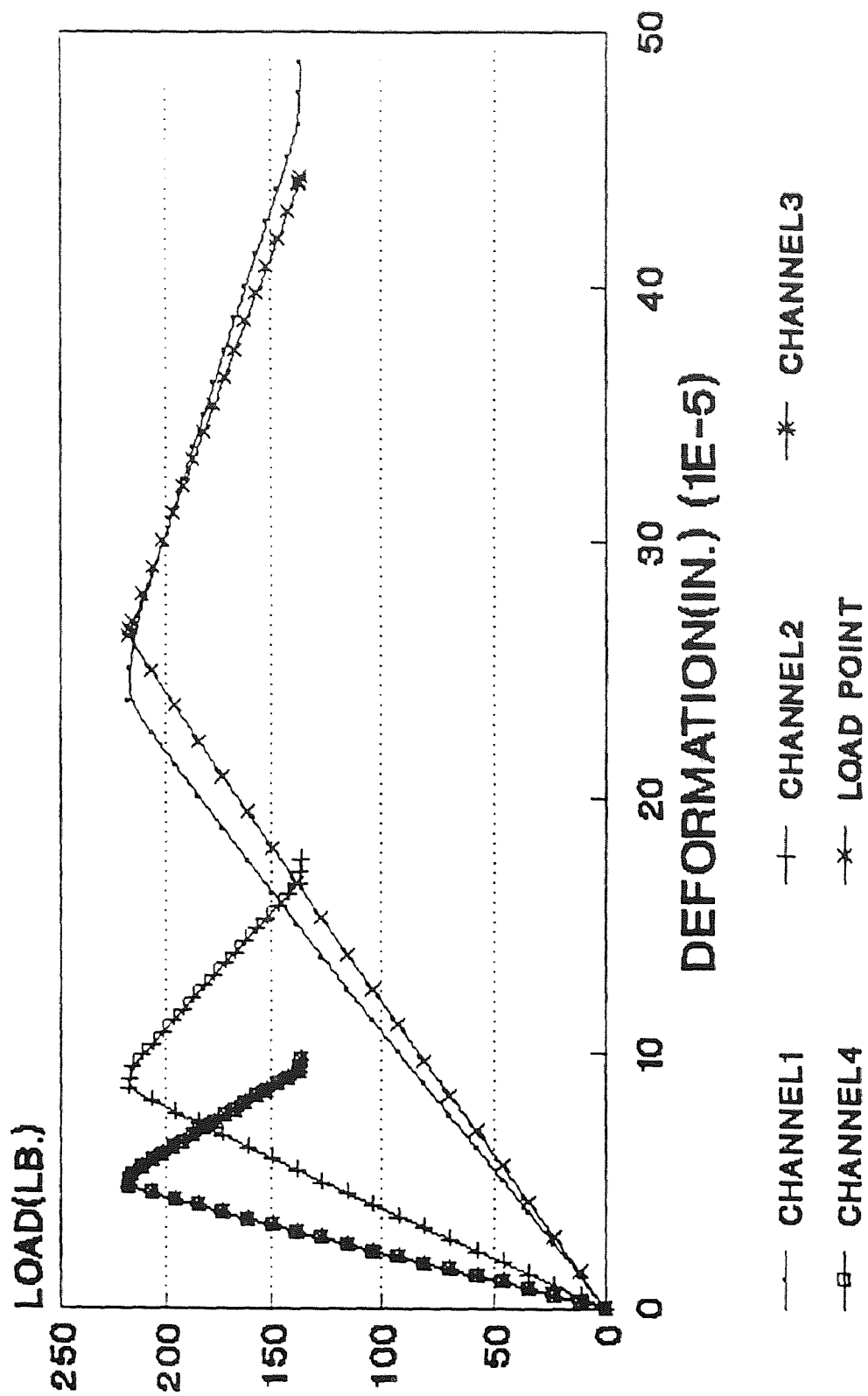


Fig.99 Internal deformation for Fig.98

some of the specimen cracks did not propagate in a straight manner , and therefore did not stretch the fibers.

Fig.100 thru 109 illustrate the deformation pattern at different load intervals for each one of the specimen tested. As indicated in these figures , COD values in almost all cases were considerably much larger than all the other deformations. For this reason , in another set of figures (110 thru 119) ,internal deformation patterns are compared separately. Results shown in Fig.110 thru 119 indicate that the critical cracking zone in compact tension is approximately 1.7 inches , whereas in the three point bend specimen is about 1.2 inches.

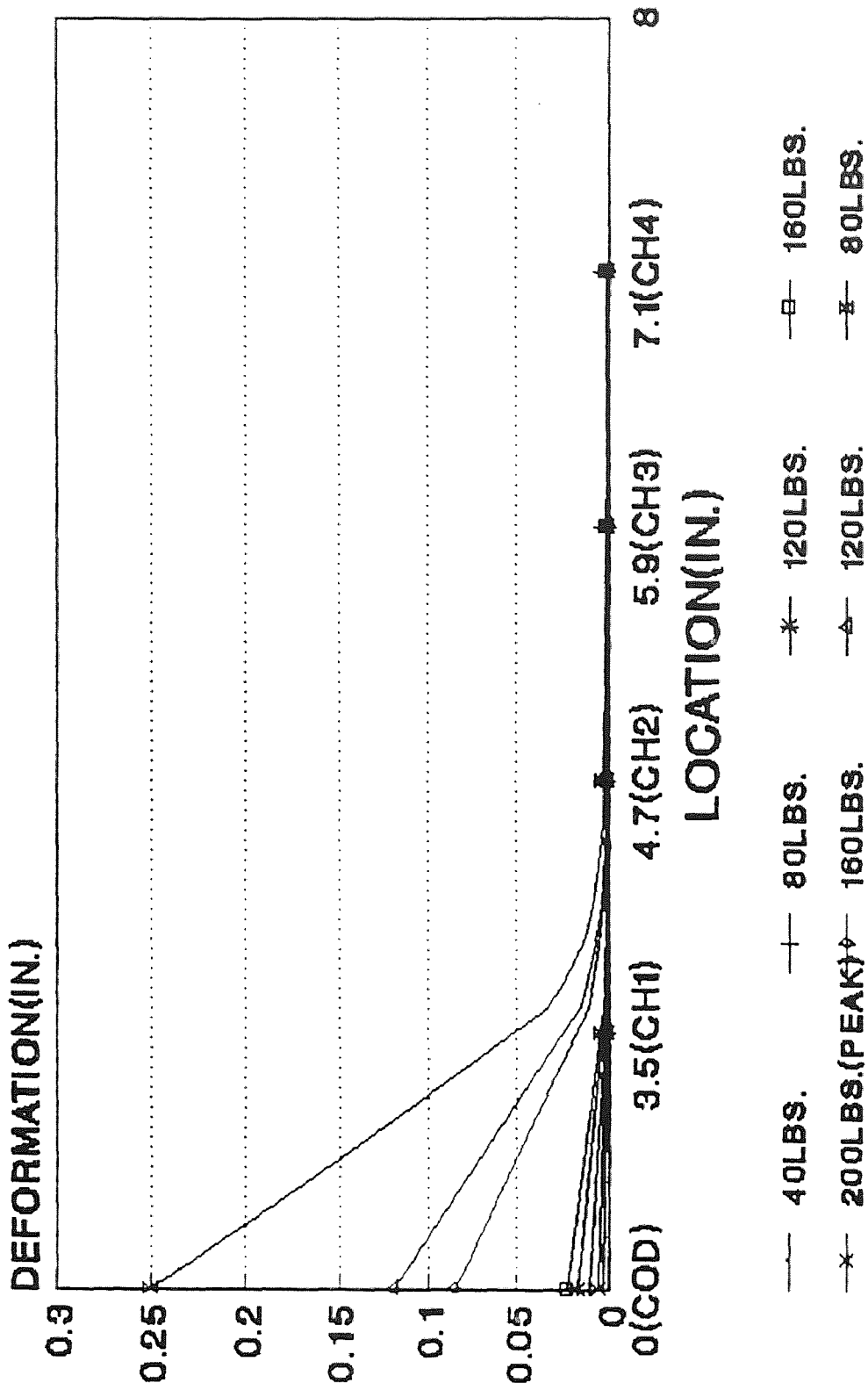


Fig.100 Deform. pattern at diff. load F2

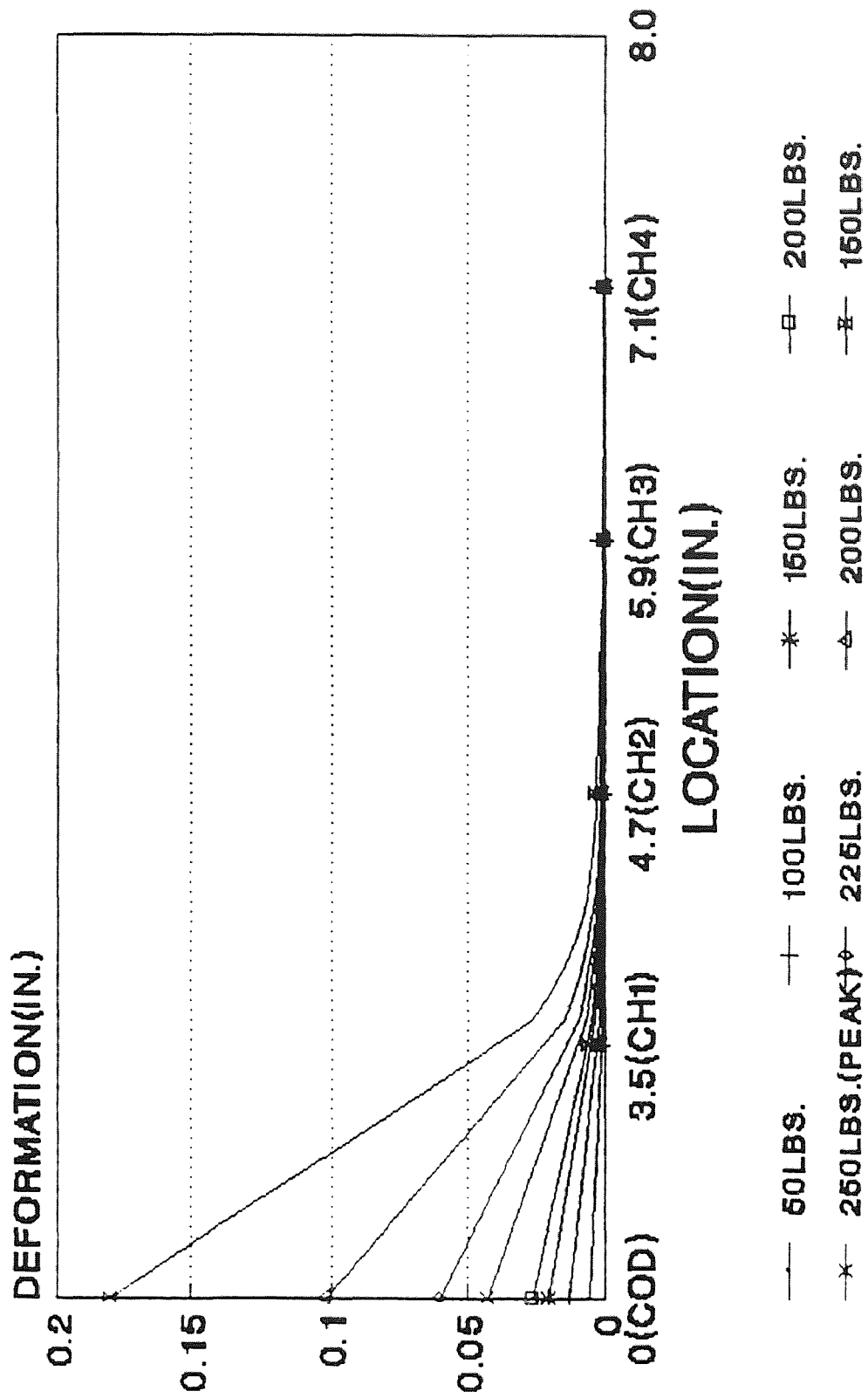


Fig.101 Deform. pattern at diff. load F8

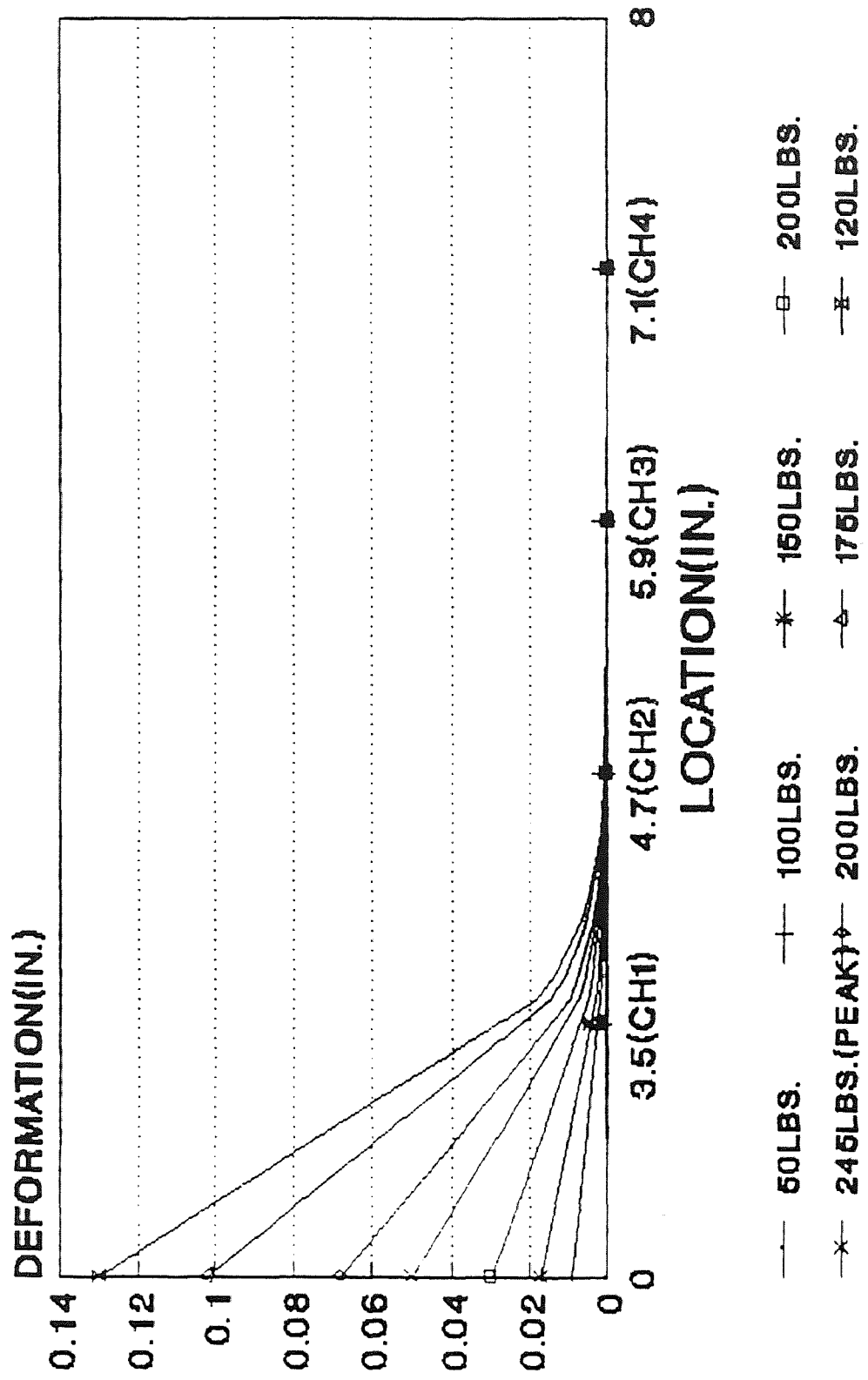


Fig.102 Deform. pattern at diff. load F11

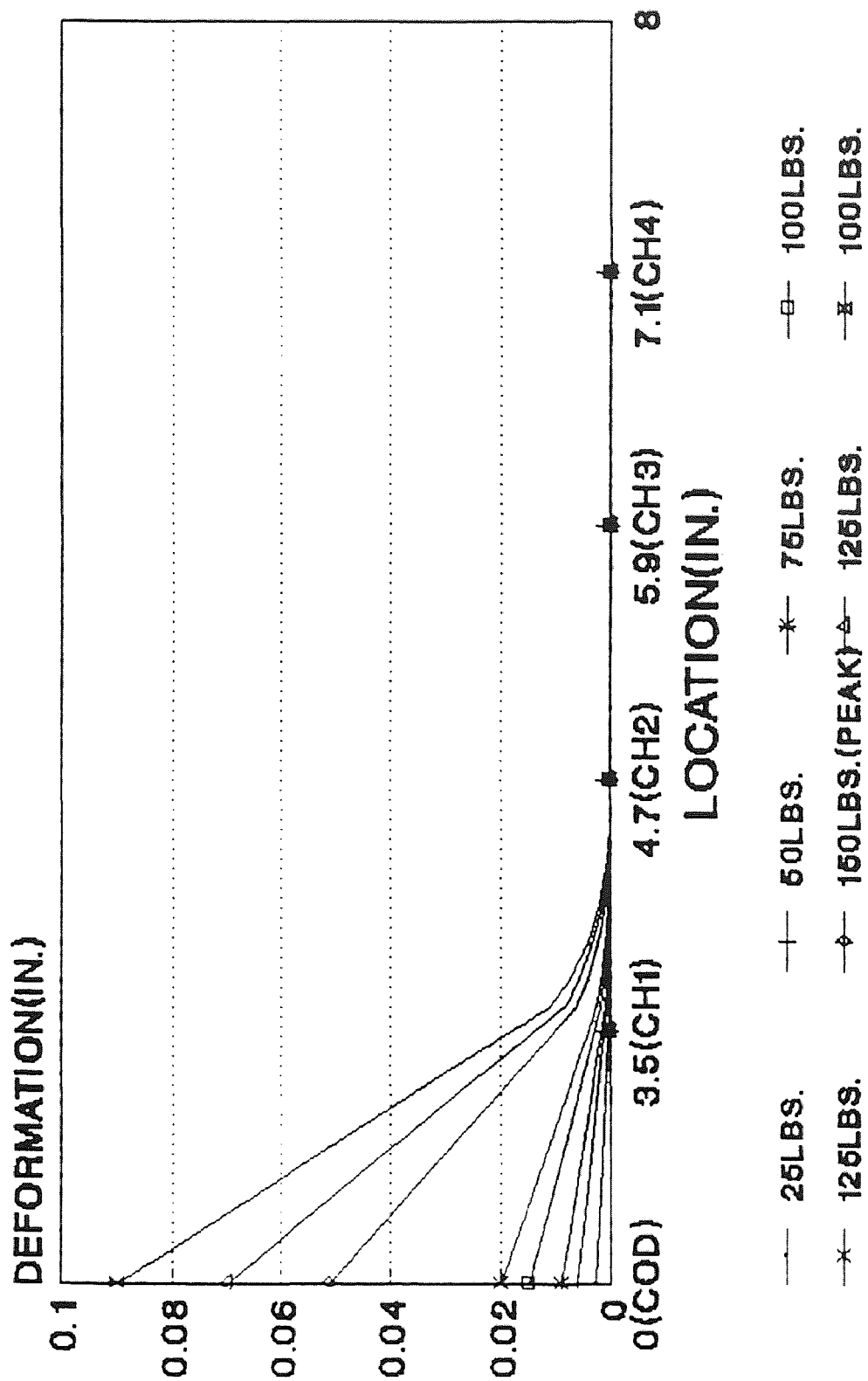


Fig.103 Deform. pattern at diff. load F12

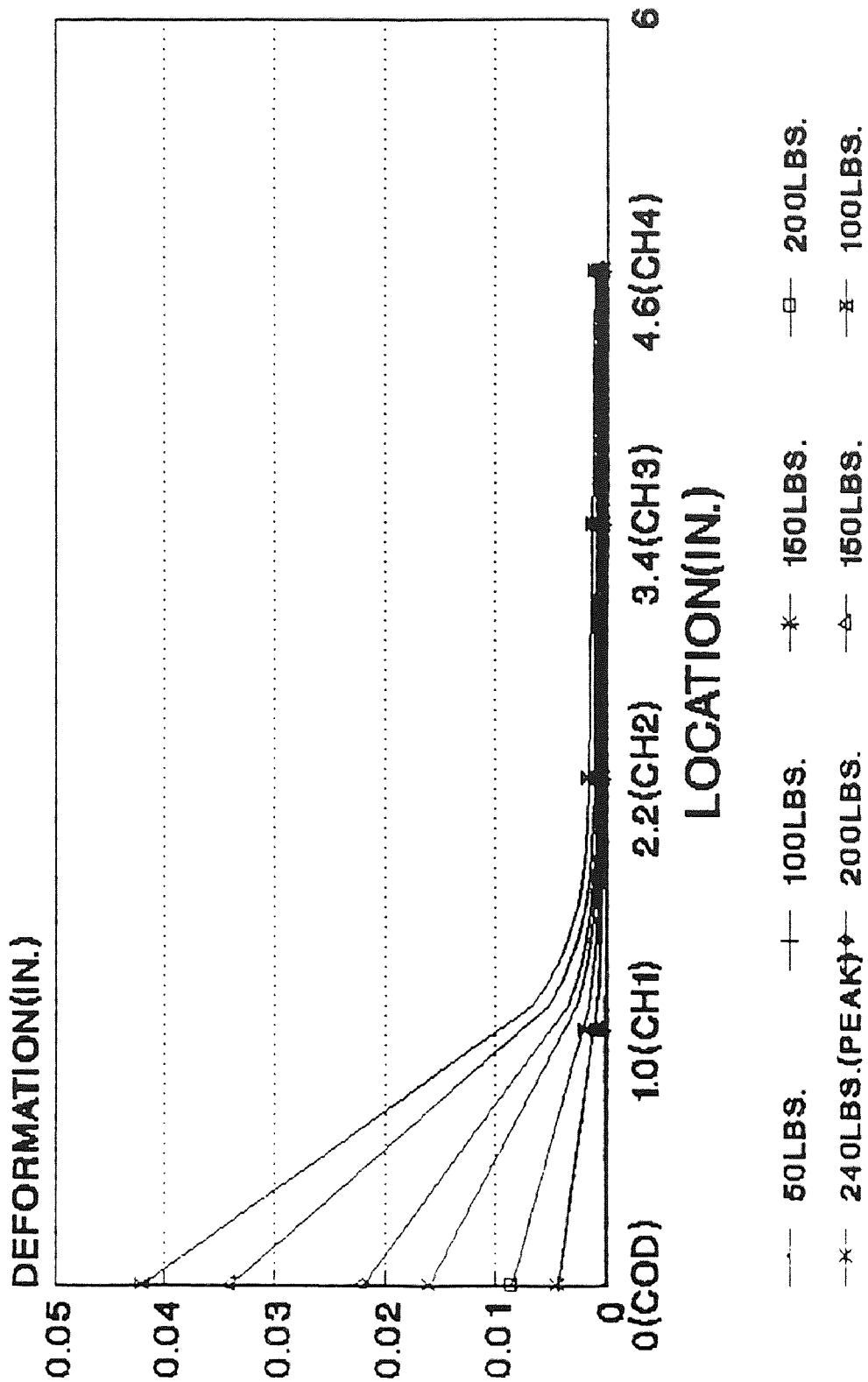


Fig.104 Deform. pattern at diff. loadF19B

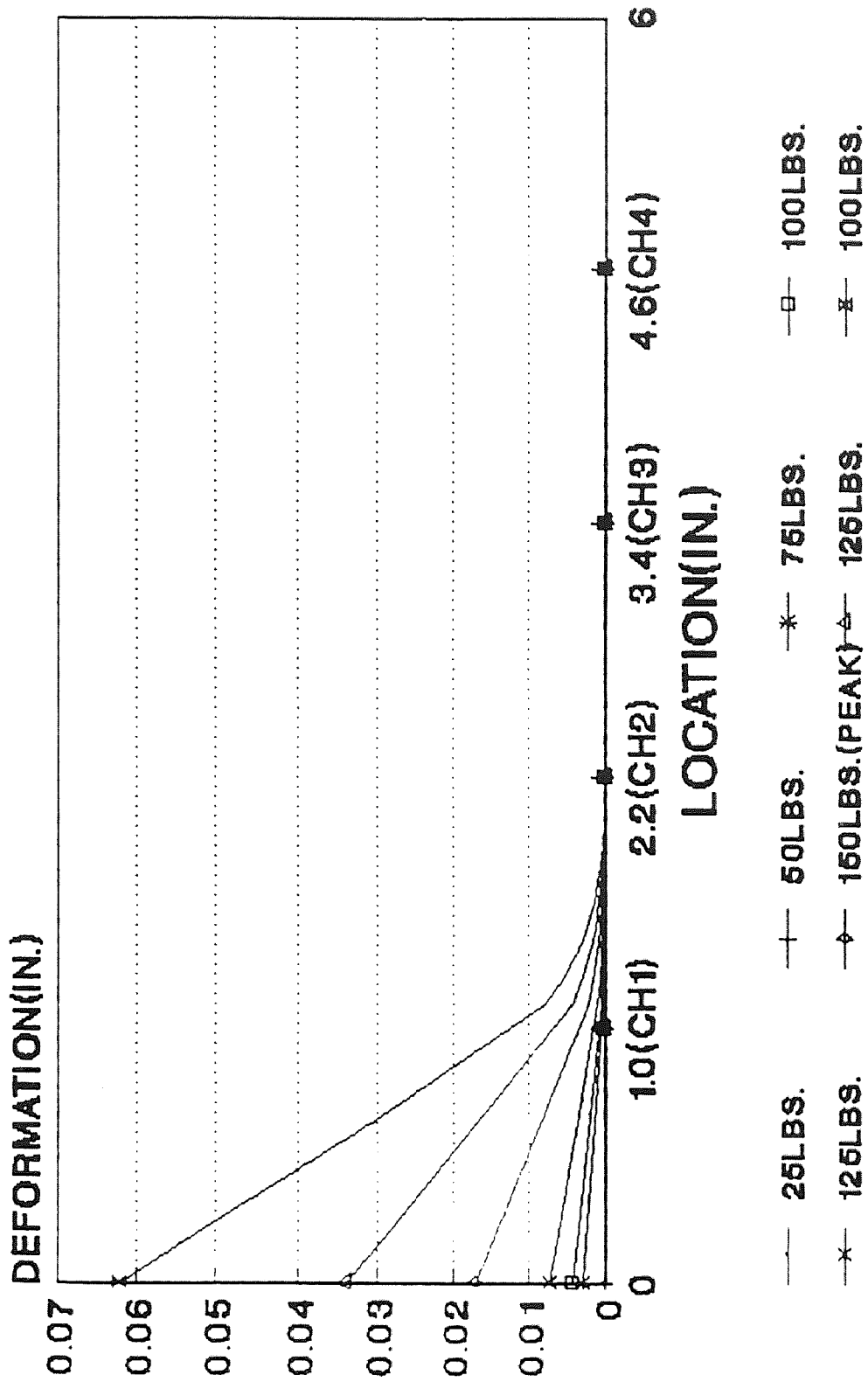


Fig.105 Deform. pattern at diff. loadF19D

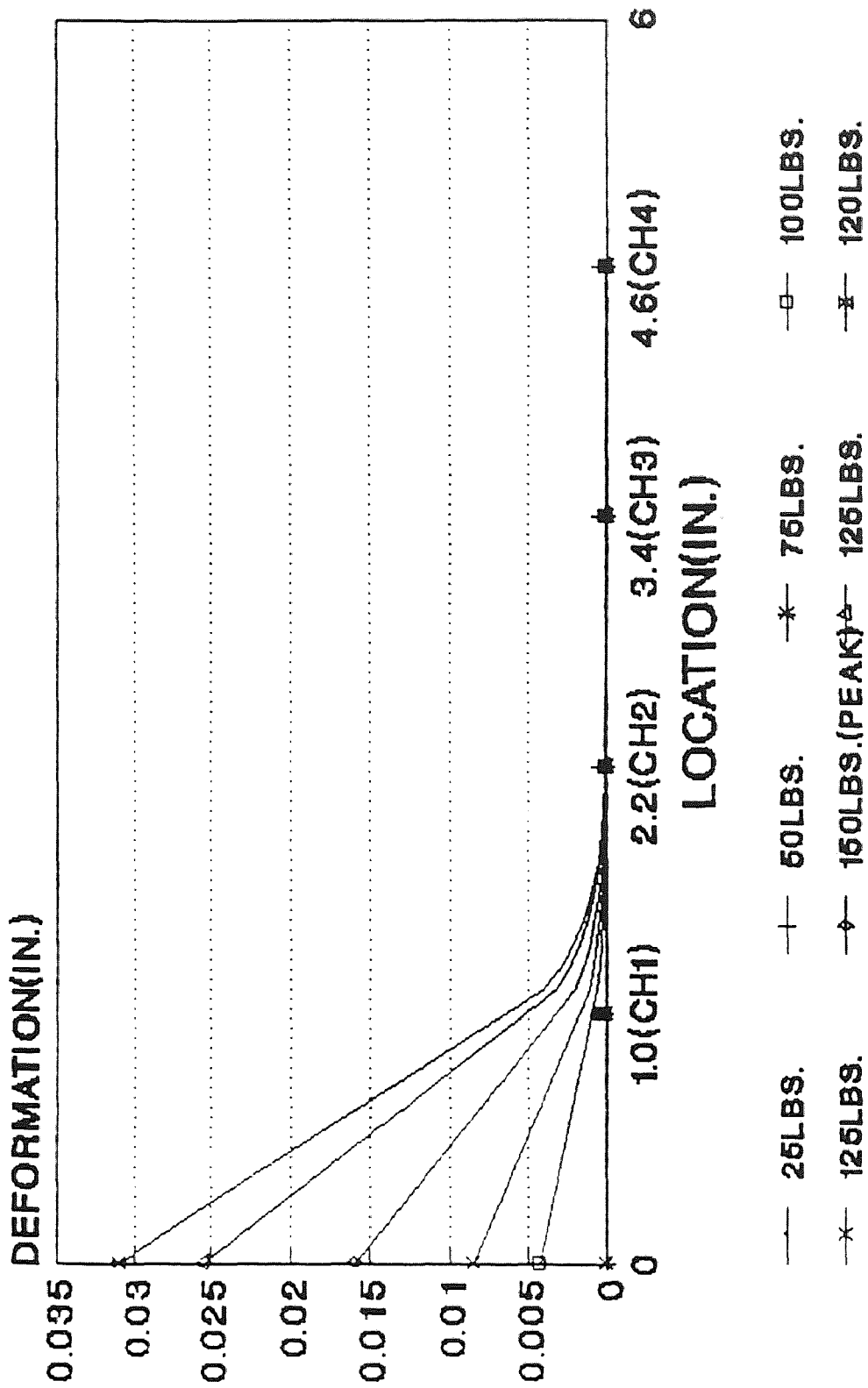


Fig.108 Deform. pattern at diff. loadF28A

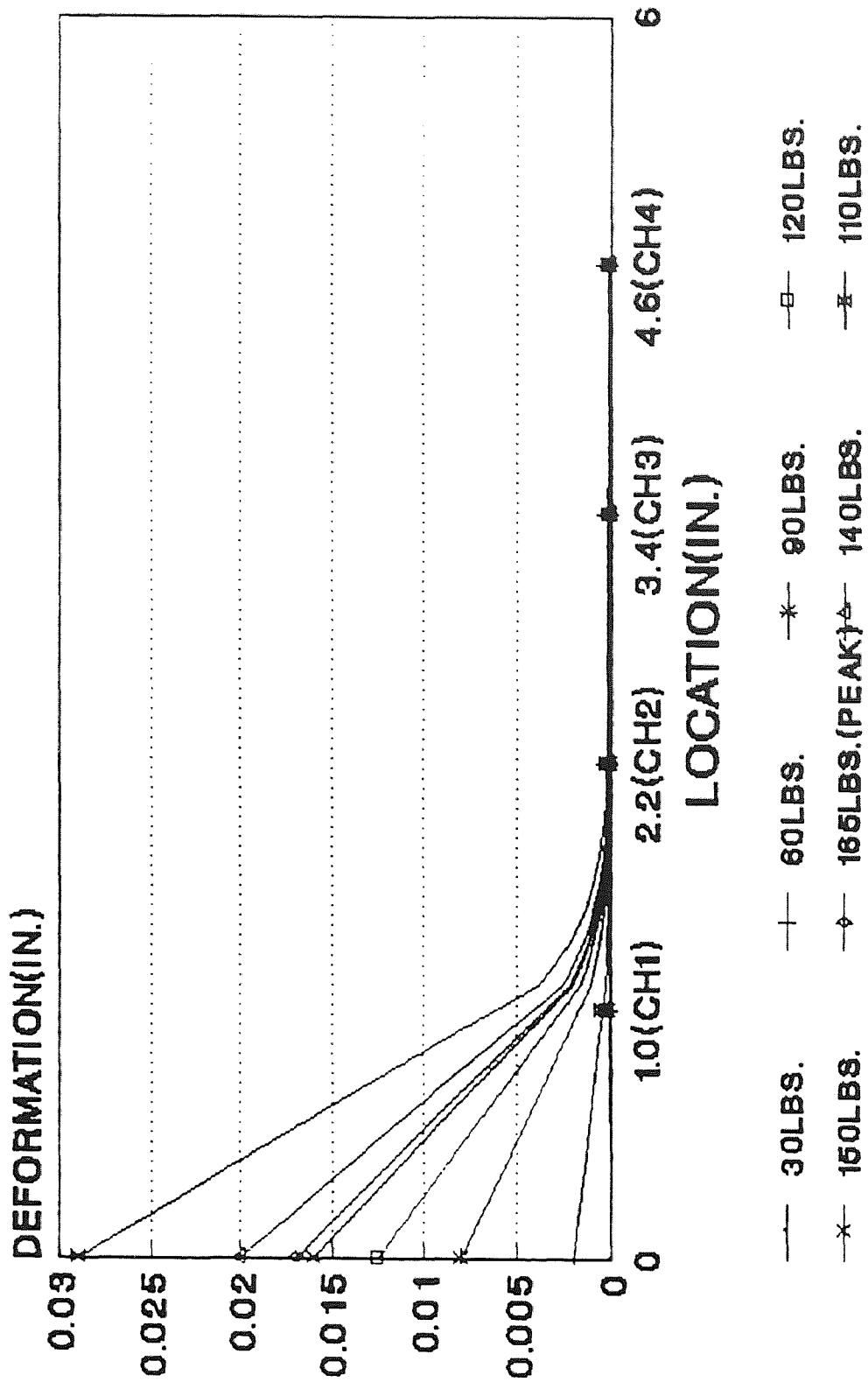


Fig.107 Deform. pattern at diff. loadF28C

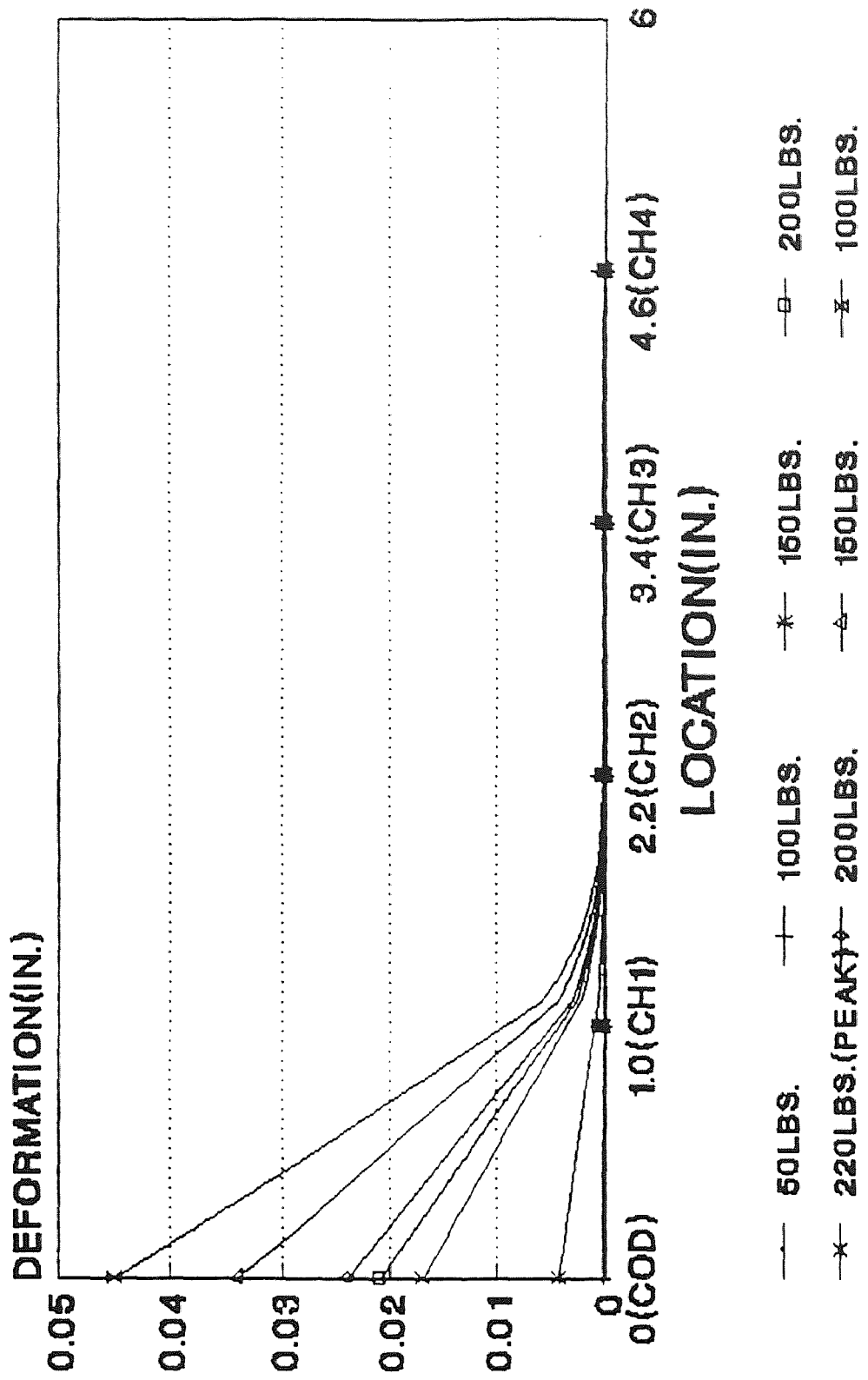


Fig.108 Deform. pattern at diff load M1A

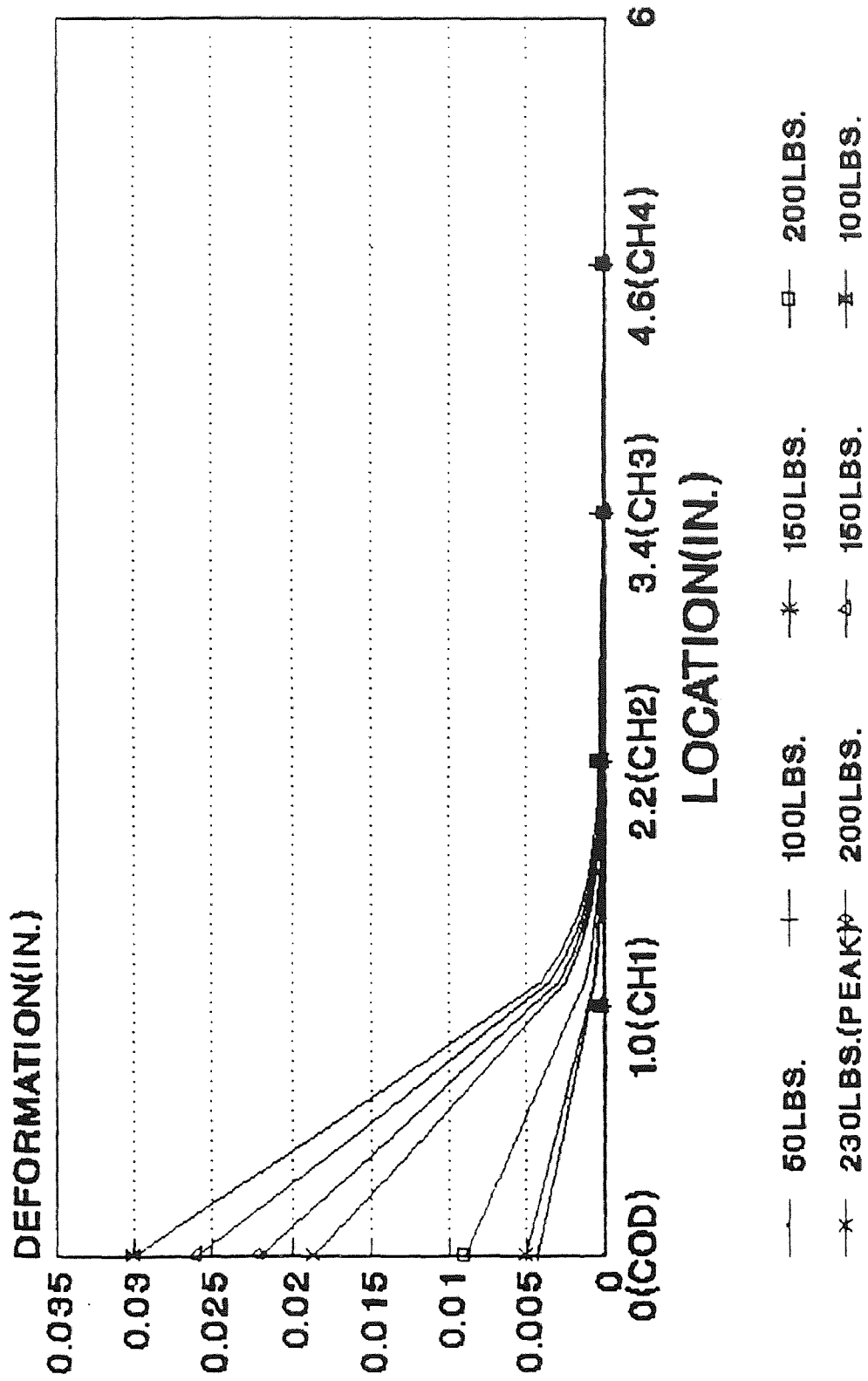


Fig.109 Deform. pattern at diff. load

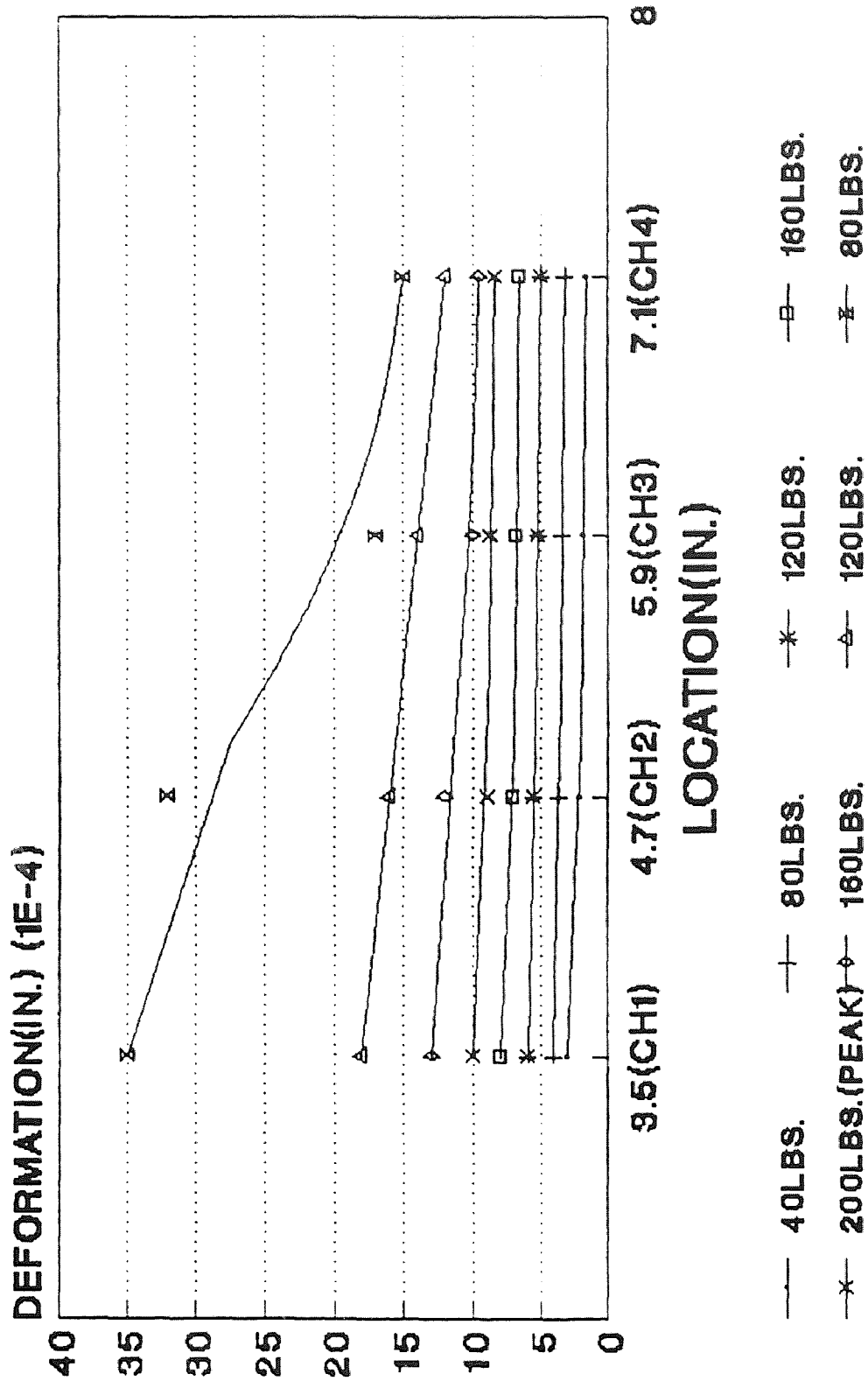


Fig.110 Deform. pattern without C 2

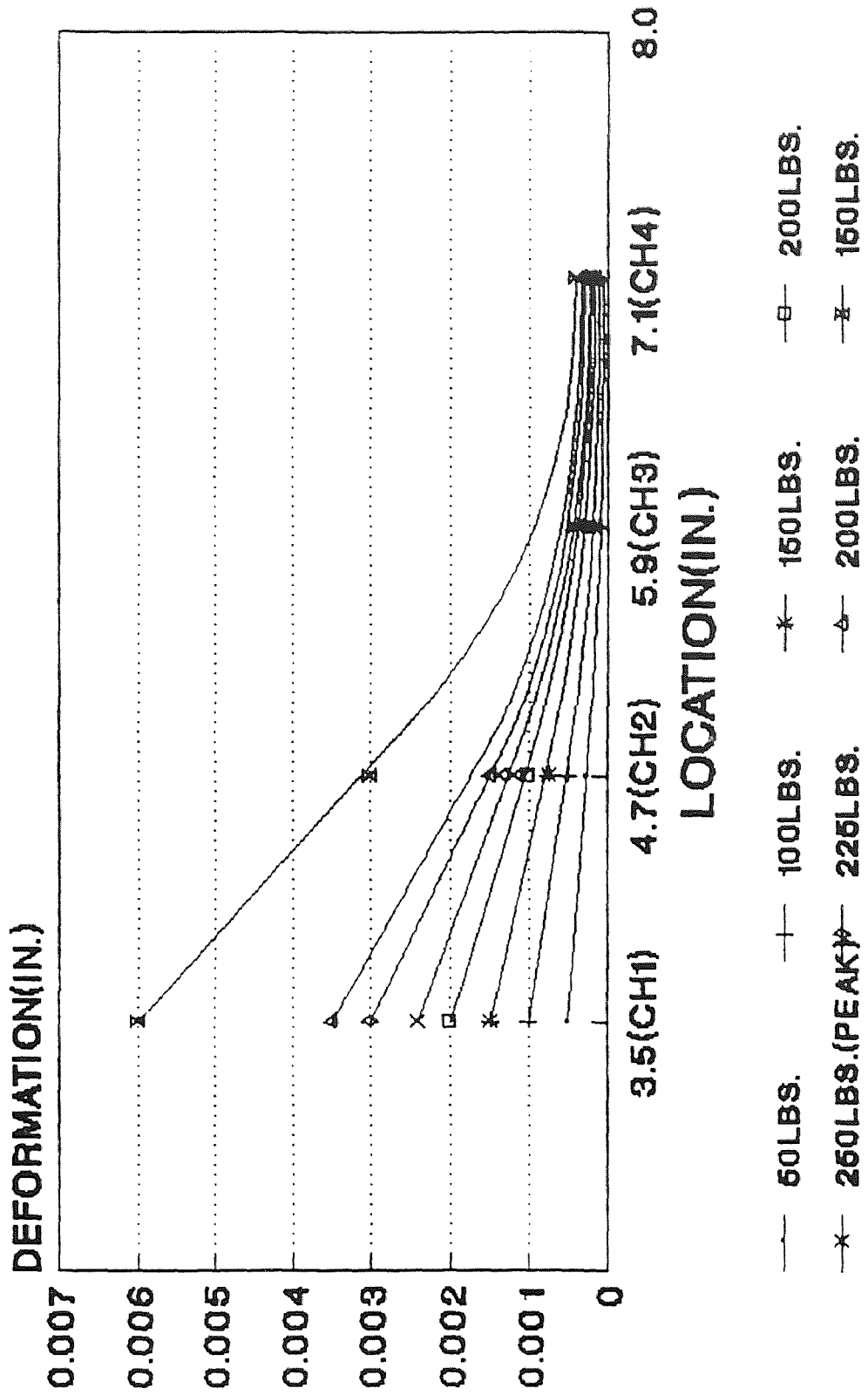


Fig.111 Deform. pattern without COL.

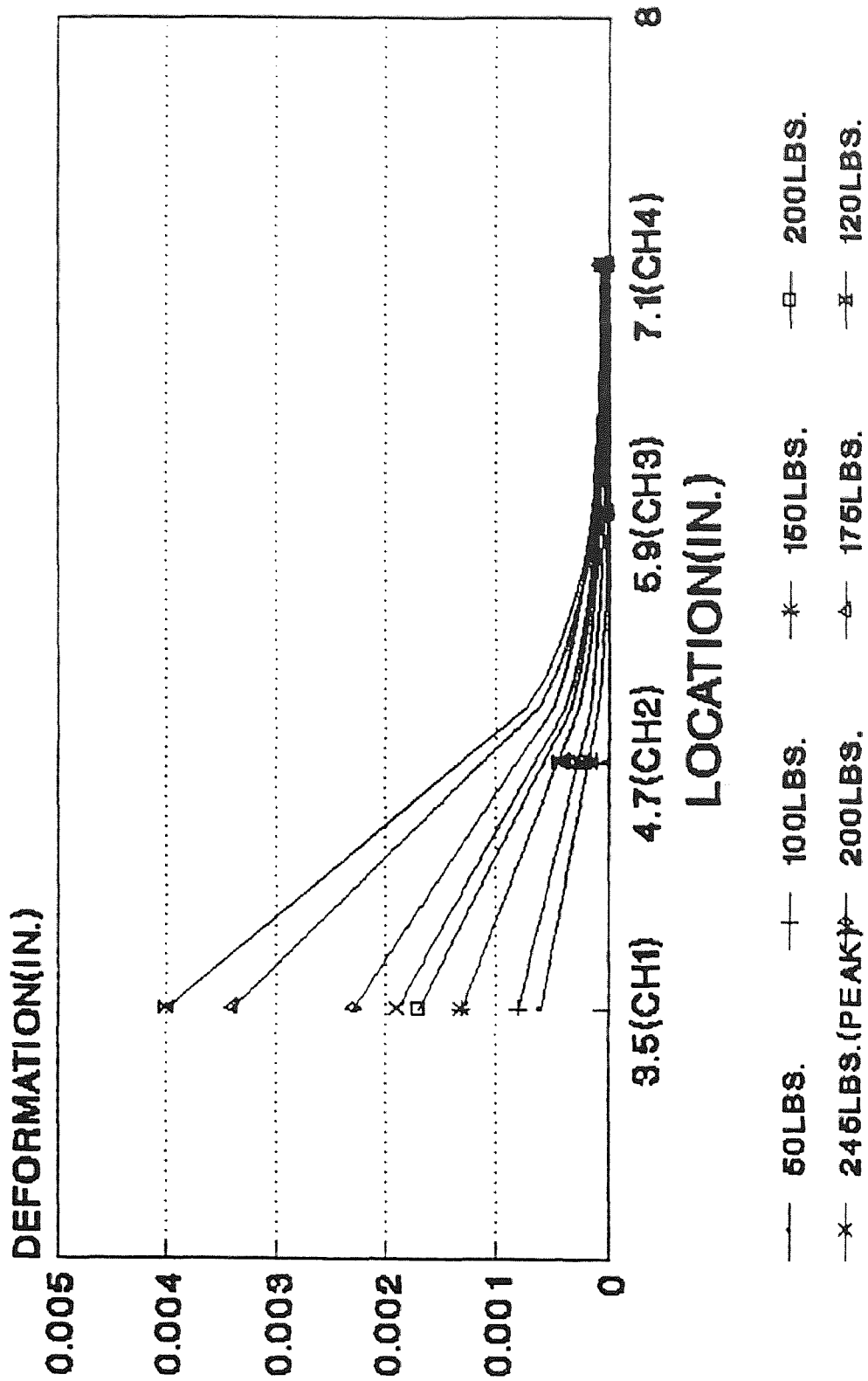
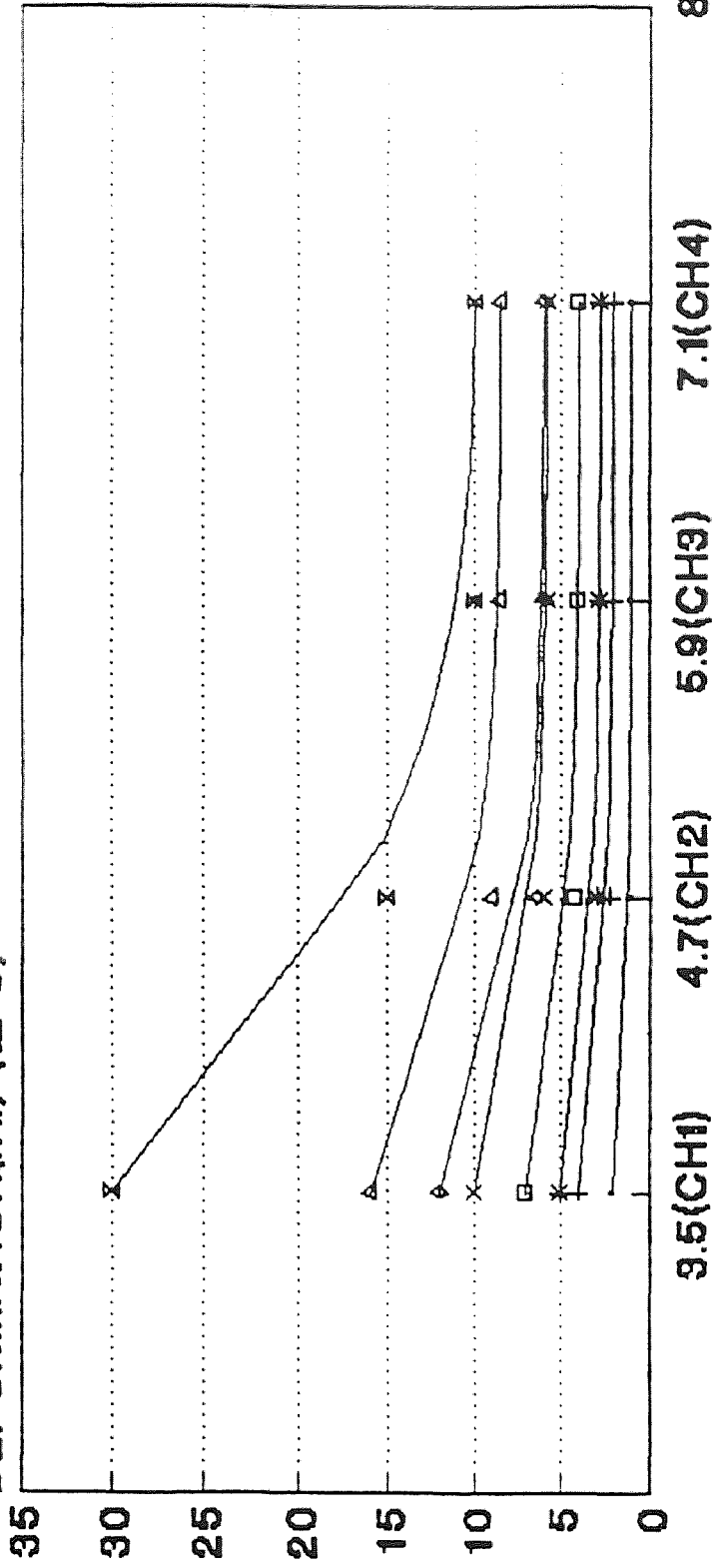


Fig.112 Deform. pattern without CO₂ F11

DEFORMATION(IN.) (1E-5)



—+— 25LBS. —+— 50LBS. —*— 60LBS. —*— 75LBS. —□— 100LBS.
—x— 125LBS. —◇— 150LBS.(PEAK) —△— 125LBS. —x— 100LBS.

Fig.113 Defor. pattern wi COD F12

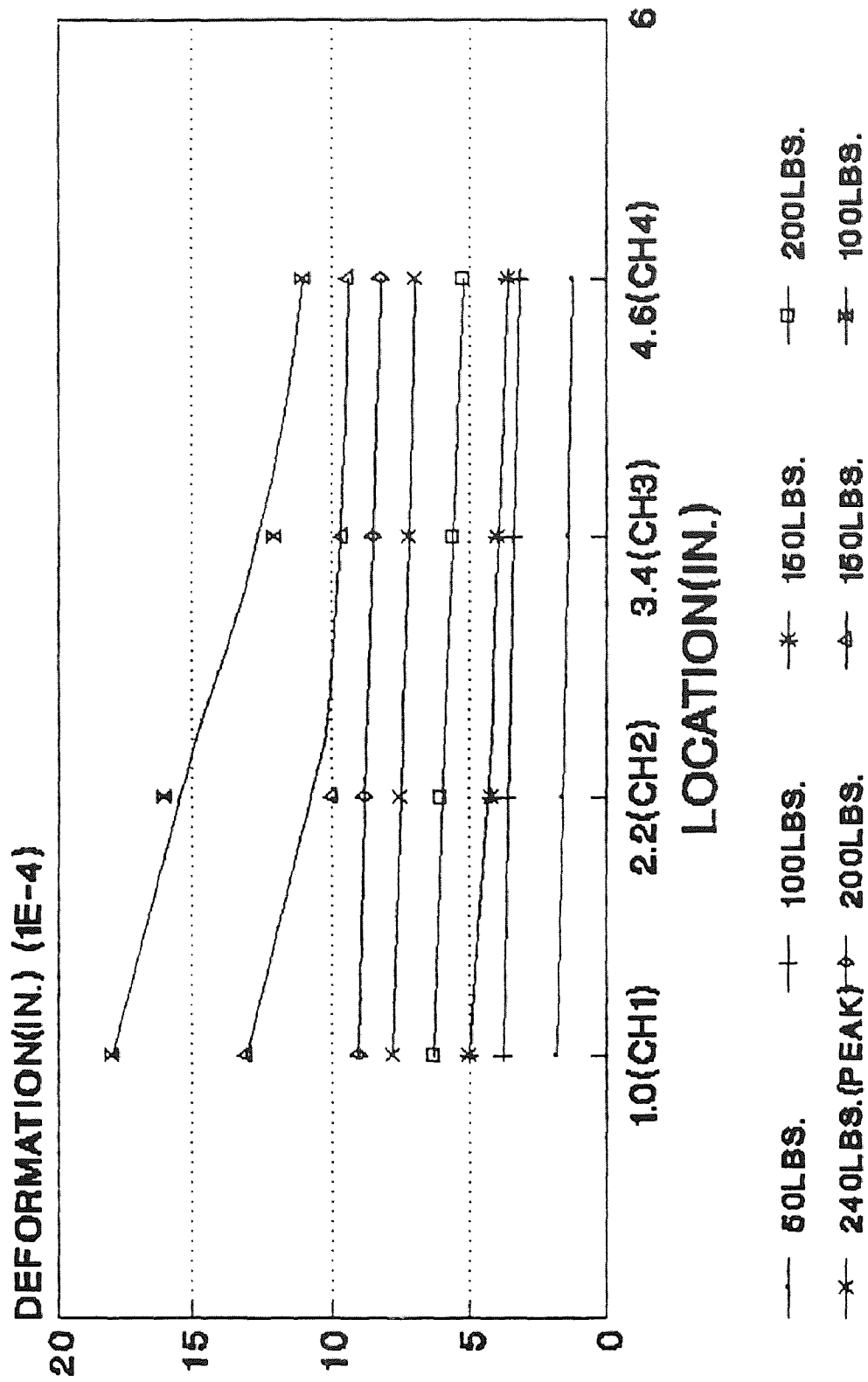


Fig.114 Deform. pattern without CO₂

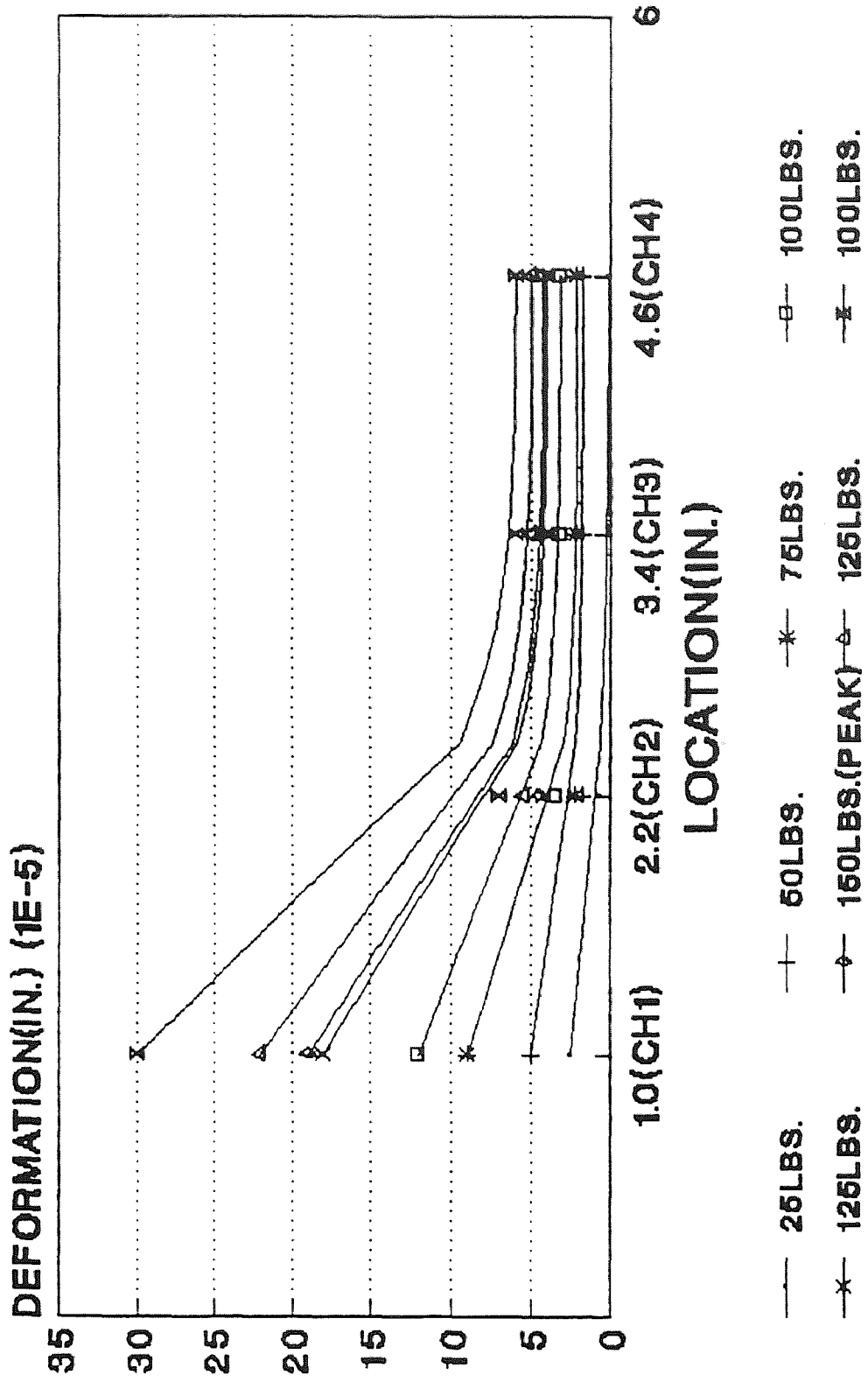


Fig.115 Deform. pattern without CC.

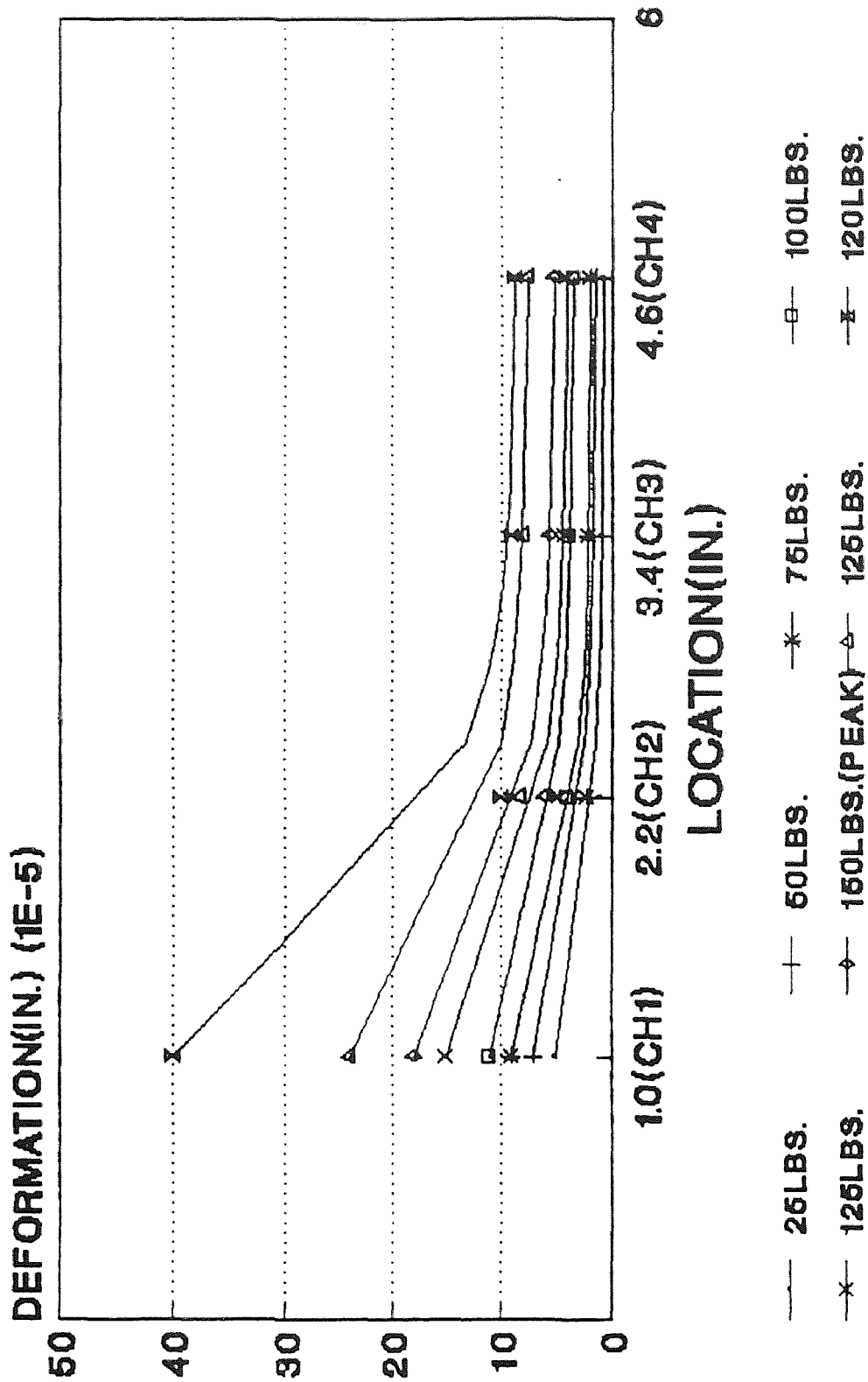


Fig.116 Deform. pattern without COI

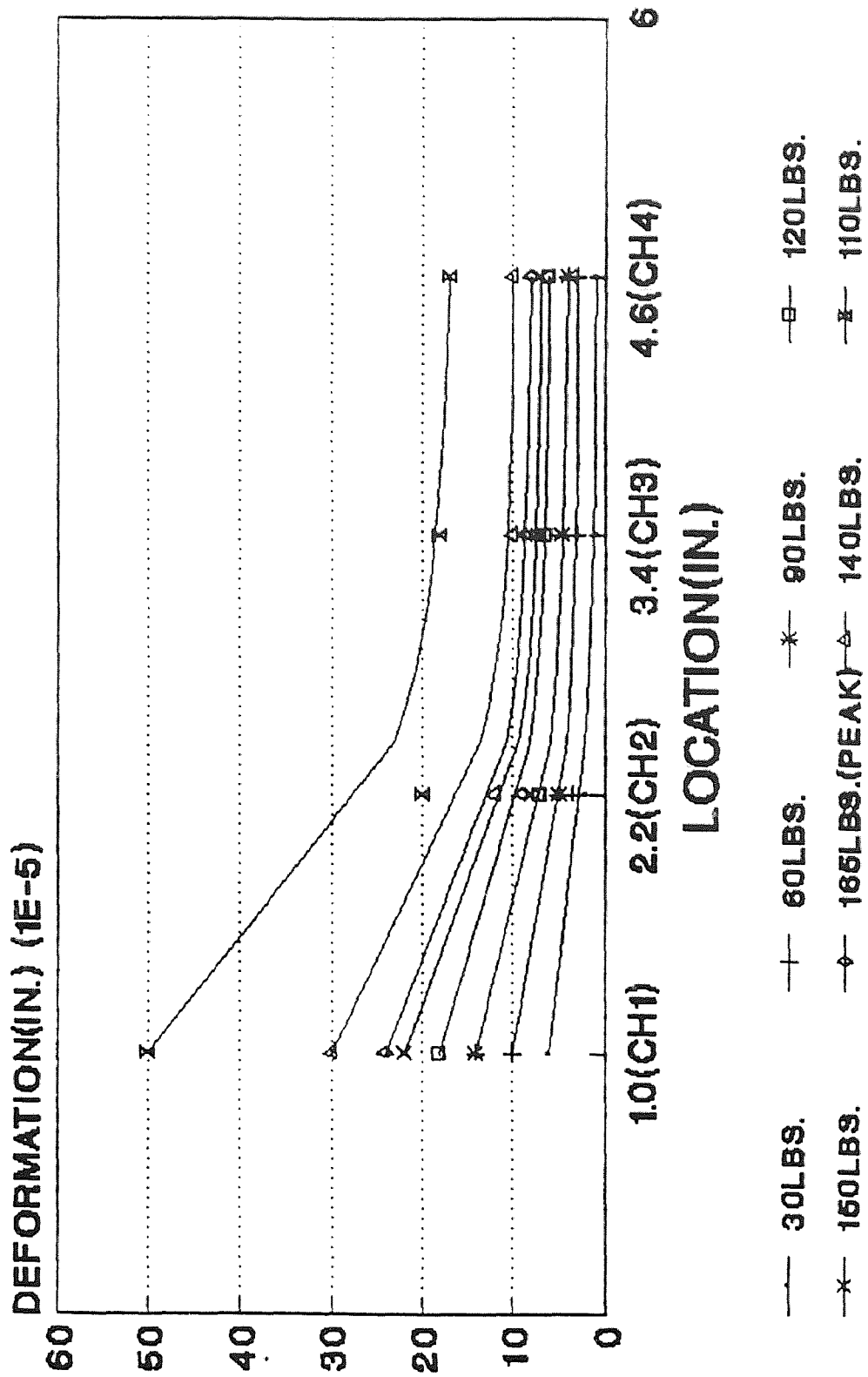


Fig.117 Deform. pattern without F28C

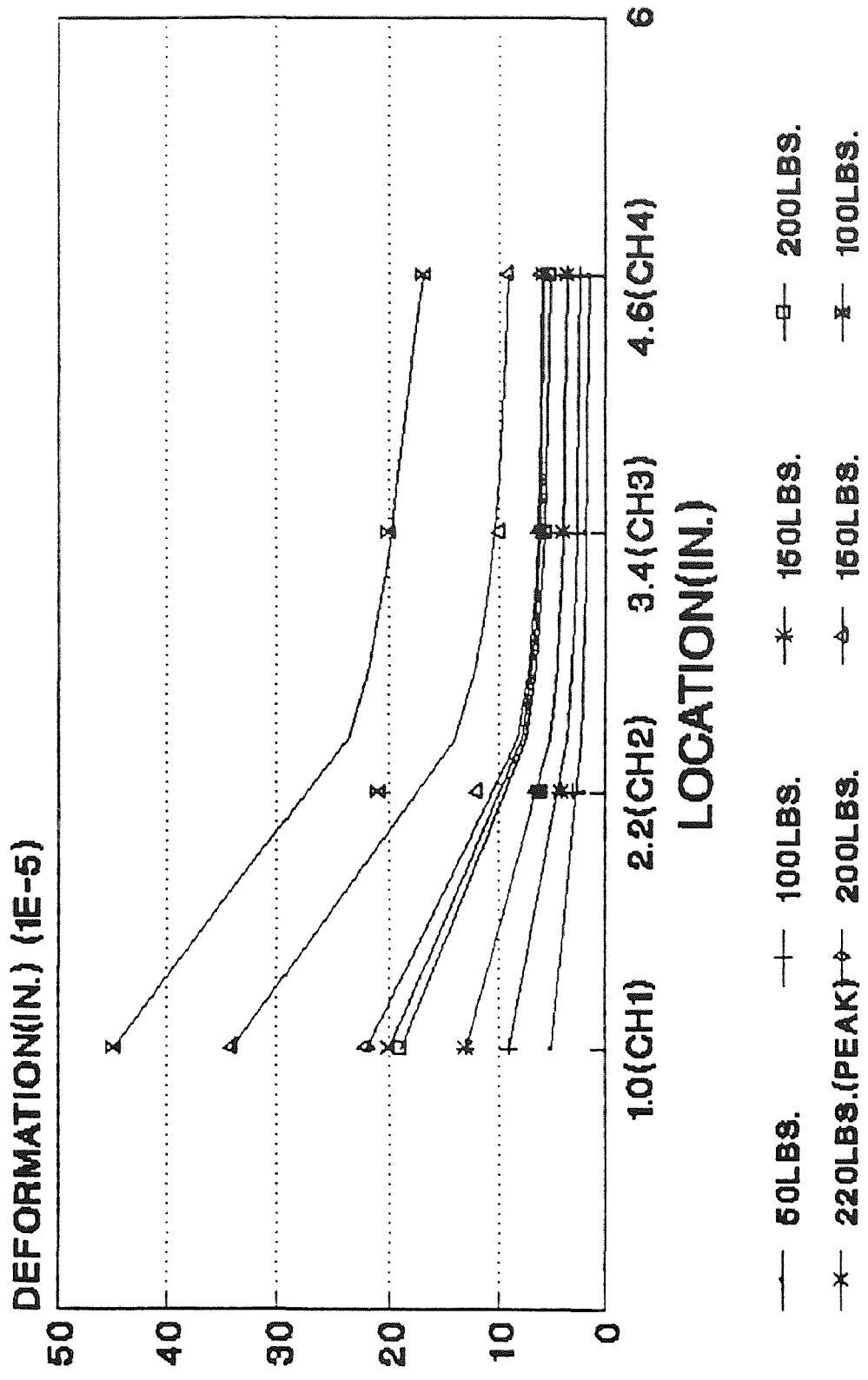


Fig.118 Deform. pattern without COD

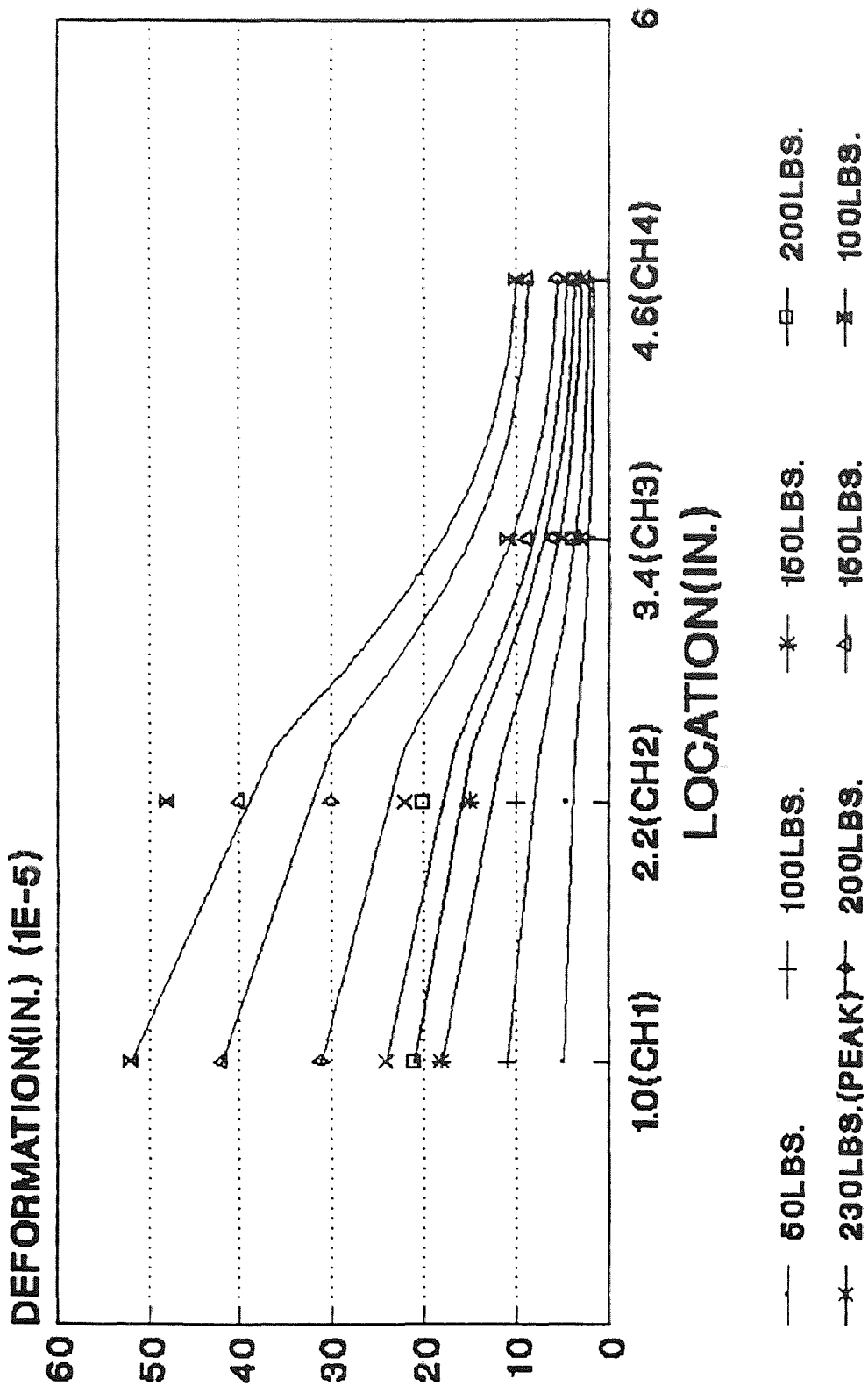


Fig.119 Defor. pattern without CO₂

CHAPTER IV Conclusion

IV.1 Conclusion

Based on the results obtained in this research , the following conclusions can be drawn :

1. The experimental techniques which were used in this study are reliable and worth further usage.
2. The critical load for CT specimen (tension test) is about 170LBS.
3. The critical load for three point bend specimen is about 220LBS.
4. The average critical COD of CT specimen (tension test) is about 0.048 inch.
5. The average critical COD of three point bend specimen is about 0.016 inch.
6. The average critical internal deformation of CT specimen for CH1 , CH2 , CH3 & CH4 is about 0.0018 , 0.0013 , 0.0004 & 0.0003 inch respectively.
7. The average critical internal deformation of BEAM specimen for CH1 , CH2 , CH3 & CH4 is about 0.0002 , 0.00016 , 0.00005 & 0.00003 respectively.

IV.2 Future Research

The experimental method presented in this study for internal deformation measurement is new and requires further research for improvements.

Possible future research might be the following :

1. Place more than four fiber optic sensors in the process zone for deformation measurements.
2. Use this technique for concrete specimen subjected to impact load for detection of cracking.

REFERENCES

1. Hillerborg, A., Modeer, M., and Petersson, P.E., "Analysis of Crack Formation and Crack Growth in Concrete by Means of Fracture Mechanics and Finite Elements," *Cement and Concrete Research*, Vol. 6, 1976, pp. 773-782.
2. Ingraffea, A.R., Henze, F.E., "Finite Element Models for Rock Fracture Mechanics," *International Journal for Numerical and Analytical Methods in Geomechanics*, Vol. 4, 1980, pp. 25-43.
3. Brown, J.H., "Measuring The Fracture Toughness of Cement Paste and Mortar," *Magnize of Concrete Research*, Vol. 24, No. 81, 1972, pp. 185-196.
4. Petersson, P.E., "Crack Growth and Development of Fracture Zones in Plain Concrete and Similar Materials," *Report No. TVBM-1006*, Lund Institute of Technology, Dec. 1981, 174 pages.
5. Visalvanich, K., Naaman, A.E., "Fracture Methods in Cement Composites," *ASCE-EMD*, Vol. 107 No. EM6, Dec. 1981, pp. 1155-1171.
6. Li, V.C., "Fracture Resistance Parameters For Cementitious Materials and Their Experimental Determinations," *Applications of Fracture Mechanics to Cementitious Composites*, NATO-ARW, Sept. 1984, Northwestern University, S.P. Shah, Editor.
7. Dugdale, D.S., "Yielding of Steel Sheets Containing Slits," *Journal of Mechanics, Physics and Solids*, Vol. 8, 1960

- , pp. 100-104.
8. Barrenblatt,G.J.,"The Mathematical Theory of Equilibrium Crack in The Brittle Fracture,"Advances in Applied Mechanics,Vol. 7,1962, pp. 55-125.
 9. Wecharatana,M.,Shah,S.P.,"Predictions of Nonlinear Fracture Process Zone in Concrete, "ASCE -EMD , Vol. 109 No. 5, October 1983, pp. 1231-1246.
 10. Cho,K.Z., Kobayashi,A.S., Hawkins,N.M., Barker,D.B., Jeang,F.L., "Fracture Process Zone of Concrete Cracks," ASCE-EMD, Vol.110, No. 8, August 1984, pp.1174-1184.
 11. Kaplan,M.F.,"Crack Propagation and The Fracture of Concrete," ACI Journal, Vol. 58, No. 5, November 1961, pp.591-610.
 12. Walsh,P.F.,"Fracture of Plain Concrete," Indian Concrete Institute, Vol. 46, No. 11, Nov. 72.
 13. Mindess,S., Nadeau,J.S.,"Effect of Notch Width on K for Mortar and Concrete,"Cement and Concrete Research, Vol. 6,1967 , pp.529-534.
 14. Ansari,F. , Yang,S.X. , "Microcomputer Controlled Closed-Loop Testing System in a Vibration Isolated Environment." Experimental Techniques (SEM) , Vol.12 , No.2 , Feb. 1988 , PP. 25-27

APPENDIX A

```

100  *-----*
110  *
120  *          MENG.BAS - DATA ACQUISITION PROGRAM
130  * MetraByte Corporation                      Rev. 1.10   8-27-84
140  *-----*
150  ?
160  ?----- STEP 1 -----
170  ?Load DASH16.BIN by contracting workspace & initialize
180  CLEAR, 49152!          ?Contract BASIC's workspace to 48K
190  DEF SEG = 0           ?Get BASIC's segment in memory
200  SG = 256 * PEEK(&H511) + PEEK(&H510)
210  SG = SG + 49152!/16
220  DEF SEG = SG         ?Load segment for CALL routine
230  BLOAD "DASH16.BIN", 0      ?Load it
240  DIM DIO%(8),A%(18000)
250  DIO%(0) = &H300        ?DASH-16 board base address
260  DIO%(1) = 2           ?Selected interrupt level for DASH-16
270  DIO%(2) = 3           ?Selected DMA level for DASH-16
280  DASH16 = 0           ?Declare & initialize other CALL parameters
290  FLAG% = 0
300  MD% = 0              ?Select Mode 0 - initialize driver

310  CALL DASH16 (MD%, DIO%(0),FLAG%) ?do it
320  IF FLAG%<>0 THEN PRINT "INITIALIZATION ERROR":STOP ?any error?
330  ?
340  ?----- STEP 2 -----
350  ?Prompt user for multiplexer scan limits
360  ?(this step can be omitted if default limits o.k.)
370  ?Set up multiplexer scanning limits
380  MD%=1                ?Mode 1 - set scan limits
390  INPUT "Lower multiplexer scanning limit (0-7 or 15)? : ",DIO%(0)
400  INPUT "Upper multiplexer scanning limit (0-7 or 15)? : ",DIO%(1)
410  CALL DASH16 (MD%, DIO%(0),FLAG%)
420  IF FLAG%<>0 THEN PRINT "Error in scan limits # ";FLAG% : STOP
430  ?
440  ?----- STEP 3 -----
450  ?SET UP SCANNING RATE (20HZ)
460  MD% = 17
470  DIO%(0) = 50 : DIO%(1) = 1000
480  CALL DASH16 (MD%, DIO%(0),FLAG%)
490  IF FLAG%<>0 THEN PRINT"Error in scan rate set up # ";FLAG% : STOP
500  ?
510  ?----- STEP 4 -----
530  DIO%(0) = 18000
540  DIO%(1) = VARPTR(A%(0)) ?Array locator
550  DIO%(2) = 1           ?Trigger source - programmable timer
560  MD%=4
570  CALL DASH16 (MD%, DIO%(0),FLAG%)
580  IF FLAG%<>0 THEN PRINT "Error in mode 4 # ";FLAG% : STOP
590  ?
600  ?----- STEP 5 -----
610  ?Display converted data
616  OPEN "C:DATA.DAT" FOR OUTPUT AS #1
620  FOR I=0 TO 18000
630  WRITE #1, A%(I)
640  NEXT I
650  END

```

```

D Line# 1      7
      1      PROGRAM   CHAN.FOR
      1      DIMENSION D1(300),D2(300),D3(300),D4(300),D5(300)
      2      *,D6(300),L1(300),L2(300),L3(300),L4(300),L5(300)
      3      *,L6(300)
      4      N=300
      5      OPEN(1,FILE='DATA.DAT',STATUS='OLD')
      6      OPEN(2,FILE='CH1.DAT',STATUS='NEW')
      7      OPEN(3,FILE='CH2.DAT',STATUS='NEW')
      8      OPEN(4,FILE='CH3.DAT',STATUS='NEW')
      9      OPEN(5,FILE='CH4.DAT',STATUS='NEW')
     10      DO 10 I=1,N
1      11      READ(1,15)L1(I)
1      12      READ(1,15)L2(I)
1      13      READ(1,15)L3(I)
1      14      READ(1,15)L4(I)
1      15      READ(1,15)L5(I)
1      16      READ(1,15)L6(I)
1      17      15 FORMAT(I5)
1      18      10 CONTINUE
      19      DO 20 J=1,N
1      20      D1(J)=((L1(J)-351.4)/182.11-1.2)*1000.0
1      21      D2(J)=(L2(J)/198.98-2.8)*1000.0
1      22      D3(J)=(L3(J)/192.23-2.6)*1000.0
1      23      D4(J)=(L4(J)/189.97-2.18)*1000.0
1      24      20 CONTINUE
      25      JJ=0
      26      DO 30 K=1,N
1      27      JJ=JJ+3
1      28      WRITE(2,25)JJ,D1(K)
1      29      WRITE(3,25)JJ,D2(K)
1      30      WRITE(4,25)JJ,D3(K)
1      31      WRITE(5,25)JJ,D4(K)
1      32      25 FORMAT(5X,I3,10X,F10.3)
1      33      30 CONTINUE
      34      STOP
      35      END

```

Name	Type	Offset	P	Class
------	------	--------	---	-------

D1	REAL	16		
D2	REAL	1216		
D3	REAL	2416		
D4	REAL	3616		
D5	REAL	4816		
D6	REAL	6016		
I	INTEGER*4	14420		
J	INTEGER*4	14432		
JJ	INTEGER*4	14440		
K	INTEGER*4	14444		
L1	INTEGER*4	7216		
L2	INTEGER*4	8416		
L3	INTEGER*4	9616		
L4	INTEGER*4	10816		
L5	INTEGER*4	12016		
L6	INTEGER*4	13216		


```

3 Line# 1
1 PROGRAM TOT.FOR
1 DIMENSION B1(40),B2(40),B3(40),B4(40),B5(40)
2 * ,AC1(39),AC2(39),AC3(39),AC4(39)
3 DIMENSION F(40),G(40),A(39)
4 DATA D1,D2,D3,D4,F/0.00035,0.0004,0.000133,
5 *0.00034,198.0;
6 OPEN(1,FILE='CD1.DAT',STATUS='NEW')
7 OPEN(2,FILE='CD2.DAT',STATUS='NEW')
8 OPEN(3,FILE='CD3.DAT',STATUS='NEW')
9 OPEN(4,FILE='CD4.DAT',STATUS='NEW')
10 OPEN(5,FILE='CD5.DAT',STATUS='NEW')
11 OPEN(6,FILE='A1.OUT',STATUS='NEW')
12 OPEN(7,FILE='A2.OUT',STATUS='NEW')
13 OPEN(8,FILE='TT.DAT',STATUS='NEW')
14 AD1=D1/40.0
15 AD2=D2/40.0
16 AD3=D3/40.0
17 AD4=D4/40.0
18 AF=F/20.0
19 B1(1)=0.0
20 B2(1)=0.0
21 B3(1)=0.0
22 B4(1)=0.0
23 B5(1)=0.0
24 WRITE(1,33)B1(1),B5(1)
25 WRITE(2,33)B2(1),B5(1)
26 WRITE(3,33)B3(1),B5(1)
27 WRITE(4,33)B4(1),B5(1)
28 DO 10 I=1,19
1 29 B1(I+1)=B1(I)+AD1
1 30 B2(I+1)=B2(I)+AD2
1 31 B3(I+1)=B3(I)+AD3
1 32 B4(I+1)=B4(I)+AD4
1 33 B5(I+1)=B5(I)+AF
1 34 WRITE(1,33)B1(I+1),B5(I+1)
1 35 WRITE(2,33)B2(I+1),B5(I+1)
1 36 WRITE(3,33)B3(I+1),B5(I+1)
1 37 WRITE(4,33)B4(I+1),B5(I+1)
1 38 10 CONTINUE
39 DO 88 K=20,21
1 40 B1(K+1)=B1(K)+AD1
1 41 B2(K+1)=B2(K)+AD2
1 42 B3(K+1)=B3(K)+AD3
1 43 B4(K+1)=B4(K)+AD4
1 44 B5(K+1)=B5(K)-AF*0.1
1 45 WRITE(1,33)B1(K+1),B5(K+1)
1 46 WRITE(2,33)B2(K+1),B5(K+1)
1 47 WRITE(3,33)B3(K+1),B5(K+1)
1 48 WRITE(4,33)B4(K+1),B5(K+1)
1 49 33 FORMAT(5X,F15.13,10X,F8.4)
1 50 88 CONTINUE
51 DO 82 IJ=22,37
1 52 B1(IJ+1)=B1(IJ)+AD1
1 53 B2(IJ+1)=B2(IJ)+AD2
1 54 B3(IJ+1)=B3(IJ)+AD3
1 55 B4(IJ+1)=B4(IJ)+AD4
1 56 B5(IJ+1)=B5(IJ)-AF*1.2

```

```

D Line#
1 57 WRITE(1,33)B1(IJ+1),B5(IJ+1)
1 58 WRITE(2,33)B2(IJ+1),B5(IJ+1)
1 59 WRITE(3,33)B3(IJ+1),B5(IJ+1)
1 60 WRITE(4,33)B4(IJ+1),B5(IJ+1)
1 61 82 CONTINUE
1 62 DO 67 IK=38,39
1 63 B1(IK+1)=B1(IK)+AD1
1 64 B2(IK+1)=B2(IK)+AD2
1 65 B3(IK+1)=B3(IK)+AD3
1 66 B4(IK+1)=B4(IK)+AD4
1 67 B5(IK+1)=B5(IK)-AP*0.05
1 68 WRITE(1,33)B1(IK+1),B5(IK+1)
1 69 WRITE(2,33)B2(IK+1),B5(IK+1)
1 70 WRITE(3,33)B3(IK+1),B5(IK+1)
1 71 WRITE(4,33)B4(IK+1),B5(IK+1)
1 72 67 CONTINUE
1 73 AC1(1)=0.0
1 74 AC2(1)=0.0
1 75 AC3(1)=0.0
1 76 AC4(1)=0.0
1 77 DO 37 I=1,39
1 78 J=I+1
1 79 AC1(J)=AC1(I)+(B1(J)-B1(I))*((B5(I)+B5(J))/2.0)
1 80 AC2(J)=AC2(I)+(B2(J)-B2(I))*((B5(I)+B5(J))/2.0)
1 81 AC3(J)=AC3(I)+(B3(J)-B3(I))*((B5(I)+B5(J))/2.0)
1 82 AC4(J)=AC4(I)+(B4(J)-B4(I))*((B5(I)+B5(J))/2.0)
1 83 37 CONTINUE
1 84 WRITE(6,66)AC1(19)
1 85 WRITE(6,66)AC2(19)
1 86 WRITE(6,66)AC3(19)
1 87 WRITE(6,66)AC4(19)
1 88 66 FORMAT(10X,'AREA=',F9.3)
1 89 F(1)=0.0
1 90 G(1)=0.0
1 91 WRITE(5,22)F(1),G(1)
1 92 DO 25 I=1,19
1 93 G(I+1)=G(I)+AP
1 94 F(I+1)=(G(I+1)*0.043)/1000*0.02801
1 95 WRITE(5,22)F(I+1),G(I+1)
1 96 25 CONTINUE
1 97 DO 91 J=20,21
1 98 G(J+1)=G(J)-AP*0.1
1 99 F(J+1)=((G(J)-G(J+1))*0.043/1000)*0.02801
1 100 91 WRITE(5,22)F(J+1),G(J+1)
1 101 DO 92 K=22,37
1 102 G(K+1)=G(K)-AP*1.2
1 103 F(K+1)=((G(K)-G(K+1))*0.043/1000)*0.02801
1 104 92 WRITE(5,22)F(K+1),G(K+1)
1 105 DO 93 L=38,39
1 106 G(L+1)=G(L)-AP*0.05
1 107 F(L+1)=((G(L)-G(L+1))*0.043/1000)*0.02801
1 108 93 WRITE(5,22)F(L+1),G(L+1)
1 109 TA=0.0
1 110 DO 94 M=1,39
1 111 N=M+1
1 112 F=F(N)-F(M)

```

```

D Line# :      7
1   113      A(N)=X*G(N)
1   114      TA=TA+A(N)
1   115      94 CONTINUE
      116      WRITE(7,14)TA
      117      22 FORMAT(5X,F15.13,10X,F8.4)
      118      14 FORMAT(10X,'AREA=',F9.3)
      119      DO 75 MN=1,40
1   120      73 FORMAT(F8.4,5X,F8.6,5X,F8.6,5X,F8.6,5X,F8.6,5X,F8.6)
1   121      75 WRITE(8,73)B5(MN),B1(MN),B2(MN),B3(MN),B4(MN),F(MN)
      122      STOP
      123      END

```

Name	Type	Offset	Class
------	------	--------	-------

A	REAL	1756	
AC1	REAL	1132	
AC2	REAL	1288	
AC3	REAL	1444	
AC4	REAL	1600	
AD1	REAL	1932	
AD2	REAL	1936	
AD3	REAL	1940	
AD4	REAL	1944	
AP	REAL	1948	
B1	REAL	12	
B2	REAL	172	
B3	REAL	332	
B4	REAL	492	
B5	REAL	652	
D1	REAL	1912	
D2	REAL	1916	
D3	REAL	1920	
D4	REAL	1924	
F	REAL	812	
G	REAL	972	
I	INTEGER*4	1952	
IJ	INTEGER*4	1980	
IK	INTEGER*4	1984	
J	INTEGER*4	1988	
K	INTEGER*4	1956	
L	INTEGER*4	2012	
M	INTEGER*4	2020	
MN	INTEGER*4	2072	
N	INTEGER*4	2024	
P	REAL	1928	
TA	REAL	2016	
X	REAL	2028	

Name	Type	Size	Class
MAIN			PROGRAM

```

D-Line# 1      7
1      PROGRAM    DEF.FOR
1      DIMENSION  B1(40),B2(40),B3(40),B4(40),B5(40),
2      *           ,AC1(39),AC2(39),AC3(39),AC4(39)
3      DATA  D1,D2,D3,D4,P/0.00035,0.0004,0.000133,
4      *0.00034,198.0/
5      OPEN(1,FILE='CD1.DAT',STATUS='NEW')
6      OPEN(2,FILE='CD2.DAT',STATUS='NEW')
7      OPEN(3,FILE='CD3.DAT',STATUS='NEW')
8      OPEN(4,FILE='CD4.DAT',STATUS='NEW')
9      AD1=D1/40.0
10     AD2=D2/40.0
11     AD3=D3/40.0
12     AD4=D4/40.0
13     AP=P/20.0
14     B1(1)=0.0
15     B2(1)=0.0
16     B3(1)=0.0
17     B4(1)=0.0
18     B5(1)=0.0
19     WRITE(1,33)B1(1),B5(1)
20     WRITE(2,33)B2(1),B5(1)
21     WRITE(3,33)B3(1),B5(1)
22     WRITE(4,33)B4(1),B5(1)
23     DO 10 I=1,19
1 24     B1(I+1)=B1(I)+AD1
1 25     B2(I+1)=B2(I)+AD2
1 26     B3(I+1)=B3(I)+AD3
1 27     B4(I+1)=B4(I)+AD4
1 28     B5(I+1)=B5(I)+AP
1 29     WRITE(1,33)B1(I+1),B5(I+1)
1 30     WRITE(2,33)B2(I+1),B5(I+1)
1 31     WRITE(3,33)B3(I+1),B5(I+1)
1 32     WRITE(4,33)B4(I+1),B5(I+1)
1 33     10 CONTINUE
34     DO 88 K=20,21
1 35     B1(K+1)=B1(K)+AD1
1 36     B2(K+1)=B2(K)+AD2
1 37     B3(K+1)=B3(K)+AD3
1 38     B4(K+1)=B4(K)+AD4
1 39     B5(K+1)=B5(K)-AP*0.1
1 40     WRITE(1,33)B1(K+1),B5(K+1)
1 41     WRITE(2,33)B2(K+1),B5(K+1)
1 42     WRITE(3,33)B3(K+1),B5(K+1)
1 43     WRITE(4,33)B4(K+1),B5(K+1)
1 44     33 FORMAT(5X,F10.7,10X,'1',10X,F8.4)
1 45     88 CONTINUE
46     DO 82 IJ=22,37
1 47     B1(IJ+1)=B1(IJ)+AD1
1 48     B2(IJ+1)=B2(IJ)+AD2
1 49     B3(IJ+1)=B3(IJ)+AD3
1 50     B4(IJ+1)=B4(IJ)+AD4
1 51     B5(IJ+1)=B5(IJ)-AP*0.43
1 52     WRITE(1,33)B1(IJ+1),B5(IJ+1)
1 53     WRITE(2,33)B2(IJ+1),B5(IJ+1)
1 54     WRITE(3,33)B3(IJ+1),B5(IJ+1)

```

```

D Line# 1      7
57          DO 67 IK=38,39
1 58          B1(IK+1)=B1(IK)+AD1
1 59          B2(IK+1)=B2(IK)+AD2
1 60          B3(IK+1)=B3(IK)+AD3
1 61          B4(IK+1)=B4(IK)+AD4
1 62          B5(IK+1)=B5(IK)-AP*0.05
1 63          WRITE(1,33)B1(IK+1),B5(IK+1)
1 64          WRITE(2,33)B2(IK+1),B5(IK+1)
1 65          WRITE(3,33)B3(IK+1),B5(IK+1)
1 66          WRITE(4,33)B4(IK+1),B5(IK+1)
1 67          67 CONTINUE
68          AC1(1)=0.0
69          AC2(1)=0.0
70          AC3(1)=0.0
71          AC4(1)=0.0
72          DO 37 I=1,39
1 73          J=I+1
1 74          AC1(J)=AC1(I)+(B1(J)-B1(I))*((B5(I)+B5(J))/2.0)
1 75          AC2(J)=AC2(I)+(B2(J)-B2(I))*((B5(I)+B5(J))/2.0)
1 76          AC3(J)=AC3(I)+(B3(J)-B3(I))*((B5(I)+B5(J))/2.0)
1 77          AC4(J)=AC4(I)+(B4(J)-B4(I))*((B5(I)+B5(J))/2.0)
1 78          37 CONTINUE
79          WRITE(6,66)AC1(19)
80          WRITE(6,66)AC2(19)
81          WRITE(6,66)AC3(19)
82          WRITE(6,66)AC4(19)
83          66 FORMAT(10X,'AREA=',F9.3)
84          STOP
85          END

```

Name	Type	Offset	F	Class
AC1	REAL	812		
AC2	REAL	968		
AC3	REAL	1124		
AC4	REAL	1280		
AD1	REAL	1456		
AD2	REAL	1460		
AD3	REAL	1464		
AD4	REAL	1468		
AP	REAL	1472		
B1	REAL	12		
B2	REAL	172		
B3	REAL	332		
B4	REAL	492		
B5	REAL	652		
D1	REAL	1436		
D2	REAL	1440		
D3	REAL	1444		
D4	REAL	1448		
I	INTEGER*4	1476		
J	INTEGER*4	1512		
K	INTEGER*4	1516		
L	INTEGER*4	1520		
M	INTEGER*4	1480		